Design with Regard to Collision Impact

Comparison of Response between a Simplified 2DOF system and FE analysis for Impact on a Simply Supported Elastic Beam

Master of Science Thesis in the Master's Programme Structural Engineering and Building Technology

ERIK ASPLUND

DANIEL STECKMEST

Design with Regard to Collision Impact

Comparison of Response between a Simplified 2DOF system and FE analysis for Impact on a Simply Supported Elastic Beam

Master of Science Thesis in the Master's Programme Structural Engineering and Building Technology

ERIK ASPLUND

DANIEL STECKMEST

Design with regard to collision impact

Comparison of Response between a Simplified 2DOF system and FE analysis for Impact on a Simply Supported Elastic Beam

Master of Science Thesis in the Master's Programme Structural Engineering and Building Technology

ERIK ASPLUND

DANIEL STECKMEST

Department of Civil and Environmental Engineering
Division of Structural Engineering
Concrete Structures
Chalmers University of Technology
SE-412 96 Göteborg
Sweden
Telephone: + 46 (0)31-772 1000

Cover:
Illustration of how a vehicle impact on a simply supported beam can be transformed into a FE model and a 2DOF system. Comparison of response in displacement u_2, support reaction force R_A and moment M_α over time between 2DOF and FEM.

Design with regard to collision impact

Comparison of Response between a Simplified 2DOF system and FE analysis for Impact on a Simply Supported Elastic Beam

Master of Science Thesis in the Master's Programme Structural Engineering and Building Technology

ERIK ASPLUND

DANIEL STECKMEST

Department of Civil and Environmental Engineering
Division of
Concrete Structures
Chalmers University of Technology

ABSTRACT

During a collision between two objects an impact load is generated. Such events could for example happen when a vehicle crashes into a barrier or when an object is thrown into a wall by strong wind. The response from such an impact can be very different from when a static load is applied. The approach regarding collision impacts presented in Eurocode is very limited and simplified, and the subject needs to be investigated further. This Master's thesis uses a simplified two degree of freedom (2DOF) system and a finite element (FE) model to analyse the responses during a collision between a moving object and a simply supported elastic beam.

Basic theory of dynamics and collision analysis are presented together with different ways of approximating the material behaviour. Several dynamical models, such as classic theory, 2DOF spring-mass system and FE analysis are described and implemented. A parameter study is performed to decide which properties are most critical. This shows that the ratio of the eigenfrequencies of the involved objects is a governing factor for how the response of the system behaves.

The response from a collision depends greatly on the structural properties of the two objects involved. Vehicle crash tests are therefore studied in order to determine reasonable properties to be used for vehicles in a collision impact analysis. It is established that the material response of a vehicle has a bilinear relationship with a stiffness increase after a certain deformation, in contrast to Eurocode where a constant stiffness value is used which also is very low compared to what is found in the tests.

To be able to implement a beam in the 2DOF system it needs to be treated as a single degree of freedom system. For this purpose, transformation factors are derived to translate the beam properties in order to be applicable in the spring-mass system.

A collision impact can be seen as a point load acting at various distances from the support. This needs to be considered in the analysis which is carried out using several different points of impact and elastic materials. A comparison of the results from the 2DOF and FE models is then made to assess how well the simplified system manages to describe the response. It can be concluded that the 2DOF system shows a good correlation with the FE analysis when the frequency ratio is low or when loading close to midspan. When the frequency ratio is high the 2DOF response will be on the unsafe side for all loading positions, but the deflection will still correlate well.

Key words: Collision impact, impulse load, 2DOF, FEM, dynamic response, moment, shear force, transformation factors, vehicle stiffness, crash test

Dimensionering med hänsyn till kollisionslast

Jämförelse av respons mellan ett förenklat tvåfrihetsgradssystem och en FE analys för kollision med en fritt upplagd elastisk balk

Examensarbete inom mastersprogrammet Structural Engineering and Building Technology
ERIK ASPLUND
DANIEL STECKMEST
Institutionen för bygg- och miljöteknik
Avdelningen för konstruktionsteknik
Betongbyggnad
Chalmers tekniska högskola

SAMMANFATTNING

Vid en krock mellan två kroppar skapas en kollisionslast. Detta kan vara när ett fordon kör in i ett hinder eller när ett objekt slungas in i en vägg av stark vind. Responsen från en sådan kollision kan vara mycket annorlunda jämfört med om lasten vore statisk. Tillvägagångssättet i Eurokod är ganska förenklat och begränsat, och detta ämne måste därför undersökas djupare. Detta examensarbete använder ett förenklat tvåfrihetsgradssystem (2DOF-system) och en finita element (FE) modell för att analysera responsen vid en kollision mellan ett inkommande föremål och en fritt upplagd elastisk balk.

Grundläggande teori om dynamik och kollisionsanalys presenteras tillsammans med olika metoder för att uppskatta materialets beteende. Flertalet dynamiska modeller, såsom klassisk stötteori, ett 2DOF-massa-fjäder-system och en FE-modell beskrivs och implementeras. En parameterstudie genomförs för att bestämma vilka egenskaper som har störst betydelse. Denna visar att kvoten av de ingående kropparnas egenfrekvenser är en viktig faktor för att beskriva hur systemet beter sig.

Den respons som uppstår vid en kollision beror till stor del på de strukturella egenskaperna hos de två aktuella kropparna. Därför har krocktester av bilar studerats för att kunna uppskatta vilka parametrar som är rimligt att använda vid en kollisionsanalys. Det visar sig att fordon har en bilinjär arbetskurva där styvheten ökar efter en viss deformation. Detta i motsats till Eurokod som använder ett konstant värde på styvheten som dessutom är mycket lägre än vad som visas i testerna.

För att kunna implementera balken i 2DOF-systemet har transformationsfaktorer härletts. Dessa omvandlar balkens egenskaper för att gälla i ett massa-fjäder-system.

En kollision kan ses som en punktlast som träffar på ett godtyckligt avstånd från stödet, vilket tas till hänsyn i beräkningarna genom att flera olika träffpunkter ingår i analysen. Resultaten från 2DOF-systemet och FE-modellen jämförs sedan för att bedöma hur väl det förenklade systemet beskriver responsen. Det kan konstateras att 2DOF-systemet visar god överrensstämmelse med FE-analysen när frekvenskvoten är låg eller när lasten träffar nära balkmitt. När frekvenskvoten istället är hög visar 2DOF-systemet resultat på osäker sida för alla träffpunkter, förutom för nedböjningen som verkar stämma bra överrens för alla testade fall.

Nyckelord: Kollisionslast, impulslast, 2DOF-system, FEM, dynamisk respons, moment, tvärkraft, transformationsfaktorer, fordonsstyvhet, krocktest.

Contents

CHALMERS *Civil and Environmental Engineering*, Master's Thesis 2014:80

Preface

In this Master's thesis the responses during a collision between a projectile and a simply supported beam have been investigated, and a comparison between a 2DOF system and FE model has been carried out.

The project has been carried out in collaboration with Reinertsen Sverige AB and the Department of Civil and Environmental Engineering, Division of Structural Engineering, Concrete Structures research group at Chalmers University of Technology. The project has been carried out with Ph.D. Morgan Johansson, Reinertsen Sverige AB, as supervisor and Ph.D. Joosef Leppänen, Chalmers University of Technology, as examiner. The work has been carried out between January and June 2014 at Reinertsen Sverige AB in Gothenburg, Sweden.

First of all we would like to thank Morgan Johansson for his devoted supervision of our thesis project, thoughtful insights and helpful feedback. Secondly we also want to thank Joosef Leppänen for his guidance as an examiner and important feedback. Additionally we also want to express appreciation to Mattias Carlsson and Sebastian Andersson who have both been very helpful when we experienced problems with the finite element software. Also a big thanks to Reinertsen Sverige AB for the big private office space of 60 square meters provided for us during the whole semester.

Finally we want to thank both each other and our fellow thesis worker colleagues for all the pleasant coffee breaks and occasional Friday pastries.

Gothenburg June 2014

Erik Asplund and Daniel Steckmest

Abbreviations

2DOF	Two Degree of Freedom
COR	Coefficient of Restitution e
EC	Eurocode
Euro NCAP	European New Car Assessment Programme
FEA	Finite Element Analysis
FEM	Finite Element Method
FWDB	Full Width Deformable Barrier
FWRB	Full Width Rigid Barrier
LCMDB	Load Cell Moving Deformable Barrier
MDOF	Multi Degree of Freedom
NHTSA	National Highway Traffic Safety Administration
ODB	Offset Deformable Barrier
SDOF	Single Degree of Freedom
ULS	Ultimate Limit State

Notations

Roman upper case letters

A	Area
A_{cc}	Area of compression zone
A_s	Amount (area) of tensile reinforcement
A_ϕ	Area of one reinforcement bar
A_{II}	Effective concrete area
C	Damping matrix
E	Modulus of elasticity (Young's modulus)
E_{II}	Equivalent modulus of elasticity
E_c	Modulus of elasticity of concrete
E_s	Modulus of elasticity of reinforcing steel
E_k	Kinetic energy
EI_b	Bending stiffness of a beam
F	(External) force
F_b	Force acting on a beam
G	Shear modulus
I	Impulse
I_c	Characteristic impulse
I_I	Moment of inertia for a cross section in state I (uncracked)
I_{II}	Moment of inertia for a cross section in state II (cracked)
K	Stiffness matrix
M	Bending moment
M_f	Bending moment in field
M_s	Bending moment at support
M_α	Bending moment at point of impact
M	Mass matrix
N	Normal force
P	Pressure
Q	Equivalent static force
R_1	Internal reaction force in body 1

R_2	Internal reaction force in body 2
R_A	Reaction force at support A
R_B	Reaction force at support B
R_{sta}	Static part of the reaction force
R_{dyn}	Dynamic part of the reaction force
R	Loading capacity (strength)
T	Period (duration of one cycle)
V	Shear force
W	Work
W_i	Internal work
W_e	External work

Roman lower case letters

a	Acceleration
a	Distance between loading and support
b	$1 - a$
c	Damping coefficient
c	Concrete cover
c	Wave speed
d	Effective depth of cross-section for tensile reinforcement
d'	Effective depth of cross-section for compressive reinforcement
e	Coefficient of restitution, COR
f	Natural frequency
f_{tk}	Characteristic strength of reinforcement
f_{yk}	Characteristic yield strength of reinforcement
f_1	Natural frequency of body 1
f_2	Natural frequency of body 2
h_b	Height of cross-section of a beam
k	Stiffness (spring constant)
k_1	Stiffness of body 1
$k_{1,1}$	Stiffness of first part of a bilinear force-displacement relationship
k_2	Stiffness of body 2
$k_{1,2}$	Stiffness of second part of a bilinear force-displacement relationship
$k_{1,3}$	Stiffness of unloading part of a bilinear force-displacement relationship
k_b	Stiffness of a beam
k_λ	Correction factor for plastic rotation capacity
l	Distance
l_0	Distance between the zero and the maximum moment section
l_b	Length of beam
m	Mass
m_1	Mass of body 1
m_2	Mass of body 2
m_b	Mass of beam
n	Number of reinforcement bars
p	Momentum
s	Spacing of bars
t	Time
Δt	Time increment
u	Displacement

u_1	Displacement of body 1
u_1	Displacement corresponding to a change in stiffness for a bilinear curve
u_2	Displacement of body 2
Δu	Displacement increment
u_{el}	Elastic displacement
u_{pl}	Plastic displacement
u_s	Displacement of system point
$\dot{u}$	Velocity
$\ddot{u}$	Acceleration
$u''(x)$	Curvature of a beam
v	Velocity
v_0	Initial velocity
v_r	Velocity at impact
w_b	Width of cross-section of a beam
x	Depth of compression zone
x	Coordinate of horizontal length axis
x_{cc}	Distance to equivalent force for compression zone
x_u	Depth of compression zone in ULS

Greek lower case letters

α	Distance between loading and support in relation to the total length
α_s	Ratio of E_s to E_c
β	$1 - \alpha$
β_{shear}	Factor regarding shear stress
β_{el}	Load factor
γ	The distribution of the load in relation to the total length of the beam
$\gamma_{1,2}$	Load factor used when determining reaction force according to Biggs
γ_I	Factor for characteristic impulse
κ_F	Transformation factor for load
κ_k	Transformation factor for stiffness
κ_m	Transformation factor for mass
$\kappa_{m,el}$	Transformation factor for mass, elastic response
$\kappa_{m,pl}$	Transformation factor for mass, plastic response
κ_{mF}	Transformation factor for both mass and load
ε_{uk}	Ultimate strain of reinforcing steel
θ	Rotation
θ_{pl}	Plastic rotation capacity
θ_s	Plastic rotation
λ	Shear slenderness
ρ	Density
ω	Natural circular frequency
φ	Angle between force and direction of displacement
φ_{dyn}	Dynamic amplification factor
ϕ	Diameter of reinforcing steel bar

1 Introduction

1.1 Background

During a collision between two objects an impact load is generated. Such events could for example happen when a vehicle crashes into a barrier, when an object is dropped onto a floor or thrown into a wall by strong wind. The response from such an impact can be very different from when a static load is applied and the structural properties of the objects will be of great importance for the dynamic behaviour.

The approach regarding collision impact presented in Eurocode is very simplified and the knowledge in this field of study is generally limited. Therefore the subject needs to be investigated further and alternative methods for analysis, both detailed and simplified, needs to be studied.

1.2 Objective

The objective of this Master's thesis is to investigate a collision impact and the resulting responses using both simplified and more advanced design approaches. The different methods, including a two degree of freedom (2DOF) system and a finite element (FE) model, will also be compared to see how well the simplified methods are able to describe the real behaviour. Furthermore it needs to be studied under what conditions it is adequate to use a simplified method and when a more refined method needs to be implemented. A literature study treating the basic theory of dynamics will also be carried out and a summary of this will be composed and implemented in the thesis.

Furthermore it will be investigated how the response from a collision depends on different structural properties of the involved objects. An important design situation in real life is vehicle impact, but the knowledge about the structural parameters of such an object is limited in the field of structural engineering. Therefore vehicle crash tests are to be studied in order to determine reasonable properties to be used for vehicles in collision impact analyses. A collision impact can be seen as a point load acting at various distances from the support and the importance of impact position for different responses, such as moment and shear force, will be examined.

1.3 Scope and limitations

In this thesis the effect of damping is omitted since it in most cases has a small influence on the response of a collision impact, due to the relatively short duration of the load. It would also make the analyses more complicated than what is needed.

Moreover this report only treats simply supported beams with elastic response. This choice is made in order to be able to be thorough enough when studying different aspects of the subject.

1.4 Method

A literature study covering the basic theory of dynamics and collision analysis, including different ways of approximating the material behaviour, is carried out.

Several dynamical models, such as classic theory, 2DOF spring-mass system and FE analysis are then described and implemented. The 2DOF system is modelled in the commercial software MATLAB and is based on the fundamental equation of motion. The central difference method is then used to find a numerical solution of the displacement in each time step. The FE analyses are performed in the commercial software ADINA 900 nodes version, ADINA R & D, Inc (2014). Here the colliding object is modelled as a point mass connected to a spring and the beam is modelled by elastic 3D beam elements. The FE analyses are used as a reference throughout the report and are assumed to be a sufficiently good representation of reality.

The response from a collision depends greatly on the structural properties of the two objects involved. A parameter study is therefore performed, using the dynamical models, to decide which properties are the most critical. Vehicle crash tests are also studied in order to determine reasonable properties to be used for vehicles in collision impact analyses.

To be able to implement a beam in the 2DOF system it needs to be treated as a single degree of freedom (SDOF) system. To be able to do this, transformation factors are derived in order to translate the beam properties. These can then be implemented in the spring-mass system.

Each analysis is carried out using several different points of impact to simulate an arbitrary impact position on the beam. This will also affect the transformation factors since the shape and size of the deflection is different for different impact positions. A comparison of the results from the 2DOF and FE models is then made to assess how well the simplified system manages to describe the response.

Finally an example of an analysis is carried out where a vehicle crashing into a beam is investigated. Here the 2DOF model, with different material responses for the vehicle, is implemented and compared to the calculation method described in Eurocode. A recommendation for which of the simplified analysis methods to use in different situations is also proposed.

1.5 Thesis outline

Chapter 2 contains most of the background theory used for this thesis including basic concepts of dynamics, how to treat different kind of material behaviours and a description of dynamic models such as the spring-mass system.

Chapter 3 implements the dynamic models, previously described in Chapter 2, and contains a parameter study to decide which variables are the most important. It also examines the effect of a rigid barrier being present.

Chapter 4 examines what structural parameters are reasonable to use for vehicles that crashes into a barrier, and also describes the beam studied in this thesis. A description and derivation of how the beam is transformed for use in the 2DOF model is presented. Furthermore a description of how impact load is treated in Eurocode is included.

Chapter 5 contains detailed analyses of impact on a simply supported beam. Both the 2DOF system and FE model are used for the analysis and the methods are well described. The models are also compared to determine how well the simplified 2DOF system is able to capture the response in the beam, and to decide when each model is proper to use. The effect of the impact position on the beam response is also studied to decide the most critical loading position. Finally a calculation example where a vehicle crashing into a column is carried out using reasonable parameters previously discussed in this thesis.

Results and the discussion of these are treated individually in each chapter, but a concluding discussion of the whole report is carried out in Chapter 6 together with recommendations for further studies. References used in this thesis can be found in Chapter 7. Several appendices are attached at the end of the report and contain additional results that are not included in the main chapters.

2 Basic Theory

2.1 Basic concepts of Dynamics

To understand the mechanics behind what is happening during a collision between two objects, it is necessary to be familiar with some basic dynamical concepts. In a collision, the impact load will act during a very short time, in opposite to a static load. Therefore some fundamental theory of dynamics is presented in this section, based on Johansson and Laine (2012).

2.1.1 Velocity and acceleration

Mean velocity $\bar{v}$ is defined as distance moved by an object, Δu, during a certain time interval Δt,

$$\bar{v} = \frac{\Delta u}{\Delta t} \tag{2.1}$$

If the time step then is considered as infinitely small, i.e. $\Delta t \rightarrow 0$, the velocity v is defined as the change of an objects position with each instant of time

$$v = \frac{du}{dt} = \dot{u} \tag{2.2}$$

This is basically the same as the speed of an object, except that speed does not describe in which direction an object is moving.

Analogously, the acceleration a is defined as the change of an objects velocity with each instant of time t

$$a = \frac{dv}{dt} = \frac{d\dot{u}}{dt} = \ddot{u} \tag{2.3}$$

2.1.2 Force and pressure

Force can be described as the ability to accelerate the mass of a body. This relation between force F, mass m and acceleration is stated in Newton's second law of motion

$$F = m \cdot a \tag{2.4}$$

To define the force per unit area A the physical quantity pressure P can be used

$$P = \frac{F}{A} \tag{2.5}$$

2.1.3 Momentum and impulse

The momentum p of a body with mass m and velocity v can be defined as

$$p = m \cdot v \tag{2.6}$$

If the body has an initial velocity of v_0 and is subjected to a force $F(t)$ during a certain time period $t_0 \leq t \leq t_1$, it will have a final momentum of

$$p = m \cdot v_1 = m \cdot v_0 + \int_{t_0}^{t_1} F(t)dt \tag{2.7}$$

The change in momentum can be described as the impulse I transferred to the body

$$I = \int_{t_0}^{t_1} F(t)dt \tag{2.8}$$

and can be seen as the area under the graph in a force-time diagram, see Figure 2.1. When studying impact loads the maximum force is often not the most relevant parameter, instead the impulse is of major importance since it relates the acting force with the duration of the impact, see Figure 2.1.
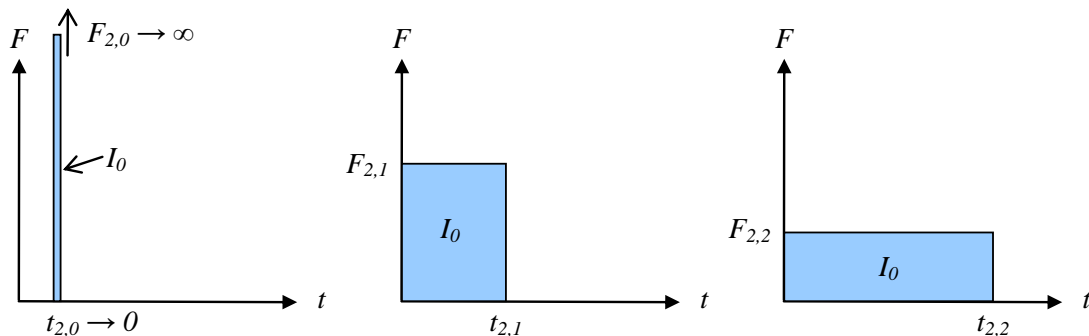
Figure 2.1   *The impulse I_0 is equal to the area under the graph in the force-time diagram. Here the impulse is of equal size in all three cases.*

2.1.4 Work and kinetic energy

A force that is acting on a body is said to do work when the action results in a displacement of the body. The work W_x done is only dependent on the force F_x that is acting in the direction of the displacement u

$$W_x = F_x \cdot u = F \cdot \cos(\varphi) \cdot u \tag{2.9}$$

where φ is the angle between the acting force and the direction of the displacement, see Figure 2.2a.

The work done by a variable force can more generally be written as

$$W_x = \int_0^u F_x(x)dx \qquad (2.10)$$

a)   *b)*
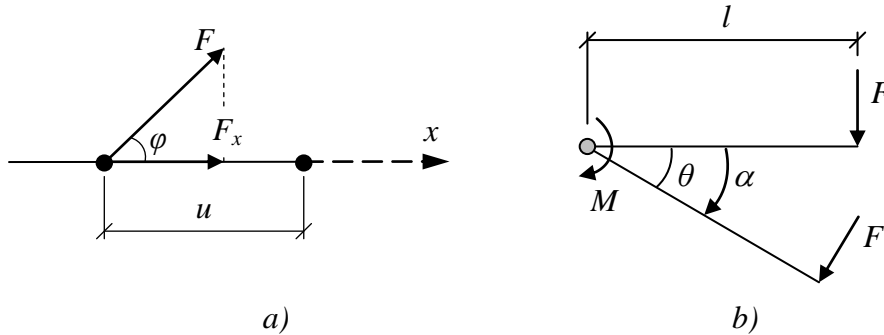
Figure 2.2   *a) A force doing work on a body, b) a moment doing work on a body.*

A moment M acting on a body can analogously do work W_α when a rotation θ is generated

$$W_\alpha = M \cdot \theta \qquad (2.11)$$

where the moment, see Figure 2.2b, is defined as

$$M = F \cdot l \qquad (2.12)$$

More generally when the moment varies with the angle α, the work can be defined as

$$W_\alpha = \int_0^\theta M(\alpha)d\alpha \qquad (2.13)$$

The kinetic energy E_k of a body with mass m and velocity v is defined as

$$E_k = \frac{m \cdot v^2}{2} \qquad (2.14)$$

Both work and kinetic energy is quantities of energy and both of them needs to be considered in a collision analysis to determine the total response of the objects.

2.1.5 Equation of motion

The equation of motion describes the behaviour of an object in terms of its motion in time and is based on equilibrium of forces and Newton's second law. The equation of motion is used when studying a spring-mass system. The forces acting on a body is divided into one external force $F(t)$ and two internal forces, R_{sta} and R_{dyn}, as shown in Figure 2.3. The internal forces are reactions due to boundary conditions, one static and one dynamic, which are dependent on the displacement and velocity respectively, this gives

$$F(t) - (R_{sta} + R_{dyn}) = m \cdot a \qquad (2.15)$$

The inner restraints can for a linearly elastic response be stated as

$$R_{sta} = k \cdot u \qquad (2.16)$$

and

$$R_{dyn} = c \cdot \dot{u} \qquad (2.17)$$

where k represents the stiffness or spring constant and c the damping coefficient. If these two expressions are combined with the equilibrium stated above, we get the final expression for the equation of motion

$$m \cdot \ddot{u} + c \cdot \dot{u} + k \cdot u = F(t) \qquad (2.18)$$
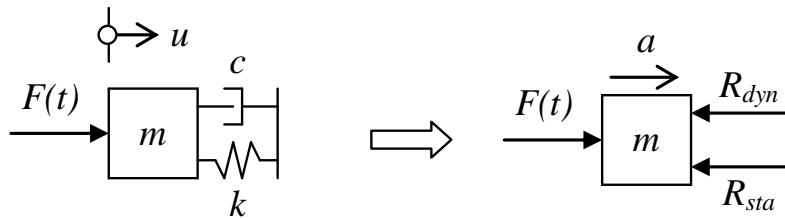
Figure 2.3   Illustration of forces acting on an accelerating body, and how this can be modelled as a spring-mass system with damping.

2.2 Structural internal resistance

2.2.1 Structural response

The response of a structure can be divided into infinitely many cases, but the following three are the most common and generalized cases; elastic, plastic and elasto-plastic response, see Figure 2.4. According to equation (2.10) the internal work W_i can be seen as the area under graphs in this figure.
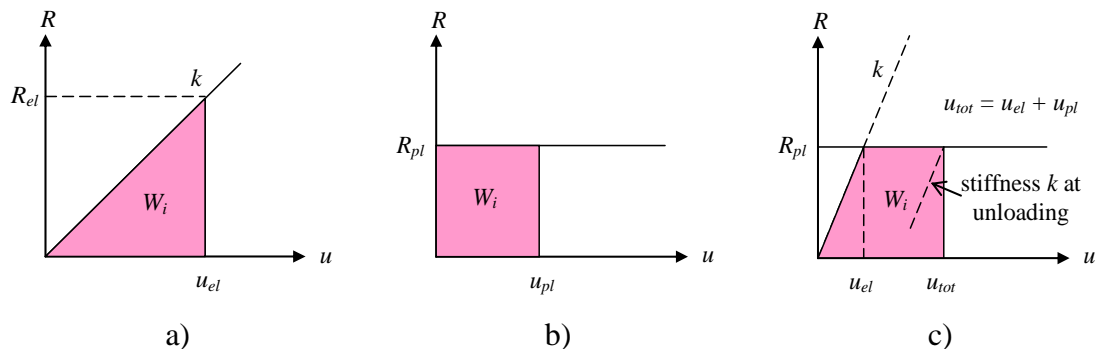
Figure 2.4   Load-displacement curves for different structural responses, a) elastic, b) plastic and c) elasto-plastic.

These responses are based on a simplification of the real behaviour of different structures and materials which gives a good and useful approximation. For the linear elastic response, the stiffness, k, is assumed to be constant and the elastic load capacity R_{el} to be infinitely large. However, a specific point of failure, or maximum load capacity, could also be specified. The deformation u_{el} is fully elastic and will return to zero after unloading. For the plastic response, the stiffness is not a relevant parameter and the plastic load capacity R_{pl} is the only parameter influencing the response. The deformation u_{pl} is fully plastic and will be permanent even after unloading. The final response, elasto-plastic response, is a combination of the former two; it has an elastic behaviour up to its load capacity and a plastic behaviour afterwards. The total displacement u_{tot} consists of both an elastic u_{el} and a plastic u_{pl} part. The elasto-plastic response is the one closest to reality for most structures and is therefore recommended for analyses. But, for simplicity, if the plastic deformation capacity of a structure is small, it can be wise to use the elastic model and if the stiffness of the structure is high, the plastic response can be used instead.

The stress-strain curves in Figure 2.5 are illustrations of the real material behaviour of concrete and steel. The response for concrete, Figure 2.5a, is often simplified to an elastic behaviour with a maximum capacity of f_{cc} in compression. For a reinforced concrete beam the strength of concrete in tension is, due to cracking, often neglected in analysis. Instead the reinforcement determines the governing strength capacity in tension. In the curve describing the reinforcement, Figure 2.5b, both an elastic and a plastic part can be distinguished. The elastic part shows substantially a linear elastic behaviour but the plastic part exhibits some strain hardening. This can be disregarded and the curve can conservatively be estimated with a simplified elasto-plastic behaviour, similar to the structural response seen in Figure 2.4c.
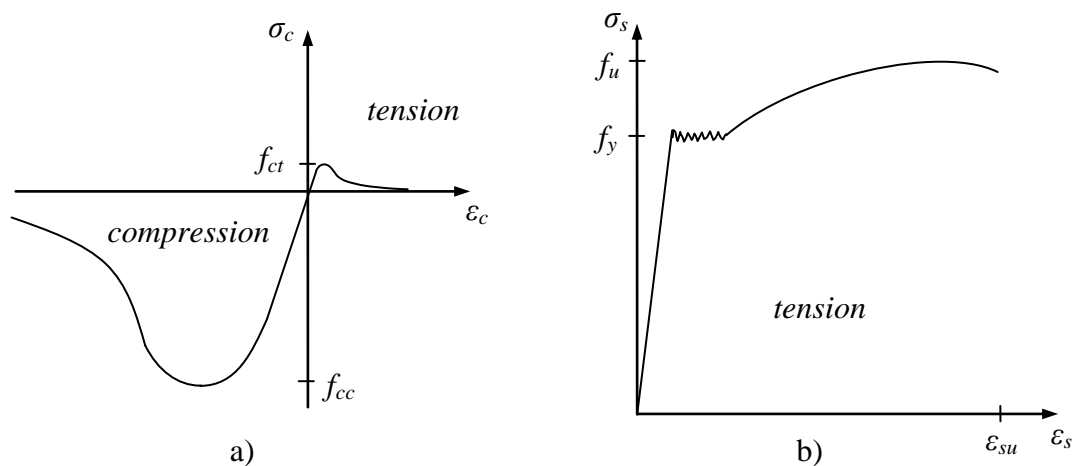
Figure 2.5   Stress-strain relationship for a) concrete and b) reinforcement in tension.

The impulse created during a collision impact can be of various different shapes depending on the structural properties of the colliding bodies, such as mass, stiffness and loading capacity. For a simplified case where a body crashes into a non-deformable barrier, three different types of impulses are illustrated in Figure 2.6, where the force F acting on the barrier is plotted against time t, Johansson and Laine (2012). However in reality both bodies will become deformed during the impact and the resulting impulse will get a more complex form, this is discussed further in Chapter 3.
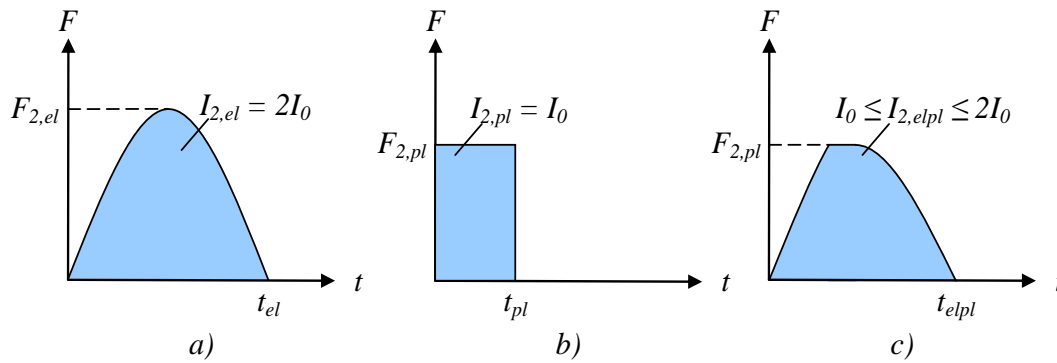
Figure 2.6   *Different shape of impulse for three different responses in a body during a collision into a rigid barrier; a) elastic response, b) plastic response and c) elasto-plastic response.*

In Figure 2.6 the different size of the impulse of reaction force I_2 is visualized for the three responses. $F_{2,el}$ and $F_{2,pl}$ are the maximum resulting load acting on the barrier in the elastic respectively in the plastic case. As seen here, the impulse is twice as large for the elastic response $I_{2,el}$, compared to the impulse for the plastic response $I_{2,pl}$. The reason for this behaviour is that the momentum of the body, during the impact, will change from p_0 to zero for the plastic case, while it will change from p_0 to $-p_0$ for the elastic case. This can be thought of as two impulses, if the total impulse in Figure 2.6a is divided at the time of maximum force, into two equally big parts. Then the first impulse is acting when the body has a positive velocity, and the second impulse is acting during the bounce back period, when the velocity is negative. For the elasto-plastic response, the impulse will be somewhere between the impulses of the other two responses.

The ability of a structure to absorb energy is vital for its performance under impulse loading. An external work is done from the impact load F and can be set equal to the kinetic energy of a projectile. An internal work, based on the internal resistance R and deformation capacity, is then created to balance up the external work, see Figure 2.7. The external and internal work, W_e and W_i, can be seen as the integrals of the force-deformation curve. The barrier is here seen as a body which can be deformed.
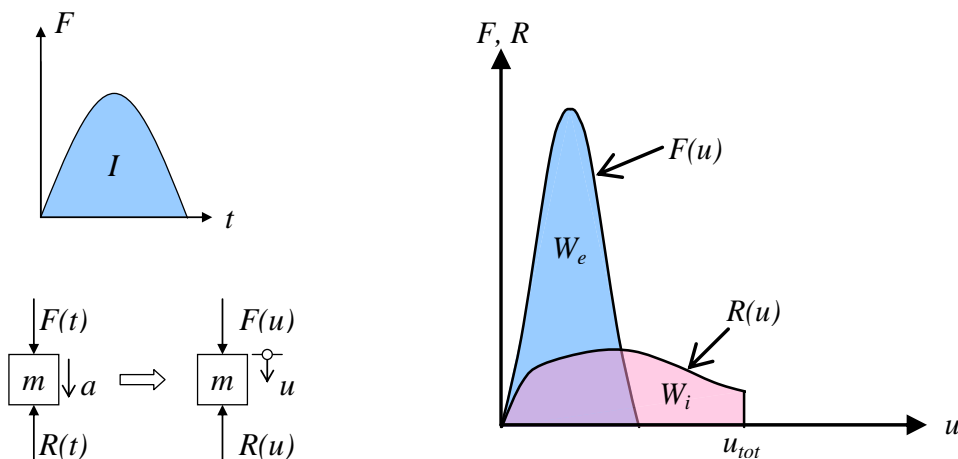
Figure 2.7   *Illustration of how internal work is created from an impulse load to balance the external work.*

Here F is the force from the incoming object acting on the barrier, and R is the reaction force acting in the barrier. The incoming object is here assumed to have an elastic response and the barrier is assumed to have a nonlinear plastic response.

This internal work can be achieved in different ways depending on the structural properties. A structure with high stiffness will get small deformations but large reaction forces, while a low stiffness will give large deformations but small reaction forces. In opposite to what is preferable for a structure subjected to static loading, it is therefore often better for a structure to have a low stiffness and large deformation capacity when subjected to impulse loading. The latter case will in general give higher energy absorption capacity by using the material in a more efficient way, see Figure 2.8.
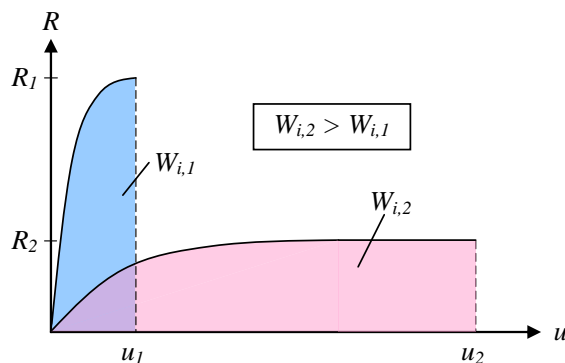
Figure 2.8   *Internal work done in two different materials, one with high strength and low deformation capacity and one with low strength and high deformation capacity.*

2.2.2 Plastic rotation capacity

When a plastic or elasto-plastic response is used for a beam it means that the concept of moment redistribution is utilized and that the maximum deflection is the governing factor for the design of the beam. This deflection can be translated, using trigonometry, into a maximum rotation, or plastic rotation θ_s, at the points where the plastic hinges are formed, see Figure 2.9. The method for determining the plastic rotation capacity described in this section is based on Eurocode 2 (CEN, 2004) and is only valid for the ultimate limit state (ULS). In design, the plastic rotation should not exceed the rotation capacity, $\theta_s \leq \theta_{pl}$.
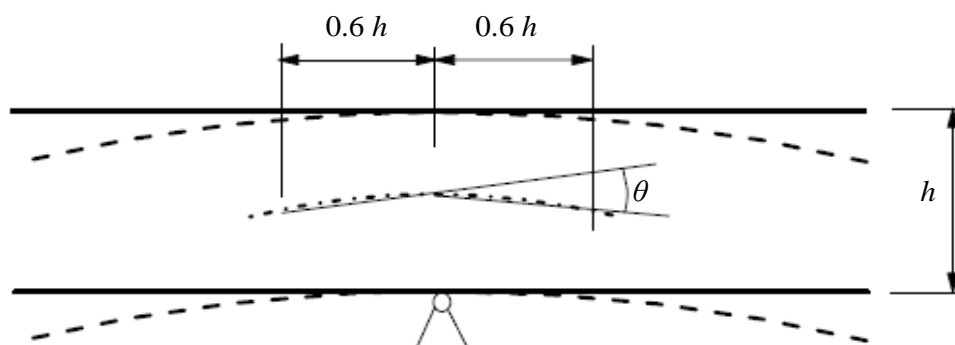
Figure 2.9   *Plastic rotation θ_s of a reinforced concrete section in a continuous beam, CEN (2004).*

The plastic analysis in Eurocode can be used, without further check of rotation capacity, if the following three conditions are fulfilled, CEN (2004)

    I.   the area of the tensile reinforcement is limited as
        a. $x_u / d < 0.25$ for concrete strength class $\leq C50/60$
        b. $x_u / d < 0.15$ if concrete class $\geq C55/67$
   II.   reinforcement used is of either class *B* or *C*, see Table 2.1
  III. the ratio between intermediate support moment M_s and field moment M_f should fulfil $0.5 \leq M_s / M_f \leq 2.0$

where x_u is the depth of the compression zone in the ultimate limit state, ULS, and d is the effective depth of the cross-section.

These conditions for use of the plastic design are presumably based on a static loading point of view and are therefore not valid for an impulse load. For this kind of load the plastic rotations can be considerably larger, and more detailed checks of the rotation capacity are therefore needed in collision analysis; this is further described below.

Table 2.1   *Definition of reinforcing steel classes according to Eurocode 2 CEN (2004).*

Class	f_{yk} [MPa]	f_{tk} / f_{yk} [-]	ε_{uk} [%]
A	400 - 600	≥ 1.05	≥ 2.5
B	400 - 600	≥ 1.08	≥ 5.0
C	400 - 600	$\geq 1.15 \ \& < 1.35$	≥ 7.5

The reinforcement classes specified in Eurocode 2 are of the new European standard which replaced the old Swedish system about 20 years ago. When analysing older structures it can therefore be difficult to translate the old types of reinforcement to today's standards. The old types were in general more ductile and some of them even more ductile than today's class *C*, meaning they allowed a greater plastic rotation, Johansson and Laine (2012). This is important to keep in mind when dealing with older structures.

The plastic rotation capacity θ_{pl} for a beam with specified reinforcement and concrete class is given as a diagram in Figure 2.10. Here is only reinforcement class *B* and *C* represented, since class A is not recommended to be used in plastic analysis. The diagram is clearly visualising how the reinforcement will fail first if the amount of reinforcement is small and how the concrete will fail first if the beam is well reinforced. For an optimal plastic behaviour it is necessary to have a reinforcement amount near the boundary between these two failure mechanisms.
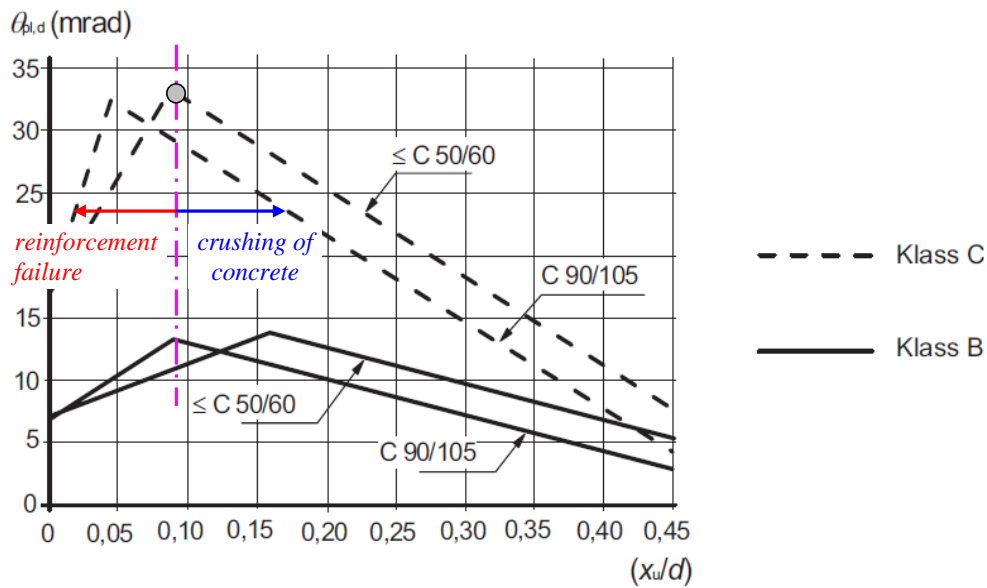
Figure 2.10 Plastic rotation capacity θ_{pl} for different reinforcement and concrete classes. Limit between reinforcement and concrete failure for one type of concrete with class C reinforcement is visualised. The values apply only for a shear slenderness λ of 3, CEN (2004).

For the plastic hinges to be formed in the considered regions, the following conditions regarding the area of the tensile reinforcement needs to be met

   I. $x_u / d < 0.45$ for concrete strength class $\leq C50/60$
  II. $x_u / d < 0.35$ if concrete class $\geq C55/67$

The values for the plastic rotation capacity given in Figure 2.10 needs to be multiplied with a correction factor k_λ for beam cross sections with a shear slenderness, λ, other than 3

$$\theta_{pl,d} = k_\lambda \cdot \theta_{pl} \tag{2.19}$$

and

$$k_\lambda = \sqrt{\frac{\lambda}{3}} \tag{2.20}$$

The shear slenderness is defined as

$$\lambda = \frac{l_0}{d} \tag{2.21}$$

where l_0 is the distance between the zero moment section and maximum moment section after redistribution and d is the effective depth. The shear slenderness can in a simplified way be calculated as

$$\lambda = \frac{M_{sd}}{V_{sd} \cdot d} \tag{2.22}$$

where M_{sd} and V_{sd} are the design bending moment and the corresponding design shear force.

Eurocode 2 is the only standard treated in this section but not the only design code which gives recommendations for how to calculate the plastic rotation capacity. Bk 25:2 (Fortifikationsförvaltningen, 1973) and Betonghandboken (Cederwall, et al., 1990) are two other handbooks, though a little bit older, that treats the same subject. In Johansson and Laine (2012) a comparison is made between the methods presented in these three standards. The result shows that Eurocode produces reasonable values for the rotation capacity that lies somewhere in between the values from the other two methods.

2.3 Dynamic models

2.3.1 Classic impact theory

A simple way to study a one-dimensional collision between two bodies is to use the classic impact theory. It is based on the assumptions that the first body has an initial velocity of v_0 and a mass of m_1 and the second body has no initial velocity and mass m_2. After the impact the velocities are assumed to be v_1 and v_2 respectively as shown in Figure 2.11.
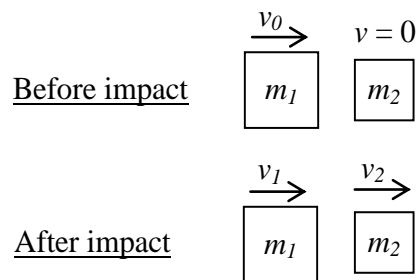
Figure 2.11   *Illustration of a body with a certain velocity colliding with another body without any velocity. After the collision both bodies will have a new velocity.*

The kinetic energy and momentum before the impact are

$$E_{k,0} = \frac{m_1 \cdot v_0{}^2}{2} \tag{2.23}$$

$$p_0 = m_1 \cdot v_0 \tag{2.24}$$

The classic impact theory can describe both an elastic and a plastic collision by changing the coefficient of restitution (COR) e, between 0 (plastic impact) and 1 (elastic impact). If the COR is $0 < e < 1$ it means that the impact is somewhere in between elastic and plastic, the COR is defined by

$$e = \frac{v_2 - v_1}{v_0} \tag{2.25}$$

The final velocities of the two bodies after the impact are consequently

$$v_1 = \frac{m_1 - e \cdot m_2}{m_1 + m_2} \cdot v_0 \tag{2.26}$$

$$v_2 = \frac{(1 + e) \cdot m_1}{m_1 + m_2} \cdot v_0 \tag{2.27}$$

For an elastic collision both the kinetic energy and momentum are preserved in the impact. This gives a COR of $e = 1$ and the final velocities become

$$v_{1,el} = \frac{m_1 - m_2}{m_1 + m_2} \cdot v_0 \tag{2.28}$$

$$v_{2,el} = \frac{2 \cdot m_1}{m_1 + m_2} \cdot v_0 \tag{2.29}$$

From these equations it can be noted that $v_{1,el}$ is negative if $m_1 < m_2$, meaning that body 1 will be moving in the opposite direction after the impact. Body 2 on the other hand will always be moving in the positive direction; i.e. the initial direction of movement of body 1. If $m_1 = m_2$ body 1 will be stationary after the impact and all energy will be transferred to body 2.

For a plastic collision only the momentum is preserved and $e = 0$. The kinetic energy is here reduced because of the transformation to potential energy during the duration of the plastic impact. The final velocity of the two bodies will be equal, thus they move together after the impact

$$v_{1,2,pl} = \frac{m_1}{m_1 + m_2} \cdot v_0 \tag{2.30}$$

From this equation it can be seen that $v_{1,2,pl}$ will be half the size of v_0 when $m_1 = m_2$ and that $v_{1,2,pl} \rightarrow 0$ when $m_1 << m_2$, meaning all kinetic energy will be transformed and absorbed in body 1.

It is also possible to describe an elasto-plastic behaviour for a case when $0 < e < 1$, which means that the response lies somewhere between the elastic and plastic case. The difficulty with this case is how to decide on what value of the COR to use.

The kinetic energy after the impact can be stated as a function of the initial kinetic energy. For an elastic collision

$$E_{k,1,el} = \frac{m_1 \cdot v_{1,el}{}^2}{2} = \frac{m_1}{2} \left(\frac{m_1 - m_2}{m_1 + m_2} \cdot v_0 \right)^2 = \left(\frac{m_1 - m_2}{m_1 + m_2} \right)^2 \cdot E_{k,0} \tag{2.31}$$

$$E_{k,2,el} = \frac{m_2 \cdot v_{2,el}{}^2}{2} = \frac{m_2}{2} \left(\frac{2 \cdot m_1}{m_1 + m_2} \cdot v_0 \right)^2 = \frac{4 \cdot m_1 \cdot m_2}{(m_1 + m_2)^2} \cdot E_{k,0} \tag{2.32}$$

and for a plastic collision the total kinetic energy is

$$E_{k,pl} = \frac{(m_1 + m_2) \cdot v_{1,2,pl}^{\,2}}{2} = \frac{m_1 + m_2}{2} \left(\frac{m_1}{m_1 + m_2} \cdot v_0 \right)^2 = \frac{m_1}{m_1 + m_2} \cdot E_{k,0} \qquad (2.33)$$

The amount of kinetic energy acting in the positive direction of the system, regardless the value of *e*, can be described as

$$E_{k,3} = \begin{cases} E_{k,2} & \text{for} \quad v_1 \le 0 \\ E_{k,1} + E_{k,2} & \quad v_1 > 0 \end{cases} \qquad (2.34)$$

With the help of this equation a ratio between the initial and final kinetic energy acting in the positive direction can be calculated, $E_{k,3} / E_{k,0}$, as a function of the ratio of the bodies masses m_1 / m_2. The relationship is here presented for different values of the COR in a graph, see Figure 2.12.
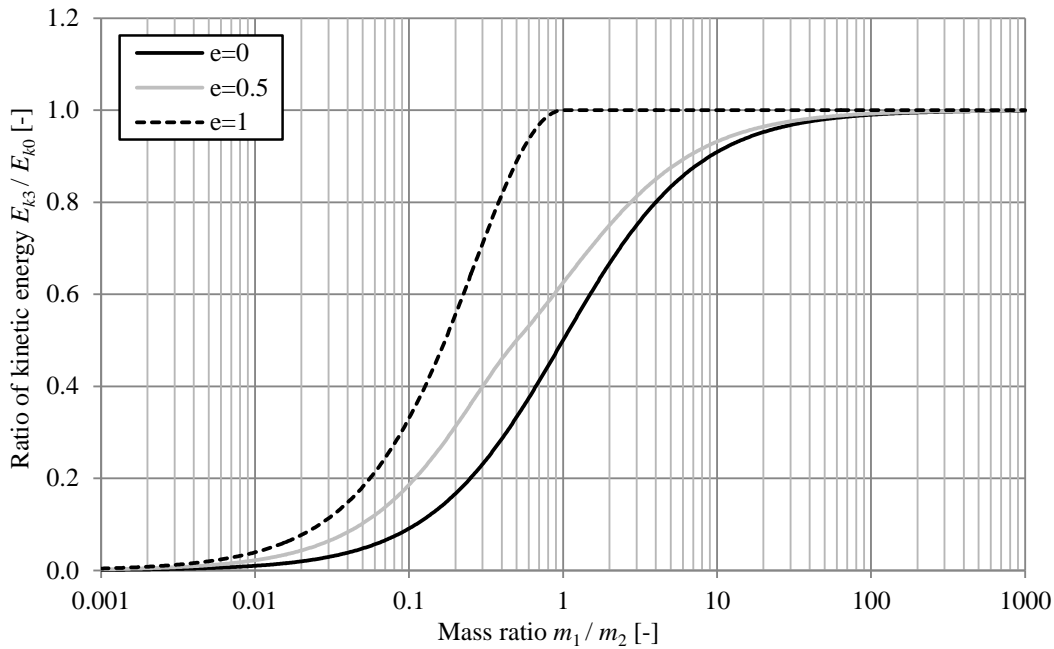
Figure 2.12 Ratio of kinetic energy, acting in the positive direction, as a function of the mass ratio, for different values of the coefficient of restitution, e.

If $m_1 < m_2$, which is usually true for the type of collision that will be studied in this report, the difference in response for an elastic and plastic collision can be expressed as a ratio of the final kinetic energies acting in the positive direction

$$\frac{E_{k,3,el}}{E_{k,3,pl}} = \frac{E_{k,2,el}}{E_{k,pl}} = \frac{4 \cdot m_2}{m_1 + m_2} = \frac{4}{\dfrac{m_1}{m_2} + 1} \qquad (2.35)$$

From this ratio it is clear that the kinetic energy for the elastic case is larger, which makes sense since, as stated before, all kinetic energy is preserved. When $m_1 / m_2 \to 0$ the kinetic energy is four times larger for the elastic case and when $m_1 / m_2 \to 1$ it is two times larger.

This relation can also be seen in Figure 2.12, and it is clear that the difference is not evened out until $m_1 / m_2 > 100$. From this, one can understand the importance of choosing a correct value for the COR.

2.3.2 Single degree of freedom

Perhaps the simplest dynamical model is a spring-mass oscillator shown in Figure 2.13.
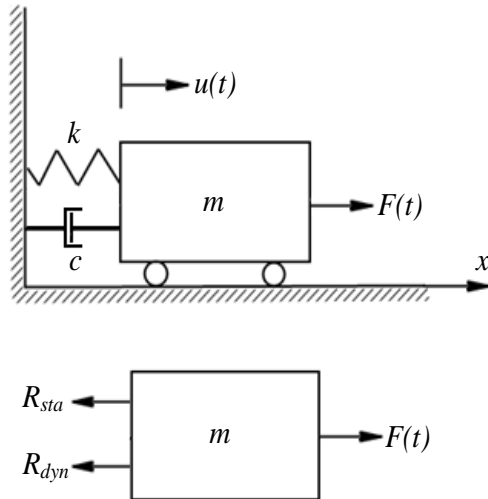
Figure 2.13   Single degree of freedom spring mass oscillator.

Since only one variable, *u,* is needed to describe the instantaneous position of the mass, this is called a single degree of freedom (SDOF) system. The equation of motion for this system can be written as

$$m\ddot{u} + c\dot{u} + ku = F(t) \tag{2.36}$$

The effect of the damping c is considered negligible for applications dealt with in this report due to the short time period of the load application and that only the maximum displacement u is of interest. If the system undergoes free vibration, meaning $F(t) = 0$, the homogeneous second-order differential equation becomes

$$m\ddot{u} + ku = 0 \tag{2.37}$$

The general solution of equation (2.37) is

$$u(t) = A_1 \cos \omega_n t + A_2 \sin \omega_n t \tag{2.38}$$

where A_1 and A_2 are constants that are chosen so that the initial conditions will be satisfied. In this case, the initial conditions for displacement and velocity are

$$u(0) = u_0 \tag{2.39}$$

$$v(0) = \dot{u}_0 = v_0 \tag{2.40}$$

Also ω_n is the undamped natural circular frequency, defined by

$$\omega_n = \sqrt{\frac{k}{m}} \qquad \left[\text{rad}\middle/\text{s}\right] \tag{2.41}$$

So by applying the initial conditions to equation (2.38), the time-dependent displacement for free vibration of an undamped mass-spring oscillator is

$$u(t) = u_0 \cos \omega_n t + \frac{v_0}{\omega_n} \sin \omega_n t \tag{2.42}$$

Equation (2.42) only applies for free vibration, and equation (2.43) is a more general solution that is used to determine the complementary solution when the external force $F(t) \neq 0$

$$u(t) = A_1 \cos \omega_n t + A_2 \sin \omega_n t + \frac{F(t)}{k} \tag{2.43}$$

A very important special case is the response of an undamped SDOF system to a short duration impulse. If we consider a force with a duration, t_d, much smaller than the period time, T, of the SDOF system, that is $t_d << T_n$, the impulse is defined as

$$I = \int_0^{t_d} F(t)dt \tag{2.44}$$

If the system is at rest for $t \leq 0$, the equation of motion and initial conditions are

$$m\ddot{u} + ku = \begin{cases} F(t) & 0 < t < t_d \\ 0 & 0 \end{cases} \tag{2.45}$$

$$u(0) = \dot{u}(0) = 0$$

By integrating equation (2.45) with respect to time and applying the initial conditions we get

$$m\dot{u}(t_d) + ku_{avg}t_d = I \tag{2.46}$$

where u_{avg} is the average displacement in the time interval $0 < t < t_d$. By letting $t_d \rightarrow 0$, mening that impulse corresponds to the characteristic impulse, the second term in equation (2.46) can be ignored, which gives

$$m\dot{u}(0^+) = I \tag{2.47}$$

Thus the impulse gives the mass an initial velocity of

$$\dot{u}(0^+) = \frac{I}{m} \tag{2.48}$$

but leaves the initial displacement to

$$u(0^+) = 0 \qquad\qquad\qquad (2.49)$$

These expressions can be used as "initial" conditions for the free vibration problem. By using these conditions in equation (2.42) we get the impulse response

$$u(t) = \frac{I}{\omega_n m} \sin \omega_n t \qquad\qquad\qquad (2.50)$$

The unit impulse response function is obtained by letting $I = 1$, and is by convention often called $h(t)$

$$h(t) = \frac{1}{\omega_n m} \sin \omega_n t \qquad\qquad\qquad (2.51)$$

2.3.2.1 SDOF loaded with characteristic impulse I_c

In Figure 2.14 a characteristic impulse for an ideal impulse load, a time dependent load with infinitely high pressure acting during an infinitely short time, is shown.
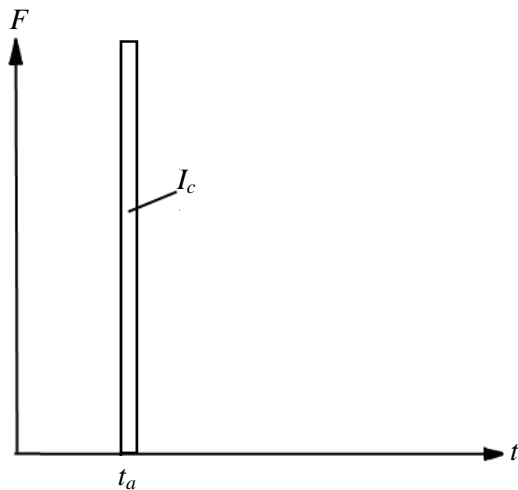
Figure 2.14   Illustration of the characteristic impulse I_c.

The action of an impulse, I_c, acting on a body with mass m can be expressed as

$$I_c = m \cdot v \qquad\qquad\qquad (2.52)$$

The kinetic energy, E_k, for the same body with velocity v is

$$E_k = \frac{m \cdot v^2}{2} \qquad\qquad\qquad (2.53)$$

which means that by combining equations (2.52) and (2.53) the kinetic energy generated by an impulse acting on a body with mass m can be expressed as

$$E_k = \frac{I^2}{2m} \tag{2.54}$$

The kinetic energy, E_k, transferred into an impulse loaded structure can be seen as exterior work, W_e. This needs to be in equilibrium with the interior work, W_i, of the body in order to counteract the initiated movement coming from the impulse. This means an energy balance is obtained

$$W_e = W_i \tag{2.55}$$

which is the basis used in the calculation model for an impulse loaded structure. The interior work can act in different ways depending on its type of response. Here an elastic, a plastic and an elasto-plastic structural response will be further examined.

2.3.2.2 Elastic system

For an elastic system, see Figure 2.15, the interior reaction force, $R(u)$, is expressed as

$$R(u) = k \cdot u \tag{2.56}$$

where k is a constant stiffness and u is the displacement. Based on this the interior work can be calculated as

$$W_i = \frac{R(u_{el}) \cdot u_{el}}{2} = \frac{k u_{el}^2}{2} \tag{2.57}$$

where u_{el} is the elastic displacement needed to absorb the external work according to Figure 2.15c. By combining equations (2.54) and (2.57) the needed elastic deformation can be expressed as

$$u_{el} = \frac{I_c}{m \omega_n} \tag{2.58}$$

a) b) c)
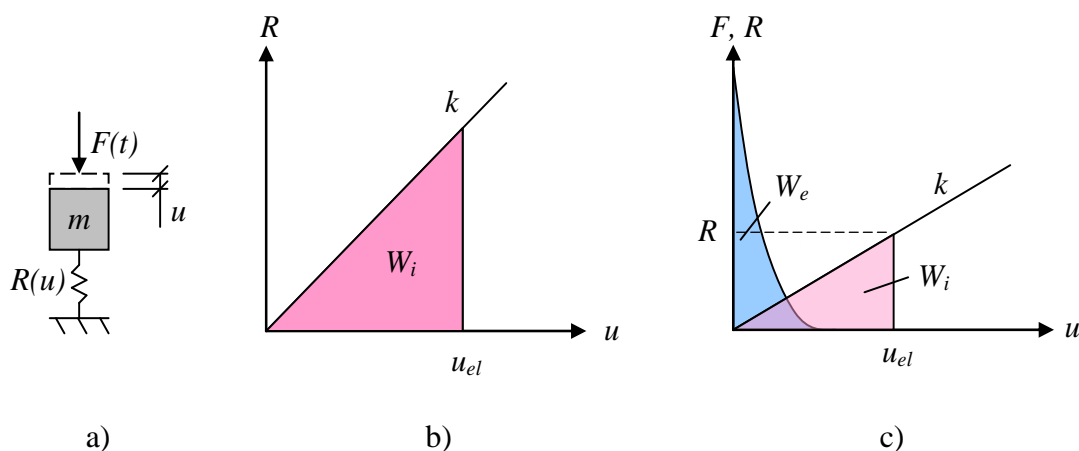
Figure 2.15   System with linear elastic response: (a) SDOF-system, (b) load-deflection relationship, (c) energy equilibrium between external and internal work.

2.3.2.3 Plastic system

When considering a plastic system, see Figure 2.16, the internal reaction force is set to a constant capacity, R. The internal work can then be expressed as

$$W_i = R(u_{pl}) \cdot u_{pl} = Ru_{pl} \tag{2.59}$$

where u_{pl} is the plastic displacement needed to absorb the external work according to Figure 2.16c. By combining equations (2.54) and (2.59) the needed elastic deformation can be expressed as

$$u_{pl} = \frac{I_c^{\,2}}{2mR} \tag{2.60}$$

a)   b)   c)
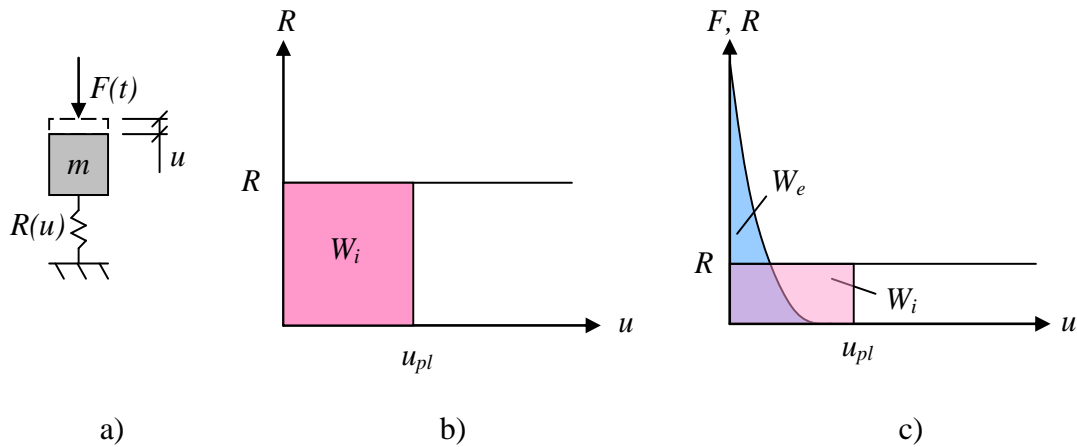
Figure 2.16   System with plastic response: (a) SDOF-system, (b) load-deflection relationship, (c) energy equilibrium between external and internal work.

2.3.2.4 Elasto-plastic system

For an elasto-plastic system, see Figure 2.17, the internal reaction force $R(u)$ is expressed as

$$R(u) = \begin{cases} ku, & u \le u_{el,1} \\ R, & u > u_{el,1} \end{cases} \tag{2.61}$$

where $u_{el,1}$ is the limit for elastic response, which is

$$u_{el,1} = \frac{R}{k} \tag{2.62}$$

The internal work can on the basis of this be expressed as

$$W_i = \frac{R}{2}\left(u_{el,1} + 2u_{pl,1}\right) \tag{2.63}$$

and by combining equation (2.63) with equations (2.54) and (2.55) the required plastic deformation can be calculated as

$$u_{pl,1} = \frac{I_k^2}{2mR} - \frac{u_{el,1}}{2} = u_{pl} - \frac{u_{el,1}}{2} \tag{2.64}$$

where u_{pl} is the plastic response for a pure plastic system. The total deformation can then be calculated to

$$u_{tot} = u_{el,1} + u_{pl,1} = u_{pl} + \frac{u_{el,1}}{2} \tag{2.65}$$
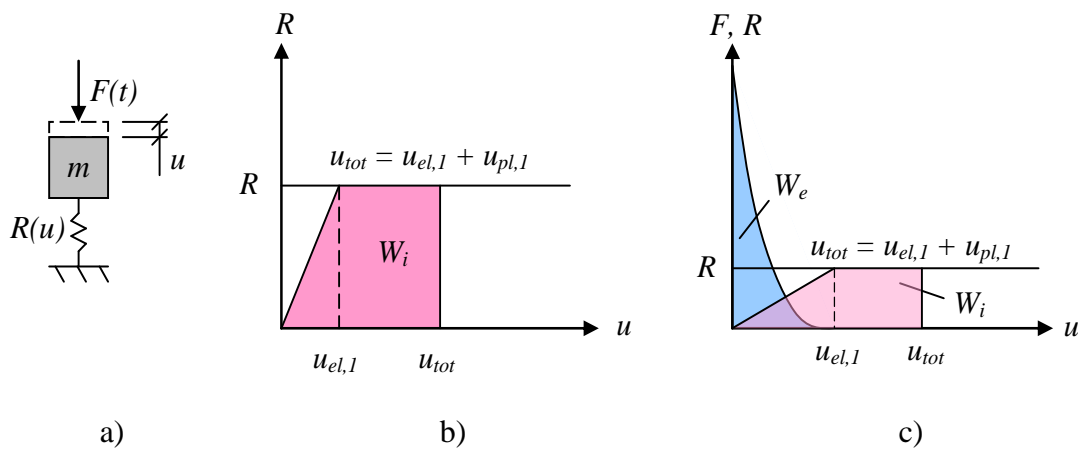
Figure 2.17   *System with elastic-plastic response: (a) SDOF-system, (b) load-deflection relationship, (c) energy equilibrium between external and internal work.*

2.3.3 Multi-degree of freedom
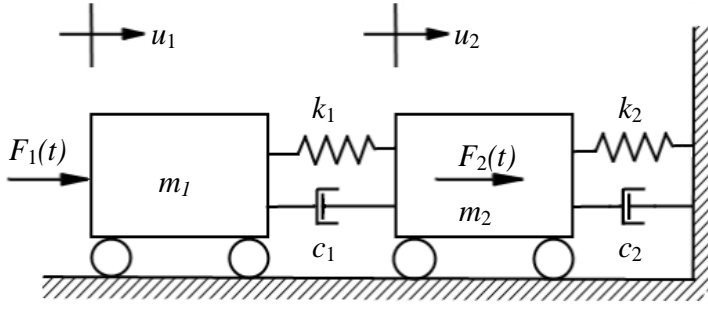
*Figure 2.18   Two-degree of freedom system (2DOF) consisting of two masses,
springs and dampers respectively.*

In Figure 2.18 we see a two-degree of freedom system (2DOF) consisting of two masses. In order to derive the equation of motion for this system Newton's Second Law is applied. Firstly free-body diagrams are drawn for each of the masses with the unknown internal forces labelled, see Figure 2.19.
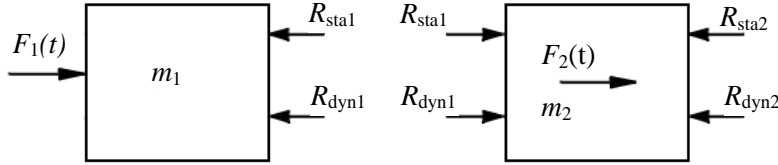
*Figure 2.19   Free-body diagrams showing all forces, both internal and external,
acting on the two masses.*

Force equilibrium for the two masses gives

$$\rightarrow: \sum F_1 = m_1 \cdot \ddot{u}_1 = F_1(t) - R_{sta1} - R_{dyn1} \tag{2.66}$$

$$\rightarrow: \sum F_2 = m_2 \cdot \ddot{u}_2 = F_2(t) + R_{sta1} + R_{dyn1} - R_{sta2} - R_{dyn2} \tag{2.67}$$

The spring forces, R_{sta1} and R_{sta2}, are related to the displacements and the viscous damping forces, R_{dyn1} and R_{dyn2}, are related to the velocities

$$R_{sta1} = k_1(u_1 - u_2) \tag{2.68}$$

$$R_{dyn1} = c_1(\dot{u}_1 - \dot{u}_2) \tag{2.69}$$

$$R_{sta2} = k_2 u_2 \tag{2.70}$$

$$R_{dyn2} = c_2 \dot{u}_2 \tag{2.71}$$

By combining and simplifying the above expressions the following is obtained

$$m_1\ddot{u}_1 - c_1(\dot{u}_1 - \dot{u}_2) - k_1(u_1 - u_2) = F_1(t) \tag{2.72}$$

$$m_2\ddot{u}_2 - c_1\dot{u}_1 + \dot{u}_2(c_1 + c_2) - k_1 u_1 + u_2(k_1 + k_2) = F_2(t) \tag{2.73}$$

Equations (2.72) and (2.73) can be written on matrix form

$$\begin{bmatrix} m_1 & 0 \\ 0 & m_2 \end{bmatrix}\begin{bmatrix} \ddot{u}_1 \\ \ddot{u}_2 \end{bmatrix} + \begin{bmatrix} c_1 & -c_1 \\ -c_1 & c_1+c_2 \end{bmatrix}\begin{bmatrix} \dot{u}_1 \\ \dot{u}_2 \end{bmatrix} + \begin{bmatrix} k_1 & -k_1 \\ -k_1 & k_1+k_2 \end{bmatrix}\begin{bmatrix} u_1 \\ u_2 \end{bmatrix} = \begin{bmatrix} F_1(t) \\ F_2(t) \end{bmatrix} \tag{2.74}$$

or with symbolic matrix notation

$$\mathbf{M\ddot{u}} + \mathbf{C\dot{u}} + \mathbf{Ku} = \mathbf{F}(t) \tag{2.75}$$

where $\mathbf{M}$ is the mass matrix, $\mathbf{C}$ is the viscous damping matrix, $\mathbf{K}$ is the stiffness matrix, $\mathbf{u}$ is the displacement vector and $\mathbf{F}(t)$ is the load vector, Craig Jr. and Kurdila (2006). When comparing equation (2.75) to the equation of motion for a SDOF system (2.18), it can be seen that they have the same arrangement.

In order to calculate the natural frequencies and mode shapes of the system the damping is set to zero. To keep it more general the equation of motion is from now on written on a more general form

$$\begin{bmatrix} m_{11} & m_{12} \\ m_{21} & m_{22} \end{bmatrix}\begin{bmatrix} \ddot{u}_1 \\ \ddot{u}_2 \end{bmatrix} + \begin{bmatrix} k_{11} & k_{12} \\ k_{21} & k_{22} \end{bmatrix}\begin{bmatrix} u_1 \\ u_2 \end{bmatrix} = \begin{bmatrix} F_1(t) \\ F_2(t) \end{bmatrix} \tag{2.76}$$

where $k_{11} = k_1$, $k_{12} = k_{21} = -k_1$ and $k_{22} = k_1 - k_2$. In the same way as for a SDOF-system the solution will consist of one complementary solution, obtained by setting the force vector to zero, plus a particular solution.

$$u(t) = u_p(t) + u_c(t) \tag{2.77}$$

The complementary solution determines the natural frequencies and natural modes of the system which is very important for further analyses. The equation of motion now has the form

$$\begin{bmatrix} m_{11} & m_{12} \\ m_{21} & m_{22} \end{bmatrix}\begin{bmatrix} \ddot{u}_1 \\ \ddot{u}_2 \end{bmatrix} + \begin{bmatrix} k_{11} & k_{12} \\ k_{21} & k_{22} \end{bmatrix}\begin{bmatrix} u_1 \\ u_2 \end{bmatrix} = \begin{bmatrix} 0 \\ 0 \end{bmatrix} \tag{2.78}$$

The system is assumed to undergo harmonic motion of the form

$$u_1(t) = U_1 \cos(\omega t - \alpha)$$
$$u_2(t) = U_2 \cos(\omega t - \alpha) \tag{2.79}$$

where U_1 and U_2 are signed constants that are used in order to determine the amplitudes of the two sinusoidal motions. This is then substituted into equation (2.78) in order to obtain the algebraic eigenvalue problem

$$\left(\begin{bmatrix} k_{11} & k_{12} \\ k_{21} & k_{22} \end{bmatrix} - \omega^2 \begin{bmatrix} m_{11} & m_{12} \\ m_{21} & m_{22} \end{bmatrix} \right)\begin{bmatrix} U_1 \\ U_2 \end{bmatrix} = \begin{bmatrix} 0 \\ 0 \end{bmatrix} \tag{2.80}$$

The only non-trivial solution to this set of homogeneous linear algebraic equations correspond to values of ω^2 that satisfy the characteristic equation

$$\begin{bmatrix} k_{11} & k_{12} \\ k_{21} & k_{22} \end{bmatrix} - \omega^2 \begin{bmatrix} m_{11} & m_{12} \\ m_{21} & m_{22} \end{bmatrix} = \begin{bmatrix} 0 \\ 0 \end{bmatrix} \tag{2.81}$$

Equation (2.81) is solved for the two roots labelled ω_1^2 and ω_2^2, these are the eigenvalues and $\omega_1 \leq \omega_2$. The parameters ω_1 and ω_2 are the circular natural frequencies of the system expressed in rad/s. In order to calculate the natural modes, or the eigenvectors, ω_1^2 is substituted back into the first row of equation (2.80) in order to obtain the mode shape ratio

$$\beta_1 = \left(\frac{U_2}{U_1} \right)_{(1)} \tag{2.82}$$

In the same way ω_2^2 is substituted into the second row to obtain

$$\beta_2 = \left(\frac{U_2}{U_1} \right)_{(2)} \tag{2.83}$$

The mode shapes is characterized by the following notation

$$\Phi = \begin{bmatrix} \phi_1 \\ \phi_2 \end{bmatrix} = A_r \begin{bmatrix} 1 \\ \beta_r \end{bmatrix} \qquad r = 1,2 \tag{2.84}$$

where A_r is a constant. The general solution of equation (2.76) is then with natural frequencies and mode shape ratios inserted

$$\begin{aligned} u_1(t) &= A_1 \cos(\omega_1 t - \alpha_1) + A_2 \cos(\omega_2 t - \alpha_2) \\ u_2(t) &= \beta_1 A_1 \cos(\omega_1 t - \alpha_1) + \beta_2 A_2 \cos(\omega_2 t - \alpha_2) \end{aligned} \tag{2.85}$$

where the constants A_1, A_2, α_1 and α_2 are determined by initial conditions, Craig Jr. and Kurdila (2006). Usually the initial conditions are $u_1(0)$, $u_2(0)$, $\dot{u}_1(0)$ and $\dot{u}_2(0)$. In this solution the damping is neglected, since it has little effect on the maximum response during a short term impact. An alternate way to write the general solution is

$$\begin{aligned} u_1(t) &= A_1 \cos(\omega_1 t) + B_1 \sin(\omega_1 t) + A_2 \cos(\omega_2 t) + B_2 \sin(\omega_2 t) \\ u_2(t) &= \beta_1 A_1 \cos(\omega_1 t) + \beta_1 B_1 \sin(\omega_1 t) + \beta_2 A_2 \cos(\omega_2 t) + \beta_2 B_2 \sin(\omega_2 t) \end{aligned} \tag{2.86}$$

Where the constants A_1, A_2, B_1 and B_2 are determined by initial conditions. It is also possible to write equation (2.86) on vector form using the notation in equation (2.84), it then becomes

$$\mathbf{u}(t) = A_1 \Phi_1 \cos(\omega_1 t) + B_1 \Phi_1 \sin(\omega_1 t) + A_2 \Phi_2 \cos(\omega_2 t) + B_2 \Phi_2 \sin(\omega_2 t) \tag{2.87}$$

2.3.4 The Central Difference Method

The Central Difference Method is an explicit solution method for the numerical solution of second-order differential equations in structural dynamics applications. Recall the equation of motion, here written on matrix form

$$\mathbf{M} \cdot \ddot{\mathbf{u}} + \mathbf{C} \cdot \dot{\mathbf{u}} + \mathbf{K} \cdot \mathbf{u} = \mathbf{F}(t) \tag{2.88}$$

where $\mathbf{M}$ is the mass matrix, $\mathbf{C}$ is the damping matrix, $\mathbf{K}$ is the stiffness matrix, $\mathbf{F}(t)$ is exterior load vector and $\ddot{\mathbf{u}}$, $\dot{\mathbf{u}}$ and $\mathbf{u}$ is acceleration-, velocity- and displacement-vectors respectively. It is a conditionally stable method where each time-step, Δt, must be less than a critical time-step Δt_{crit}, otherwise there will be an error that grows to such proportions that the obtained solution quickly becomes worthless. The critical time step can be expressed as

$$\Delta t_{crit} = \frac{2}{\omega_{max}} = 2 \cdot \sqrt{\mathbf{M}\mathbf{K}^{-1}} \tag{2.89}$$

where ω_{max} is the highest eigenfrequency of the system. It should be noted that in particular for SDOF-systems, a substantially smaller time-step might still be necessary in order to obtain an accurate solution. Which time-step to use in different situations depends on a combination of the load configuration and the response time of the system, but usually a time-step in the magnitude of one hundredth of the duration of the load works well, Johansson and Laine (2012).

The basis of the Central Difference Method is the simple finite-difference expressions for velocity and acceleration

$$\dot{\mathbf{u}}_t = \frac{\mathbf{u}_{t+\Delta t} - \mathbf{u}_{t-\Delta t}}{2 \cdot \Delta t} \tag{2.90}$$

$$\ddot{\mathbf{u}}_t = \frac{\mathbf{u}_{t+\Delta t} - 2 \cdot \mathbf{u}_t + \mathbf{u}_{t-\Delta t}}{\Delta t^2} \tag{2.91}$$

When the finite-difference expressions for the first and second derivatives are substituted into the governing equation of motion evaluated at time t, the discrete governing equation results in

$$\left(\frac{\mathbf{M}}{\Delta t^2} + \frac{\mathbf{C}}{2 \cdot \Delta t} \right) \mathbf{u}_{t+\Delta t} + \left(\mathbf{K} - \frac{2 \cdot \mathbf{M}}{\Delta t^2} \right) \mathbf{u}_t + \left(\frac{\mathbf{M}}{\Delta t^2} + \frac{\mathbf{C}}{2 \cdot \Delta t} \right) \mathbf{u}_{t-\Delta t} = \mathbf{F}(t) \tag{2.92}$$

Ultimately the deflection at time $t+\Delta t$ can be written as

$$\mathbf{u}_{t+\Delta t} = \left(\Delta t^2 \mathbf{M}^{-1} + 2 \cdot \Delta t \mathbf{C}^{-1} \right) \left(\mathbf{F}(t) - \left(\mathbf{K} - \frac{2 \cdot \mathbf{M}}{\Delta t^2} \right) \mathbf{u}_t - \left(\frac{\mathbf{M}}{\Delta t^2} + \frac{\mathbf{C}}{2 \cdot \Delta t} \right) \mathbf{u}_{t-\Delta t} \right) \tag{2.93}$$

As seen all terms on the right hand side in equation (2.93) is from the time t or $t - \Delta t$, which means that the deflection $\mathbf{u}_{t+\Delta t}$ can be solved using already known information. Also a reasonable approximation, which is on the safe side for an impulse loaded structure, is to put the damping to zero, $\mathbf{C} = \mathbf{0}$. This is due to the fact that an impulse load is normally acting during a very short time, meaning that the effect of the

damping on the maximum deflection is negligible, Johansson and Laine (2012). This simplifies equation (2.93) to

$$\mathbf{u}_{t+\Delta t} = \left(\Delta t^2 \mathbf{M}^{-1}\right)\left(\mathbf{F}(t) - \left(\mathbf{K} - \frac{2 \cdot \mathbf{M}}{\Delta t^2}\right)\mathbf{u}_t - \left(\frac{\mathbf{M}}{\Delta t^2}\right)\mathbf{u}_{t-\Delta t}\right) \tag{2.94}$$

From equation (2.94) it can be seen that the Central Difference Method needs a special starting step since in the first step when calculating the displacement $\boldsymbol{u}_{\Delta t}$ information about the deflection at time $-\Delta t$ is needed. For this reason a special starting step is used, expressed as

$$\mathbf{u}_{-\Delta t} = \mathbf{u}_0 - \Delta t \cdot \dot{\mathbf{u}}_0 + \frac{\Delta t^2}{2} \cdot \ddot{\mathbf{u}}_0 \tag{2.95}$$

in order to start the numerical analysis.

The Central Difference Method is summarized as an algorithm in Appendix A.

There is several other related methods to solve this type of problem, for example the Newmark-β Method and the Wilson-θ Method. These methods are not discussed further in this thesis; instead readers are referred to Craig Jr. and Kurdila (2006).

Earlier in this section the stiffness, $\mathbf{K}$, is assumed to show a linear elastic behaviour. However, it is relatively easy to use the same expressions but with a non-linear material response. Since the stiffness, $\mathbf{K}$, is given for time t when calculating the displacement at time $t+\Delta t$, it is possible to use a secant stiffness in order to describe a non-linear response, see Figure 2.20. That is, by letting the stiffness at time t be a function of the present deflection, $u(t)$, meaning, $k_t = k_t(u_t)$, it is possible to compute the stiffness for an arbitrary material response. In equation (2.94) it is not really of interest to describe the stiffness per se, but the internal force, R_t, acting in the current time-step

$$R_t = k_t \cdot u_t \tag{2.96}$$

The secant stiffness is therefore expressed as

$$k_t = \frac{R_t}{u_t} \tag{2.97}$$
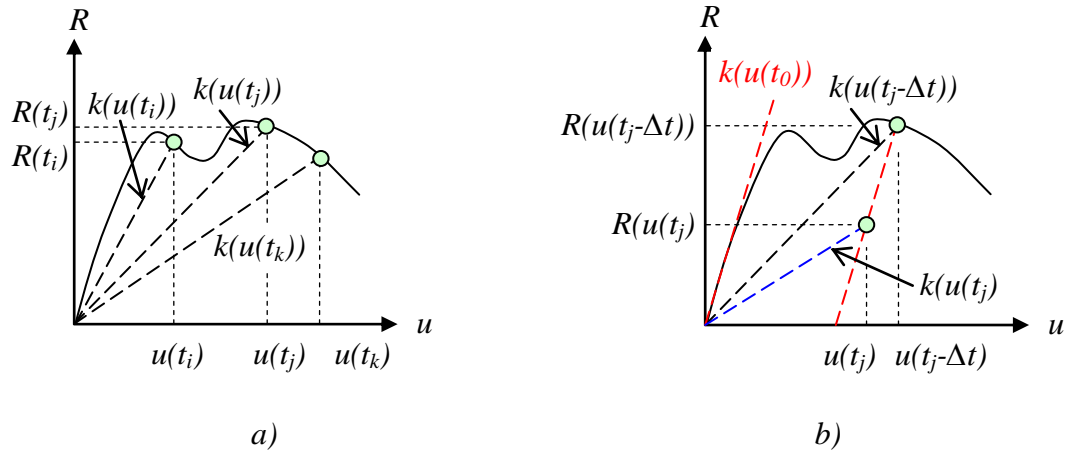
Figure 2.20   Secant stiffness at time t for a system with arbitrary material properties.

In the same way it is possible to adapt the stiffness during off-loading. By keeping track of if the current stiffness should correspond to loading or off-loading it is possible to adapt the stiffness to the present case. For example, it is possible that for a plastic response allow the off- and on-loading correspond to a desired linear-elastic stiffness up to a certain yield-stress, and for further loading, with growing plastic deformations, let the secant stiffness take over.

3 Analysis of Collision Models and Parameter Study

In this chapter collisions will be simulated and their responses studied. For this purpose an algorithm for a 2DOF spring-mass system was created using the commercial software MATLAB, see Appendix H, where the central difference method is used to find a numerical solution of the displacement in each time step.

3.1 2DOF system without barrier

In this section the response of a system during a collision will be studied. With the starting point in the classic impact theory the 2DOF system, with the stiffness of body 2 k_2 set to zero, can be utilized for the analysis, see Figure 3.1.
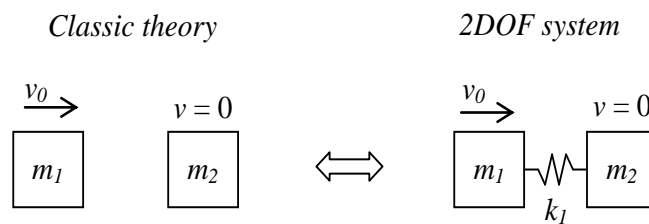
Figure 3.1   Illustration of how the classic theory can be analysed using a 2DOF spring-mass system.

The response of an impact according to the classic theory is presented in Figure 2.12. Based on this four points were chosen, to be studied further in this section. These correspond to elastic and plastic response, $e = 1$ and $e = 0$, when the mass ratio is equal to 0.1 and when it is equal to 10, see Figure 3.2.
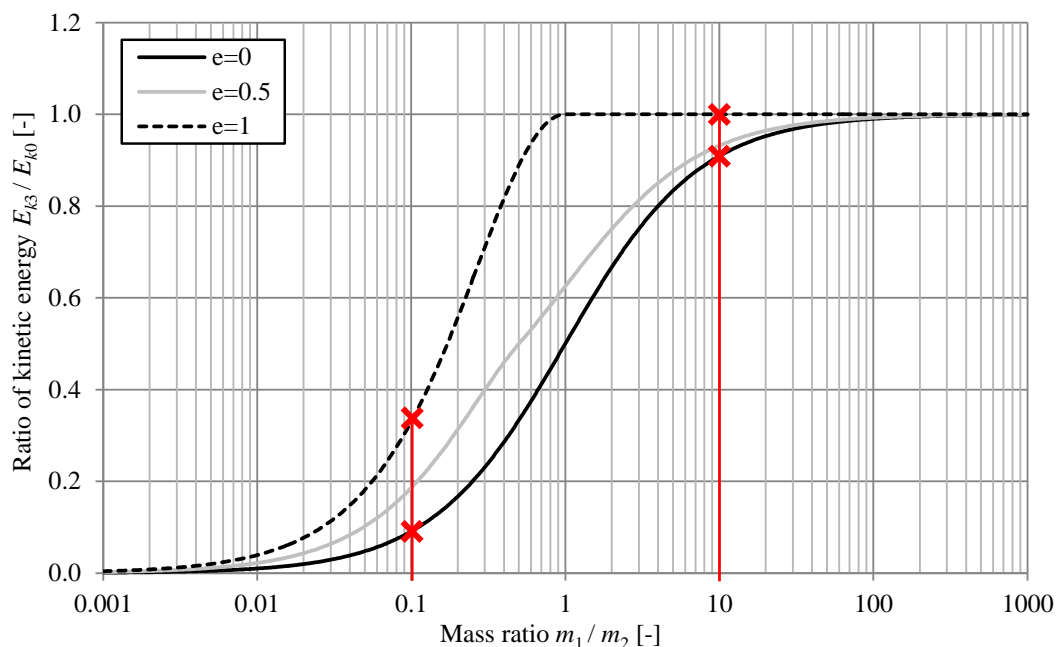
Figure 3.2   Points of interest in the classic impact theory to be studied further, based on Figure 2.12.

3.1.1 Elastic response

The collision with elastic response is first studied. The spring will have a linear elastic behaviour when the deformation is positive and a stiffness of zero when the deformation is negative. This is due to the fact that the two bodies should only interact through compression forces, not tension forces, see Figure 3.3.
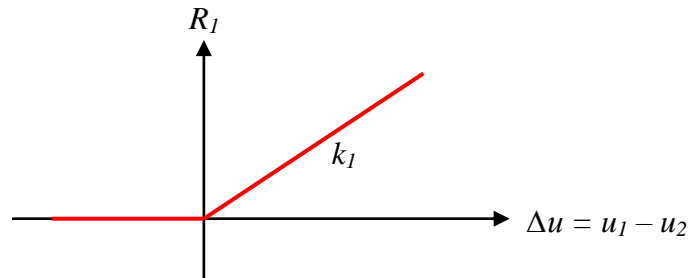
Figure 3.3   The force-displacement relationship used for the spring when studying a classic impact with elastic response.

The parameters for the analyses are chosen to correspond to the points marked in Figure 3.2 by letting the mass of the second body m_2 be constant and varying the mass of the first body m_1 in order to obtain the correct mass ratio. For the collisions with a mass ratio of ten, two different stiffnesses are also considered, see Table 3.1.

Table 3.1   Input parameters for the elastic classic collision analyses.

Case	m_1 [kg]	m_2 [kg]	k_1 [kN/m]	v_0 [m/s]
Collision 1	1 000	10 000	100	20
Collision 2	100 000	10 000	100	20
Collision 3	100 000	10 000	1 000	20

The results from the analyses are compared in a force-time diagram where the force in the spring during the impact period is shown in Figure 3.4. This and all other analyses in this section are studied during a time period of 1.0 second, and with an initial velocity v_0 of 20 m/s (72 km/h).
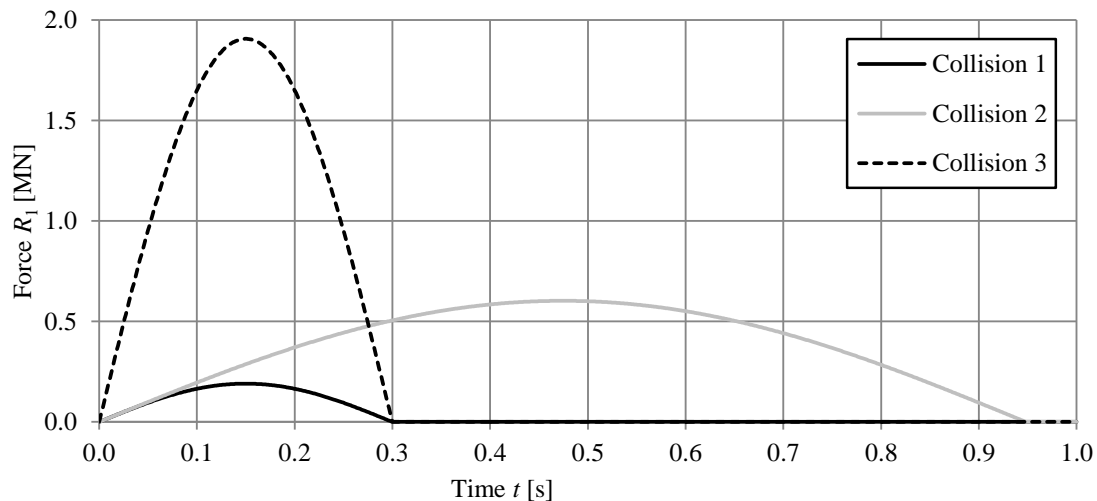
Figure 3.4   Force vs time during an impact in an elastic classic collision, for parameters in the different cases see Table 3.1.

In Figure 3.4 for Collision 2 the duration of the impact is roughly 0.95 seconds, while it is only about 0.3 seconds for Collision 1. This is due to that a larger impulse needs to be transferred to the second body when the momentum of the first body is larger. For Collision 3 the stiffness is ten times larger, but the mass ratio is the same as for Collision 2. Here the impulse, the area under the force-time graph, is equally large as for Collision 2 because of the same momentum. But the duration of the impact is now the same as for Collision 1 because of the higher stiffness, and the maximum force therefore needs to be higher.

In Figure 3.5 various other results from the analysis of Collision 1 are presented, namely the displacement u, the velocity v, the impulse I and the work W, for both bodies and as a function of time. Figure 3.5a shows the displacement over time for the two bodies. During the impact body 1 is deformed initially before body 2 is set in motion. After about 0.15 seconds body 1 is stationary, velocity equal to zero, before it changes direction and the deformation decreases again. After about 0.3 seconds the impact is over and the two bodies are no longer in contact with each other, this can also be seen in Figure 3.5b. As discussed in Section 2.3.1, the first body will obtain a negative velocity after impact if it has smaller mass compared to the second body, and this is confirmed in this analysis, see Figure 3.5b. Figure 3.5c clearly shows how the impulse, or momentum, is transferred from the first body to the second body, as the two curves are exactly mirrored. Finally Figure 3.5d shows how the internal work develops in body 1 and how an external work is transferred to body 2. The work done in body 1 increases in the beginning of the impact, but decreases after the object changes direction, due to that a negative work is done. The work done on body 2 increases slowly and ends up at the same level as the work done in object 1. The results for collision 1 are compared with the classic impact theory in Table 3.2. As seen they are almost identical and gives the same energy ratio E_{k3} / E_{k0} as in Figure 3.2

For the corresponding results for Collision 2 and Collision 3, see Appendix B.

Table 3.2   *Comparison of results between classic impact theory and the 2DOF system for elastic response, collision 1.*

	Classic	2DOF
e [-]	1	1.000
v_1 [m/s]	-16.364	-16.364
v_2 [m/s]	3.636	3.636
E_{k0} [kJ]	200	200
E_{k3} [kJ]	66.120	66.117
E_{k3}/E_{k0}	0.331	0.331
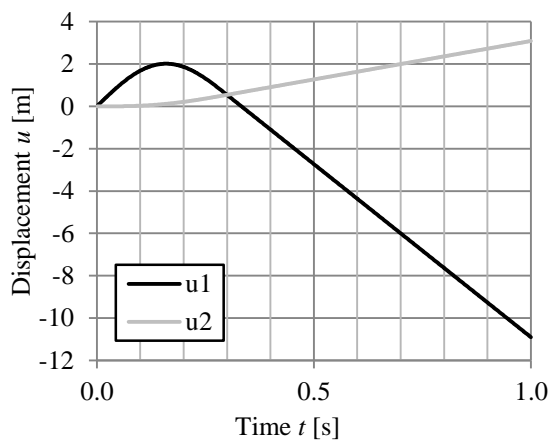
a)
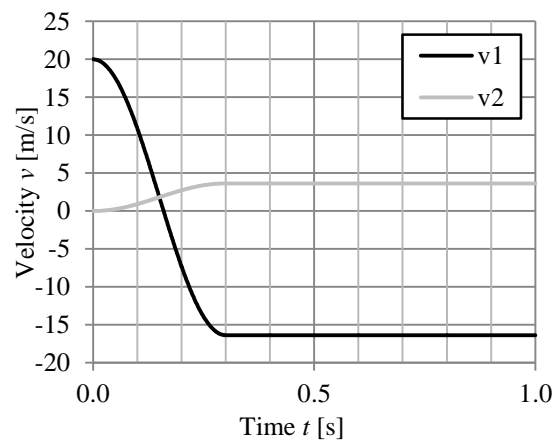
b)
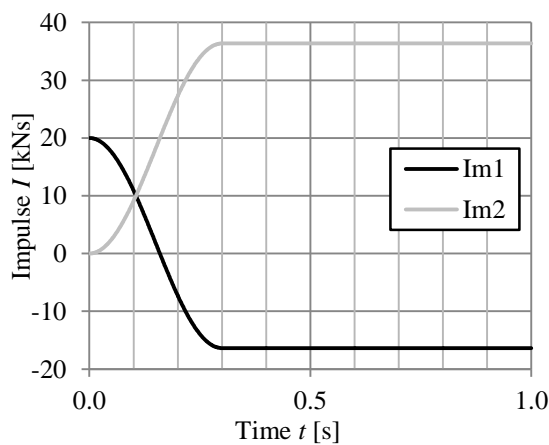
c)
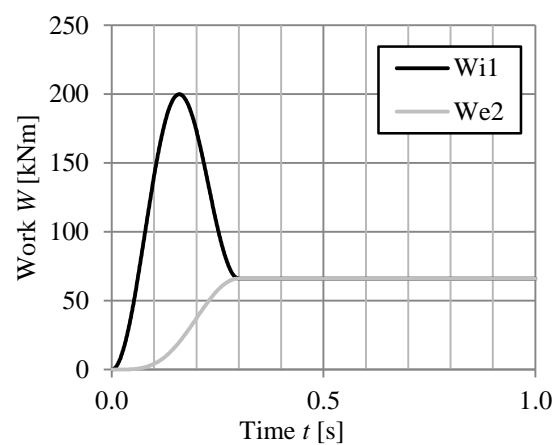
d)

Figure 3.5   *Results from an elastic collision, Collision 1, where $m_1 = 1\,000$ kg, $m_2 = 10\,000$ kg, $k_1 = 100$ kN/m and $v_0 = 20$ m/s.*

3.1.2 Plastic response

The collision with plastic response is now studied. The spring will have a plastic behaviour when the deformation is positive, and as before, a stiffness of zero when the deformation is negative, see Figure 3.6.
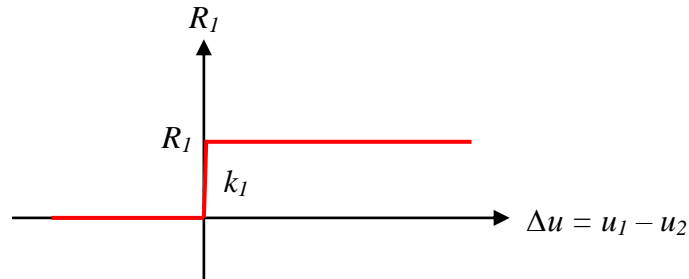
Figure 3.6   The force-displacement relationship used for the spring when studying a classic impact with plastic response.

The parameters for the analyses are chosen to correspond to the points in Figure 3.2, this time the points on the curve for plastic response where $e = 0$. This is accomplished by again letting the mass of the second body m_2 be constant while varying the mass of the first body m_1. For the higher mass ratio two different load capacities are considered in the analysis. To be able to simulate an entirely plastic behaviour, the stiffness of the spring is given a sufficiently high value, see Table 3.3. The COR e is subsequently calculated for the three analyses according to equation (2.25), to ensure that it is close to zero.

Table 3.3   Input parameters for the plastic classic collision analyses.

Case	m_1 [kg]	m_2 [kg]	k_1 [MN/m]	R_1 [kN]	v_0 [m/s]	e
Collision 4	1 000	10 000	100	200	20	0.033
Collision 5	100 000	10 000	100	200	20	0.011
Collision 6	100 000	10 000	100	400	20	0.021

The results from the analyses are compared in a force-time diagram where the force in the spring during the impact period is visualized in Figure 3.7.
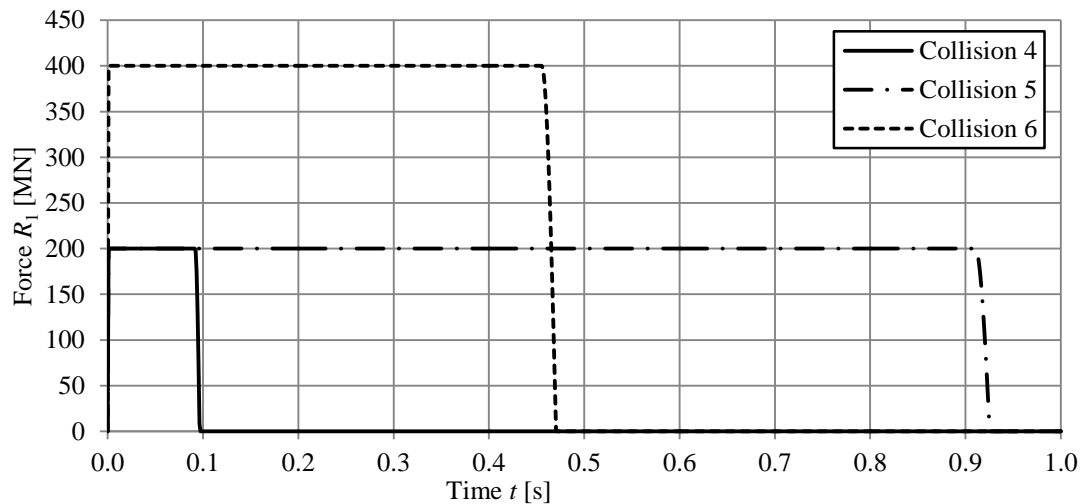
Figure 3.7   Force vs time during an impact in a plastic classic collision, for parameters in the different cases see Table 3.3.

The shape of the impulse for all three cases in Figure 3.7 is almost a perfect rectangle, which is characteristic for a plastic response. The fact that the stiffness is not infinitely large is the reason for the small inclinations of the loading and unloading curves. The plastic response gives a constant force applied to the second body during most of the impact period. This leads to that the duration of impact for Collision 5 is much longer, about 0.93 seconds, compared to Collision 4 which has a duration of about 0.1 seconds. This is due to the larger impulse that needs to be transferred in Collision 5, where the mass m_1 is larger. When the load capacity, or yield force, is doubled in Collision 6 the impact duration is half as long, roughly 0.47 seconds, compared to Collision 5. This means that the transferred impulse is equal in the two collisions, which should also be the case because of the same momentum the bodies have prior to the collision.

In Figure 3.8 several other results from the analysis of Collision 4 are presented, namely the displacement u, the velocity v, the impulse I and the work W, for both bodies and as a function of time. In Figure 3.8a the displacement over time is visualized, and it can be seen how the plastic deformation of the first body takes place entirely during the first 0.1 seconds of the impact. After this time, the impact is over and the two bodies are not in contact any more. This is however not correct since in a fully plastic impact the bodies will stay in contact with each other. What is seen here is because of the elastic behaviour at loading and unloading that are used in the calculations. That the plasticization process is finished is confirmed in Figure 3.8b where it is seen that the velocities will be constant after this period, with body 2 having the highest velocity. Figure 3.8c shows how the impulse is transferred between the bodies, and it is exactly mirrored as it was for the elastic collisions. Figure 3.8d shows a different behaviour of body 1 compared to the elastic analysis. Here the work done in body 1 is larger than in body 2 due to the fact that plastic deformation takes place in the former. The work done on body 2 is on the other hand a lot smaller. This is interpreted as that the impact energy is mostly consumed in the plasticization process of body 1, instead of acting on body 2. Another observation is that for a plastic analysis the first body will never bounce back and get a negative velocity, in opposite to what happens in the elastic analysis when $m_1 < m_2$. The results for collision 4 are compared with the classic impact theory in Table 3.4. There is a small difference in the results, but the energy ratio E_{k3} / E_{k0} is still very close to each other

and has the same value as given in Figure 3.2. For a better correlation with the classic theory a higher stiffness could be used, i.e. a lower value of the COR would be obtained.

For the corresponding results for Collision 5 and Collision 6, see Appendix B.

Table 3.4   *Comparison of results between classic impact theory and the 2DOF system for plastic response, collision 4.*

	Classic	2DOF
e [-]	0	0.033
v_1 [m/s]	1.8182	1.214
v_2 [m/s]	1.8182	1.879
E_{k0} [J]	200 000	200 000
E_{k3} [J]	18 182	18 382
E_{k3}/E_{k0}	0.091	0.092

a)

b)

c)

d)
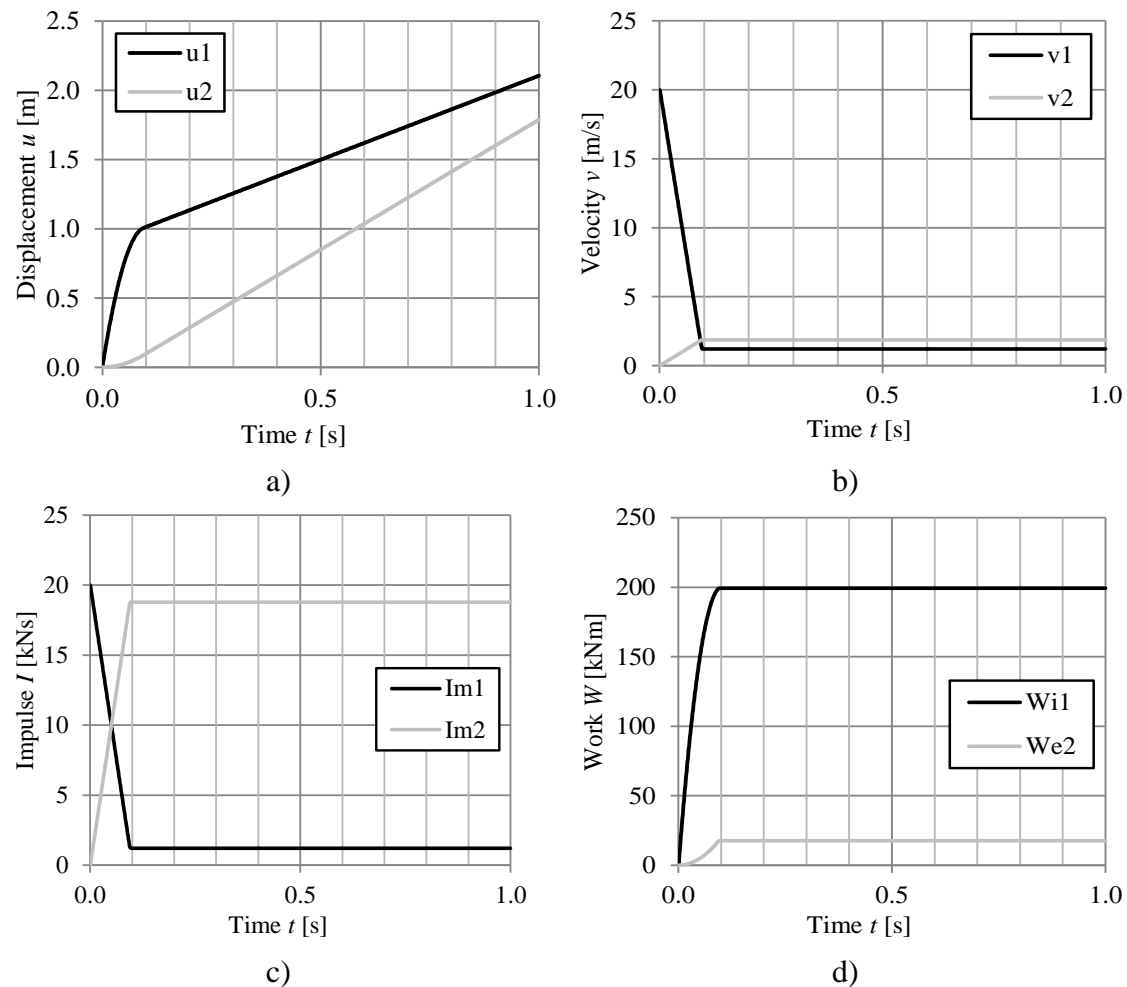
Figure 3.8   *Results from a plastic collision, Collision 4, where $m_1 = 1\,000$ kg, $m_2 = 10\,000$ kg, $k_1 = 100$ MN/m, $R_1 = 200$ kN and $v_0 = 20$ m/s.*

CHALMERS, *Civil and Environmental Engineering*, Master's Thesis 2014:80

3.2 Analysis of 2DOF system with a barrier

For impact against a non-rigid barrier, for example body 2 in a 2DOF system, the load response $R_2(t)$ will depend on the mass and stiffness of both bodies.
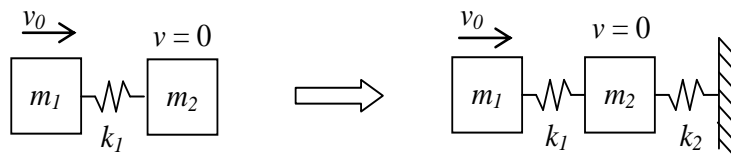
Figure 3.9   Illustration of a) Previous system used in section 3.1 b) 2DOF system used in this section.

3.2.1 Elastic response
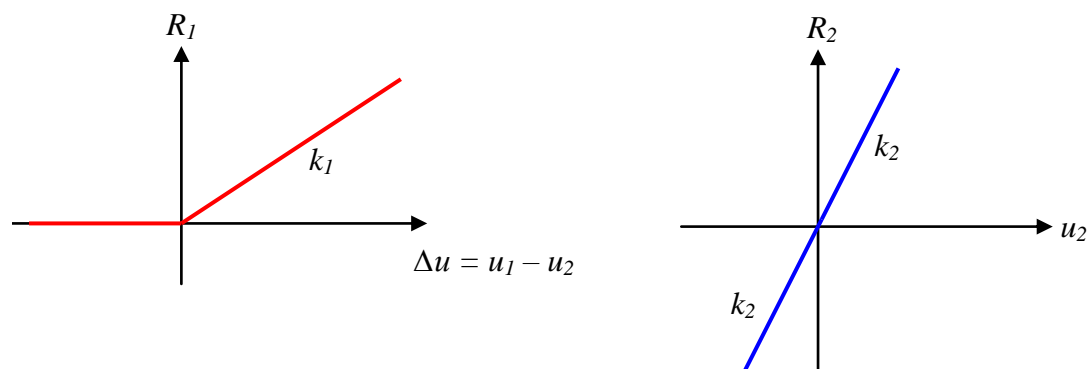
Figure 3.10   The force-displacement relationship used for the two springs when studying a 2DOF system with elastic responses.

The spring stiffness k_1 has a linear elastic behaviour when the deformation is positive and a stiffness of zero when the deformation is negative. This is due to the fact that the two bodies should only interact through compression forces, not tension forces. The stiffness of the second spring k_2 is considered to be linear elastic, see Figure 3.10.

The displacement of the second body, u_2, and thereby also the response in time $R_2(t)$ is affected by the eigenfrequency of both body 1, f_1, and body 2, f_2, thereby giving it a more complex appearance. This relation can be expressed as a mass ratio m_1 / m_2 and a frequency ratio, f_1 / f_2, for body 1 and body 2. The approach presented here is based on the assumption that the dynamic load that arises during impact can be transformed to an equivalent static load, $F_{2,sta}$, which can be used for static analysis of the structure in question. A useful tool is then to use a loading factor β_{el} that describes the relation between the equivalent static load $F_{2,sta}$ and the maximum dynamic load $F_{2,el}$

$$F_{2,sta} = \beta_{el} \cdot F_{2,el} \tag{3.1}$$

It should be noted that the equivalent static load corresponds to the interior force R_2 acting on body 2 as seen in Figure 2.19

$$F_{2,sta} = R_2 = k_2 u_{el,2} \qquad (3.2)$$

The dynamic load $F_{2,el}$ for a hard impact, i.e impact against a rigid barrier, can be found by letting the initial kinetic energy $E_{kinetic}$ be equal to the elastic strain energy E_{strain} of the colliding object

$$E_{kinetic} = E_{strain} \qquad (3.3)$$

The external work W_e which is equal to the initial kinetic energy is expressed as

$$W_e = E_{kinetic} = \frac{m v_0^2}{2} \qquad (3.4)$$
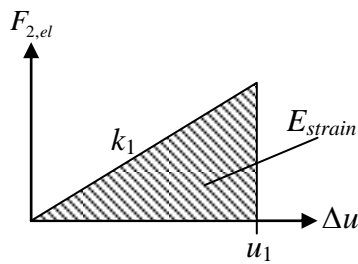
Figure 3.11   Stress-strain curve showing the elastic strain energy.

The area under the stress-strain curve is the elastic strain energy E_{strain}, which is equal to the internal work

$$W_i = E_{strain} = \frac{F_{2,el} u_1}{2} \qquad (3.5)$$

where the deflection u can be expressed as

$$u_1 = \frac{F_{2,el}}{k_1} \qquad (3.6)$$

Thereby the elastic strain energy can be expressed as

$$E_{strain} = \frac{F_{2,el}^2}{2 k_1} \qquad (3.7)$$

By putting the initial kinetic energy equal to the elastic strain energy

$$\frac{m_1 v_0^2}{2} = \frac{F_{2,el}^2}{2 k_1} \qquad (3.8)$$

the dynamic load can be expressed as

$$F_{2,el} = v_0 \sqrt{k_1 \cdot m_1} \qquad (3.9)$$

The load factor in equation (3.1) can be defined as

$$\beta_{el} = \frac{R_2}{F_{2,el}} \qquad (3.10)$$

In Johansson (2014a) a diagram showing the relation between the load factor β_{el} and the frequency ratio f_1 / f_2 is presented for different values of the mass ratio m_1 / m_2, this is shown in Figure 3.12. The tabulated values for the load factor β_{el} can be found in Appendix C.
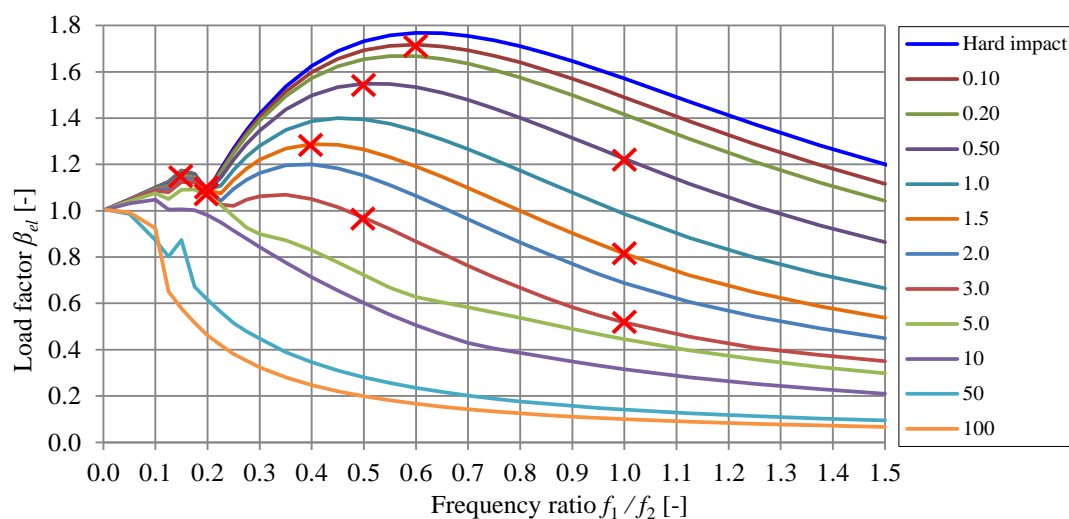
Figure 3.12   *Relationship between load factor β_{el} and frequency ratio f_1 / f_2 for different relations of the mass ratio m_1 / m_2 based on Johansson (2014a).*

A total amount of ten comparisons thought to be interesting have been carried out using different combinations of the mass ratio m_1 / m_2 and frequency ratio f_1 / f_2 in order to demonstrate the behaviour of an elastic impact, see Table 3.5. These combinations are marked in Figure 3.12.

Table 3.5   *Table showing the coordinates of tested impacts from Figure 3.12.*

Impact test number	Mass ratio m_1 / m_2	Frequency ratio f_1 / f_2	Loading factor β_{el} $F_{2,sta} / F_{2,el}$
1	0.1	0.6	1.72
2	0.5	0.5	1.55
3	1.5	0.4	1.29
4	0.2	0.2	1.08
5	2.0	0.2	1.09
6	0.2	0.15	1.17
7	2.0	0.5	0.97
8	3.0	1.0	0.52
9	1.5	1.0	0.81
10	0.5	1.0	1.22

Impact test number 2 is presented in Figure 3.13 and Figure 3.14 and impact test number 8 is presented in Figure 3.15 and Figure 3.16. The rest of the impact tests are presented in Appendix C.

a) Deformation

b) Velocity

c) Impulse for body 1

d) Impulse for body 2
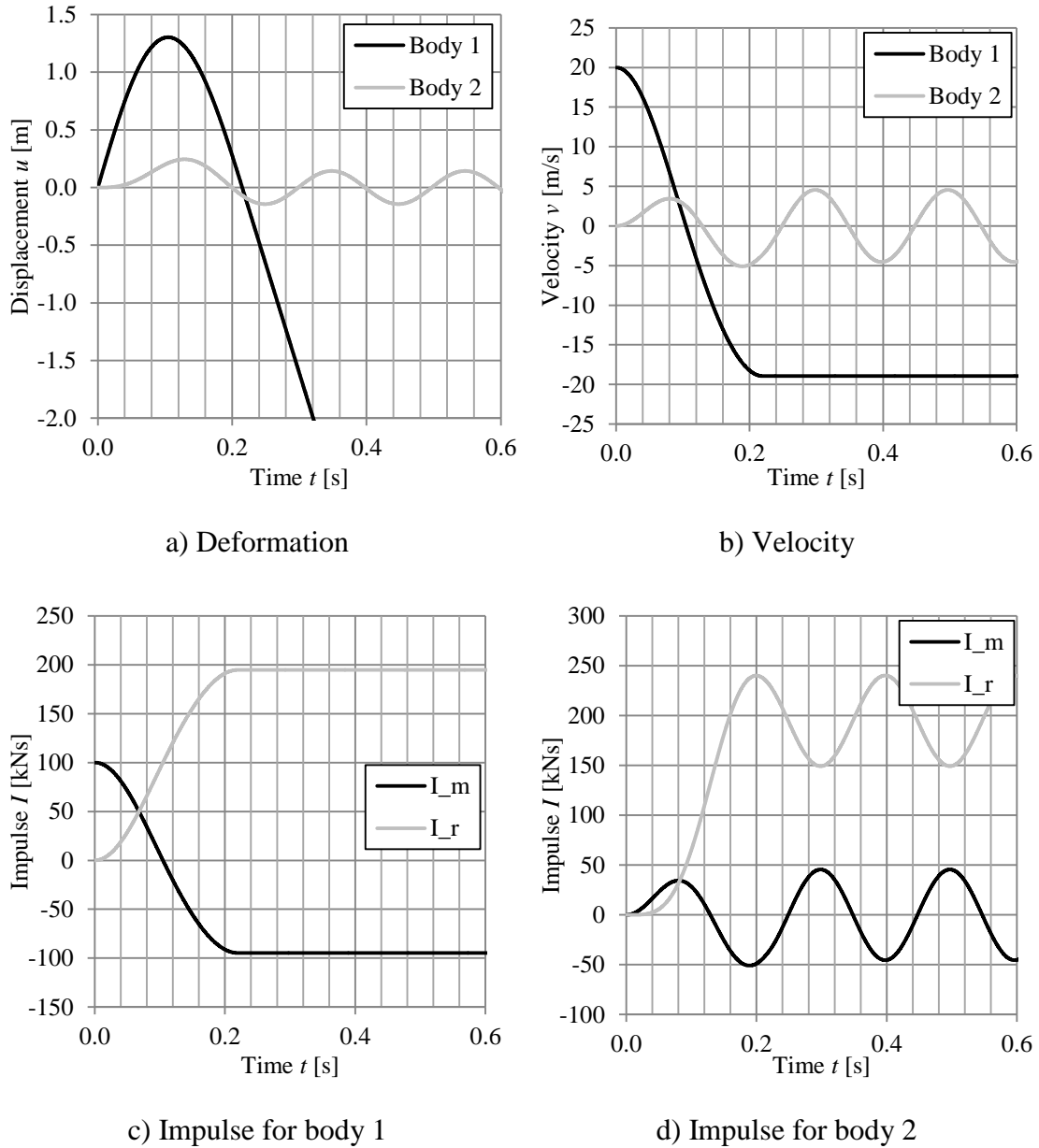
Figure 3.13   Impact test number 2: $m_1 = 5\,000kg$, $m_2 = 10\,000kg$ $k_1 = 1.25\ MN/m$, $k_2 = 10\ MN/m$, $v_0 = 20\ m/s$.

In impact test number 2 it can be seen from Figure 3.13 that the impact lasts for about 0.2 seconds. One thing that might seem a bit strange at first glance is that the impulse of reaction force I_r from body 1 shown in Figure 3.13c has an almost twice as large value as the original impulse of mass I_m, or momentum, of body 1. This is due to the fact that body 1 bounces back with a velocity $v_1 \approx -v_0$ as seen in Figure 3.13b. In order to achieve a change in the momentum for body 1 from p_0 to $p_1 \approx -p_0$ an impulse of $I_r \approx 2p_0$ is needed, see also Figure 2.6.
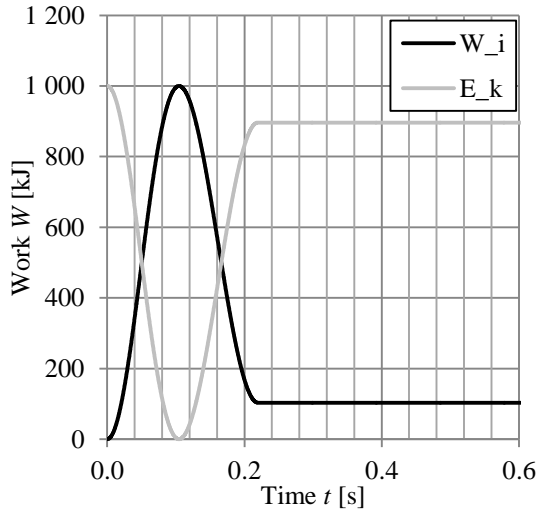
a) Kinetic energy - internal work body 1
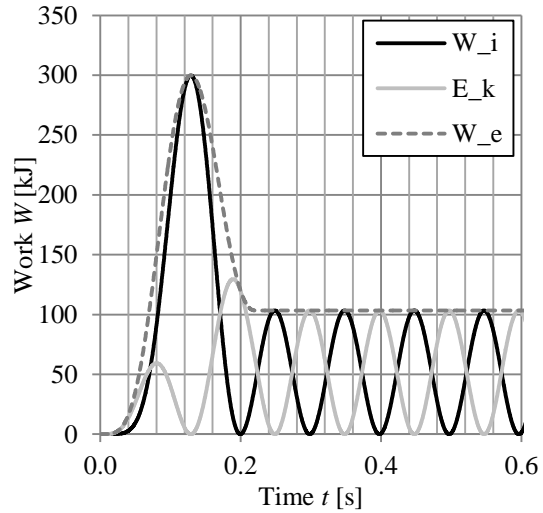
b) Kinetic energy - work body 2
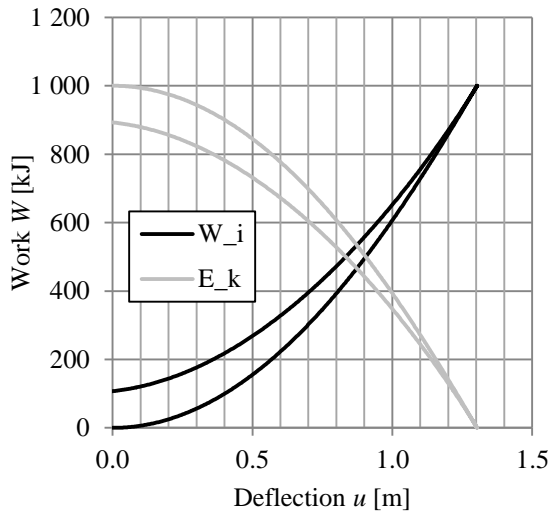
c) Kinetic energy - internal work body 1
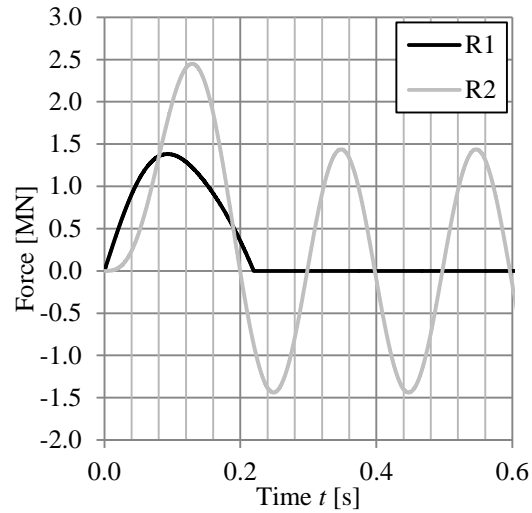
d) Load pulse

Figure 3.14   Impact test number 2: m_1 = 5 000 kg, m_2 = 10 000 kg, k_1 = 1.25 MN/m, k_2 = 10 MN/m, v_0 = 20 m/s.

In Figure 3.14a it can be seen how the internal work and kinetic energy of body 1 interact with each other with regard to time. The kinetic energy reduces with the same amount as the internal energy increases, this can also be seen in Figure 3.14c which shows the same plot but with regard to the deflection of body 1 instead of time.
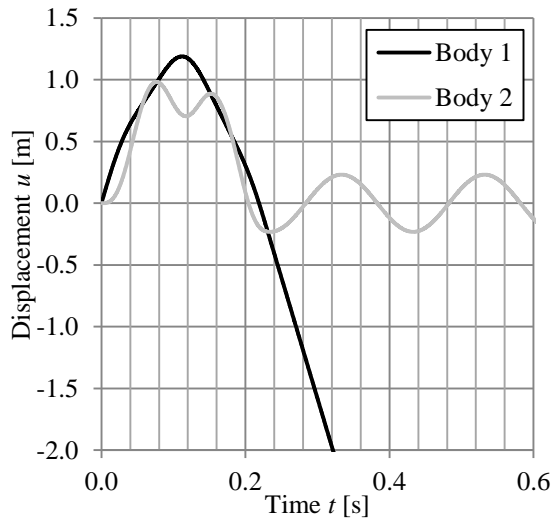
a) Deformation
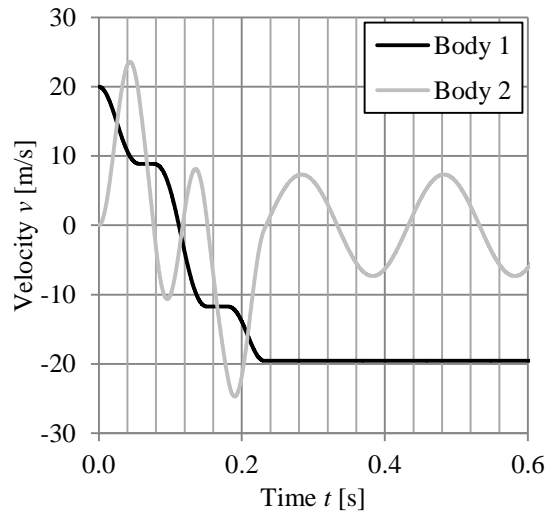
b) Velocity
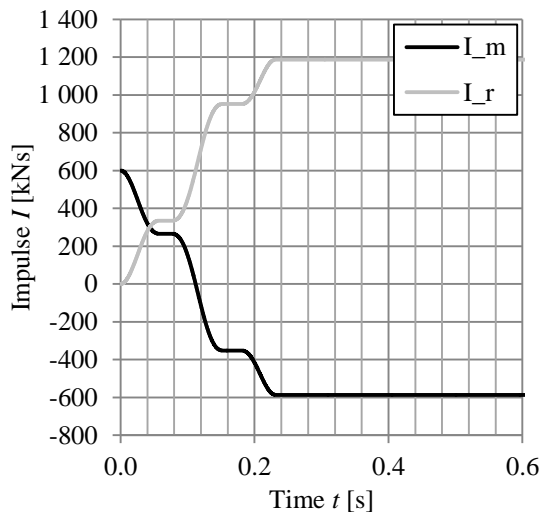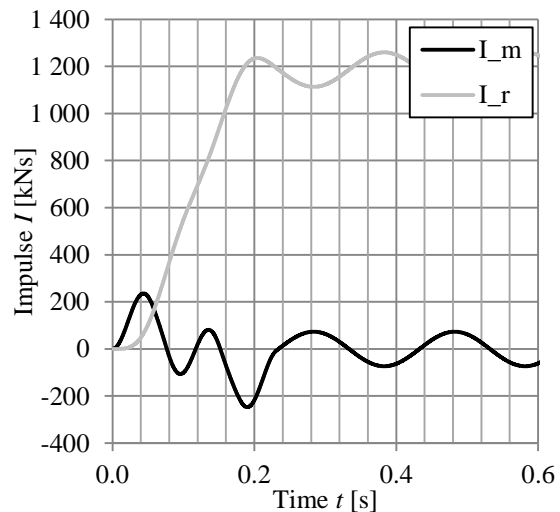
c) Impulse for body 1

d) Impulse for body 2

Figure 3.15   *Impact test number 8: m_1 = 30 000 kg, m_2 = 10 000 kg, k_1 = 30 MN/m, k_2 = 10 MN/m, v_0 = 20 m/s.*

In impact test number 8 it can be seen from Figure 3.15 that the impact lasts for a little bit more than 0.2 seconds, but compared to impact test number 2 the behaviour of the impact is different. Both the velocity and the impulse of body 1, see Figure 3.15b and Figure 3.15c, change in a step-like behaviour over time. This is due to that there are multiple impacts between body 1 and body 2, this phenomenon is discussed further with Figure 3.17. Except from this, the impulse displays again the same behaviour of having a larger value than the original impulse of body 1.
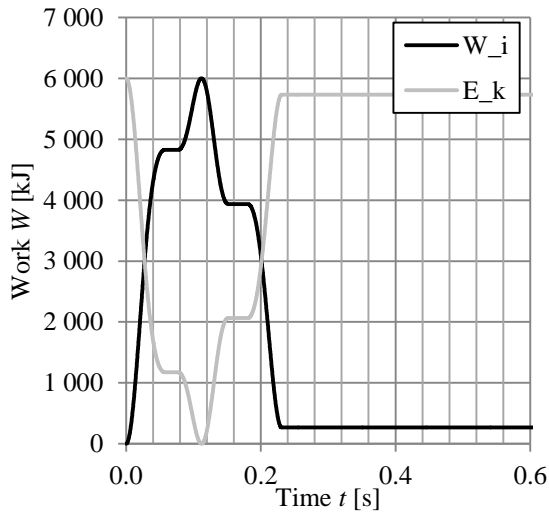
a) Kinetic energy - internal work body 1
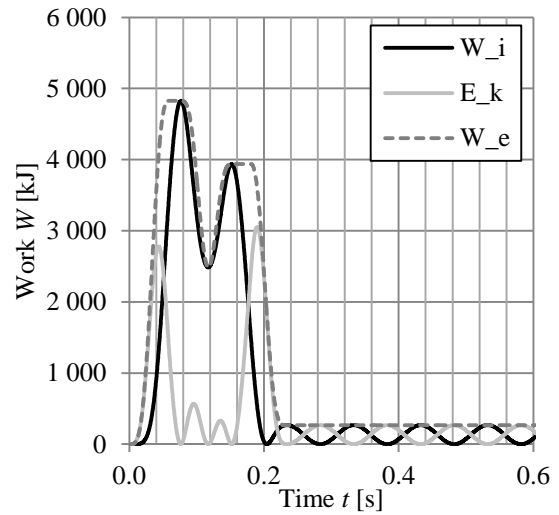
b) Kinetic energy - work body 2
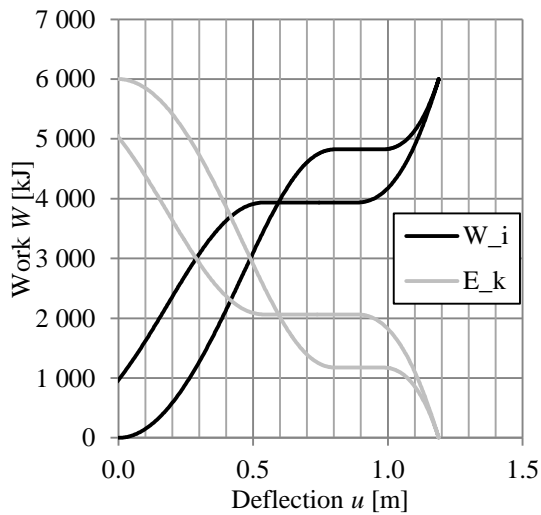
c) Kinetic energy - internal work body 1
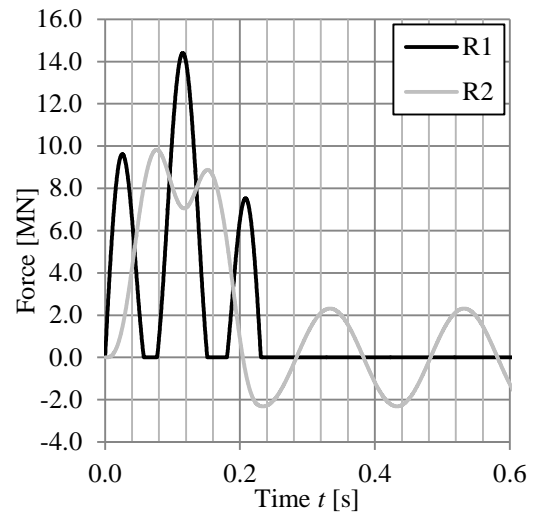
d) Load pulse

Figure 3.16   Impact test number 8: m_1 = 30 000 kg, m_2 = 10 000 kg, k_1 = 30 MN/m, k_2 = 10 MN/m, v_0 = 20 m/s.

In Figure 3.16a it can be seen how the internal work and kinetic energy of body 1 interact with each other with regard to time. The step-like behaviour is visible and the kinetic energy is mirrored by the internal energy, this can also be seen in Figure 3.16c that shows the same plot but with regard to the deflection of body 1 instead of time.

The shape of the load pulse that arises during impact between body 1 and body 2 has great influence on the response of the latter. How the shape of the load pulse is affecting the response is fairly complicated and depends on a combination of different properties such as mass ratio and frequency ratio for the two bodies.

a) $m_1 / m_2 = 0.5, f_1 / f_2 = 0.5$

b) $m_1 / m_2 = 2, f_1 / f_2 = 0.2$

c) $m_1 / m_2 = 3, f_1 / f_2 = 0.5$

d) $m_1 / m_2 = 3, f_1 / f_2 = 1$
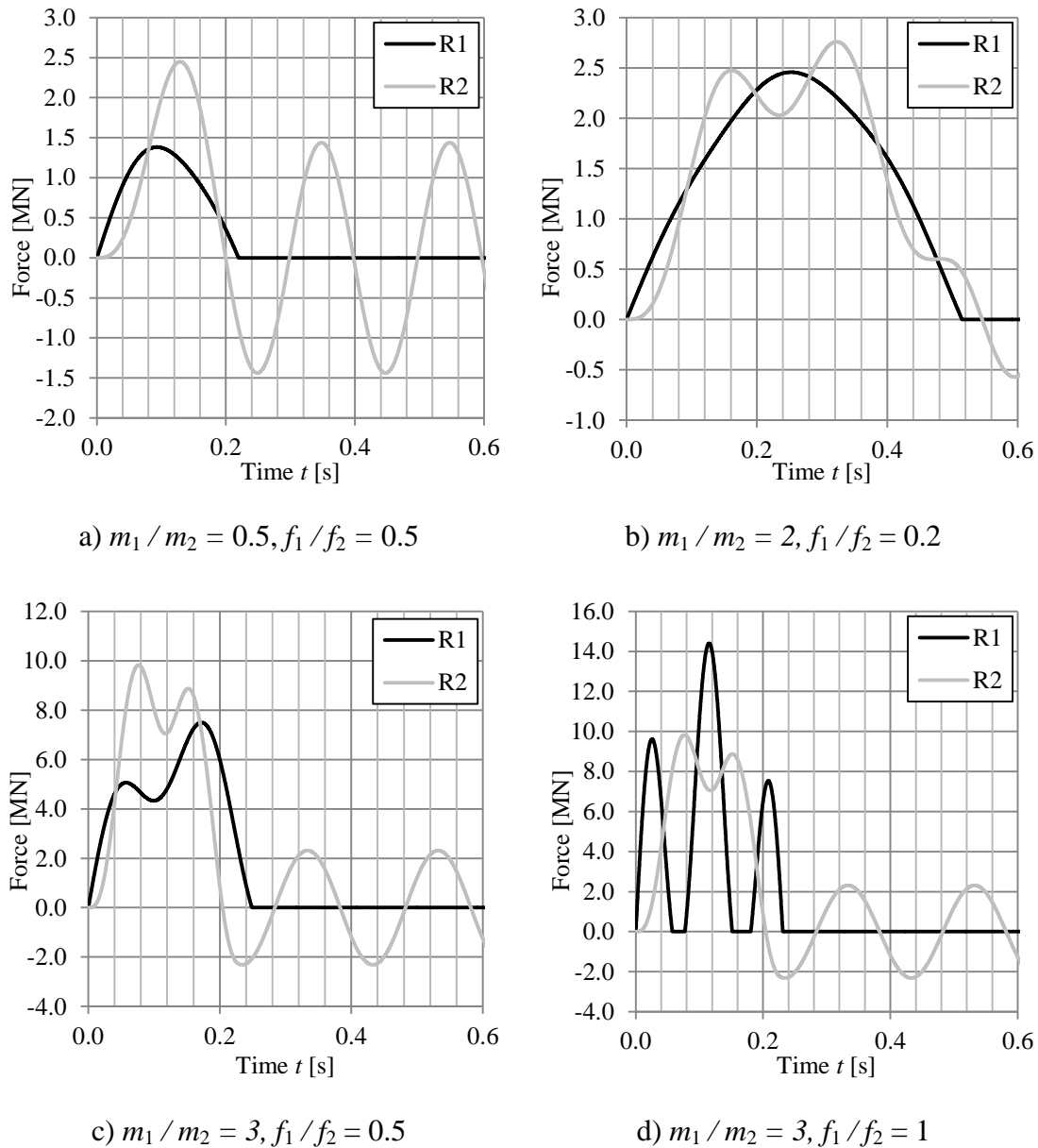
Figure 3.17   Load pulses for impact test numbers 2,5,7 and 8.

The relations presented for an elastic impact using classic impact theory in section 2.3.1 is valid when body 2 does not have a support, meaning $k_2 = 0$. In that case there will only be a single impact between the bodies as described by equations (2.28) and (2.29). However for a case where $k_2 \neq 0$ and $v_1 > 0$ after impact, body 1 will catch up with body 2 and thereby causing one or several secondary impacts. This can be seen in Figure 3.17d where R_1 after the initial impact reduces until body 1 again comes into contact with body 2. This phenomenon is especially common when both mass ratio m_1 / m_2 and frequency ratio f_1 / f_2 has relatively high values.

3.2.2 Elasto-plastic response

The case with elasto-plastic response is a combination of the elastic and the plastic responses, for both bodies. The material has a maximum load capacity R for which the plasticization starts. These results are not discussed in the main report but are included in Appendix C since it might be interesting to see how an elasto-plastic system behaves.

3.3 Comparison of impact with and without barrier

In order to get a clearer picture of what the difference in response is for an impact with and without a barrier some impact tests are made where all properties are the same except for the use of a barrier, represented in the 2DOF system by the stiffness k_2. Three collisions are demonstrated, one without a barrier, one with a relatively weak barrier and one with a relatively stiff barrier, see Table 3.6.

Table 3.6   The properties used for each impact test.

	m_1 [kg]	m_2 [kg]	k_1 [N/m]	k_2 [N/m]	v_0 [m/s]
No barrier	1000	10000	1e6	0	20
Weak barrier	1000	10000	1e6	1e7	20
Strong barrier	1000	10000	1e6	1e10	20

The difference in response for various parameters are shown in Figure 3.18

From Figure 3.18a it can be seen that the impulse, the area under the force-time graph, varies both in size and duration depending on the stiffness of the barrier. Since the impulse can be expressed as $I = mv$ it means that the soft barrier should take the longest time to reach its final velocity. This can also be seen in Figure 3.18c, which shows how the velocity of body 1 changes. For the tests using a barrier body 1 bounces back with almost the same velocity as the incoming, while it in the test without a barrier receives a much lower velocity. The velocity of body 2, illustrated in Figure 3.18d, shows that for the impact without a barrier the velocity remains constant after the impact while the impact with a weak barrier receives a sinusoidal movement due to the lack of damping. The stiff barrier also gets this behaviour but here both the amplitude and period time is so small that it is not possible to see in this diagram. Figure 3.18b displays how the kinetic energy E_k of body 1 varies with time. Since this is also dependent on the velocity the impacts gets different final energy levels.
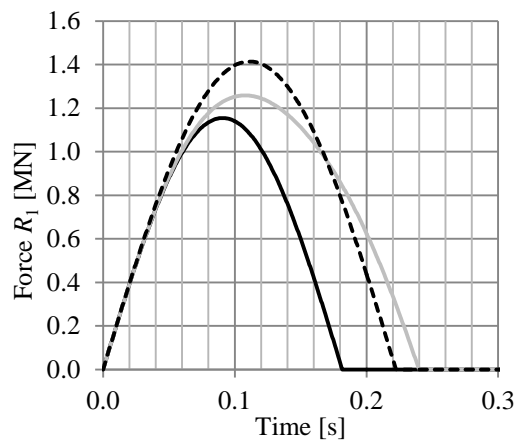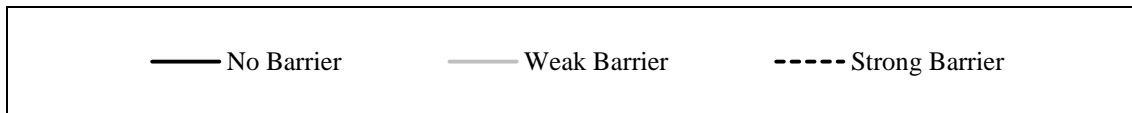
a) Force Body 1
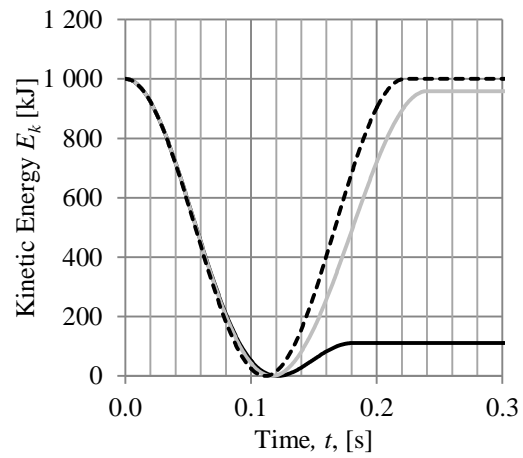
b) Kinetic Energy Body 1
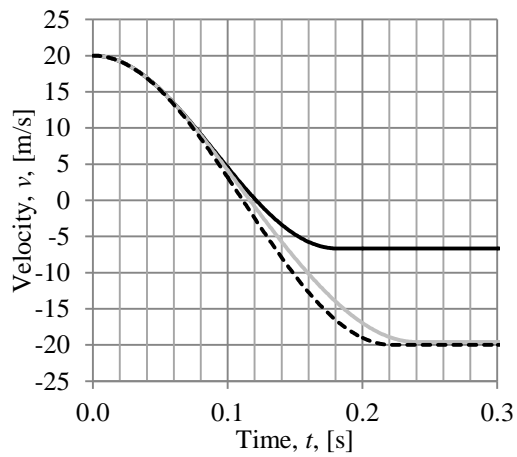
c) Velocity Body 1
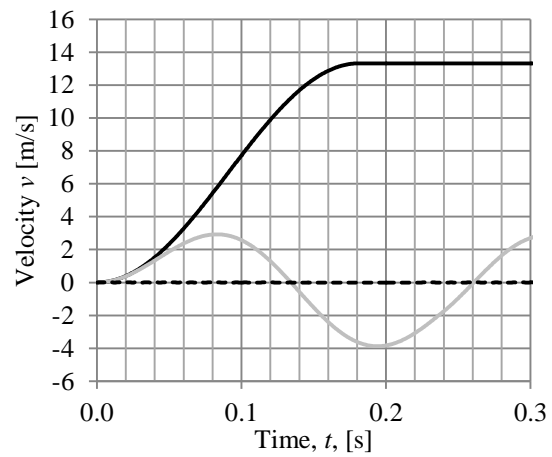
d) Velocity Body 2

Figure 3.18   Comparison of response between impacts with and without a barrier.

CHALMERS, *Civil and Environmental Engineering*, Master's Thesis 2014:80

4 Collision Impact Design

This chapter will treat how to analyse a collision in different ways and with different tools. The objects studied here is a projectile colliding with a barrier of some kind. The barrier is seen as a simply supported beam and the projectile mainly as a vehicle.

The projectile and the barrier can be translated into two bodies, each with a certain mass and stiffness, see Figure 4.1. This way the collision can be studied either according to the classic impact theory, as a 2DOF spring-mass system or with a finite element analysis (FEA).
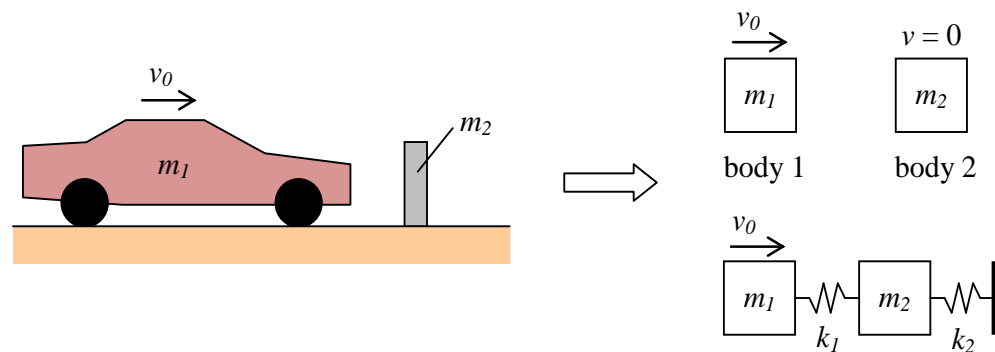
Figure 4.1   Illustration of how the two colliding objects can be translated into a model with two bodies with certain stiffness and mass.

4.1 Structural parameters

Structural parameters such as mass, stiffness and load capacity for the studied objects can be of great importance in an analysis and needs to be chosen carefully. In this section it is studied which values of the structural parameters that are appropriate to use for different objects.

4.1.1 Reasonable parameters for vehicles

Before 1951 vehicle designers believed that a stiffer vehicle body resulted in a safer vehicle for passengers subjected to a collision. This thinking, however, changed when Béla Barényi, a Mercedes-Benz engineer, invented the concept of crumple zones, Wikipedia (2014). According to this a vehicle is divided into three parts, a safety cage around the passenger compartment and two crumple zones, one in the front and one in the rear, see Figure 4.2.
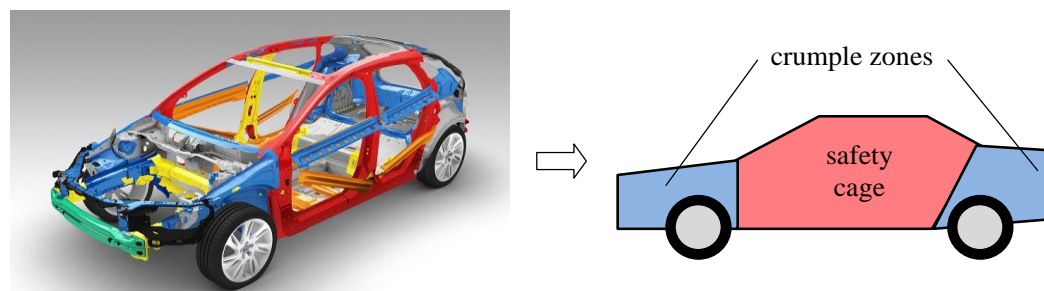
Figure 4.2   The crumple zones in a modern vehicle are made out of lower strength material and have embedded weaknesses, Volvo Cars (2013).

The crumple zone can be described as a deformation zone with lower stiffness and load capacity than the safety cage, see Figure 4.3. This means that the crumple zone will absorb most of the energy during the impact due to large plastic deformations. The duration of the impact will then also be prolonged, resulting in a decreased deceleration of the vehicle which is desirable for the passengers. In analysis it is on the safe side to assume the safety cage to be infinitely stiff and that all internal work is done by the crumple zone.

$$W_i = W_{i,cz} + W_{i,sc}$$
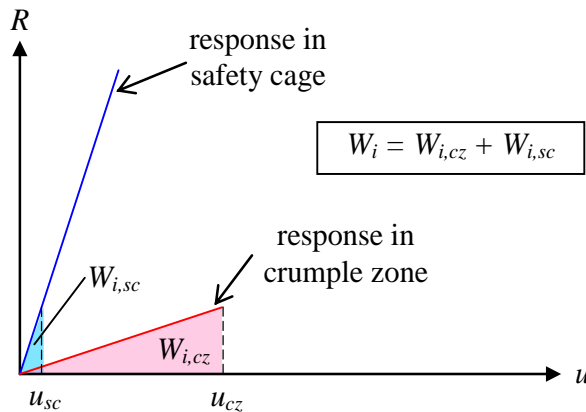
Figure 4.3   *Load-deflection curves and internal work for the safety cage and crumple zone, assuming there is a low load capacity for the crumple zone.*

To get a better picture of how load-deflection curves for vehicles really look like and what structural property values are appropriate to use, it is necessary to study results from real life crash tests. The response from different vehicles can vary quite a lot, depending on its size and weight. The results can also depend on which testing facility carried out the tests and how they were made. Different crash test results are therefore analysed and discussed in this section, to find appropriate structural values to use in the analyses to be carried out. The common types of crash tests discussed in this section are presented in Table 4.1.

Table 4.1   *Common types of crash tests discussed in this section.*

Description	Abbreviation
<u>Offset deformable barrier test</u> – There is an overlap between the vehicle and the barrier. The barrier is made out of a aluminium honeycomb material to simulate another vehicle.	ODB
<u>Full width deformable barrier test</u> – The barrier width equals the entire width of the vehicle. The barrier is made out of a aluminium honeycomb material to simulate another vehicle.	FWDB
<u>Full width rigid barrier test</u> – The barrier is the entire width of the vehicle and is assumed non-deformable.	FWRB

The Euro NCAP frontal impact crash test is performed with a 40 percent overlap between the vehicle and the barrier, called an offset deformable barrier (ODB) test, see Figure 4.4. The barrier consists of a honeycomb structure made out of aluminium,

which will get a plastic deformation under loading in a controlled manner, see Figure 4.5.

540 mm

1000 mm

40 % overlap = 40 % of the width of the car

64 km/h
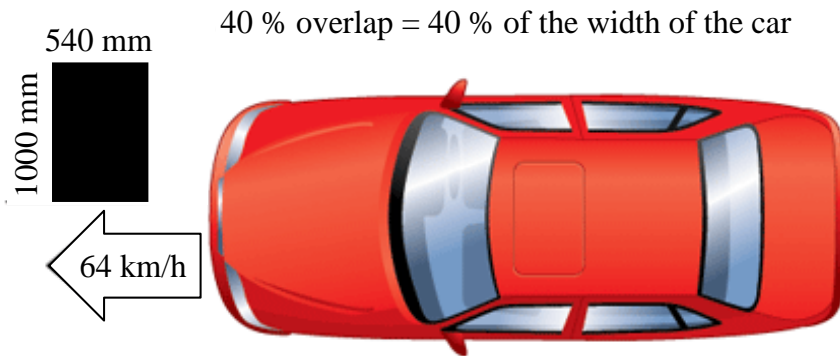
Figure 4.4   *Frontal offset impact test according to Euro NCAP, based on EURO NCAP (2014).*

a)   b)
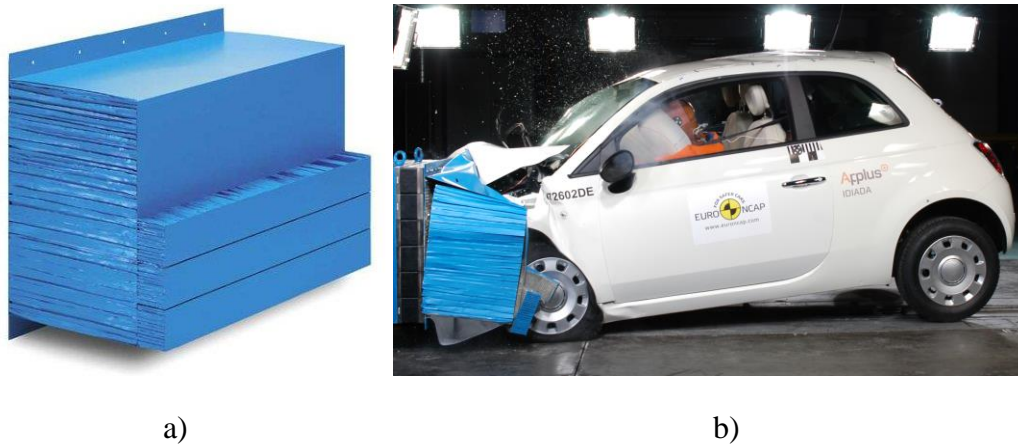
Figure 4.5   *a) deformable barrier consisting of an aluminium honeycomb structure b) deformable barrier used in Euro NCAP ODB crash test, Dynamore GmbH (2014) and EURO NCAP (2007).*

The first results come from a test discussed in a paper by Huibers and de Beer (2001). In this paper was the front stiffness of modern European vehicles studied, by comparing results from Euro NCAP frontal impact crash tests carried out by TNO Crash Safety Centre in the Netherlands. Some of these results, in form of force-displacement diagrams, are presented for different types of vehicles in Figure 4.6 and the corresponding vehicle properties are presented in Table 4.2. The vehicles are grouped into three different categories, medium family cars such as Toyota Corolla, large saloon cars such as Volvo S70 and MPV's or minivans such as Chrysler Voyager. To estimate the behaviour of these three vehicle categories a bilinear curve was fitted to the graphs and the stiffnesses were calculated. These approximated stiffnesses are also presented in Figure 4.6, where $k_{1,1}$ and $k_{1,2}$ are the two stiffnesses during loading, u_{bi} is the deformation where the stiffness is changed and $k_{1,3}$ is the stiffness at unloading.

Table 4.2   *Vehicle properties from crash tests with a 40 % overlap and a velocity of about 17.8 m/s, based on Huibers and de Beer (2001).*

Car model	Kerb mass [kg]	Test mass [kg]	Velocity [m/s]
Medium size family cars			
VW Golf	1140	1336	17.8
Citroen Xsara	1080	1100	17.8
Mitsubishi Lancer	1244	1257	17.8
Renault Megane	1060	1296	17.8
Suzuki Baleno	960	1170	17.8
Toyota Corolla	1060	1275	17.8
VW Beatle	1228	1518	17.8
Ford Focus	1080	1383	17.9
Opel Astra	1100	1325	17.8
Ford Escort	1080	1363	17.9
Mercedes A-class	1070	1267	17.8
Large saloon cars			
BMW 520I	1485	1682	17.9
Saab 95	1485	1713	17.7
Toyota Camry	1385	1604	17.8
Mercedes E200	1440	1650	17.8
Opel Omega	1455	1666	17.8
Audi A6	1400	1663	17.8
Volvo S70	1430	1597	17.8
MPV's			
Renault Espace	1520	1713	17.9
Chrysler Voyager	1800	2040	17.8
Mitsubishi Space wagon	1570	1768	17.9
VW Sharan	1690	1906	18
Peugeot 806	1550	1748	17.8
Vauxhall Sintra	1650	1933	17.8

Kerb mass in Table 4.2 is the mass of the vehicle without passengers or cargo, but with standard equipment and fuel included.
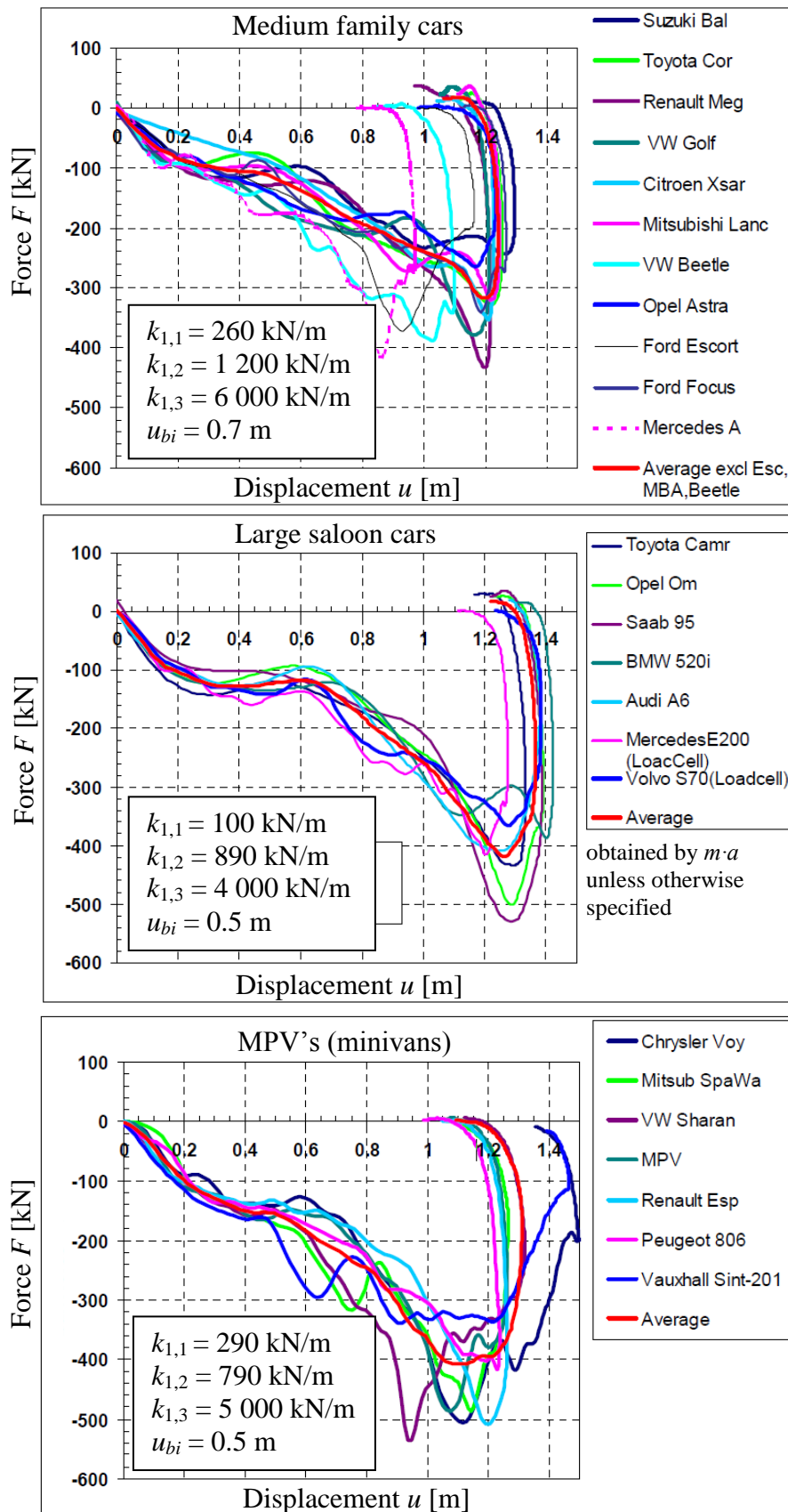
Figure 4.6 *Force-displacement graphs from crash tests with a 40 % overlap and a velocity of about 17.8 m/s, based on Huibers and de Beer (2001). Approximate stiffnesses for different parts of the curves are presented.*

The fact that the Euro NCAP frontal impact crash test is performed with a 40 percent overlap is a problem for the analysis in this thesis since a full width collision is of higher interest. This is because of the higher vehicle stiffnesses it exhibits, due to larger impacting area, thus leading to larger impact forces. In order to adjust the values from this kind of tests to better fit the purpose of this thesis, the stiffnesses are later multiplied by two to simulate a full frontal impact, see Table 4.3. This corresponds quite well to a full frontal crash test, as will be shown later in this section. The breakpoints where the stiffness changes however, are supposed to be the same regardless of the size of the overlap. The velocity of the vehicles are set to 64 km/h (17.8 m/s) in the above crash tests, but the stiffnesses are here assumed to be constant in a limited interval around this impact speed.

Another problem with the Euro NCAP crash test, for the subject of this thesis, is that a deformable barrier is used in order to simulate a collision with another vehicle. This means that the barrier will absorb some of the impact energy and give a lower overall stiffness, see Figure 4.5. In order to minimize the effect of the barrier on the stiffness distribution, the first 40 centimetres of the force-displacement curve is ignored when approximating the stiffnesses, as proposed by Huibers and de Beer (2001).

The next crash test studied was found in Struble (2014) where the topic, how to analyse load cell barrier data, was discussed. This is a full width rigid barrier (FWRB) collision which means that the full width of the car crashes into a non-deformable barrier. The test was performed by the National highway traffic safety administration (NHTSA). The force-displacement graph from the test with an approximated bilinear curve superimposed on top can be seen in Figure 4.7.
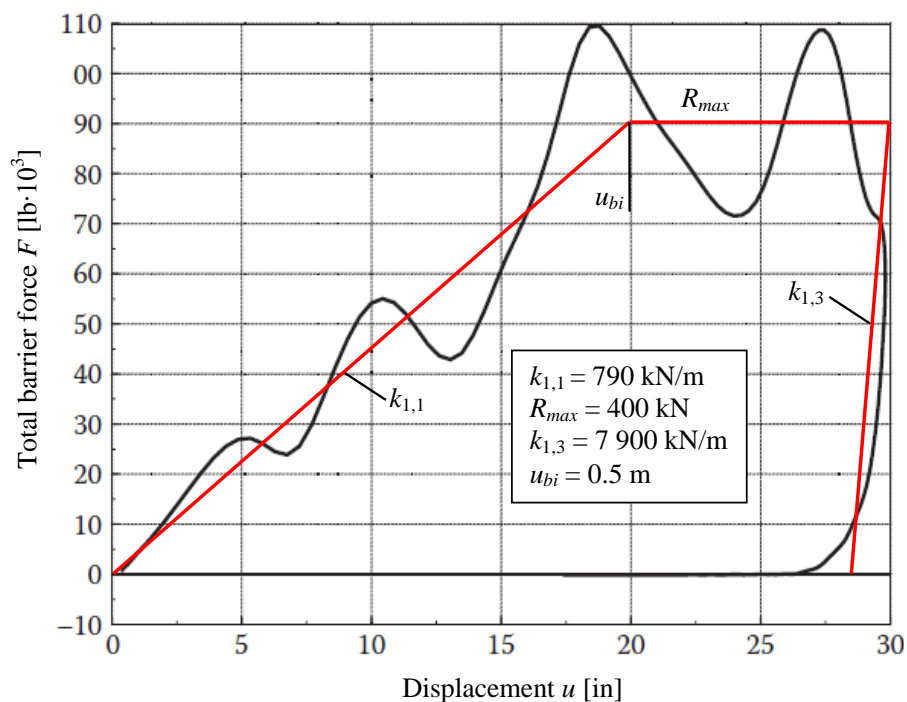
Figure 4.7   Force-displacement graphs from full frontal crash test (fixed barrier NCAP test) of a Toyota Corolla 2004 with a velocity of 15.6 m/s, obtained from load cells in NHTSA test no 5404, based on Struble (2014).

The results in Figure 4.7 clearly display a much higher stiffness than the results in Figure 4.6. This seems reasonable since, as discussed above, a full frontal impact

should exhibit a stiffer response. Figure 4.7 also indicates a maximum load capacity beyond which no further increase of load can be made, but where the deformations continues to grow.

Another crash test study is described in a paper by Takizawa, et al. (2005) for Honda R&D Co. Ltd., where load cell moving deformable barrier (LCMDB) crash tests were evaluated. Here both full width deformable barrier (FWDB) and offset deformable barrier (ODB) tests were studied. Two force-displacement graphs for a Honda from this paper with approximated bilinear curves superimposed on top can be seen in Figure 4.8.
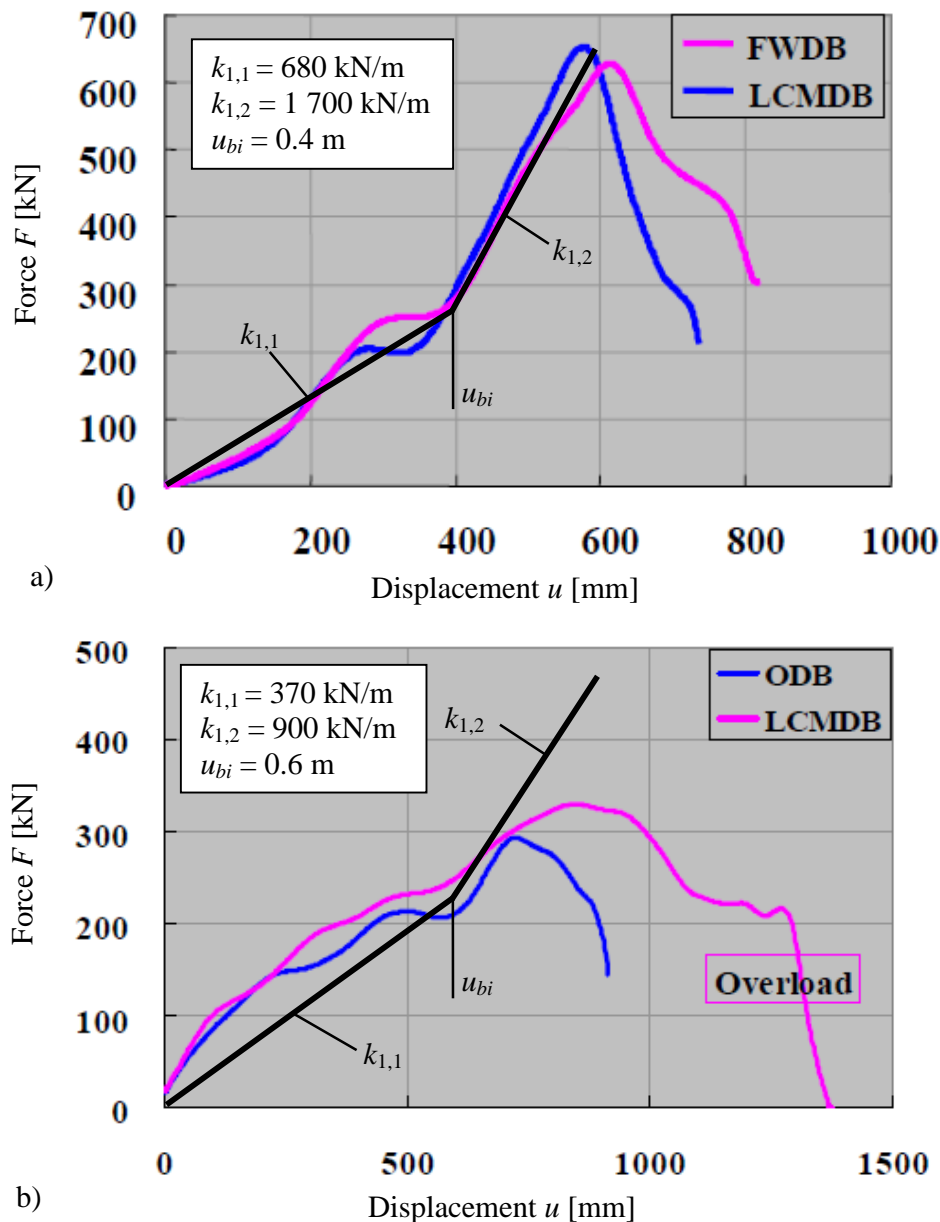
Figure 4.8   Force-displacement graphs from two different crash tests of Honda cars obtained from load cells, a) full width frontal impact with a velocity of 15.6 m/s and b) offset frontal impact with a velocity of 17.8 m/s, based on Takizawa, et al. (2005).

From these two tests one can see that the previous assumption about a doubled stiffness for full width impact, compared to offset impact, is reasonable.

The last crash test results studied are taken from a master thesis carried out at the University of Utah, Tolman (2008). In this thesis several results from FWRB tests were compared for different vehicles with different impact velocities. In Figure 4.9 are the results for a Volvo S40 presented in shape of force-displacement graphs, with approximated bilinear curves superimposed on top, for two different velocities.
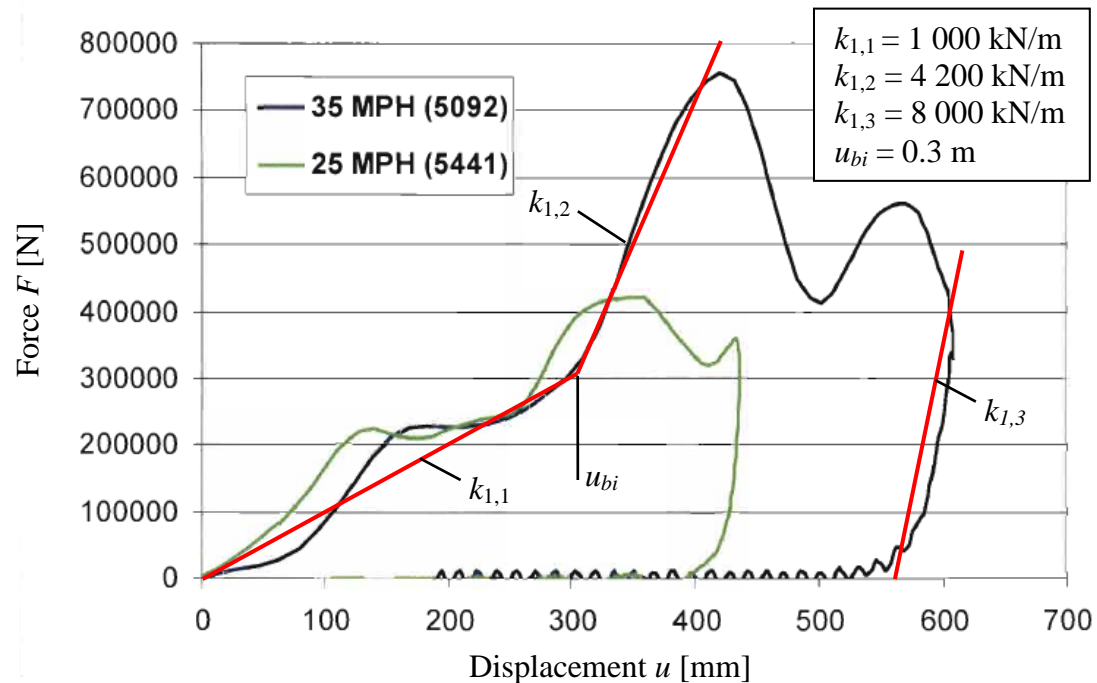
Figure 4.9   *Force-displacement graphs from two full width impact crash tests of a Volvo S40, one with a velocity of 11.2 m/s and one with 15.6 m/s. Results from NHTSA tests no 5092 and no 5441, data is obtained from load cells, based on Tolman (2008).*

From Figure 4.9 can it be concluded that the force-displacement relationship for different velocities shows a similar behaviour, and the same stiffnesses can, approximately, be used independent of the velocity. One can also see that this test shows a much higher stiffness than the former tests discussed. This is probably due to the full width barrier that is also rigid, and can thus not deform.

The respective calculated stiffnesses and breakpoints between them for all seven crash tests are presented together with the mean masses for each type of vehicle, in Table 4.3. The corresponding force-displacement curves, for an internal work equal to the kinetic energy before the impact for each vehicle, are illustrated in Figure 4.10. The stiffnesses from the ODB tests are here multiplied by two, as proposed earlier.

Table 4.3   *Frontal stiffness for different stages of loading and for different types of vehicles, based on Figure 4.6, Figure 4.7, Figure 4.8 and Figure 4.9.*

	m [kg]	$k_{1,1}$ [kN/m]	$k_{1,2}$ [kN/m]	$k_{1,3}$ [kN/m]	u_{bi} [m]
Medium family cars, ODB	1 300	520	2 400	12 000	0.70
Large saloon cars, ODB	1 700	200	1 800	8 000	0.50
MPV's (minivans), ODB	1 900	580	1 600	10 000	0.50
Toyota Corolla 04, FWRB	1 300	790	0	7 900	0.50
Honda, ODB	-	740	1 800	∞	0.60
Honda, FWDB	-	680	1 700	∞	0.40
Volvo S40, FWRB	1 600	1 000	4 200	8 000	0.30
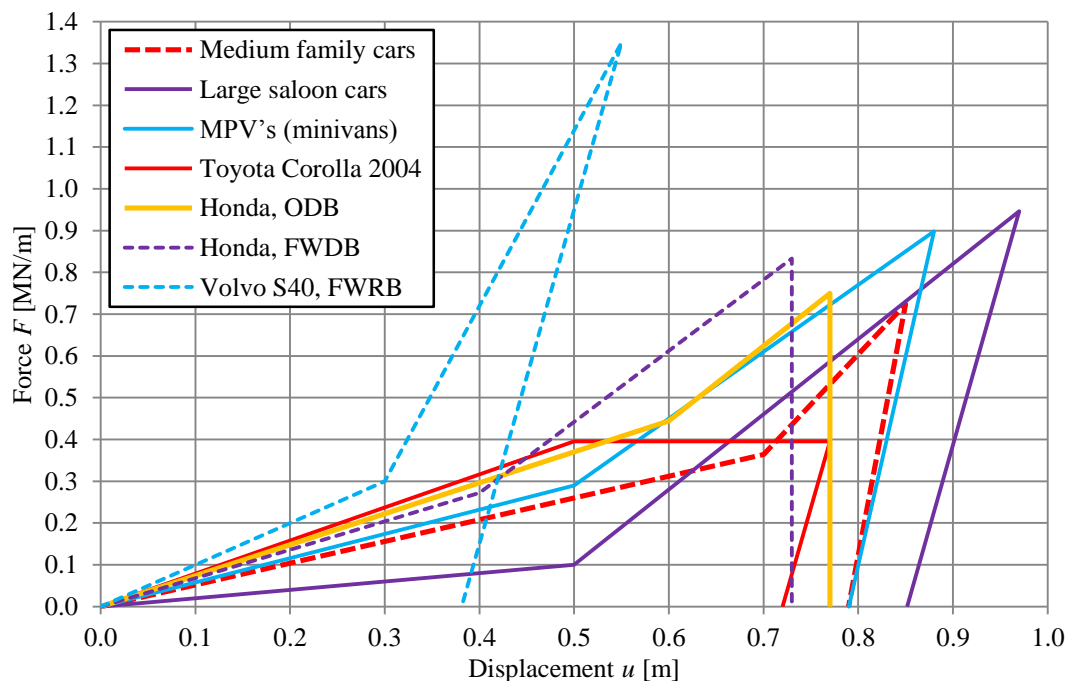
Figure 4.10   *Force-displacement diagrams for three different types of vehicles, data from Table 4.3. Internal work done for each type corresponds to the kinetic energy prior to impact.*

The behaviour of the different vehicles is quite similar, with a few exceptions, see Figure 4.10. The saloon cars generally have a large crumple zone and it is therefore possible to have a low stiffness. This fact together with their relatively high weight is the reason for the large deformations seen in this type of vehicle. The Toyota Corolla is the only vehicle that does not exhibit a stiffening behaviour after a certain displacement. Instead it shows an ideal plastic behaviour, which probably would look different in an impact with higher velocity, i.e. larger deformations. One of the vehicles has a much higher stiffness than all the others, the Volvo S40. The reasons therefore are hard to identify, one is that the barrier is rigid but that should not make such an apparent difference. The impact speed in this test, 15.6 m/s, was also lower than in some of the other tests. It has to be considered though, that the approach used

to determine all of the stiffnesses was very approximate, and the error margin is therefore of noticeable size.

4.1.2 Parameters for concrete beam

The concrete beam represents a low protective barrier of some kind and can, for simplicity reasons, be seen as simply supported, see Figure 4.11.

a)   b)
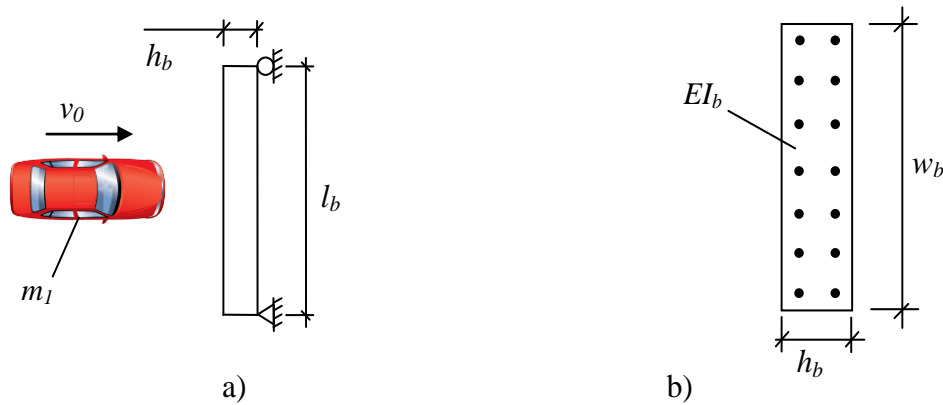
Figure 4.11   Illustration of the beam representing the barrier, a) top view and b) cross section. For dimensions and reinforcement specifications see Table 4.4.

A beam with reasonable geometry and amount of reinforcement is chosen, to be studied further in collision impact analyses in later sections, see Table 4.4. The section and stiffness properties are calculated according to Appendix G.

Table 4.4   Properties of the beam, representing a barrier, studied in this thesis.

Length l_b	5 m
Height h_b	0.3 m
Width w_b	1 m
Mass m_b	3600 kg
Concrete class	C30/37
E_c	33 GPa
Reinforcement	B500B Φ16 s100
E_s	200 GPa
Concrete cover c	40 mm
Effective height d	252 mm
I_I	$2.25 \cdot 10^9$ mm^4
I_{II}	$6.10 \cdot 10^8$ mm^4
$EI_b = E_c \cdot I_{II}$	18.30 MNm^2

4.2 Transformation of beam to spring-mass system

4.2.1 General principle

To be able to use the simplified 2DOF model for the collision, the beam needs to be transformed into a SDOF spring-mass system, see Figure 4.12. From this figure it is clear that the displacement in the system point of the beam and in the spring-mass system is the same. Here the system point coincides with the section with largest deflection in the beam, but it can also be chosen to be placed at the section where a point load is acting Johansson and Laine (2012). As said before, damping is neglected when dealing with impact loads due to the very short duration of the impact.
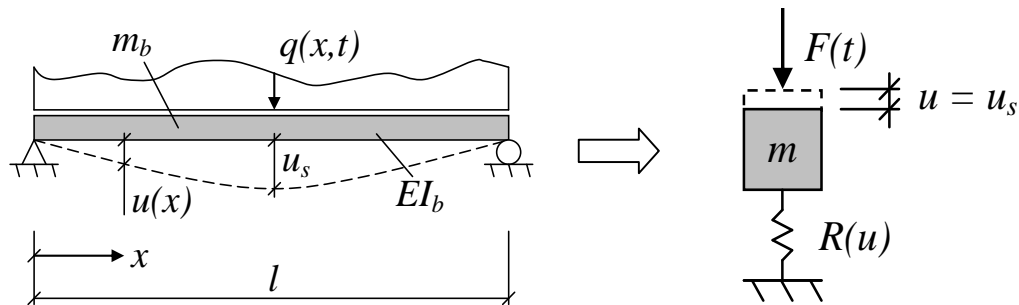
Figure 4.12   Illustration of how a loaded beam is transformed into an equivalent SDOF system.

The relationship between the properties of the beam and the SDOF system, assuming a linear elastic response in the spring, can be stated as

$$m = \kappa_m \cdot m_b \qquad (4.1)$$

$$k = \kappa_k \cdot k_b \qquad (4.2)$$

$$F = \kappa_F \cdot F_b \qquad (4.3)$$

where m_b and k_b are the mass and stiffness of the beam and F_b is the external force acting on the beam. κ_m, κ_k and κ_F are the corresponding transformation factors for the three properties. The equation of motion for a SDOF system without damping from equation (2.36)

$$m\ddot{u} + ku = F(t) \qquad (4.4)$$

can now be written as

$$\kappa_m m_b \ddot{u} + \kappa_k k_b u = \kappa_F F_b(t) \qquad (4.5)$$

By utilizing that the response in the beam under static load is

$$R_b(u) = k_b \cdot u \qquad (4.6)$$

equation (4.5) finally becomes

$$\kappa_m m_b \ddot{u} + \kappa_k R_b(u) = \kappa_F F_b(t) \tag{4.7}$$

The transformation factors are decided based on the theory of energy conservation between the beam model and the spring-mass system. The kinetic energy of the mass and the work done by the external and the internal force should in the two systems, according to this, be equal, Johansson and Laine (2012).

4.2.1.1 Conservation of kinetic energy

The conservation of kinetic energy between the two systems gives

$$E_k = \frac{m \cdot v_s^{\ 2}}{2} = \int_{x=0}^{x=l} \frac{m'(x) \cdot v(x)^2}{2} dx \tag{4.8}$$

where v_s is the velocity of the SDOF system as well as the system point and $m'(x)$ and $v(x)$ are the mass per unit length and the velocity at section x of the beam respectively.

For a beam with constant mass per unit length equation (4.8) becomes

$$m \cdot v_s^{\ 2} = \frac{m_b}{l} \int_{x=0}^{x=l} v(x)^2 dx \tag{4.9}$$

By using that

$$v_s = \frac{\Delta u_s}{\Delta t} \tag{4.10}$$

and

$$v(x) = \frac{\Delta u(x)}{\Delta t} \tag{4.11}$$

where Δu_s and $\Delta u(x)$ are the displacements at the system point and along the beam respectively, equation (4.9) can, for an arbitrary time step, be written as

$$m \cdot u_s^{\ 2} = \frac{m_b}{l} \int_{x=0}^{x=l} u(x)^2 dx \tag{4.12}$$

By combining this with equation (4.1) the transformation factor can be stated as

$$\kappa_m = \frac{1}{l} \int_{x=0}^{x=l} \frac{u(x)^2}{u_s^{\ 2}} dx \tag{4.13}$$

4.2.1.2 Conservation of external work

The conservation of external work between the two systems gives

$$W_e = F \cdot u_s = \int_{x=0}^{x=l} q(x) \cdot u(x) dx \tag{4.14}$$

where $q(x)$ is the load per unit length along the beam. The total external force acting on the beam is

$$F_b = \int_{x=0}^{x=l} q(x) dx = \int_{x=0}^{x=l} \frac{F_b}{l} dx \tag{4.15}$$

and if inserted in equation (4.14)

$$F \cdot u_s = \frac{F_b}{l} \cdot \int_{x=0}^{x=l} u(x) dx \tag{4.16}$$

By now using equation (4.3) the transformation factor can be written as

$$\kappa_F = \frac{1}{l} \int_{x=0}^{x=l} \frac{u(x)}{u_s} dx \tag{4.17}$$

For a beam with concentrated load equation (4.14) becomes

$$W_e = F \cdot u_s = F_b \cdot u_s \tag{4.18}$$

which will, by using equation (4.3), give a transformation factor of

$$\kappa_F = \frac{u_s}{u_s} = 1 \tag{4.19}$$

4.2.1.3 Conservation of internal work

The conservation of internal work between the systems finally needs to be studied. The equilibrium yields

$$W_i = \frac{ku_s^2}{2} = \frac{1}{2} \int_{x=0}^{x=l} \left(\frac{N(x)^2}{EA} + \frac{\beta_{shear}V(x)^2}{GA} + M(x) \cdot u''(x) \right) dx \tag{4.20}$$

where $N(x)$, $V(x)$ and $M(x)$ are normal force, shear force and bending moment along the beam and E is the elastic modulus, A is the cross sectional area, β_{shear} is a factor regarding the shear stress, G is the shear modulus and $u''(x)$ is the curvature of the beam. In general the contributions from normal and shear force are small in comparison to the effect of the moment, thus they can be neglected and equation (4.20) is simplified to

$$ku_s^2 = \int\limits_{x=0}^{x=l} M(x) \cdot u''(x)dx \qquad (4.21)$$

By combining this with equation (4.2), the transformation factor becomes

$$\kappa_k = \int\limits_{x=0}^{x=l} \frac{M(x) \cdot u''(x)}{k_b \cdot u_s^2}dx \qquad (4.22)$$

The stiffness of the beam can also be written as

$$k_b = \frac{F_b}{u_s} \qquad (4.23)$$

and by using this the transformation factor can now be written

$$\kappa_k = \int\limits_{x=0}^{x=l} \frac{M(x) \cdot u''(x)}{F_b \cdot u_s}dx \qquad (4.24)$$

4.2.2 Determination of transformation factors

According to Chapter 5 in Biggs (1964)

$$\kappa_k = \kappa_F \qquad (4.25)$$

This fact can be used by dividing all terms in equation (4.5) by κ_F

$$\frac{\kappa_m}{\kappa_F}m_b\ddot{u} + \frac{\kappa_k}{\kappa_F}k_b u = F_b(t) \qquad (4.26)$$

and by introducing the factor κ_{mF}

$$\kappa_{mF} = \frac{\kappa_m}{\kappa_F} \qquad (4.27)$$

Equation (4.26) can now be stated as

$$\kappa_{mF}m_b\ddot{u} + k_b u = F_b(t) \qquad (4.28)$$

which shows that only the mass of the beam needs to be transformed when the equation of motion is formed for the SDOF system.

To determine both κ_m and κ_F the variables $u(x)$ and u_s needs to be determined. u_s can be determined from $u(x)$ by defining the position of the system point, which is chosen to coincide with the point load. The factor κ_F, is as stated in equation (4.19), equal to 1 for a point load.

4.2.2.1 Elastic response for a point load

When the beam is assumed to have an elastic response and is subjected to a point load, the displacements $u(x)$ and u_s can be defined as

$$u_s = \frac{F_b l^3}{3EI_b} \alpha^2 \beta^2 \qquad (4.29)$$

and

$$u(x) = \begin{cases} \dfrac{F_b \beta}{6EI_b}((1-\beta^2)l^2 x - x^3) & 0 \le x \le \alpha l \\[4mm] \dfrac{F_b \alpha}{6EI_b}((1-\alpha^2)l^2(l-x)-(l-x)^3) & \alpha l \le x \le l \end{cases} \quad \text{for} \qquad (4.30)$$

where α, β, F_b, l, x and EI_b are explained in Figure 4.13, and $\beta = 1-\alpha$, based on Lundh (2000).
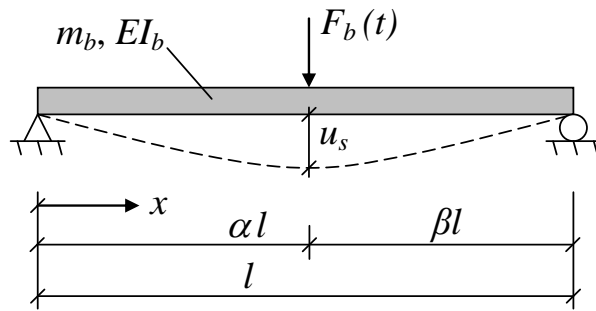
Figure 4.13   Elastic response of a beam subjected to a point load.

By using equation (4.13) together with equation (4.29) and (4.30), the transformation factor can be stated as

$$\kappa_{m,el} = \frac{1}{l}\int_{x=0}^{x=\alpha l} \frac{\left(\dfrac{F_b \beta}{6EI_b}((1-\beta^2)l^2 x - x^3)\right)^2}{\left(\dfrac{F_b l^3}{3EI_b}\alpha^2 \beta^2\right)^2}\,dx\ldots$$

$$+\frac{1}{l}\int_{x=\alpha l}^{x=l} \frac{\left(\dfrac{F_b \alpha}{6EI_b}((1-\alpha^2)l^2(l-x)-(l-x)^3)\right)^2}{\left(\dfrac{F_b l^3}{3EI_b}\alpha^2 \beta^2\right)^2}\,dx \qquad (4.31)$$

and after solving the integrals it can be written as a function of α and β

$$\kappa_{m,el} = \frac{\alpha^3}{28\beta^2} + \frac{(23\alpha^2 + 10\alpha + 2)\beta}{105\alpha^2} + \frac{\beta^2 - 2}{12\alpha} - \frac{\alpha}{10\beta^2} + \frac{1}{12\alpha\beta^2} + \frac{\alpha}{10} \qquad (4.32)$$

4.2.2.2 Plastic response for a point load

If the beam instead is assumed to have a plastic response when it is subjected to a point load, the displacement $u(x)$ can be defined as

$$u(x) = \begin{cases} u_s \dfrac{x}{\alpha l} & 0 \le x \le \alpha l \\[2mm] u_s \dfrac{l-x}{\beta l} & \alpha l \le x \le l \end{cases} \quad \text{for} \qquad (4.33)$$

where α, β, x and l are explained in Figure 4.14.
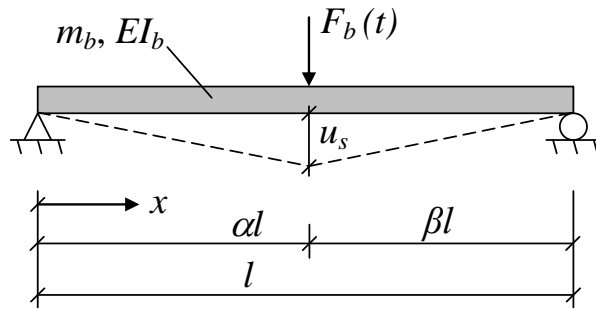
Figure 4.14   Plastic response of a beam subjected to a point load.

By using equation (4.13) together with equation (4.33), the transformation factor for the mass is then stated as

$$\kappa_{m,el} = \frac{1}{l} \int_{x=0}^{x=\alpha l} \frac{\left(u_s \dfrac{x}{\alpha l}\right)^2}{u_s^{\,2}} dx + \frac{1}{l} \int_{x=\alpha l}^{x=l} \frac{\left(u_s \dfrac{l-x}{\beta l}\right)^2}{u_s^{\,2}} dx \qquad (4.34)$$

and finally the transformation factor can be defined as a function of α and β

$$\kappa_{m,pl} = \frac{\alpha}{3} + \frac{1}{\beta^2}\left(\frac{1}{3} - \alpha + \alpha^2 - \frac{\alpha^3}{3}\right) = \frac{1}{3} \qquad (4.35)$$

4.2.2.3 Transformation factors for different cases

The transformation factors κ_m, κ_F and κ_{mF} are now calculated for different values of α and β, using equations (4.19), (4.32) and (4.35), for both the elastic and the plastic response and the results are presented in Table 4.5.

Table 4.5   Transformation factors for point loads at different distances from the support, with the system point coinciding with the point load.

α	0.5	0.4	0.3	0.2	0.1
Elastic response					
κ_m	0.486	0.518	0.642	1.011	2.803
κ_F	1.000	1.000	1.000	1.000	1.000
κ_{mF}	0.486	0.518	0.642	1.011	2.803
Plastic response					
κ_m	0.333	0.333	0.333	0.333	0.333
κ_F	1.000	1.000	1.000	1.000	1.000
κ_{mF}	0.333	0.333	0.333	0.333	0.333

In reality, the incoming object in a collision always has a certain area and the load should therefore more accurately be treated as a distributed load, see Figure 4.15.
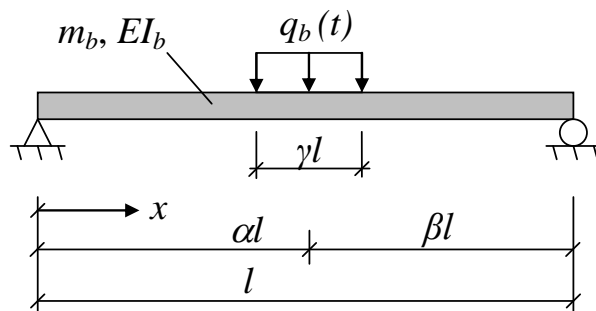
Figure 4.15   Beam subjected to a distributed load with limited distribution.

Transformation factors for a distributed load, acting at different distances from the support and with different lengths of the distribution, were calculated numerically and are presented in Table 4.6, Table 4.7 and Table 4.8, based on work by Johansson (2014b). In these tables $\gamma = 0$ corresponds to a point load, and only the elastic response is treated for the distributed load.

Table 4.6   *Comparison of transformation factors for different values of the distribution γ, when α = 0.5.*

$\alpha = 0.5$					
γ	0.0	0.1	0.2	0.3	0.4
Elastic response					
κ_m	0.486	0.486	0.488	0.491	0.494
κ_F	1.000	0.995	0.982	0.961	0.933
κ_{mF}	0.486	0.489	0.497	0.511	0.529

Table 4.7   *Comparison of transformation factors for different values of the distribution γ, when α = 0.3.*

$\alpha = 0.3$					
γ	0.0	0.1	0.2	0.3	0.4
Elastic response					
κ_m	0.642	0.644	0.650	0.658	0.668
κ_F	1.000	0.994	0.979	0.955	0.919
κ_{mF}	0.642	0.648	0.664	0.689	0.727

Table 4.8   *Comparison of transformation factors for different values of the distribution γ, when α = 0.1.*

$\alpha = 0.1$			
γ	0.0	0.1	0.2
Elastic response			
κ_m	2.803	2.853	2.988
κ_F	1.000	0.955	0.942
κ_{mF}	2.803	2.989	3.171

When studying Table 4.6, Table 4.7 and Table 4.8 one can conclude that the difference in the transformation factor κ_{mF} is slightly increased when the distribution is larger. This difference also grows larger when α get smaller, i.e. when the load acts close to the support. As can be seen in Table 4.6, when the load acts at midspan, the difference in κ_{mF} is only about 8 percent when $\gamma = 0.4$ compared to a point load, i.e. $\gamma = 0$. For the case when $\alpha = 0.3$, see Table 4.7, the same difference in κ_{mF} is about 12 percent. When $\alpha = 0.1$, see Table 4.8, the difference in κ_{mF} is about 12 percent when $\gamma = 0.2$ compared to a point load. With this in mind, it can be assumed safe to treat a load with limited distribution as a concentrated point load, as long as the distribution is not too large and not acting too close to the support.

4.2.3 Stiffness of simply supported beam subjected to a point load

During the elastic response, the stiffness of the beam k_b can be determined by using the fundamental correlation between load and displacement. For a point load this correlation can be written as

$$F_b = k_b \cdot u_s \tag{4.36}$$

If now the definition of u_s in equation (4.29) is utilized together with equation (4.36), the stiffness k_b as a function of α and β can be defined as

$$k_b = \frac{3EI_b}{l^3 \alpha^2 \beta^2} \tag{4.37}$$

The beam stiffness was calculated for different values of α using equation (4.37) and the results and presented in Table 4.9.

Table 4.9   Beam stiffness k_b for point loads at different distances from the support, with the system point coinciding with the point load.

α	0.5	0.4	0.3	0.2	0.1
Elastic response					
k_b	$48.00 \cdot \left(\frac{EI_b}{l^3} \right)$	$52.08 \cdot \left(\frac{EI_b}{l^3} \right)$	$68.03 \cdot \left(\frac{EI_b}{l^3} \right)$	$117.2 \cdot \left(\frac{EI_b}{l^3} \right)$	$370.4 \cdot \left(\frac{EI_b}{l^3} \right)$

In Table 4.9 it can be seen that the beam stiffness k_b is proportional to the bending stiffness of the beam EI_b, while it is inversely proportional to the length of the beam to the power three, l^3. This means that the length of the beam will have much more influence on the stiffness than the bending stiffness EI_b. Regarding the position of loading, the stiffness grows exponentially when the load acts closer and closer to the support. The stiffness is almost eight times higher when $\alpha = 0.1$ compared to loading at midspan.

4.2.4 Equivalent static load

Since most civil engineers are more familiar working with static loads, it is convenient to translate the dynamic impulse load into an equivalent static load. This is done by determining the static load F_{sta} that generates the same amount of exterior work W_e on the structure as the dynamic impulse I. For an elastic structure the equivalent static load is obtained by using the relationship for the external work

$$W_y = \frac{F_{sta}u_{el}}{2} \qquad (4.38)$$

which if combined with equation (4.39)

$$W_y = \frac{k_b u_{el}^2}{2} \qquad (4.39)$$

results in

$$F_{sta} = k_b u_{el} \qquad (4.40)$$

where k_b is the stiffness of the beam and u_{el} is the elastic deformation. An alternative way to find the equivalent static load for an elastic response is to use the load factor β_{el} discussed in section 3.2.1.

4.3 Impact load according to Eurocode

Impact is, according to annex C in Eurocode 1-7, defined in the following way: *"Impact is an interaction phenomenon between a moving object and a structure, in which the kinetic energy of the object is suddenly transformed into energy of deformation"*, CEN (2010).

According to Eurocode, actions that depend on impact should be determined by a dynamic analysis or represented by an equivalent static force that gives the same effects on the structure. For cars the collision force should be applied at an height h of 0.5 m above the carriageway, over an application area, a, of 0.25 m (height) × 1.5 m (width) or the member width. For trucks the collision force may be applied at any height between 0.5 m-1.5 m above the carriageway and over an application area of 0.5 m (height) x 1.5 m (width) or the member width, see Figure 4.16.
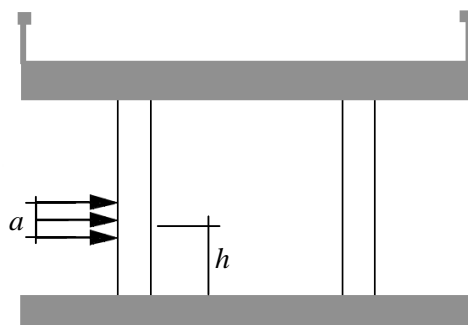
Figure 4.16   Application area of collision force on supporting substructure, based on CEN (2010).

Eurocode uses two different approaches to determine the equivalent static force. The first approach is based on suggested equivalent static forces in the direction of vehicle travel, given in section 4.3 of EC 1-7. These have a magnitude of 1 000 kN, 750 kN and 500 kN for structures adjacent to national roads, rural roads and roads in urban areas, respectively, CEN (2010). It should be noted that this method involves many uncertainties since the effects of mass and stiffness for both the vehicle and structure is not taken into account here. Therefore the result may be inaccurate, Al-Thairy and Wang (2013).

The alternative approach can be found in annex C in EC 1-7, called the dynamic impulse approach, where a distinction is made between hard impact and soft impact. For hard impact the colliding object is assumed to deform linearly during the impact phase while the structure is considered to be rigid and immovable. For a soft impact it is the other way around, the colliding object is considered as rigid and the structure is assumed to absorb all of the impact energy. This means that preventive measures should be made so that the ductility of the structure is sufficient enough to absorb the total kinetic energy of the colliding object. The maximum resulting dynamic interaction force is derived by letting the initial kinetic energy be equal to the elastic strain energy of the colliding object, for a complete derivation see section 3.2.1.

$$\frac{m \cdot v^2}{2} = \frac{F^2}{2k} \tag{4.41}$$

So the force is

$$F = v_r \sqrt{k \cdot m} \tag{4.42}$$

where v_r is the object velocity at impact, k is the equivalent elastic stiffness of the object in case of hard impact or the stiffness of the structure in case of soft impact and m is the mass of the incoming colliding object.

The force may also be considered as a rectangular pulse on the surface of the structure with a pulse duration, Δt, that is derived by substituting equation (4.42) into the momentum conservation stated in equation (4.43).

$$F \cdot \Delta t = m \cdot v_r \tag{4.43}$$

which gives

$$v_r \sqrt{k \cdot m} \cdot \Delta t = m \cdot v_r \tag{4.44}$$

that leads to

$$\Delta t = \sqrt{\frac{m}{k}} \tag{4.45}$$

It is not specified in the code but the way that equation (4.43) is stated implies that a plastic material response for the vehicle is used. If an elastic response was used the change in momentum would create an impulse twice as large compared to the one used here, see also section 3.2.1.

Equation (4.42) gives the maximum dynamic force on the surface of the structure, but inside the structure these forces may give rise to dynamic effects. An upper limit for these effects can be determined if the structure is considered elastic and the load is applied by a step function. In that case the dynamic amplification factor $\varphi_{dyn} = 2.0$. If the rise time of the impulse is taken into consideration, calculations will lead to amplification factors ranging from below 1.0 up to 1.8, depending on the dynamic characteristics of both structure and object. For a general case it is recommended that a direct dynamical analysis is used to determine φ_{dyn} CEN (2010). The amplification factor corresponds well to the load factor β_{el} described in section 3.2.1, even though it is only derived for elastic material response.

In this approach either the deformations of the impacting object or the structure is not considered depending on the assumption of hard or soft impact. This is a simplification since in most cases both the vehicle and the structure will undergo some deformation and hence absorb some of the impact energy. This means that the impact force between the vehicle and structure is overestimated for hard impact and underestimated for soft impact, Al-Thairy and Wang (2013).

5 Collision Impact on a Simply Supported Beam

This chapter presents and discusses the results from two computational models, the 2DOF system and a FE model, and compares the difference in their responses.

5.1 2DOF - Effect of impact position on a beam

To analyse the effect of the position of impact on a beam, the theory of beam to spring-mass system transformation from section 0 was implemented in the 2DOF algorithm, described in Chapter 3. The impact load is seen as a point load, meaning that the distribution is seen as infinitely small. The mass m_b was adjusted using the transformation factor $\kappa_{m,el}$ from equation (4.32) giving the corresponding mass in the 2DOF system m_2 and the stiffness of the beam k_b was calculated using equation (4.37), see Appendix G. This means that the beam is seen as both stiffer and heavier when the load is applied closer to the support. This can be seen in Figure 5.1 where the relative size of the mass and stiffness, $k_{b,rel}$ and $\kappa_{m,el,rel}$, is plotted against the loading position α on the beam, which describes the magnitude of the parameter in comparison to when loading at midspan, i.e. $\alpha = 0.5$, see equation (5.1) and (5.2).

$$k_{b,rel} = \frac{k_b(\alpha)}{k_b(0.5)} \tag{5.1}$$

$$\kappa_{m,el,rel} = \frac{\kappa_{m,el}(\alpha)}{\kappa_{m,el}(0.5)} \tag{5.2}$$
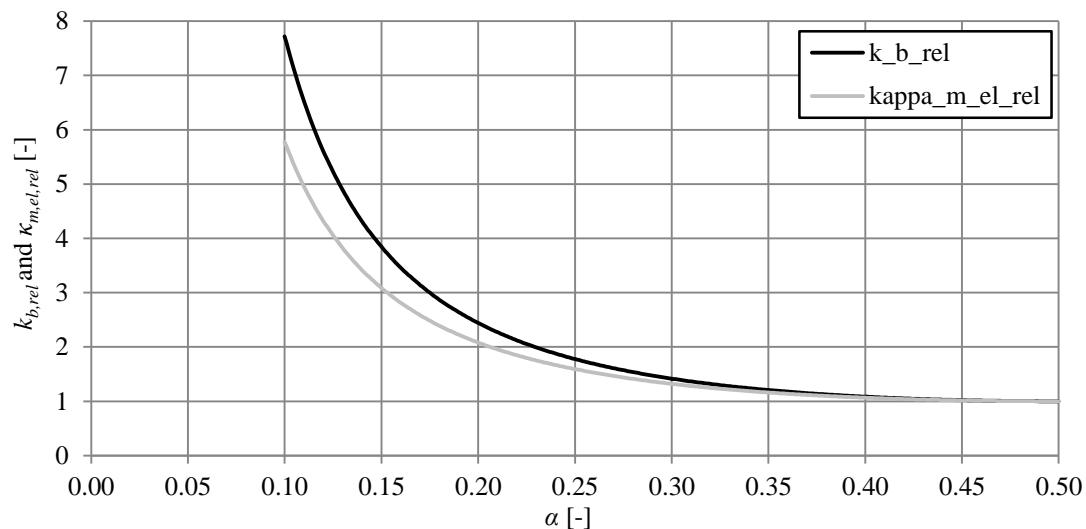
Figure 5.1   Relative size of the mass and stiffness is plotted against the loading position.

Not only the mass and stiffness of the beam will grow larger closer to the support, but also the eigenfrequency of the beam f_b. This is because k_b changes more than $\kappa_{m,el}$ and can be understood from equation (5.3), which is based on equation (2.41).

$$f_b(\alpha) = \frac{1}{2\pi} \sqrt{\frac{k_b}{\kappa_{m,el} \cdot m_b}} \quad [\text{Hz}] \tag{5.3}$$

The relative size of the eigenfrequency $f_{b,rel}$, see equation (5.4), and the theoretical natural frequency $f_{natural}$ of the beam are plotted against α in Figure 5.2.

$$f_{b,rel} = \frac{f_b(\alpha)}{f_{natural}} \tag{5.4}$$

The difference between these is small close to midspan but is over twenty percent at $\alpha = 0.05$, which could lead to a difference in response between the 2DOF and the FE model.
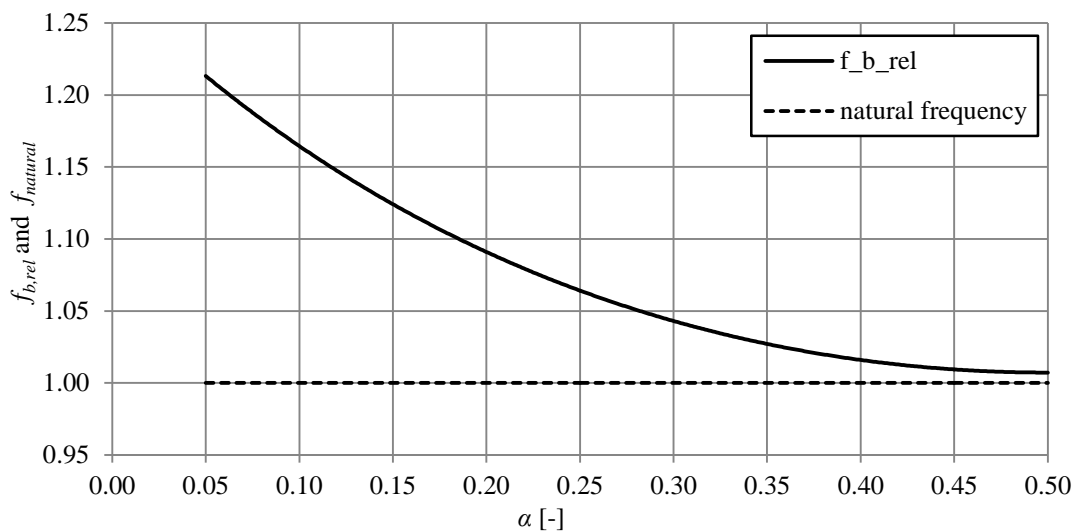
Figure 5.2   Relative size of the calculated frequency of the beam and the theoretical natural frequency is plotted against the loading position.

The study in this section is based on the concrete beam described in section 4.1.2. The velocity v_0 of the incoming object is set to 20 m/s, the mass m_1 is set to 1 000 kg and the stiffness k_1 is set to 300 kN/m. These values correspond sufficiently well with a vehicle, and the same stiffness is recommended in Eurocode, see section 4.3. The stiffness values are then varied to create five different property sets for the analyses, where property set 1 corresponds to the original case described above, see Table 5.1.

CHALMERS, *Civil and Environmental Engineering*, Master's Thesis 2014:80

Table 5.1   The different sets of properties used in the analyses.

Property set number	Spring stiffness k_1 [kN/m]	EI_b [MNm^2]
1	300	18.302
2	75	18.302
3	1 200	18.302
4	300	4.576
5	300	73.208

The study is first performed with the original values for the stiffnesses, while then also the other property sets are analysed. In the following sections are only results presented for some of the property sets, but all of the results can be seen in Appendix D.

5.1.1 Original beam – Property set 1

The first study is made with the exact same beam as described in section 4.1.2. The results are presented in form of graphs for how the reaction force R, displacement u and velocity v for the two bodies depend on time during the impact. Five different positions of impact, from $\alpha = 0.5$ to $\alpha = 0.1$, are treated and described in this section. See Figure 5.3 for the response of the incoming object and Figure 5.4 for the response of the beam.

In Figure 5.3 it can be seen that the responses for the incoming object does not change very much when α varies. The reaction force R_1 is a little bit higher and the maximum force is reached a little bit earlier for lower α values. The displacement u_{bi} and velocity v_1 are on the other hand nearly identical for the different loading positions. This is probably due to that the stiffness of the beam is, already in midspan, over twenty times larger than the stiffness of the incoming object. The influence of the increased stiffness closer to the support is therefore negligible.

If instead Figure 5.4 is studied, it is clear that the responses differs a little bit more for the beam. The reaction force R_2 is this time lower for lower values of α, which is the opposite case compared to the force R_1. This may seem odd since from a static point of view a higher force from the incoming object should result in a higher reaction force in the beam. The reason for this however is that the load factor β_{el} decreases when α decreases, in this particular case. When α decreases both the frequency ratio and the mass ratio decreases. This reasoning can be seen in the graphs in Figure 3.12, together with the fact that the frequency ratio is roughly 0.27 and the mass ratio 0.57 when the impact load is applied at midspan.

For the displacement u_2 and velocity v_2 the difference is really significant. The values gets smaller and smaller with decreasing α while the shape of the graphs is virtually maintained. This is understandable since a higher stiffness and larger mass should give smaller displacements and velocities.
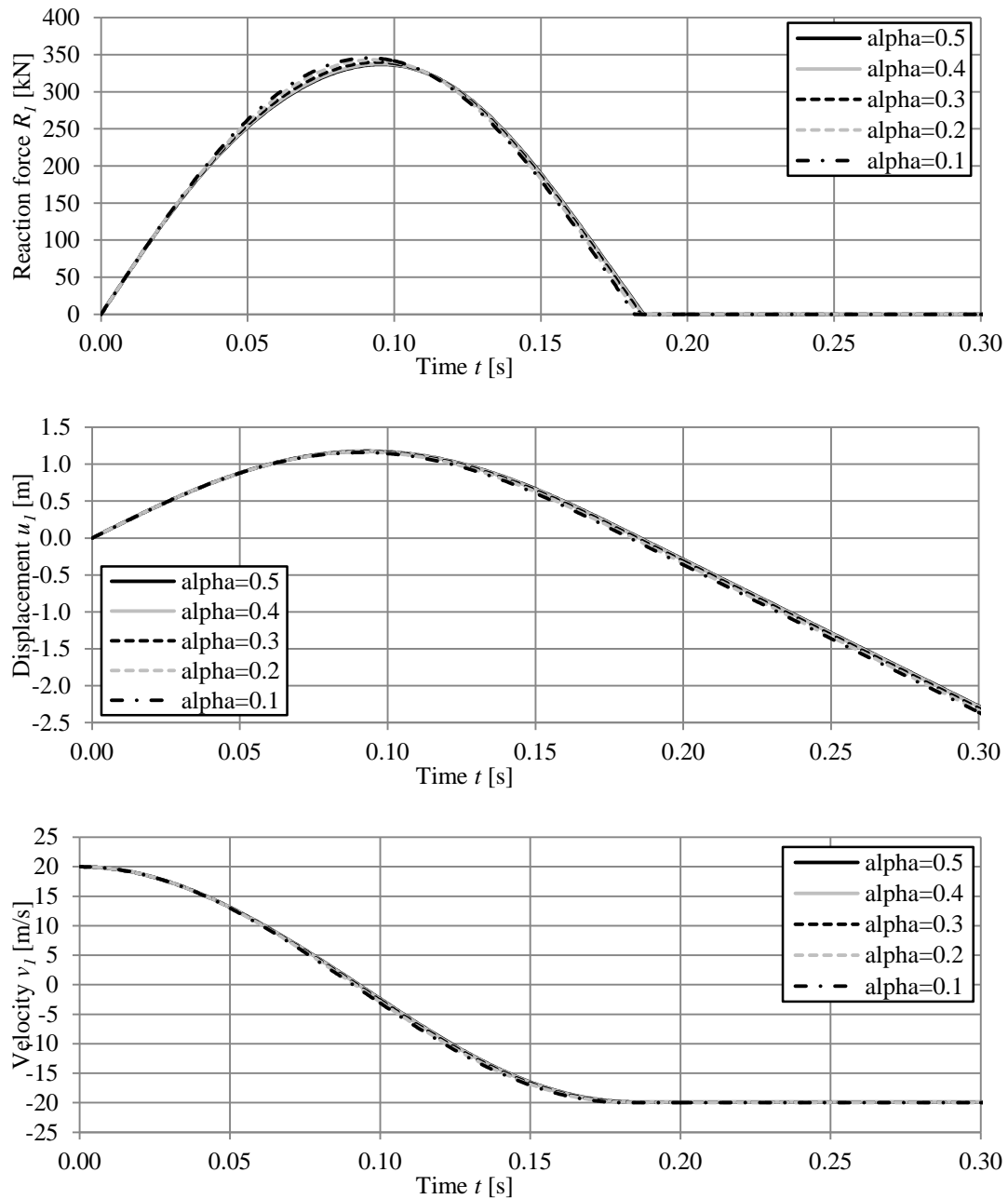
Figure 5.3   Results from the simulated collision describing the differences in position of impact, for the incoming object. Reaction force R_1, displacement u_1 and velocity v_1 are plotted against time.

CHALMERS, *Civil and Environmental Engineering*, Master's Thesis 2014:80
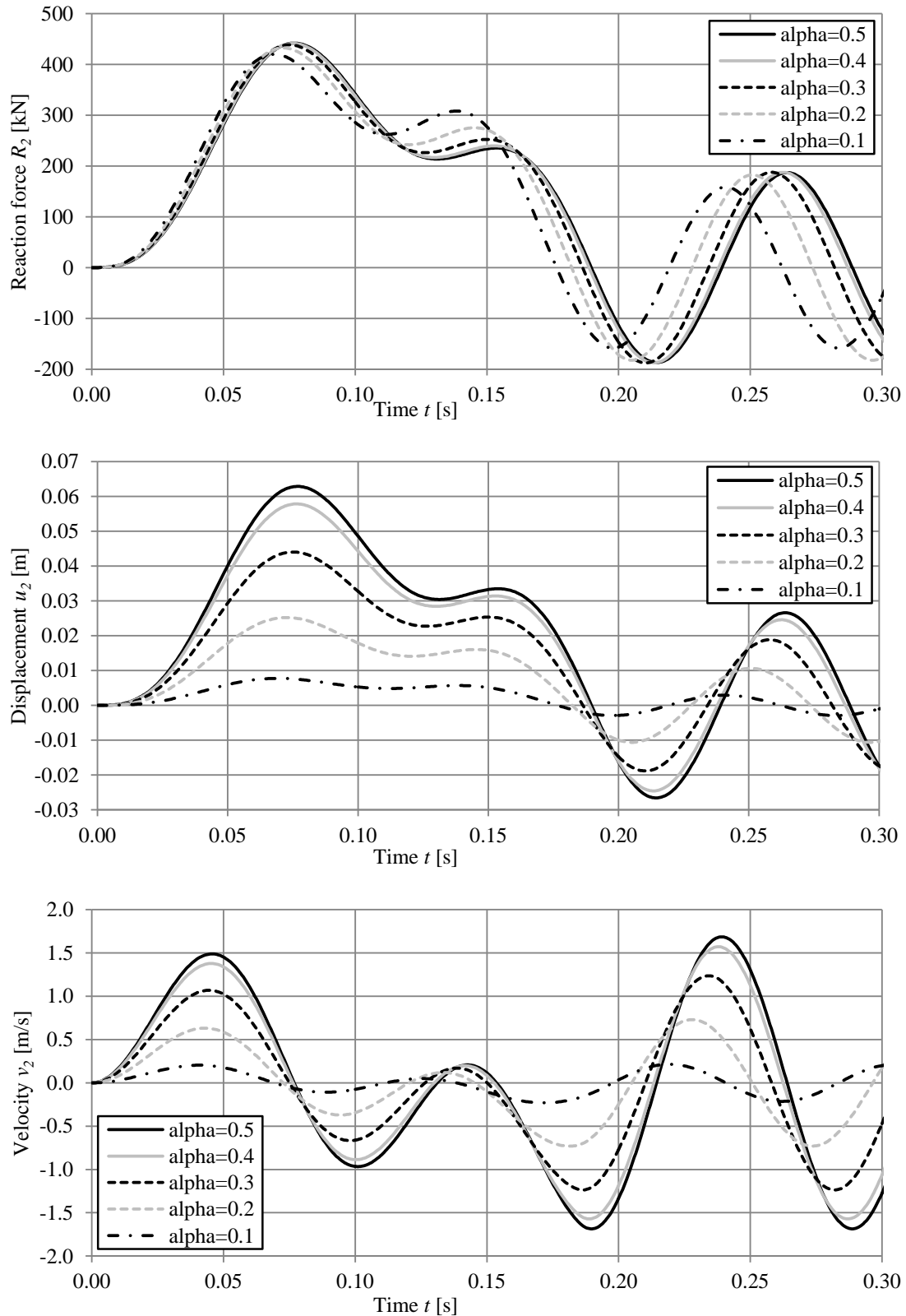
Figure 5.4 *Results from the simulated collision describing the differences in position of impact, for the beam. Reaction force R₂, displacement u₂ and velocity v₂ are plotted against time.*

5.1.2 Effect of beam stiffness

5.1.2.1 Stiffer beam – Property set 5

The beam from section 4.1.2, studied in the previous section, is now made four times as stiff, to be able to examine the difference in response. The results are again presented in form of graphs, but this time only displaying how the reaction force R for the two bodies varies during the impact. Five different positions of impact are treated and described here with the corresponding value of α, see Figure 5.5. The rest of the results can be found in Appendix D.
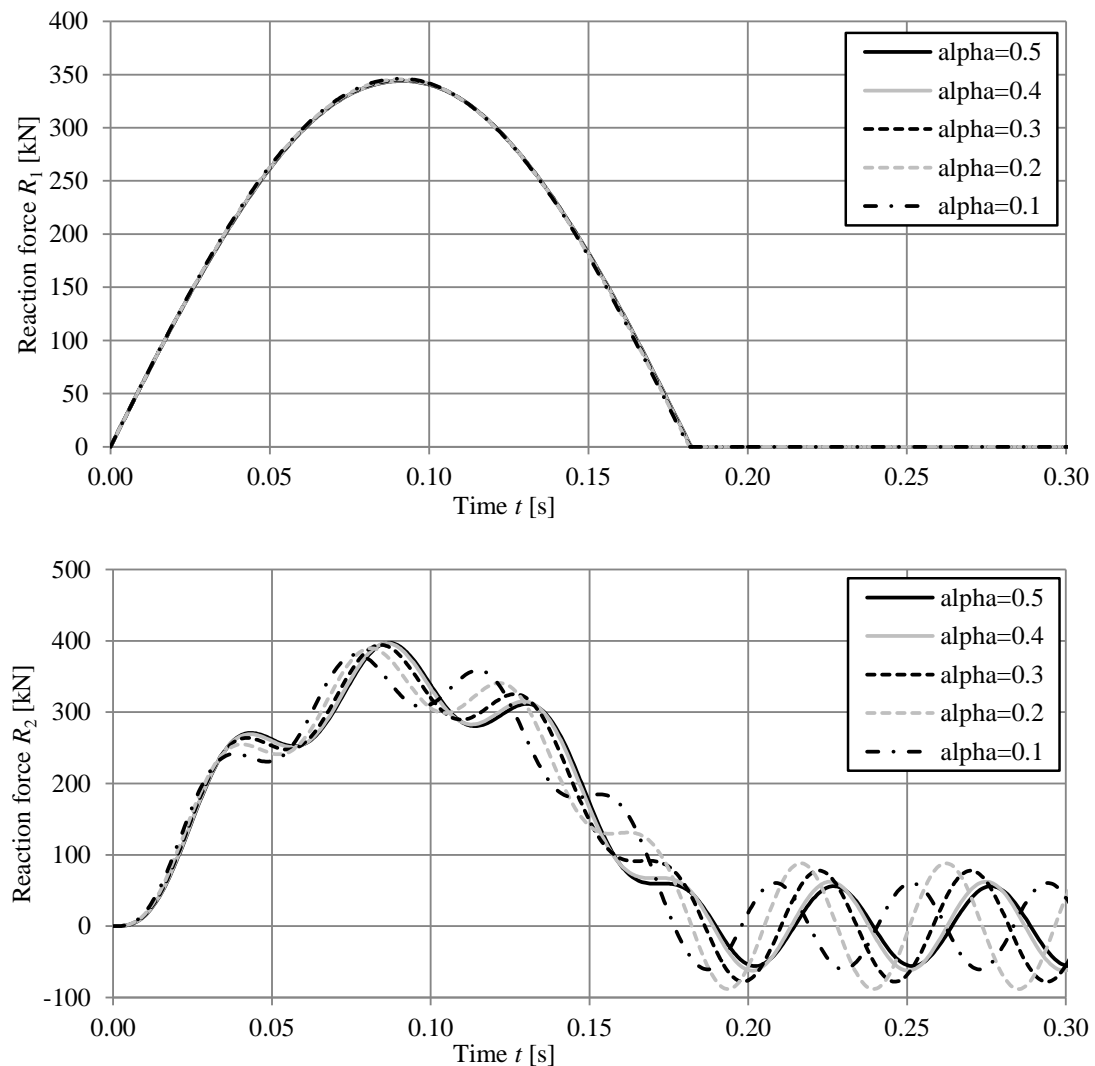
Figure 5.5   *Results from the simulated collision with a stiffer beam, describing the differences in position of impact for both the incoming object and the beam.*

The reaction force R_1 in the object displays in this case almost the exact same response regardless the position of loading, see Figure 5.5. The reason is the same as discussed in the previous case, that the beam is so much stiffer than the colliding object. And this time the beam is even stiffer, making it over 80 times as stiff as the object when loading at midspan. The reaction force in the beam R_2 behaves in a similar way as for the original beam, when loading at different positions.

5.1.2.2 Softer beam – Property set 4

The same beam from section 4.1.2 is now made one fourth as stiff, to be able to examine new differences in the response. The results are again presented in form of graphs, displaying how the reaction force R for the two bodies varies during the impact. Five different positions of impact are treated and described here with the corresponding value of α, see Figure 5.6. The rest of the results can be found in Appendix D.
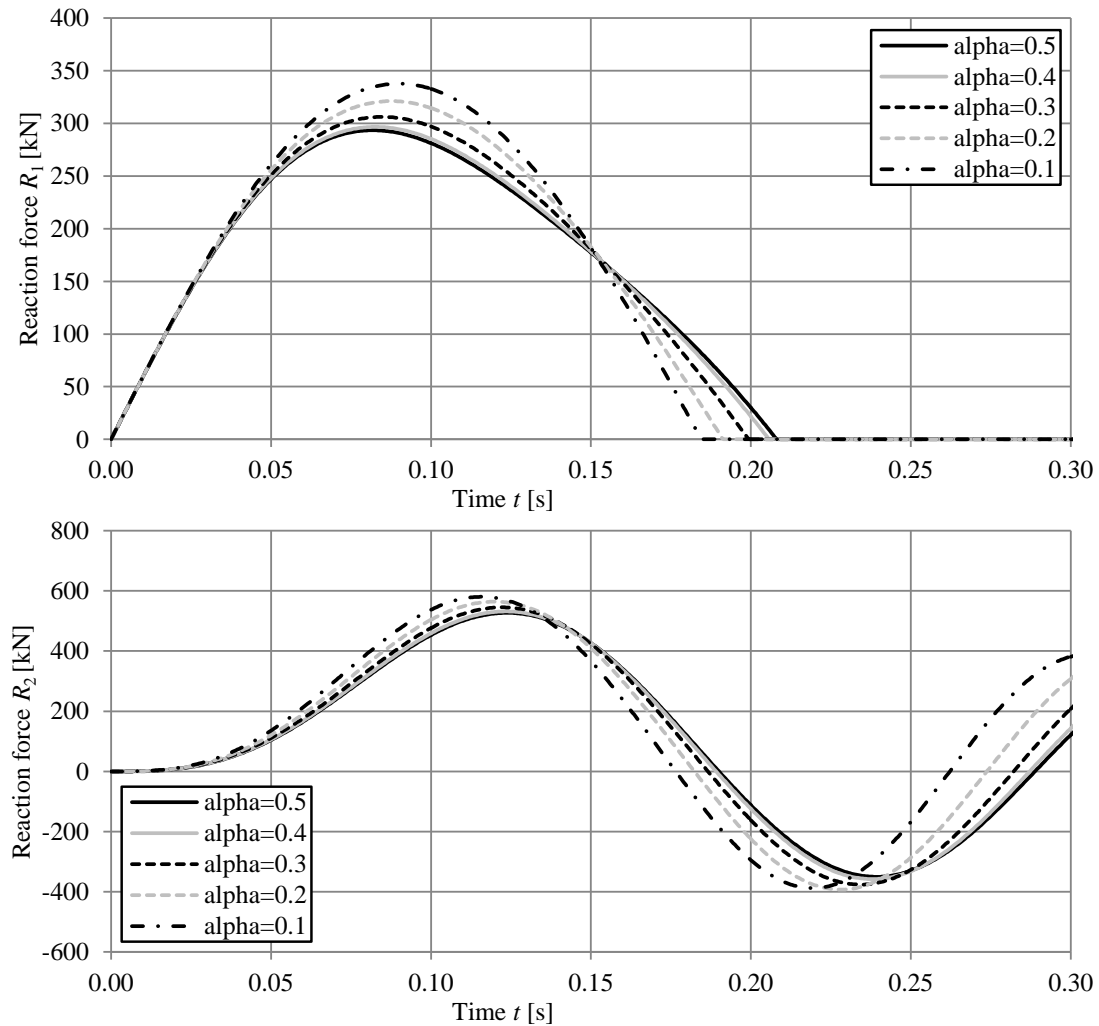
Figure 5.6   Results from the simulated collision with a softer beam, describing the differences in position of impact for both the incoming object and the beam.

For the softer beam the difference in reaction force R_1 for different loading positions is more significant, see Figure 5.6. This is due to that the difference in stiffness between the object and the beam is now smaller, with a beam that is five times stiffer than the incoming object when loading at midspan. So the increase in stiffness when moving towards the support now has a larger impact. The reaction force in the beam R_2 for different α values has the same relation as before, but this time the force increases when α decreases. This is because the lower beam stiffness gives a new position in the graphs in Figure 3.12, as discussed before, and this leads to that the load factor β_{el} this time increases when α decreases. The frequency ratio f_1 / f_2 is for this case approximately 0.55.

5.1.3 Effect of spring stiffness

If instead the stiffness of the spring is changed by a factor four, property sets 2 and 3 from Table 5.1, the behaviour are identical to when the stiffness of the beam is changed, but the magnitude of the response is different. This is due to that the deciding factor when determining the response of the system is the frequency ratio between the beam and the impacting body. Since this remain unchanged compared to before the response also remains constant. Increasing the spring stiffness a certain amount is equivalent to decreasing the beam stiffness with the same amount and will produce results with equal behaviour. Therefore these results are only presented in Appendix D.

5.2 Finite element model

To perform detailed analyses of the system the finite element software ADINA is used ADINA R & D, Inc (2014). The FE model consists of a simply supported concrete beam that is connected to a moving mass through a spring which represents the impacting object. If this beam model is compared with the 2DOF system used previously the beam represents the second mass and spring, see Figure 5.7.
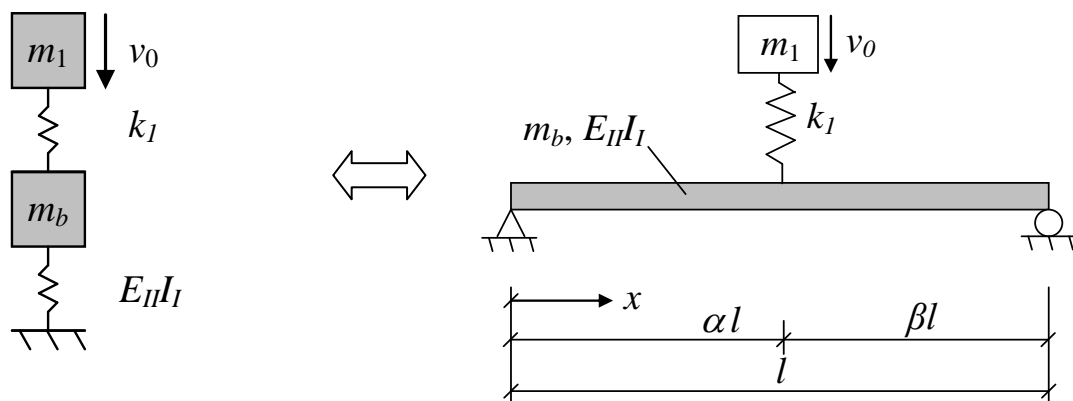
Figure 5.7   The 2DOF system implemented in the FE software.

Elastic 3D beam elements with an element length of 2 percent of the total length are used to model the beam. The impacting object is modelled by a spring element with a point mass travelling with an initial velocity. One potential problem when using ADINA is that when calculations of a concrete beam in state II are performed, ADINA is not able to recognise that the section is cracked. Instead the software uses the moment of inertia for the uncracked concrete section and thereby greatly overestimates the stiffness of the beam. In order to overcome this problem an equivalent Young's modulus E_{II} is used to obtain the correct state II bending stiffness of the beam. This is done by multiplying the original Young's modulus with the ratio between the moment of inertia in state II and state I

$$E_{II} = \frac{I_{II}}{I_{I}} E_c \qquad (5.5)$$

See also Appendix G for calculation of the equivalent Young's modulus and Appendix A for ADINA command files.

By changing the Young's modulus the speed of the force wave in the material is also changed. The wave speed is dependent on Young's modulus and the density of the material

$$c = \sqrt{\frac{E}{\rho}}$$ (5.6)

Firstly, a reference test is performed using a beam with what is assumed to be of a reasonable size and stiffness with properties according to section 4.1.2. The spring is considered to be linear elastic and the stiffness k_1 is chosen to be 300 kN/m, in accordance with what is used for a vehicle impact in Eurocode 1-7, CEN (2010). The impacting object is assumed to have a mass of 1 000 kg and an initial velocity of 20 m/s. In the following analyses the stiffness of the beam and spring respectively is altered by a factor 4, thereby changing the natural frequency f and period time T of the system with a factor 2, in accordance with equation (2.41). From this five different sets of properties are created and summarized in Table 5.2.

Table 5.2   The different set of properties used in each analysis.

Property set number	Spring stiffness k_I [kN/m]	Equivalent Young's modulus E_{II} [GPa]	$EI_b = E_{II}{\cdot}I_I$ [MNm^2]
1	300	8.134	18.302
2	75	8.134	18.302
3	1200	8.134	18.302
4	300	2.034	4.576
5	300	32.537	73.208

For each set of properties there is also five different load application points on the beam to simulate an arbitrary impact position, see Figure 5.8.

α	0.5	0.4	0.3	0.2	0.1
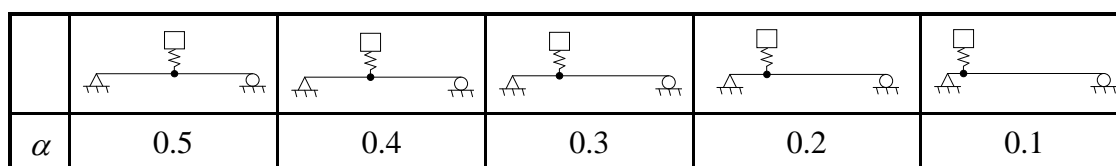
Figure 5.8   The different load application points.

To understand the results from an FE analysis it is important to know how they are obtained and what they really describe. In the FE software used the shear force in each element is taken as a mean value over the element. When extracting the shear force results the value in the first local node of each element had to be chosen, see Figure 5.9. This leads to that the obtained curve is offset to the left with the length of half an element and the values are a little bit lower than they should be. But because of the large amount of elements used, namely fifty, the error will be negligible. The moment along the beam is obtained in the same way as the shear force. The

displacement, on the other hand, can be obtained specifically for each node along the beam and the response will more or less be exact, see Figure 5.9 again.
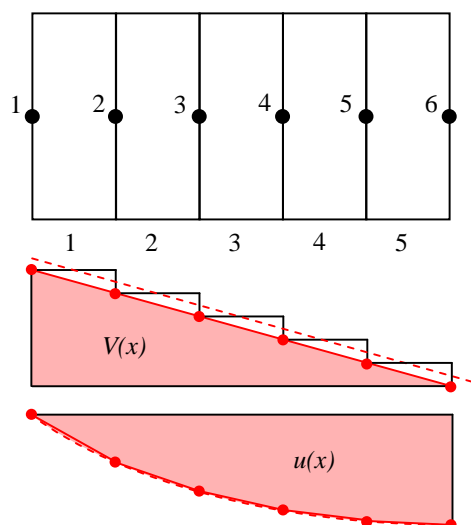
Figure 5.9   Illustration of how the shear force and displacement is extracted from the FE results, with the beam elements and nodes numbered.

5.2.1 Eigenmodes of a simply supported beam

The beam corresponding to property set 1, called the original beam, is studied with a modal analysis in ADINA. This in order to find the mode shapes for the most important eigenmodes, i.e. the eigenmodes that contribute the most to the actual deflection shape of the beam. These mode shapes can be seen in Figure 5.10, where five eigenmodes are presented. The eigenfrequencies of these modes are presented in Table 5.3. In the figure and table are some mode numbers missing, because they correspond to deflections that do not take place in the two dimensional x-y plane. These eigenmodes exist because three dimensional elements are used, but they are not of interest here.

Table 5.3   The five most important eigenmodes and their corresponding eigenfrequency for the original beam, property set 1.

Mode number	Eigenfrequency f_b [Hz]	Theoretical Eigenfrequency $f_{natural}$ [Hz]
1	10.00	10.09
2	39.83	40.36
5	88.98	90.81
8	156.60	161.44
11	241.70	252.25
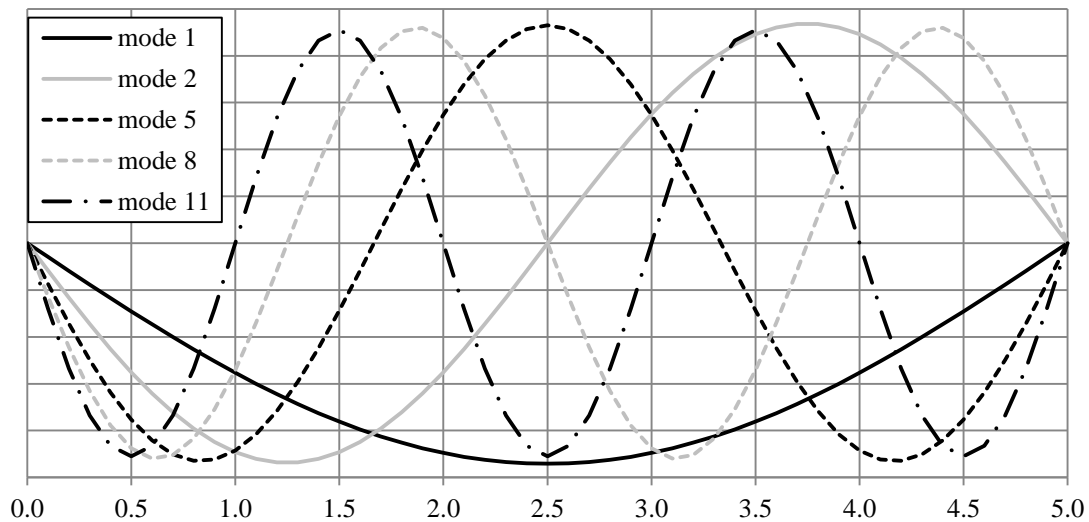
Figure 5.10   The mode shapes corresponding to the five most important eigenmodes of the studied beam.

From Figure 5.10 it can be seen that the first mode shape has a simple shape consisting of one curved line, while the higher mode shape numbers have more local extrema along the beam. It can also be seen that loading at different positions on the beam would give deflection shapes that trigger different mode shapes. Eigenmodes of higher number are more important when the load is applied closer to the support, compared to loading at midspan. This will be discussed more in the following sections.

5.2.2 Original beam - Property set 1

The first study is with a beam and spring of property set 1, as described in Table 5.2. The results presented in Figure 5.11 shows the shape of the response at the time when the maximum value is reached for each load case. As expected, the maximum moment increases as the impact position moves closer to the middle of the beam, and in the opposite way the shear force increases for impacts closer to the support. The deflection is largest close to the midspan regardless of where the impact occurs. In Figure 5.12 it can be seen that both the moment at the impact node and the support reaction force R_A occurs at almost the same time regardless of where on the beam the impact is. It is also visible that the second bump on the curve becomes less pronounced when the impact is close to the support. This is probably due to that in addition to the first most dominant eigenmode some additional eigenmodes becomes more important close to the support.
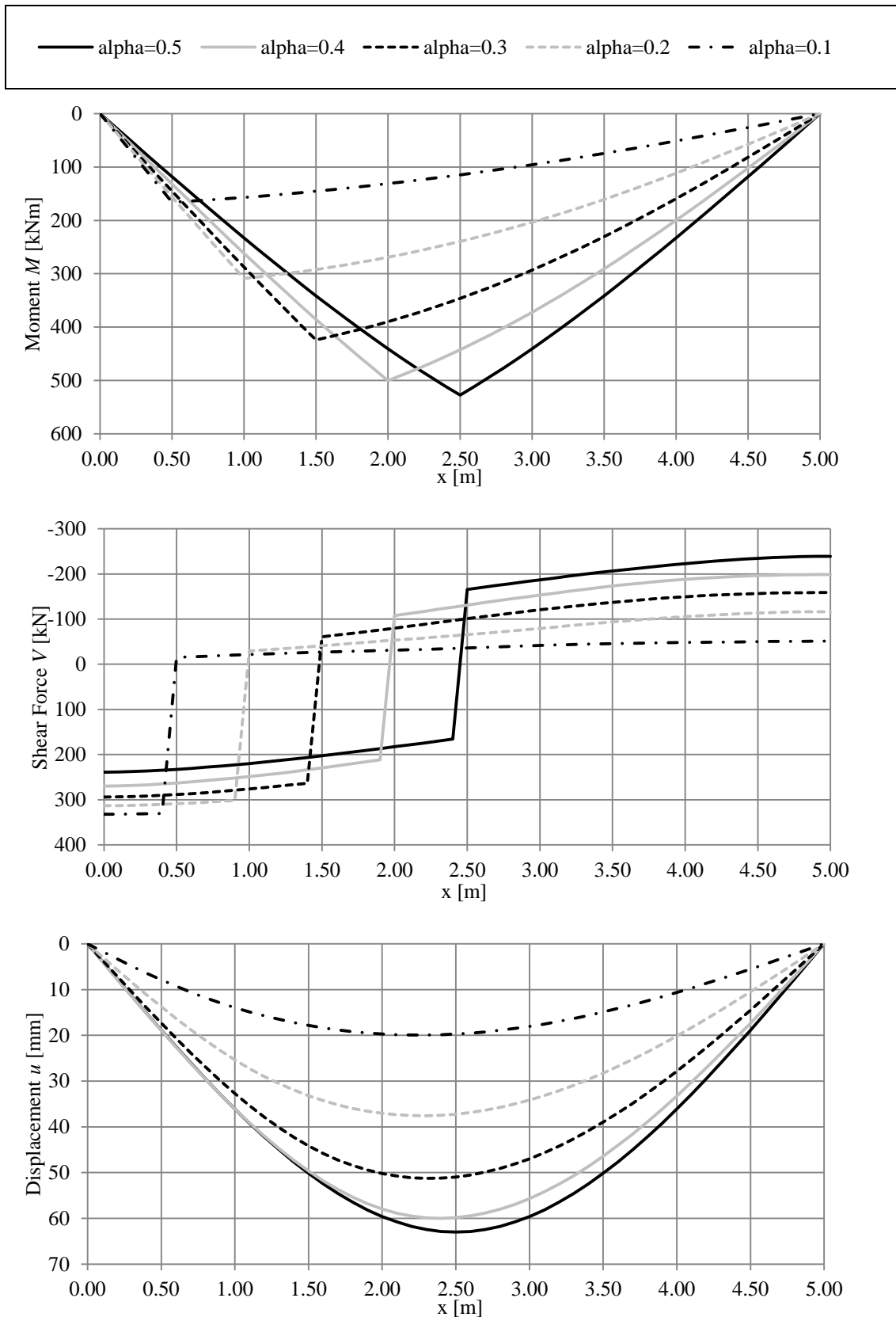
Figure 5.11   Maximum moment M, shear force V and displacement u over the length of the original beam for different impact positions, at the time when the maximum response is reached for each load case.
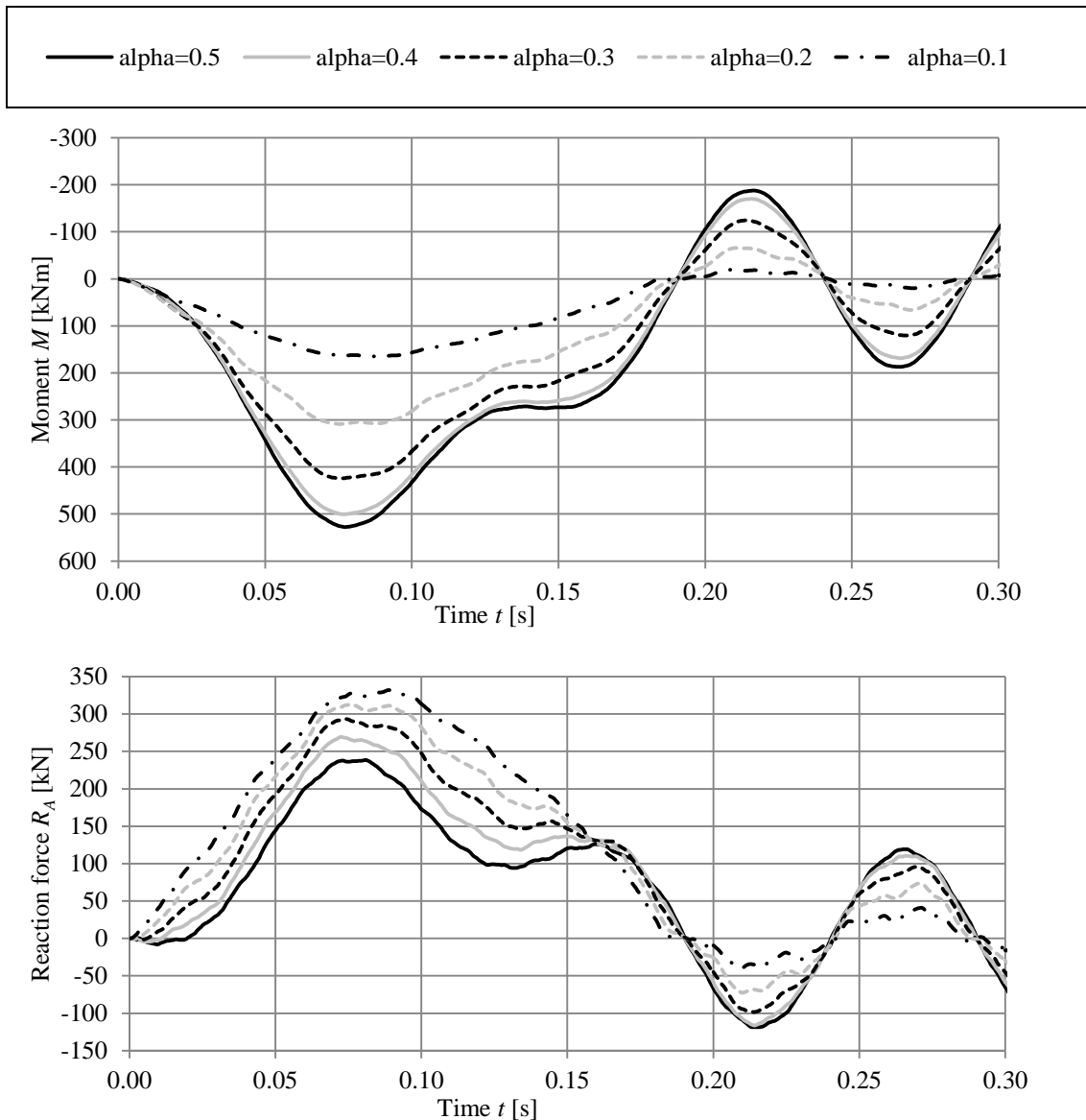
Figure 5.12   Moment at impact node with regard to time and support reaction force R_A with regard to time for different impact positions.

It can also be of interest to study how the reactions along the beam increases with time, this is essentially what leads up to the graphs in Figure 5.11 and can be seen in Figure 5.13 for $\alpha = 0.1$. Here it can be seen how the shape of the moment curve changes with time. Early during the impact, the moment is even negative at the opposite half of the beam to where the load is applied. The shape then changes as the moment grows and becomes more curved in the positive direction. But when the maximum moment is reached, the shape has gone back to consist of almost straight lines, similar to the shape of a static response. The shear force, on the other hand, grows larger with time without changing its shape very much. One interesting observation is that the shear force at the opposite support stays very close to zero during the first half of the studied time interval, while it grows constantly at the support closest to the load. When looking at the displacement curve it may be observed that the maximum displacement occurs at different positions at different times. At first the maximum is close to the point of loading, but with time it moves closer and closer to the midspan.
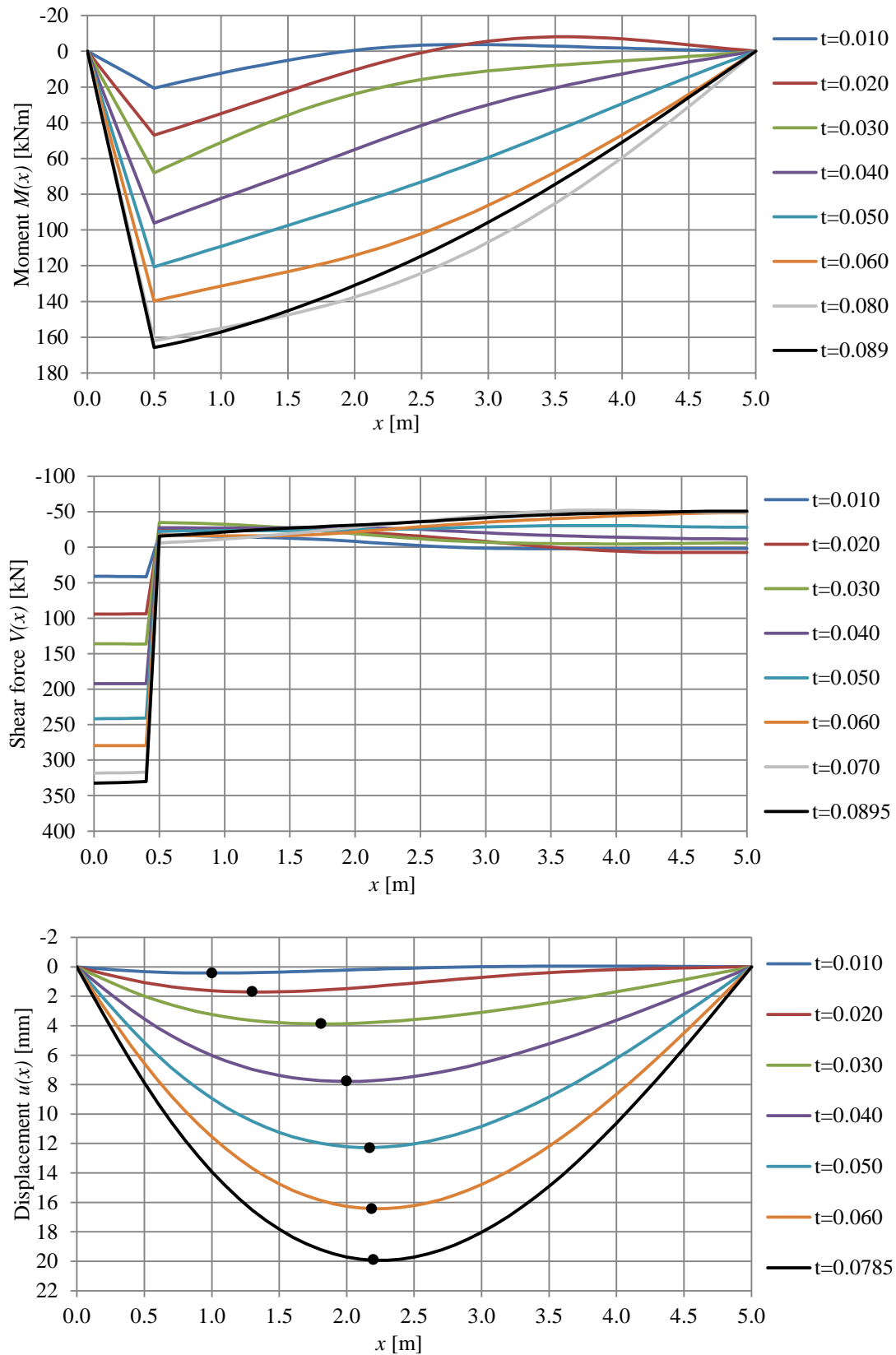
Figure 5.13   Moment M, shear force V and displacement u over the length of the original beam at different times during the impact up to when the maximum response is reached, when loading at α = 0.1.

5.2.3 Effect of beam stiffness

5.2.3.1 Stiffer beam – Property set 5

For property set 5, see Table 5.2, the maximum moment M, shear force V and deflection u along the beam shows almost identical behaviour to property set 1, see Figure 5.11, with only small differences in magnitude. These results are therefore only shown in Appendix E. The moment and reaction force over time, seen in Figure 5.14, is however displaying a different behaviour showing three bumps. This is due to that the stiffness of the beam is so large that the eigenfrequency has a much shorter period time than the duration of the impact. Again, these smaller bumps become less pronounced closer to the support due to additional eigenmodes coming into play.
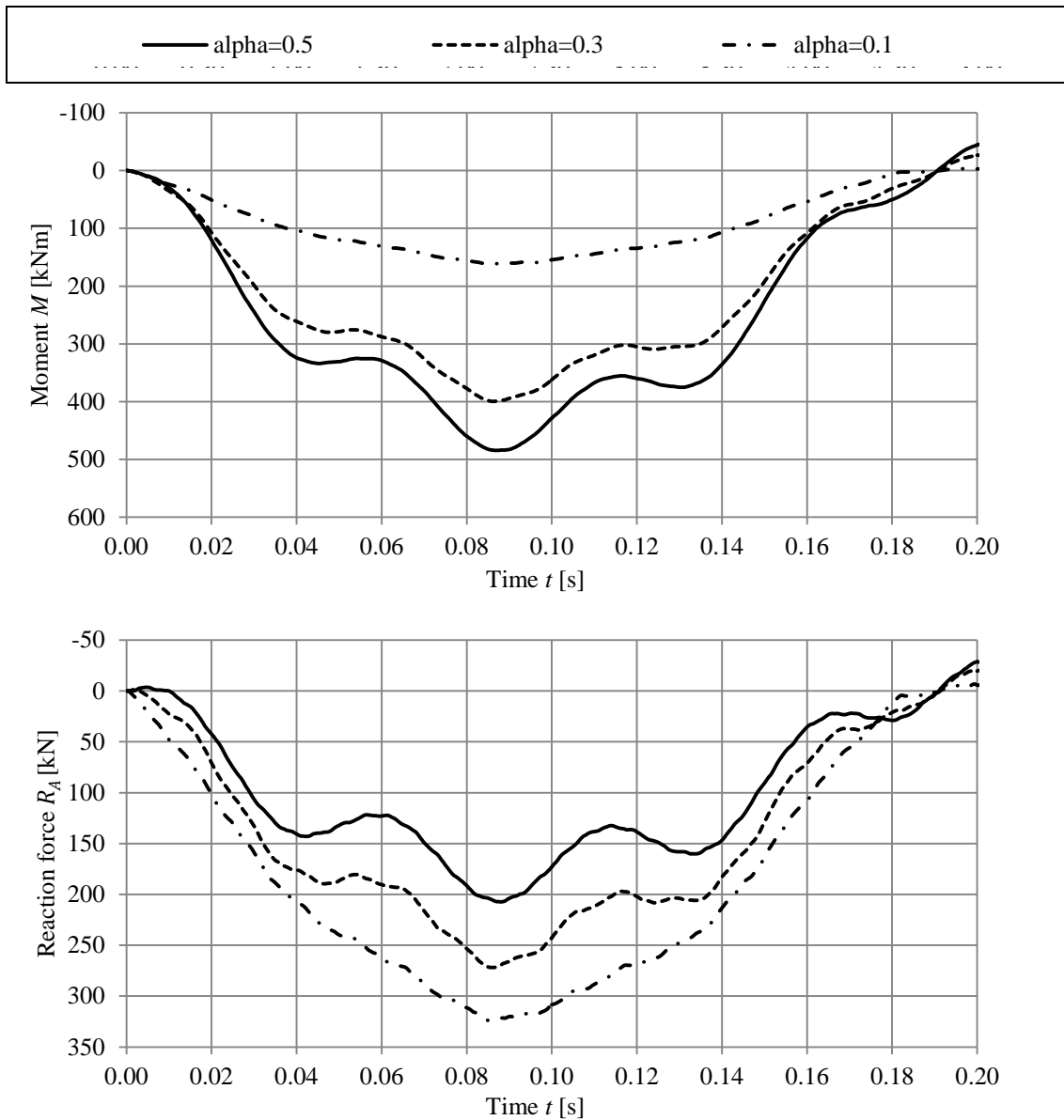
Figure 5.14   Moment M at impact node with regard to time and support reaction force R_A with regard to time for different impact positions.

5.2.3.2 Softer beam – Property set 4

The bending stiffness is now made four times smaller compared to the original beam, see Table 5.2. One interesting thing about this case, shown in Figure 5.15, is that the increase in shear force does not show the step like behaviour seen in other cases when the impact moves closer to the support. Instead the increase in shear force between $\alpha = 0.3$ and $\alpha = 0.1$ is more or less negligible. This phenomenon occurs when the beam has a relatively low stiffness compared to the stiffness of the impacting object. One reason for this to happen may be that some additional eigenmodes becomes more dominant close to the support, thereby influencing the result. These eigenmodes have higher natural frequencies and therefore the frequency ratio will decrease.

It can also be seen from Figure 5.16 that when the impact is close to the support it reaches its maximum reaction force much faster compared to if the impact is at the midspan, 0.08 seconds compared to 0.12 seconds. This time difference is due to that the beam is so soft that it takes some extra time for the force wave in the beam to reach the support section. This is because the wave speed is changed when using the equivalent Young's modulus E_{II} to modify the bending stiffness EI_b of the beam, see equation (5.6).
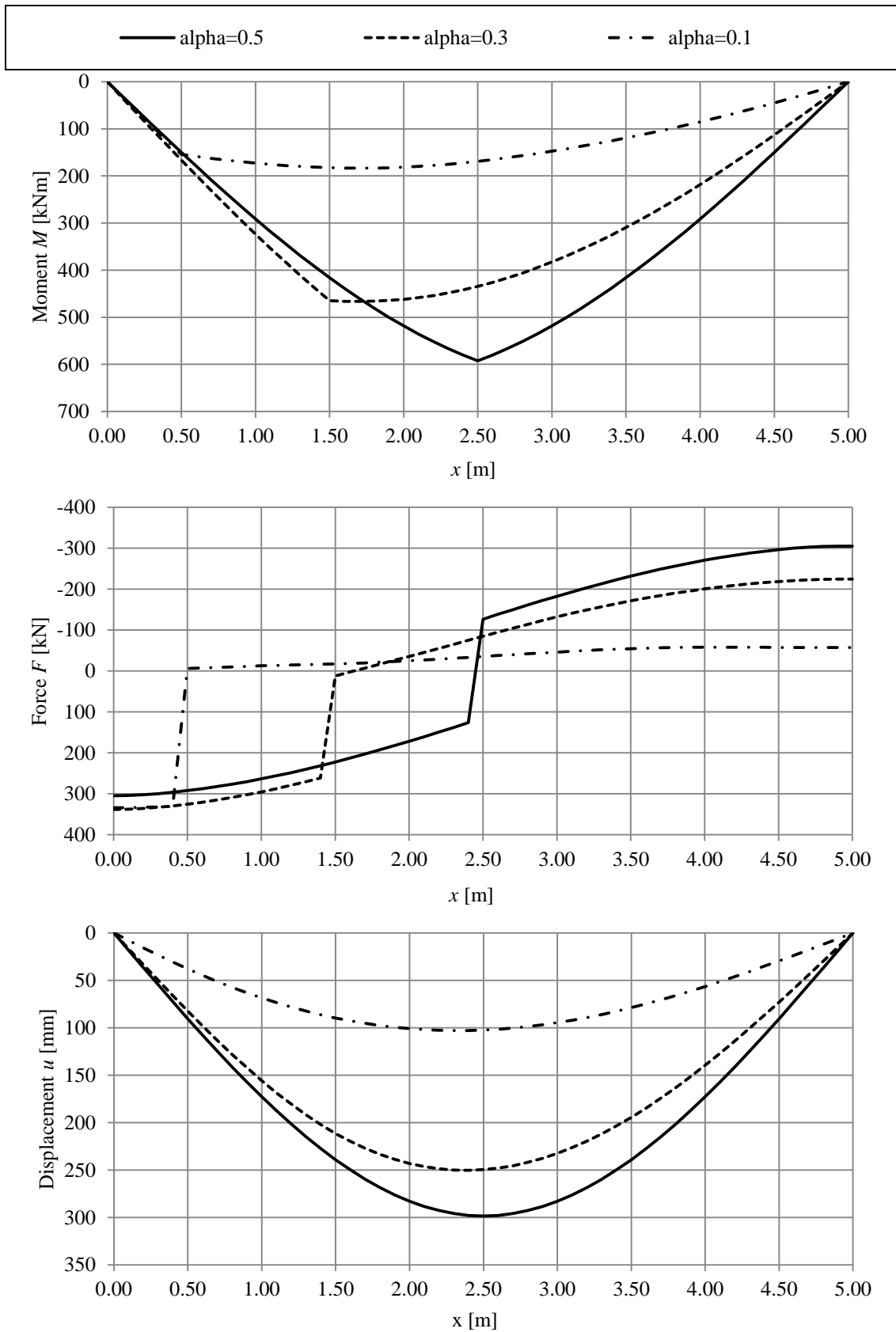
Figure 5.15   Maximum moment, shear force and deflection over the length of the soft beam for different impact positions, at the time when the maximum response is reached for each load case.
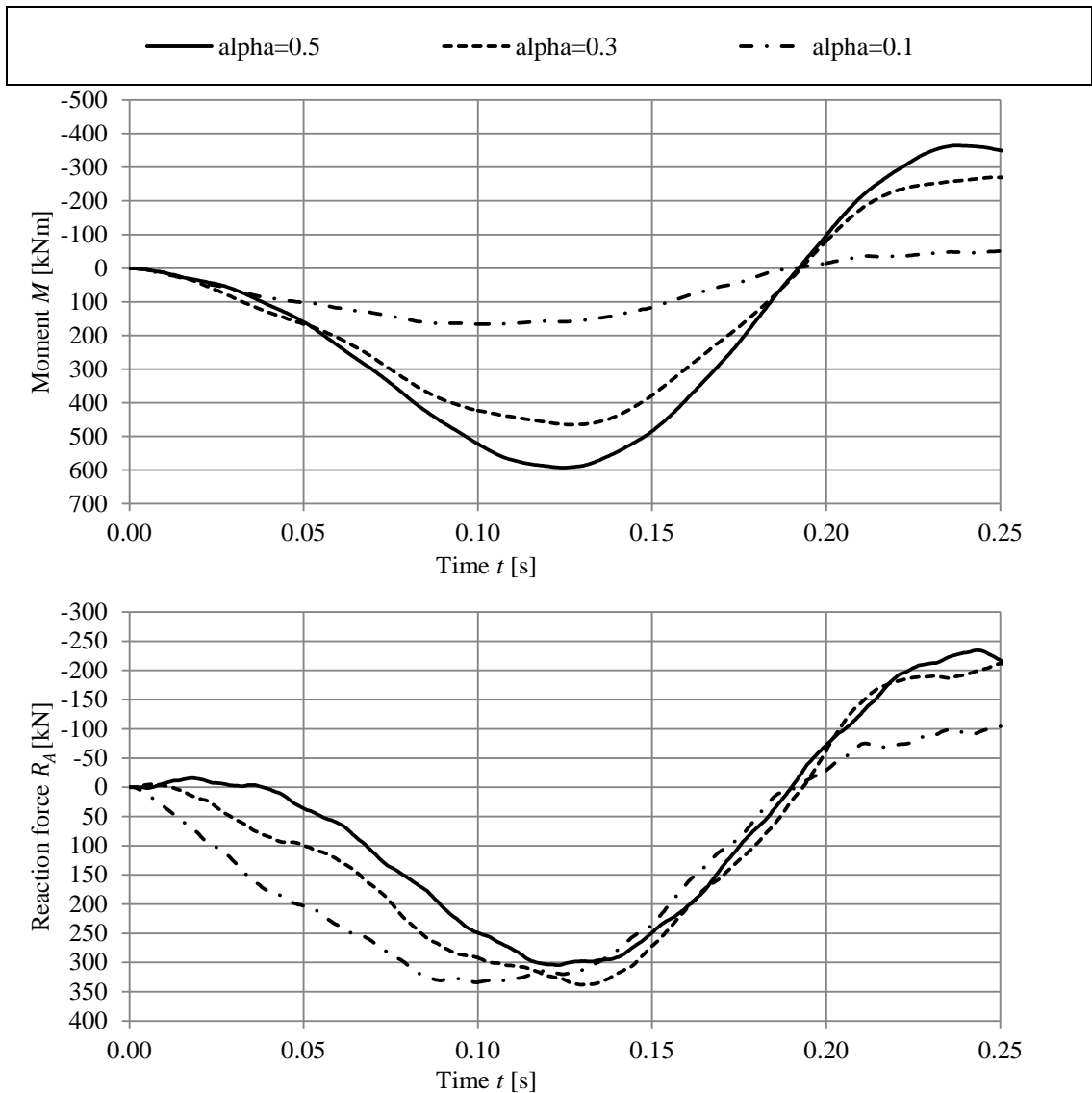
Figure 5.16   Moment at impact node with regard to time and support reaction force R_A with regard to time for different impact positions.

In Figure 5.17 it is presented how the moment and shear force along the beam increases with time, for impact at $\alpha = 0.3$ and $\alpha = 0.1$. For $\alpha = 0.3$ the moment behaves in a similar way to the original beam, see section 5.2.2, except that the shape of the moment is more curved when the maximum response occurs. For $\alpha = 0.1$ the moment curve behaves in a different way. In the beginning the moment grows in a similar way to the other cases. But this time the maximum moment occurs not directly under the point of impact, but closer to midspan. This behaviour is very different compared to the moment curve of a static response, and appears to occur when the frequency ratio f_1 / f_2 is large. The shear force for the two loading positions behaves in a similar way as the original beam. However the shape when loading at $\alpha = 0.3$ is a lot more curved with a larger force at the supports. In the beginning of the impact though the shear force is largest at the point of impact.
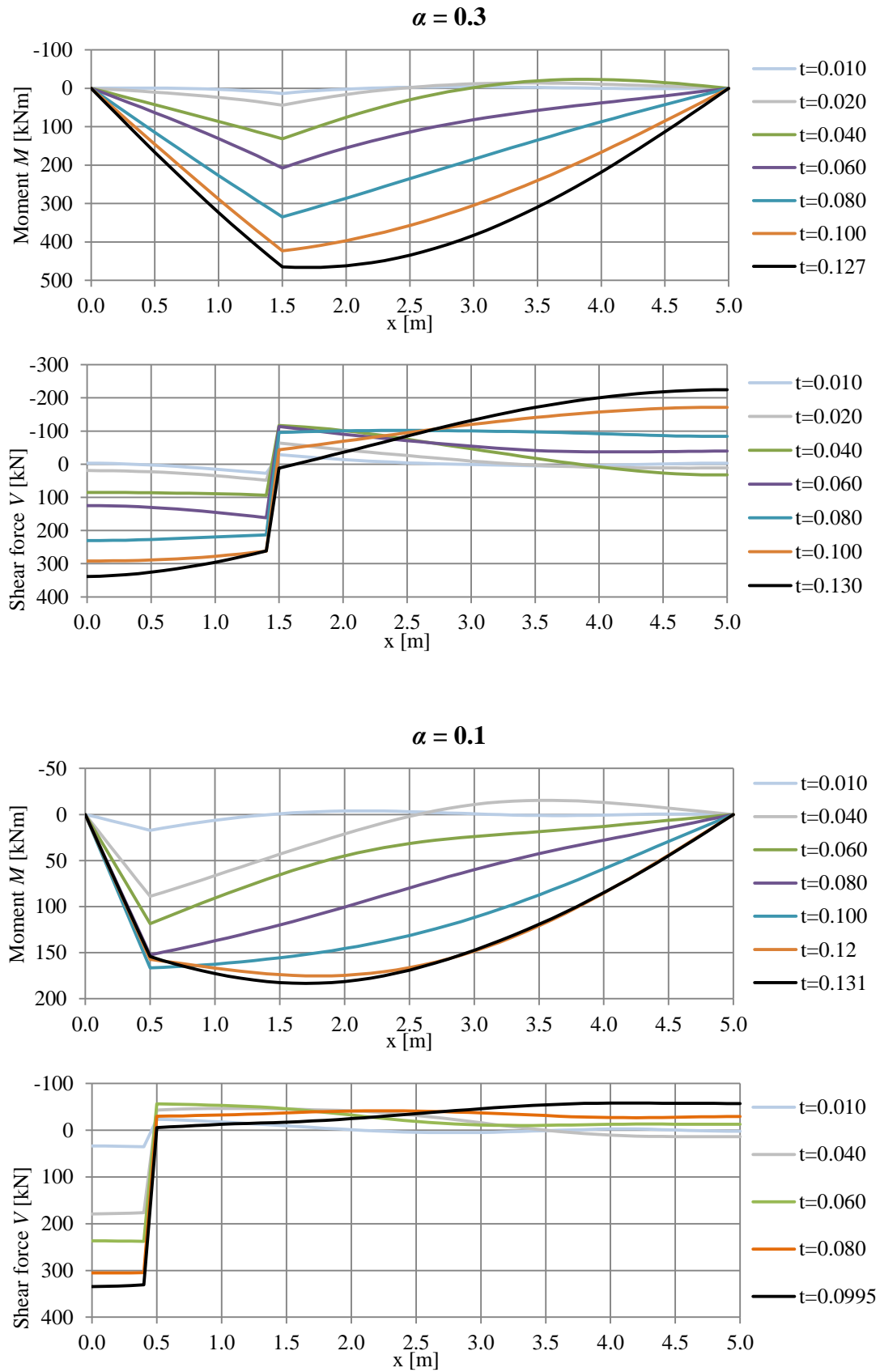
Figure 5.17   Moment M and shear force V over the length of the soft beam at different times during the impact up to when the maximum response is reached, when loading at α = 0.3 and α = 0.1.

5.2.4 Effect of spring stiffness

As mentioned for the 2DOF system in section 5.1.3 the behaviour of the response is identical when the spring stiffness is changed, compared to when the bending stiffness of the beam is changed, as long as the frequency ratio remains constant. The results for property sets 2 and 3, see Table 5.2, are therefore only presented in Appendix E.

5.3 Comparison of model responses

The collision responses for the 2DOF system and FE model presented in section 5.1 and 5.2 are in this section compared. The incoming object has a velocity v_0 of 20 m/s, the mass m_1 is set to 1 000 kg and the stiffness k_1 is set to 300 kN/m. The beam stiffness k_b is based on the beam from section 4.1.2, which corresponds to property set 1.

Five different property sets are defined and analysed with both the 2DOF system and the FEM software, see Table 5.4. This table also shows the properties for different loading positions and what the frequency ratio is for each case. In property set 2 and 3 the spring stiffness k_1 is varied and in property set 4 and 5 the bending stiffness EI_b and subsequently the beam stiffness k_b is varied. The stiffnesses are changed with multiples of four, in order to change the eigenfrequencies by a factor two.

In the following sections the comparisons for property set 1, 4 and 5 are presented, i.e. for the original beam and when the stiffness of the beam changes. The comparisons for the cases with changed stiffness of the colliding object , property sets 2 and 3, are here omitted because the responses are equal in both shape and relative size, see instead Appendix F. The reason for this is that the frequency ratio is exactly equal for the two cases; property set 2 is equal to property set 5 and property set 3 is equal to property set 4, see Table 5.4.

The responses presented in this comparison are the displacements u_1 and u_2, the support reaction force R_A, which is the maximum shear force, and the moment at the section where the load is applied M_α, all with regard to time. The support reaction force for the 2DOF system is calculated according to

$$R_{A,2DOF} = \frac{R_2 \cdot (l - \alpha l)}{l} = R_2 \cdot \beta \tag{5.7}$$

where R_2 is the force in the beam at the position of impact and $\beta = 1 - \alpha$. The moment is then calculated according to

$$M_\alpha = R_{A,2DOF} \cdot \alpha l = R_2 \cdot \beta \cdot \alpha l \tag{5.8}$$

All of the results from the comparison can be seen in Appendix F.

Table 5.4   *Input parameters for the different property sets and for three different loading positions.*

α	Property set	k_1 [kN/m]	EI_b [MNm^2]	k_b [MN/m]	m_1 [kg]	m_2 [kg]	$\dfrac{m_1}{m_2}$	f_1 [Hz]	f_2 [Hz]	$\dfrac{f_1}{f_2}$
	1	300	18.302	7.028	1 000	1 748.6	0.572	2.757	10.09	0.273
	2	75	18.302	7.028	1 000	1 748.6	0.572	1.378	10.09	0.137
0.5	3	1 200	18.302	7.028	1 000	1 748.6	0.572	5.513	10.09	0.546
	4	300	4.576	1.757	1 000	1 748.6	0.572	2.757	5.045	0.546
	5	300	73.208	28.112	1 000	1 748.6	0.572	2.757	20.18	0.137
	1	300	18.302	9.960	1 000	2 310.8	0.433	2.757	10.45	0.264
	2	75	18.302	9.960	1 000	2 310.8	0.433	1.378	10.45	0.132
0.3	3	1 200	18.302	9.960	1 000	2 310.8	0.433	5.513	10.45	0.528
	4	300	4.576	2.490	1 000	2 310.8	0.433	2.757	5.225	0.528
	5	300	73.208	39.842	1 000	2 310.8	0.433	2.757	20.90	0.132
	1	300	18.302	54.229	1 000	10 092	0.099	2.757	11.67	0.236
	2	75	18.302	54.229	1 000	10 092	0.099	1.378	11.67	0.118
0.1	3	1 200	18.302	54.229	1 000	10 092	0.099	5.513	11.67	0.473
	4	300	4.576	13.557	1 000	10 092	0.099	2.757	5.833	0.473
	5	300	73.208	216.92	1 000	10 092	0.099	2.757	23.33	0.118

5.3.1 Original beam - Property set 1

The first comparison is made with the same beam as described in section 4.1.2. The results are presented in form of graphs for how the reaction force R_A, moment M_α and displacements u_1 and u_2 for the two bodies during the impact. Three different positions of impact, from $\alpha = 0.5$ to $\alpha = 0.1$, are treated and described in this section.
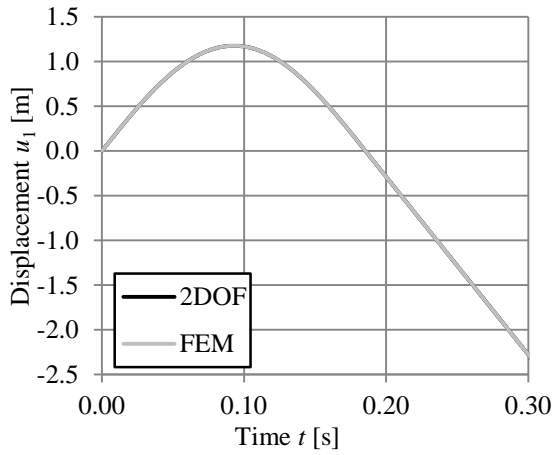
a) u_1, $\alpha = 0.5$
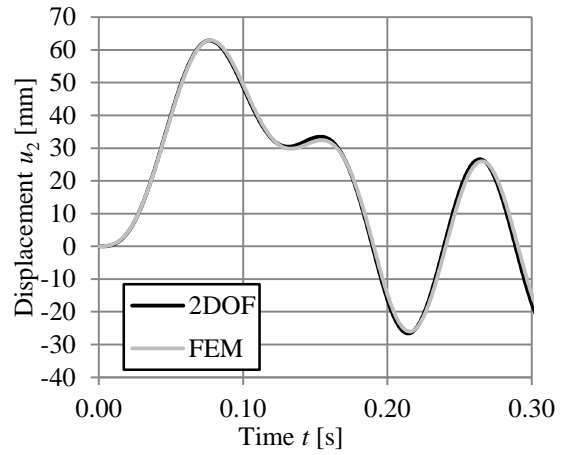
b) u_2, $\alpha = 0.5$
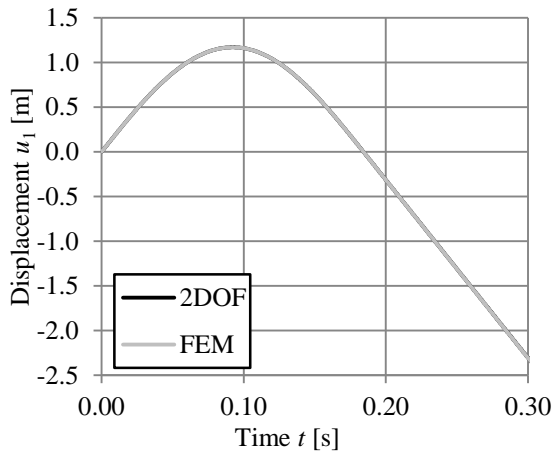
c) u_1, $\alpha = 0.3$
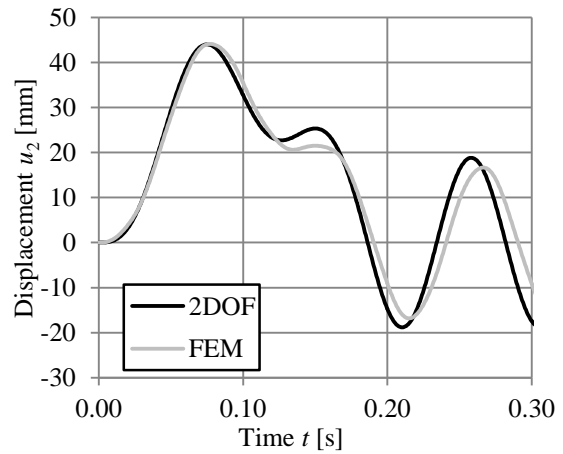
d) u_2, $\alpha = 0.3$
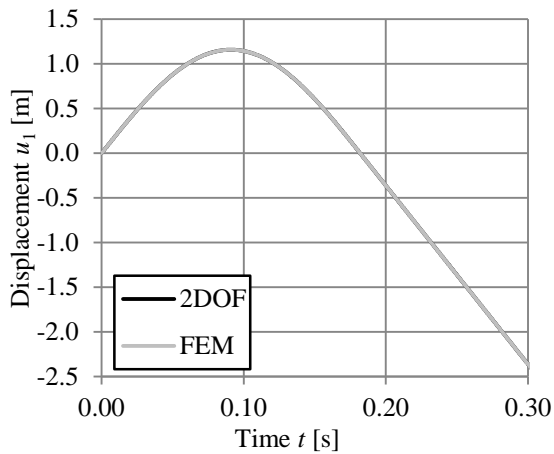
e) u_1, $\alpha = 0.1$
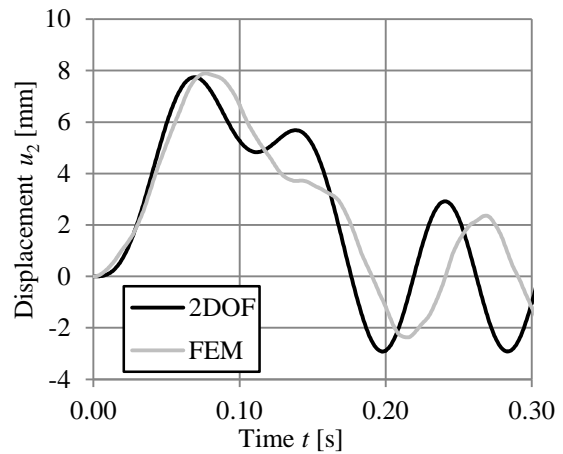
f) u_2, $\alpha = 0.1$

Figure 5.18   Comparison of response in displacement u_1 and u_2 over time between 2DOF and FEM, for three different positions of loading and with property set 1.

a) R_A, $\alpha = 0.5$

b) M_α, $\alpha = 0.5$

c) R_A, $\alpha = 0.3$

d) M_α, $\alpha = 0.3$
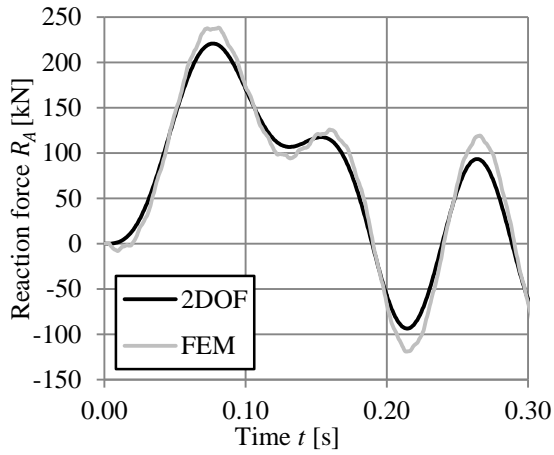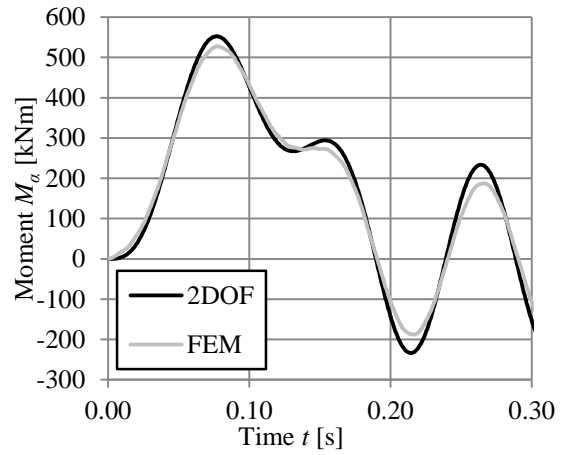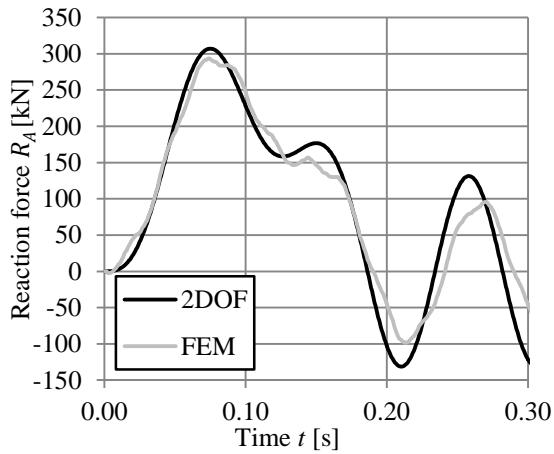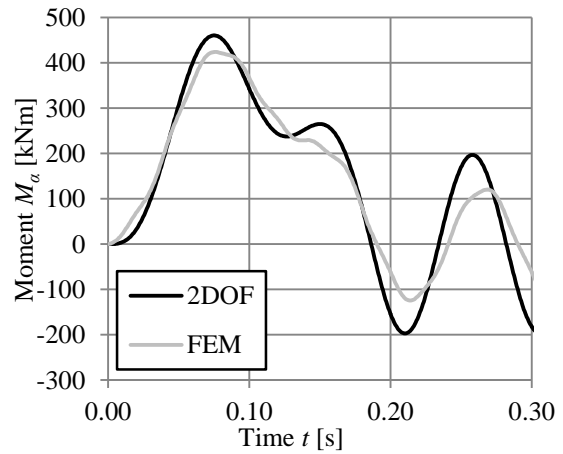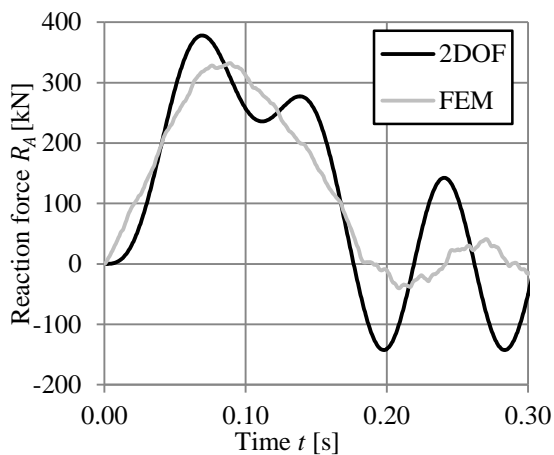
e) R_A, $\alpha = 0.1$
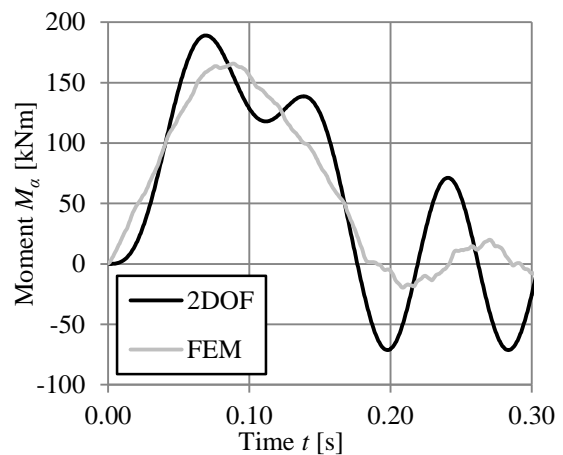
f) M_α, $\alpha = 0.1$

Figure 5.19   Comparison of response in support reaction force R_A and moment M_α over time between 2DOF and FEM, for three different positions of loading and with property set 1.

From Figure 5.18 the conclusion can be made that the correlation for the displacement u_1 is very good and no difference can be seen in any of the loading positions. This is also the case for all the other property sets, which is why this comparison is left out in the following sections. The reason for this is probably that the incoming object is modelled as a simple spring-mass system with the same stiffness k_1 in both models.

If instead u_2 is analysed a difference between the models can be observed. The correlation is almost perfect when loading at midspan, while it gets worse when loading closer to the support. The difference is still small at $\alpha = 0.3$ and the shape of the responses is almost equal. At $\alpha = 0.1$, though, the difference is larger and the shape of the curves differ quite a lot. The 2DOF response has a noticeable increase in displacement at the second impact while the FEM response shows only a small saddle point. The maximum displacement for u_2 is on the other hand quite similar in both models, with a slightly larger value from the FE model response. Hence, the 2DOF is able to predict the maximum displacement rather well

In Figure 5.19 the support reaction force R_A and moment M_α is compared, and the difference are here more evident; again more so when the load is applied closer to the support. For the support reaction force R_A the response is slightly higher for the FE model when loading at midspan, while it is the other way around when loading at $\alpha = 0.3$. When $\alpha = 0.1$ the reaction force is noticeable larger for the 2DOF model, while the shape of the graphs is clearly different. Neither does the FE model have a noticeable second bump on the curve here, which it does when the load is applied at midspan. The 2DOF system shows a similar behaviour in all three cases with a second bump after approximately 0.15 seconds.

The moment diagrams show a similar behaviour as the reaction force, but here the response from the 2DOF model is always larger. It can also be noted that for $\alpha = 0.1$ the shape of the response from the FE analysis regarding moment and support reaction force is almost identical with the values for the reaction force being roughly twice as large compared to the moment.

One conclusion from these comparisons is that the correlation between 2DOF and FEM always gets worse when moving closer to the support, i.e. making α smaller. This probably has to do with that other eigenmodes than the first one have a large impact when loading close to the support. For the case when loading at midspan the first eigenmode is the most significant one. The 2DOF system created can on the other hand only simulate the first eigenmode of the beam.

Another way of presenting the comparison between the 2DOF system and FE model is to create envelopes of the moment and shear force curves along the beam. This is done by superimposing the maximum responses for five different positions of loading. For the FE response this can be explained as superimposing the curves from Figure 5.11. The envelopes are mirrored to be valid for impacts on both sides of the midspan. The comparison of the envelopes can be seen in Figure 5.20. As seen previously in this section, the 2DOF system response is on the safe side for the whole length of the beam.
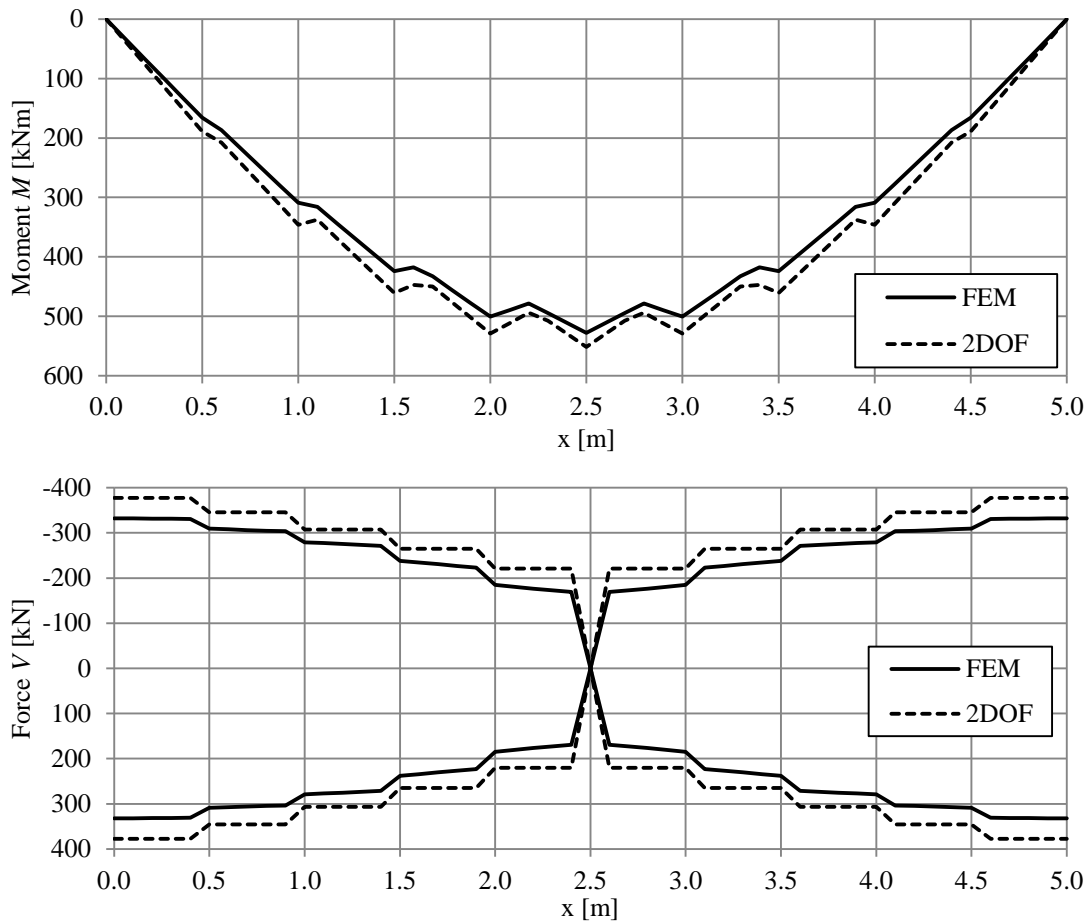
Figure 5.20   Comparision of the envelopes for the Moment M and shear force V over the length of the beam, between the 2DOF and FE responses.

5.3.2 Effect of beam stiffness

The beam stiffness is now made one fourth as stiff and four times as stiff compared to the original beam, to study the outcome of varying stiffnesses, see Table 5.4.

5.3.2.1 Stiffer beam – Property set 5

The correlation in displacement u_2 for the stiffer beam is about the same as for the original beam, see Figure 5.21. The correlation is again very good when loading at midspan and it gets worse when loading closer to the support. As for the original beam the FE model displays the highest values in all loading positions, but the difference is small. The shape also for this case differs more when loading closer to the support, where the FE model loses some of the peaks which was visible closer to midspan, while the 2DOF model virtually preserves its shape regardless of loading position.

a) u_2, $\alpha = 0.5$

b) u_2, $\alpha = 0.3$

c) u_2, $\alpha = 0.1$
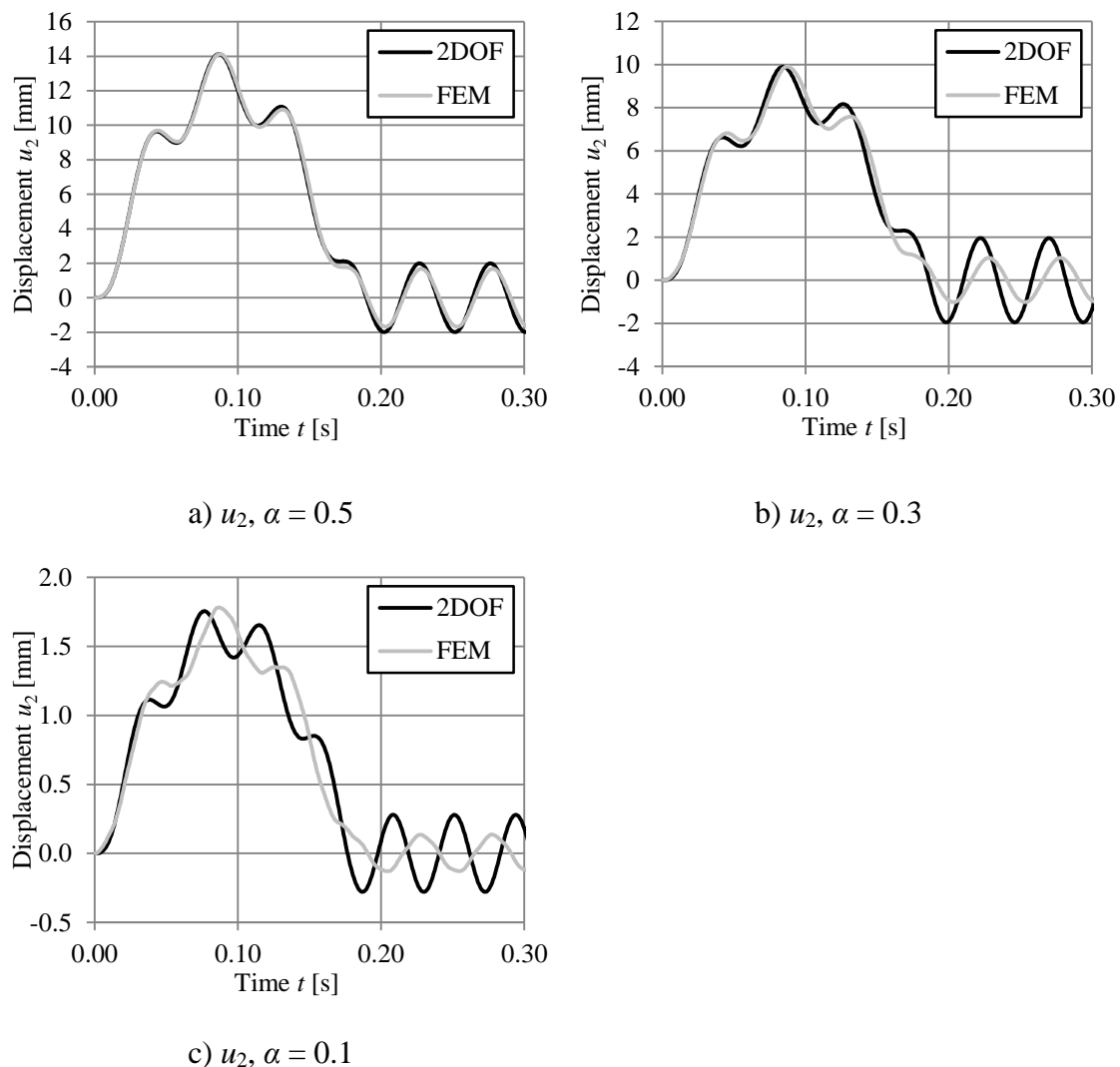
Figure 5.21   Comparison of response in displacement u_2 over time between 2DOF and FEM, for three different positions of loading and with property set 5

The correlation of reaction forces and moments have the same behaviour as for the original beam, with a much smaller difference in response compared to the weak beam, see Figure 5.22. At $\alpha = 0.3$ the correlation is still very good, as was the case with the original beam. For $\alpha = 0.1$ the difference is larger but still relatively small, and thus, fully acceptable.

a) R_A, $\alpha = 0.5$

b) M_α, $\alpha = 0.5$

c) R_A, $\alpha = 0.3$

d) M_α, $\alpha = 0.3$

e) R_A, $\alpha = 0.1$

f) M_α, $\alpha = 0.1$
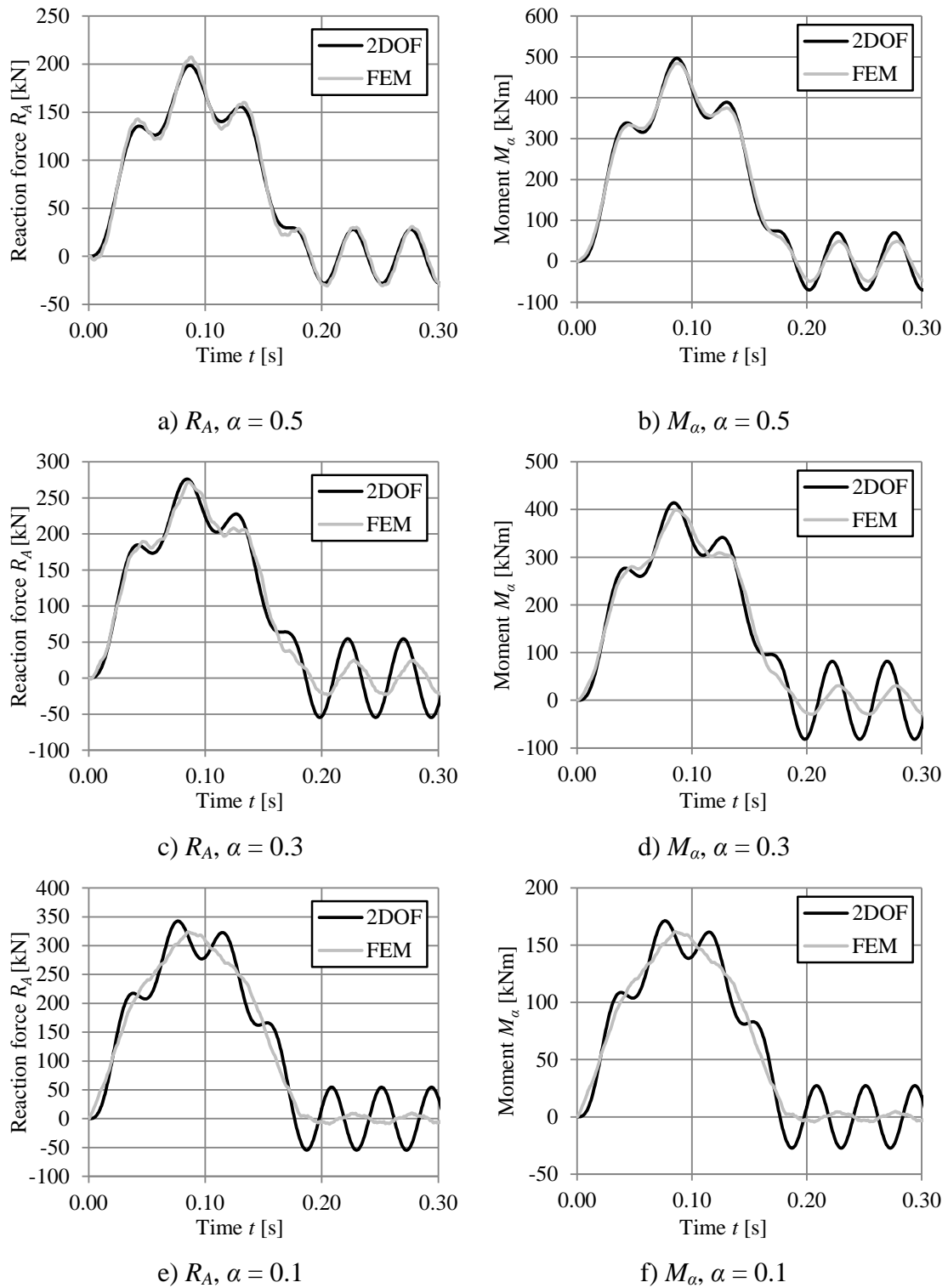
Figure 5.22   Comparison of response in support reaction force R_A and moment M_α over time between 2DOF and FEM, for three different positions of loading and with property set 5.

The comparison of the envelopes for moment and shear force between the 2DOF system and the FE model can be seen in Figure 5.23. Also this time the 2DOF system response is on the safe side for the whole length of the beam, but the difference is small.
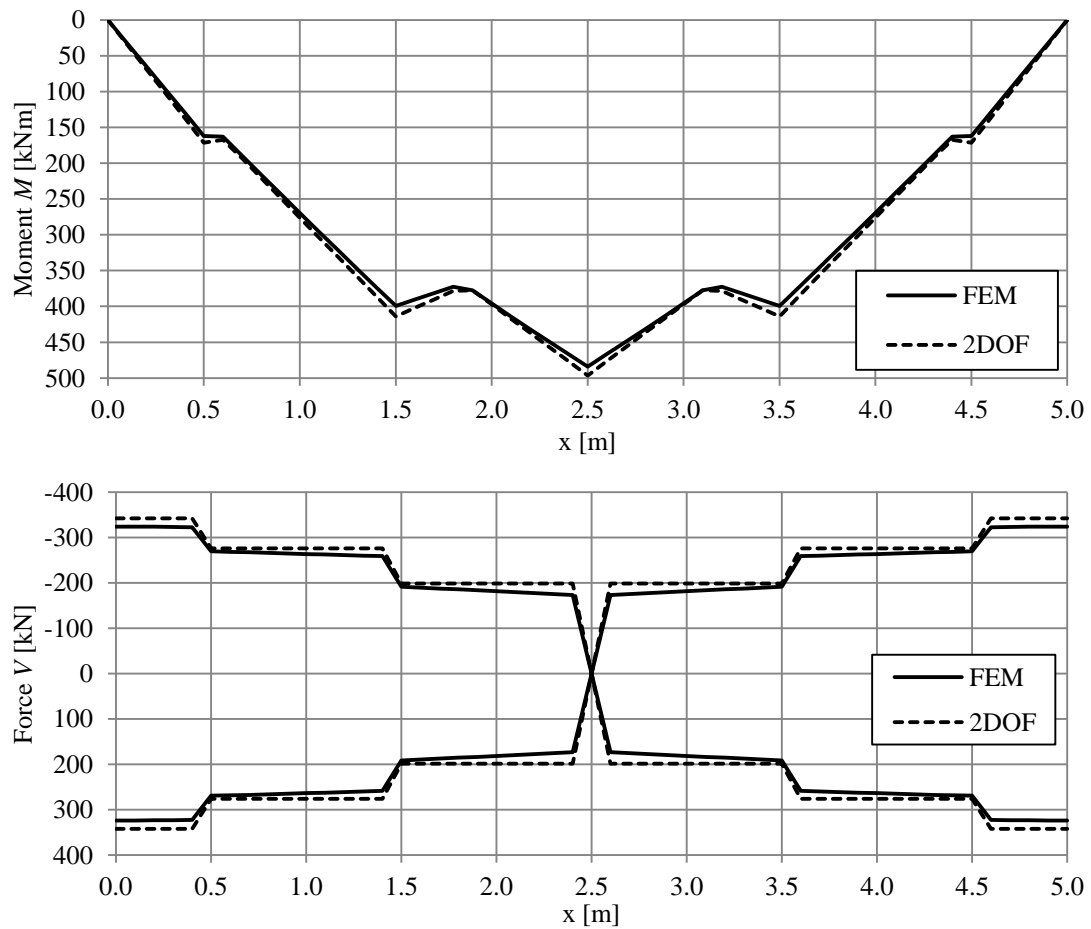
Figure 5.23   Comparision of the envelopes for the Moment M and shear force V over the length of the stiffer beam, between the 2DOF and FE responses.

5.3.2.2 Softer beam – Property set 4

The correlation in displacement u_2 is for the softer beam a little bit worse than for the original beam, compare Figure 5.24 and Figure 5.18. For loading at midspan the correlation is still very good but it gets worse when loading closer to the support. This time the 2DOF model displays the highest values in all loading positions, in contrast to the original beam.

a) u_2, $\alpha = 0.5$

b) u_2, $\alpha = 0.3$

c) u_2, $\alpha = 0.1$
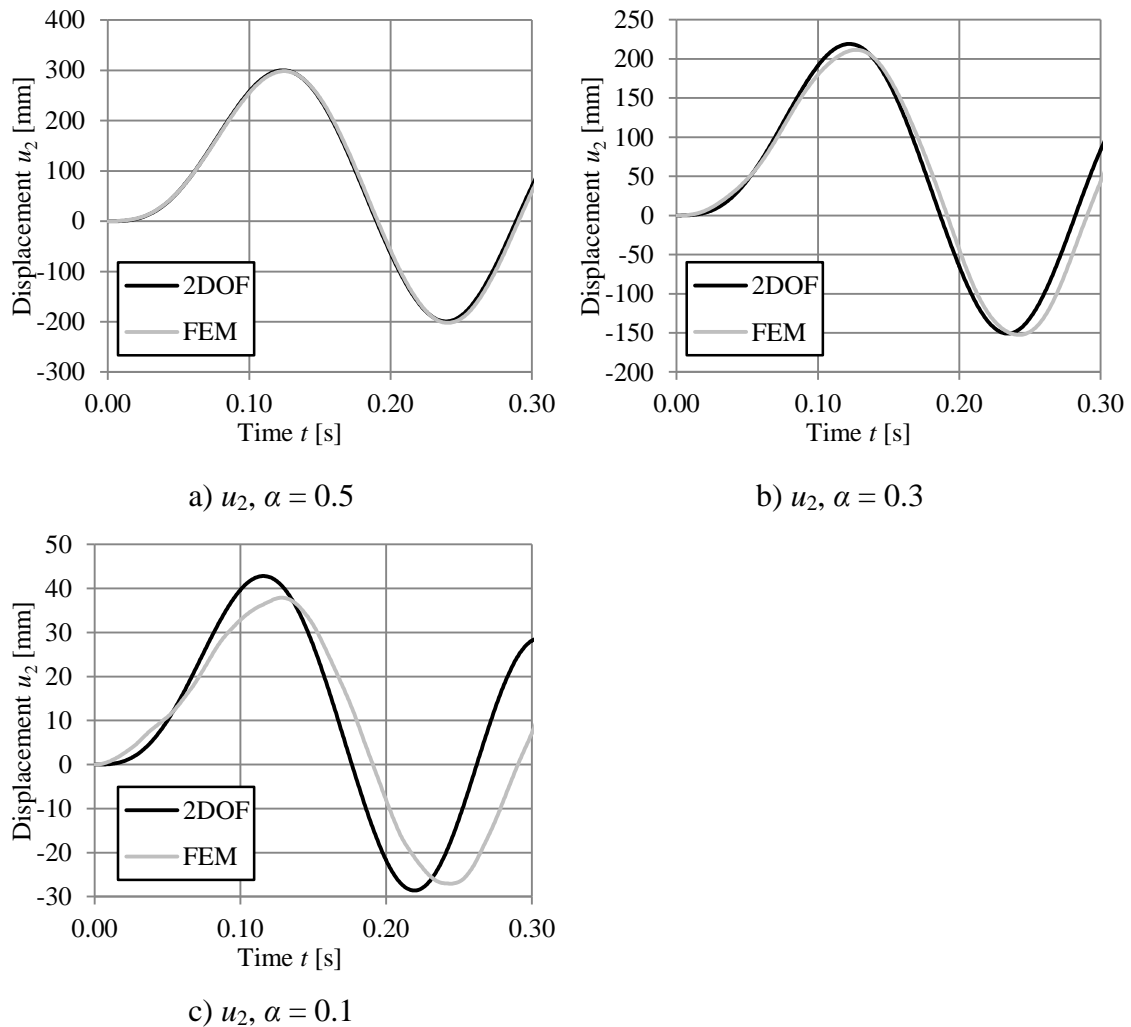
Figure 5.24   Comparison of response in displacement u_2 over time between 2DOF and FEM, for three different positions of loading and with property set 4.

The correlation of reaction forces and moments show the same behaviour as for the original beam, with higher differences closer to the support, see Figure 5.25. However, this time the differences is a lot larger than before, as the 2DOF system overestimates the response by over 50 percent compared to the FE analysis, when loading at $\alpha = 0.1$.

a) R_A, $\alpha = 0.5$ b) M_α, $\alpha = 0.5$

c) R_A, $\alpha = 0.3$ d) M_α, $\alpha = 0.3$
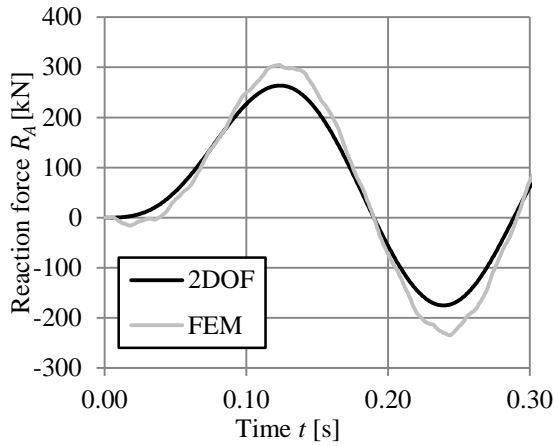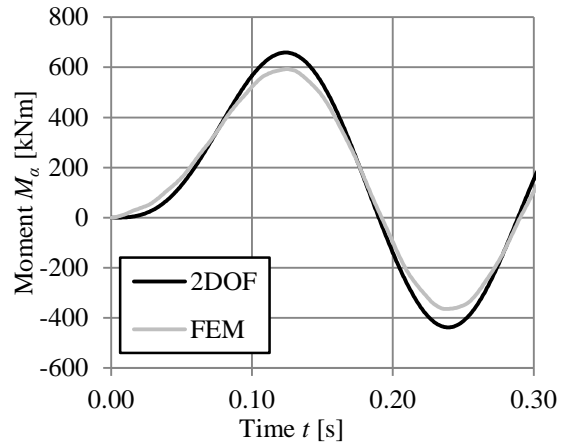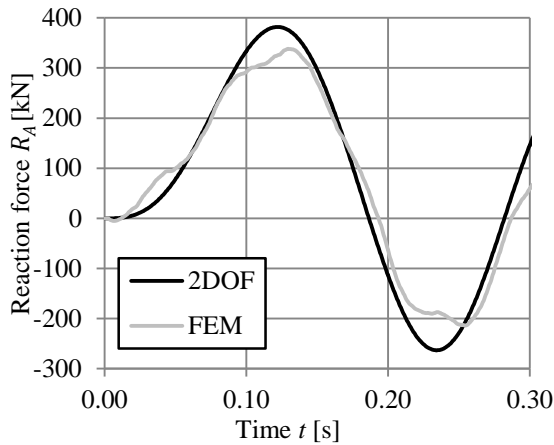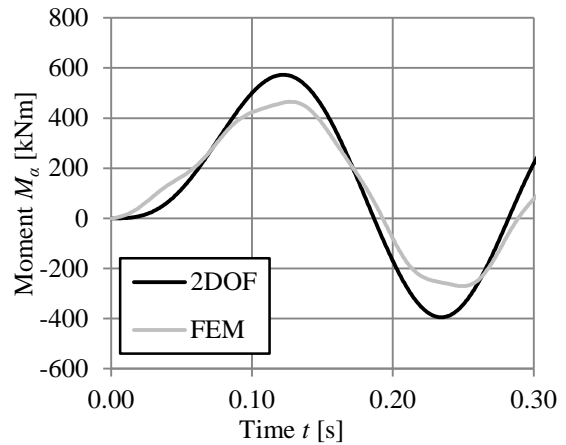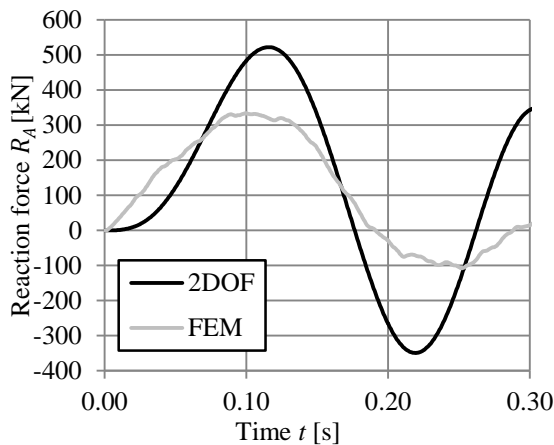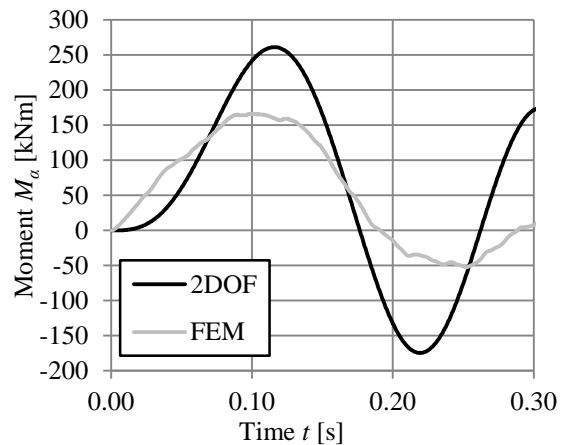
e) R_A, $\alpha = 0.1$ f) M_α, $\alpha = 0.1$

Figure 5.25   *Comparison of response in support reaction force R_A and moment M_α over time between 2DOF and FEM, for three different positions of loading and with property set 4.*

The comparison of the envelopes for moment and shear force between the 2DOF system and the FE model can be seen in Figure 5.26. Also this time the 2DOF system response is on the safe side for the whole length of the beam, and the overestimation is significant.
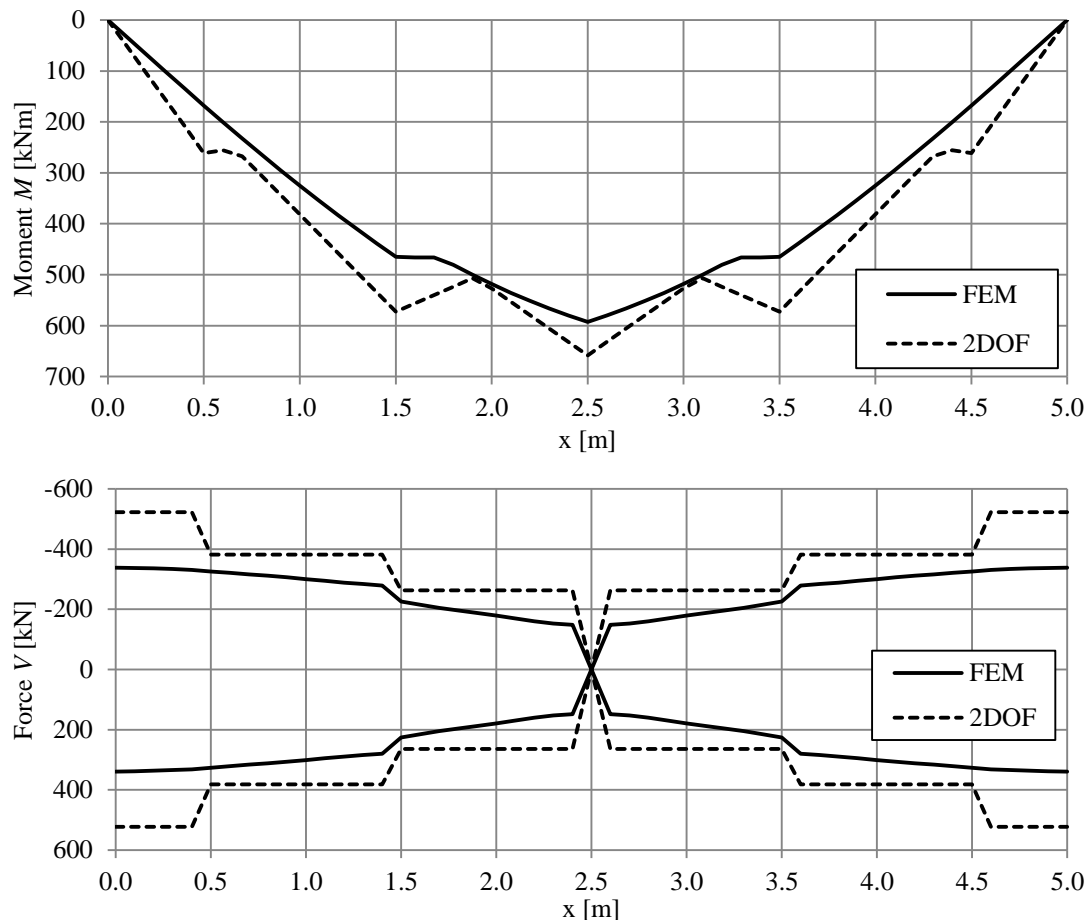
Figure 5.26   Comparison of the envelopes for the Moment M and shear force V over the length of the soft beam, between the 2DOF and FE responses.

5.3.3 Observations from the comparison

From the comparisons in the previous sections it is clear that the correlation between the 2DOF and FE models are quite good for all property sets when the load is applied close to midspan. When the load is applied closer to the support, the correlation will be worse. The cause of this could be that other eigenmodes than the first one is important when loading close to the support and, as discussed earlier, the 2DOF system cannot simulate these properly.

When making the beam softer the difference in response increased a lot, in comparison to the original and stiffer beam which had similar difference in response. If at the same time looking at the frequency ratios f_1 / f_2 for the different cases, it gets clear that the higher the frequency ratio the worse the correlation.

This phenomenon is quite interesting and needs to be investigated further. From now on the focus is set on the correlation of the shear force, because it often is more critical and of bigger importance when collision impacts are treated. The bending

moment could also be of importance, but it does not in general lead to a beam failure because of yielding and plastic redistribution.

5.3.4 Comparison of support reaction forces

To study the shear force the support reaction force R_A is investigated, since it is in general equal to the maximum shear force in a beam. The correlation between the 2DOF and FE models are studied by using the ratio of the reaction forces $R_{A,2DOF} / R_{A,FEM}$. In Table 5.5 this ratio is presented together with the frequency ratio f_1 / f_2, for all of the loading positions and for even more property sets than presented before. To clearly be able to see how the correlation of reaction forces depends on the frequency ratio, these values are also plotted in Figure 5.27 and Figure 5.28. If the original beam corresponded to a vehicle colliding with a barrier, one could think of the highest frequency ratios as a rigid steel projectile colliding with a barrier, rather than a vehicle colliding with an unreasonably soft barrier.

In Figure 5.27 it can be seen once again that the correlation is best when loading at $\alpha = 0.3$. When loading at midspan, $\alpha = 0.5$, the 2DOF system underestimates the response, meaning it is not on the safe side. This could still be acceptable since the moment utilizes plastic redistribution and the shear force is considerably larger when the load is applied close to the support. When $\alpha = 0.1$ the largest differences in reaction force can be seen and here the 2DOF system overestimates the shear forces. What is positive about this is that using the 2DOF system is on the safe side and the response when loading close to the support is likely the governing one in a design process, i.e. the largest one. The downside is that using the 2DOF system could result in very oversized structures, which is not sustainable from an environmental and economic viewpoint.

The trend in Figure 5.27 shows a decreasing correlation when the frequency ratio increases. After further studies, it was found out that this is not really true when the frequency ratio has a higher value than 1, see Figure 5.28. From this it can be seen that the ratio of the reaction forces starts to decrease for higher values of the frequency ratio. This results in a better correlation at first, but subsequently leads to that the 2DOF model underestimates the response for all loading positions, making it not safe to use anymore. For the case when $\alpha = 0.1$ the 2DOF model will not be safe to use anymore when the frequency ratio exceeds 2.5. When the frequency ratio exceeds a value of approximately 3.5 for the same loading position the ratio of the reaction force is even lower than for the case when $\alpha = 0.3$. This occurrence could be interesting to study further to see what happens to the force ratio at even higher frequency ratios than 4.5, because it looks like it could decrease even more.

Table 5.5   *Input parameters and reaction forces for the different property sets and for three different loading positions.*

α	Property set	Max of $R_{A,2DOF}$ [kN]	Max of $R_{A,FEM}$ [kN]	$\dfrac{R_{A,2DOF}}{R_{A,FEM}}$	k_1 [kN/m]	EI_b [MNm^2]	k_b [MN/m]	f_1 [Hz]	f_2 [Hz]	$\dfrac{f_1}{f_2}$
0.5	1	221.0	238.5	**0.927**	300	18.302	7.028	2.757	10.09	**0.273**
	4	263.5	304.6	**0.865**	300	4.576	1.757	2.757	5.045	**0.546**
	5	198.6	207.3	**0.958**	300	73.208	28.112	2.757	20.18	**0.137**
	6	191.2	250.6	**0.763**	300	1.144	0.439	2.757	2.523	**1.093**
	7	185.5	189.5	**0.979**	300	292.83	112.45	2.757	40.36	**0.068**
	8	254.3	285.9	**0.890**	300	9.151	3.514	2.757	7.135	**0.386**
	9	192.3	201.3	**0.955**	300	36.604	14.056	2.757	14.27	**0.193**
	10	240.3	293.4	**0.819**	300	2.288	0.879	2.757	3.567	**0.773**
	11	99.89	152.3	**0.656**	300	0.286	0.110	2.757	1.262	**2.186**
	12	90.55	140.7	**0.644**	300	0.071	0.028	2.757	0.630	**4.371**
0.3	1	307.0	293.5	**1.046**	300	18.302	9.960	2.757	10.45	**0.264**
	4	381.8	338.1	**1.129**	300	4.576	2.490	2.757	5.225	**0.528**
	5	276.1	271.9	**1.015**	300	73.208	39.842	2.757	20.90	**0.132**
	6	294.6	243.2	**1.211**	300	1.144	0.623	2.757	2.612	**1.055**
	7	259.3	256.7	**1.010**	300	292.83	159.37	2.757	41.79	**0.066**
	8	359.7	339.0	**1.061**	300	9.151	4.980	2.757	7.388	**0.373**
	9	273.8	259.0	**1.057**	300	36.604	19.921	2.757	14.78	**0.187**
	10	358.7	294.3	**1.219**	300	2.288	1.245	2.757	3.694	**0.746**
	11	203.0	229.4	**0.885**	300	0.286	0.156	2.757	1.306	**2.111**
	12	102.7	127.7	**0.804**	300	0.071	0.039	2.757	0.653	**4.221**
0.1	1	378.0	332.2	**1.138**	300	18.302	54.229	2.757	11.67	**0.236**
	4	522.3	334.0	**1.564**	300	4.576	13.557	2.757	5.833	**0.473**
	5	342.7	324.0	**1.058**	300	73.208	216.92	2.757	23.33	**0.118**
	6	478.6	281.7	**1.699**	300	1.144	3.389	2.757	2.917	**0.945**
	7	326.5	317.7	**1.028**	300	292.83	867.66	2.757	46.66	**0.059**
	8	462.5	353.8	**1.307**	300	9.151	27.114	2.757	8.249	**0.334**
	9	364.3	308.4	**1.181**	300	36.604	108.46	2.757	16.50	**0.167**
	10	531.6	313.9	**1.694**	300	2.288	6.779	2.757	4.125	**0.668**
	11	285.3	255.9	**1.115**	300	0.286	0.847	2.757	1.458	**1.890**
	12	148.2	205.6	**0.721**	300	0.071	0.212	2.757	0.729	**3.781**
	13	105.5	177	**0.596**	300	0.036	0.106	2.757	0.516	**5.349**
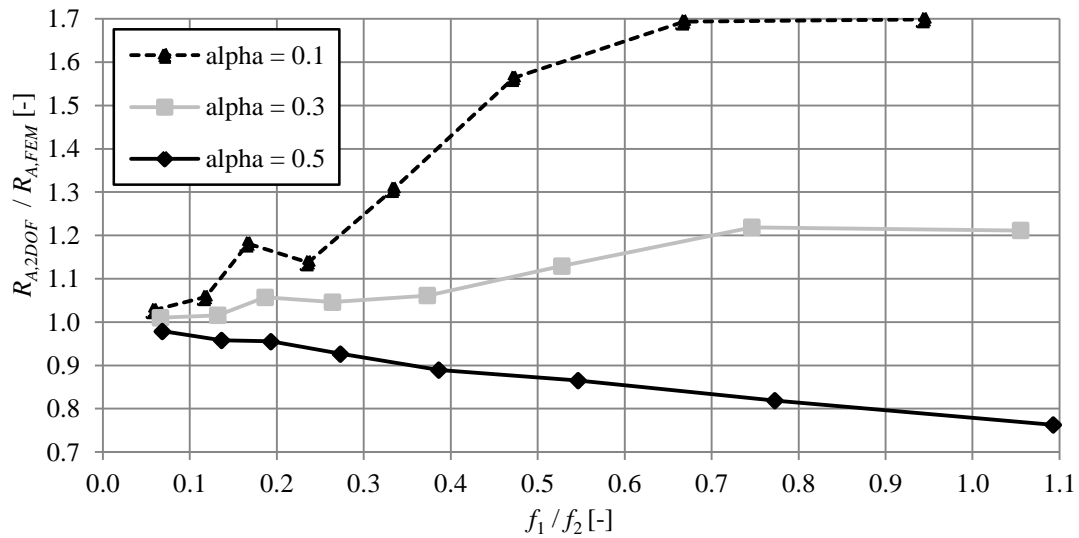
Figure 5.27   Illustration of how the ratio of the support reaction force R_A for the 2DOF and FE model varies with the frequency ratio of the two objects.
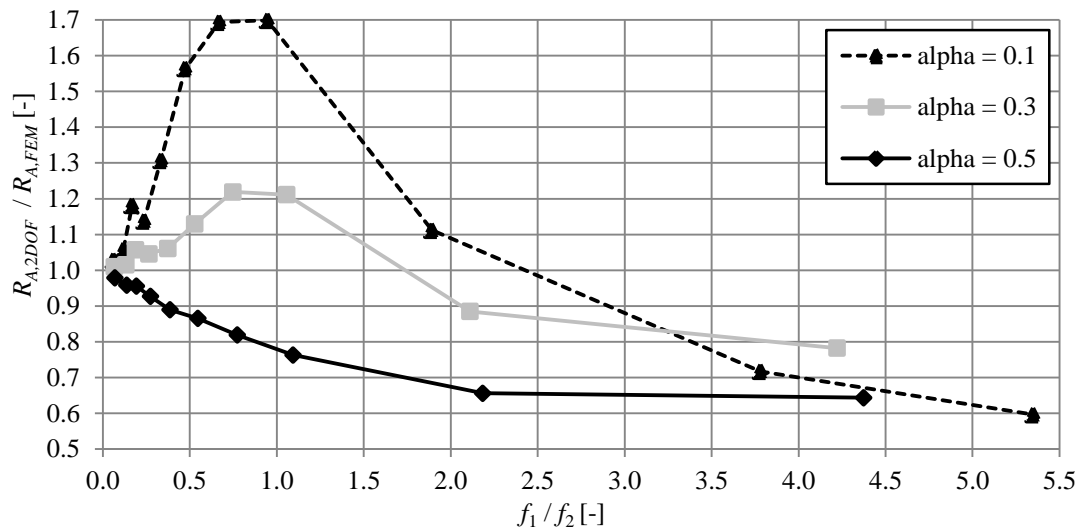
Figure 5.28   Illustration of how the ratio of the support reaction force R_A for the 2DOF and FE model varies with the frequency ratio of the two objects. Same as Figure 5.27 but for higher values of the frequency ratio.

It is now known how the ratio of the reaction force varies with the frequency ratio. It can also be of interest to see how the two reaction forces behave separately from each other, to understand why the ratio looks like it does. This is shown for the FE model in Figure 5.29 and for the 2DOF model in Figure 5.30.
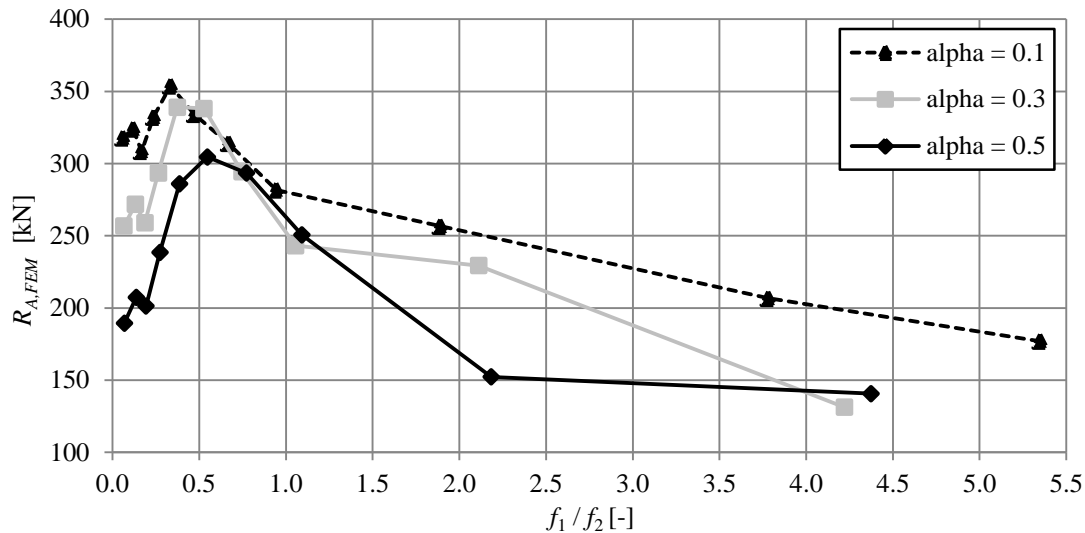
Figure 5.29   Illustration of how the reaction force from the FE model $R_{A,FEM}$ varies with the frequency ratio of the two objects.
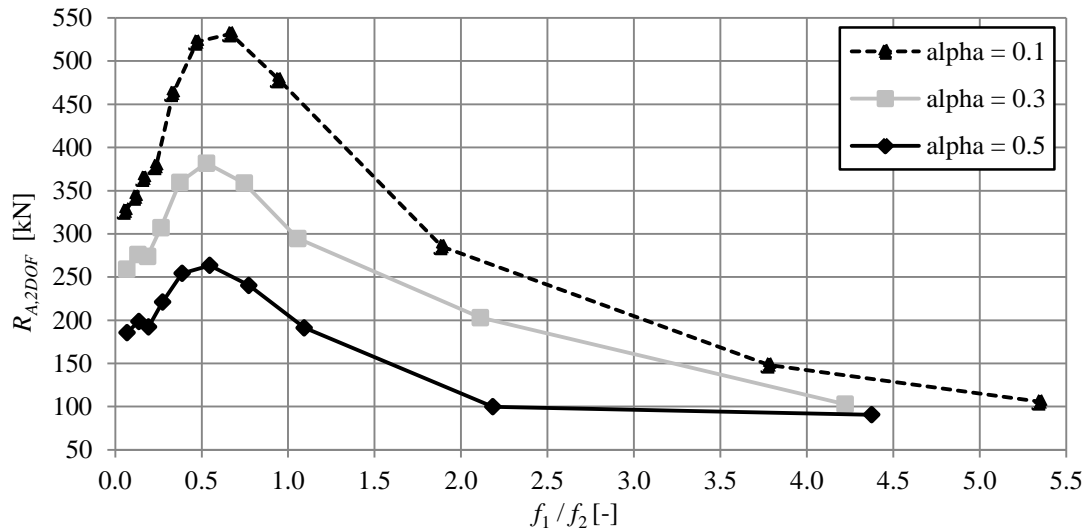
Figure 5.30   Illustration of how the reaction force from the 2DOF model $R_{A,2DOF}$ varies with the frequency ratio of the two objects.

In Figure 5.29 it is seen that the support reaction force $R_{A,FEM}$ has its largest value for all loading positions at a frequency ratio of about 0.5. In the region close to this frequency ratio the difference is also the smallest between the loading positions. The reaction force when loading at $\alpha = 0.1$ is generally the largest one for all frequency ratios, which confirms that it can be the governing load case in a design process.

The reaction force from the 2DOF system $R_{A,2DOF}$ also has its maximum for all loading positions at a frequency ratio of about 0.5. In opposite to the FE model, the difference in response between load cases is largest here, while the responses seem to come closer to each other when the frequency ratio increases. The behaviour of these lines virtually follows the behaviour of the load factor β_{el}, which is plotted for two mass ratios, approximately corresponding to the three loading positions, in Figure 5.31. This is also expected since the load factor diagram is based on a 2DOF model.
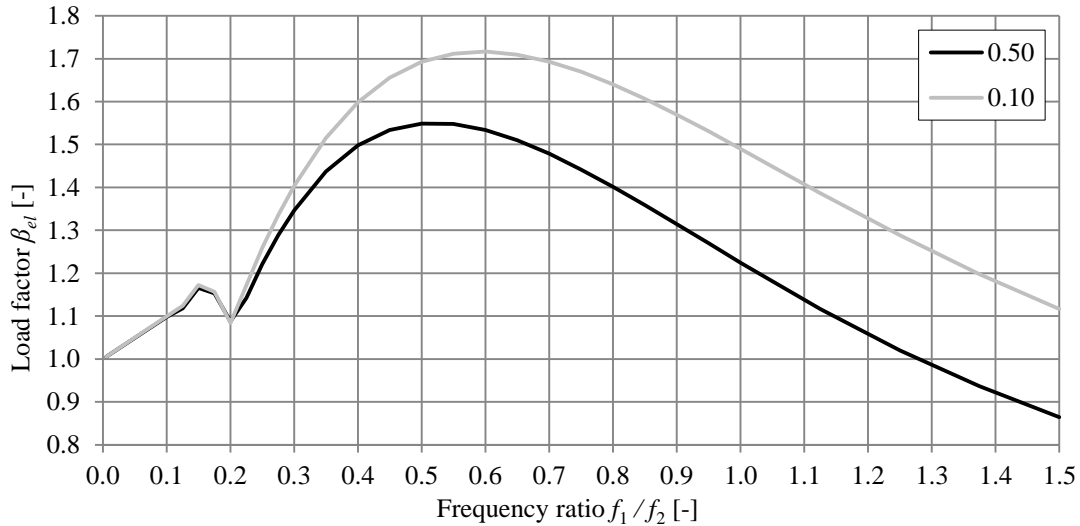
Figure 5.31   Illustration of how the load factor β_{el} varies with the frequency ratio for two different mass ratios, corresponding to the different loading positions.

From Figure 5.29 it can also be seen that the FE response has a slightly different appearance than the 2DOF response, and this gives the idea that a diagram for a load factor corresponding to the FE response could be created, similar to Figure 3.12. This can also be a topic of further studies.

5.3.5 Comparison with calculation model from Biggs

To try and find a more accurate approximation of the support reaction force R_A, compared to FE analysis, that is on the safe side for frequency ratios above 2.0, the conventional calculation model according to Biggs (1964) is implemented. Here the support reaction force R_A is calculated by

$$R_{A,Biggs} = \gamma_1 R_2(t) + \gamma_2 R_1(t) \tag{5.9}$$

where $R_1(t)$ is the external load and $R_2(t)$ is the reaction force obtained from the 2DOF system. The two load factors γ_1 and γ_2 depend on the impact position on the beam and are for impact at midspan, $\alpha = 0.5$, presented by Biggs (1964). The load factors used for other impact positions have previously been determined by Johansson (2014b) and are presented in Table 5.6. If the load factors are studied it can be seen that adding them together gives a value of β corresponding to each loading position in the table

$$\gamma_1 + \gamma_2 = \beta \tag{5.10}$$

where, according to Figure 5.7

$$\beta = 1 - \alpha \tag{5.11}$$

See also equation (5.7) for similarities with equation (5.9) and both equations gives the same response when $R_1(t) = R_2(t)$.

Table 5.6   *Load factors used to determine support reaction force $R_{A,Biggs}$ by conventional method, values from Johansson (2014b).*

α	γ_1	γ_2
0.05	1.429	-0.479
0.10	1.357	-0.457
0.15	1.286	-0.436
0.20	1.214	-0.414
0.25	1.143	-0.393
0.30	1.071	-0.371
0.35	0.999	-0.349
0.40	0.926	-0.326
0.45	0.854	-0.304
0.50	0.781	-0.281

In the following analyses only impacts close to the support, $\alpha = 0.1$, is studied since these are the most critical both with regard to shear force and the ability of the 2DOF system to represent an accurate structural response at this impact position. In order to study the response of the system for even higher frequency ratios than before an additional property set with a beam stiffness 512 times lower than the original beam (property set 1) is created giving a frequency ratio f_1 / f_2 of 5.35 see Table 5.7.

Table 5.7   *The property sets used with Biggs, only impacts at α=0.1 is tested.*

Property set	Max of $R_{A.FEM}$ [kN]	Max of $R_{A.Biggs}$ [kN]	$\dfrac{R_{A.Biggs}}{R_{A.FEM}}$	k_1 [kN/m]	EI_b [MNm^2]	k_b [MN/m]	f_1 [Hz]	f_2 [Hz]	$\dfrac{f_1}{f_2}$
1	332.2	424.1	**1.277**	300	18.302	54.229	2.76	11.67	**0.236**
8	353.8	540.9	**1.529**	300	9.151	27.114	2.76	8.25	**0.334**
4	334.0	648.9	**1.943**	300	4.576	13.557	2.76	5.83	**0.473**
10	313.9	767.2	**2.444**	300	2.288	6.779	2.76	4.13	**0.668**
6	281.7	721.6	**2.562**	300	1.144	3.389	2.76	2.92	**0.945**
11	256.6	430.1	**1.676**	300	0.286	0.847	2.76	1.46	**1.891**
12	206.7	223.5	**1.081**	300	0.071	0.212	2.76	0.739	**3.782**
13	177.0	159.0	**0.898**	300	0.0357	0.106	2.76	0.516	**5.349**
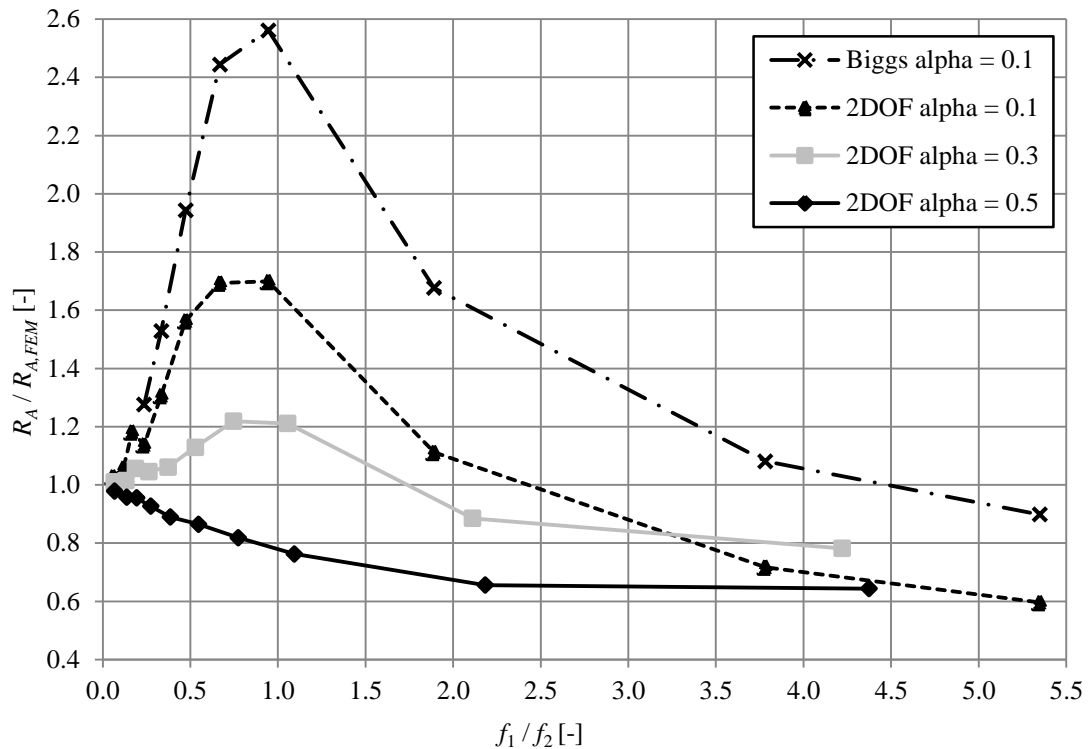
Figure 5.32   Illustration of how the utilization of the reaction force from the 2DOF model and Biggs, compared to the FE model, varies with the frequency ratio of the two objects.

As seen in Figure 5.32 the correlation between Biggs and FEM is similar to the 2DOF model used before up to a frequency ratio of about 0.4, but as the reaction force ratio for 2DOF do not longer increase at a frequency ratio of about 0.7, the overestimation using Biggs still increases, reaching a maximum value of more than 2.5 for a frequency ratio of 0.95. It then starts to decrease but is on the safe side all the way up to a frequency ratio of around 4, and then appears to be converging at a utilization ratio of around 0.8. But further studies are needed to confirm that this is the case for even higher frequency ratios.

In Figure 5.33a it is seen that both 2DOF and Biggs gives a reasonably good approximation of the maximum reaction force, but both shows double bumps that is not visible in the FE-analysis. From Figure 5.33b and Figure 5.33c it can be seen that the reaction force is overestimated but the shape of the curve shows the same sinusoidal behaviour. The behaviour in Figure 5.33b shows that the force becomes almost zero after the initial impact, a response that occurs in all three calculation models. Figure 5.33d shows that neither 2DOF nor Biggs gives a good approximation of the reaction force, instead both methods greatly overestimates it. The maximum value is also delayed by 0.1 seconds compared to the FE analysis. In Figure 5.33e is the 2DOF and Biggs responses again delayed, but this time the 2DOF gives a very good maximum value for the reaction force. In Figure 5.33f it can be seen that 2DOF now gives a smaller maximum value compared to the FE analysis, putting it on the unsafe side, while Biggs give a really good approximation of the maximum support reaction force R_A. However both 2DOF and Biggs shows a much longer loading pulse that reaches its maximum 0.3 seconds later than the FE-analysis. Evidently neither method is able to represent the result in the FE analysis.
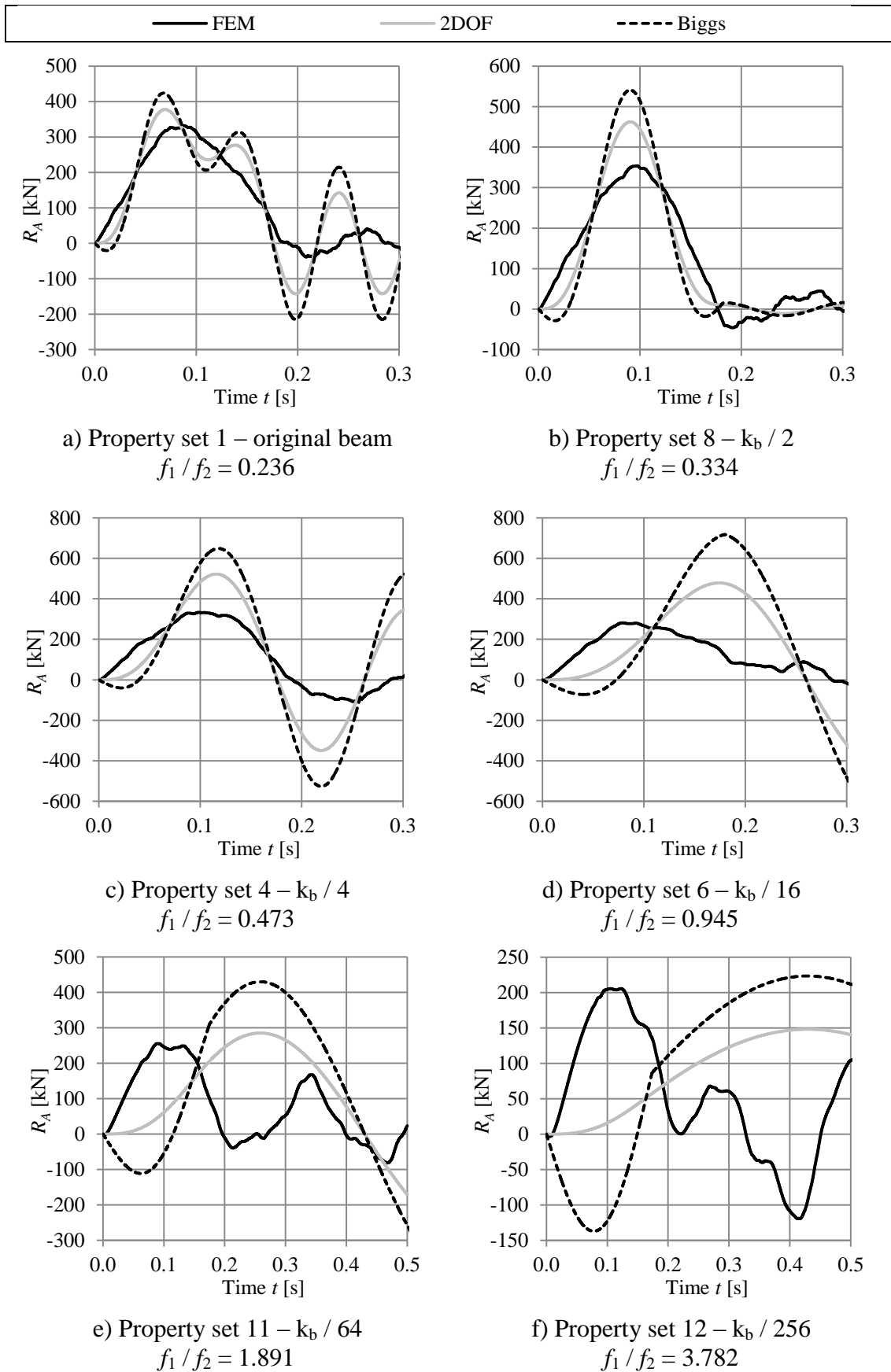
Figure 5.33   Curves comparing how the support reaction force R_A changes over time for the different calculation models, when impact at $\alpha = 0.1$.

a) Property set 1 − original beam
$f_1 / f_2 = 0.236$

b) Property set 8 − k_b / 2
$f_1 / f_2 = 0.334$

c) Property set 4 − k_b / 4
$f_1 / f_2 = 0.473$

d) Property set 6 − k_b / 16
$f_1 / f_2 = 0.945$

e) Property set 11 − k_b / 64
$f_1 / f_2 = 1.891$

f) Property set 12 − k_b / 256
$f_1 / f_2 = 3.782$

One conclusion that can be drawn on the basis of this is that, for frequency ratios below 2.5, the 2DOF system produces the most accurate result and is on the safe side. For frequency ratios above 2.5, Biggs is still on the safe side up to a frequency ratio of about 4.5. For higher frequency ratios the utilization ratio seems to converge at a value around 0.8, meaning the reaction force is underestimated by 20 percent, but further studies are needed to be able to confirm whether this is really the case.

It also needs to be clarified again that the beam stiffness EI_b in the FE software is modified by changing the value of the Young's modulus, instead of changing the moment of inertia. This implies that also the wave speed, dependent on Young's modulus and the density, in the material is changed, see equation (5.6). This could be a reason why the response behaves so different when the beam is very soft and should be investigated further.

When dealing with very soft beams one also needs to remember that damping is ignored in this project. The assumption to do so was valid for stiffer beams but one can argue that the importance of damping is larger when the beam is soft, i.e. for high frequency ratios. This could be because the response is much slower and the effect of damping would have time to make an impact.

5.3.6 Deflection of weak beams

As seen in Figure 5.33 the difference in time between 2DOF and FEM to reach the maximum support reaction force R_A increases for the softer beams with the 2DOF system being much slower. Therefore further studies are performed to study the behaviour of the deflection as the stiffness of the beam k_2 decreases. In this section, the deflection at the point of impact u_2 is compared, this is however not the maximum deflection of the beam that instead will occur close to the midspan regardless of impact position as previously shown in Figure 5.13. The comparison presented in Figure 5.34 shows the deflection u_2 over time when loading at $\alpha = 0.1$. As seen in Figure 5.34a to Figure 5.34d the 2DOF system gives a good estimate of both the size of the maximum deflection and at which time it occurs. In Figure 5.34e and Figure 5.34f the FE analysis shows a double top with the second one being the larger. This is thought to be due to that the impact is so close to the support that the force wave, created from the impact, bounces back from the support with mirrored amplitude. This creates the local minimum that occurs before the absolute maximum is reached. This behaviour is not captured by the 2DOF system which shows a sinusoidal behaviour. The maximum from 2DOF is reached almost at the same time as the FE model has a local minimum but the overall period time seem to correlate well.

Figure 5.34   Comparison of how the deflection u_2 changes over time at position $\alpha = 0.1$ for different property sets.

To see if the phenomenon occurring in Figure 5.34e and Figure 5.34f continues throughout the beam the deflection is also examined at midspan for the same loading position, $\alpha = 0.1$, see Figure 5.35. There it can be seen that the curve from the FE analysis becomes smoother and more stable, showing the same behaviour as the 2DOF model. The maximum response is a little bit delayed in the FE analysis, which is probably due to that it takes some time for the midspan of the beam to react to the impact. This is more noticeable for the soft beams since the wave speed is lower, see equation (5.6).

In opposite to the reaction force the deflection from 2DOF seems to always be on the safe side. This suggests that the reason for the decreasing reaction force for softer beams has something to do with how the reaction force is obtained from the deflection by using the equivalent static load.

a) Property set $11 - k_b / 64$
$f_1 / f_2 = 1.891$

b) Property set $12 - k_b / 256$
$f_1 / f_2 = 3.782$
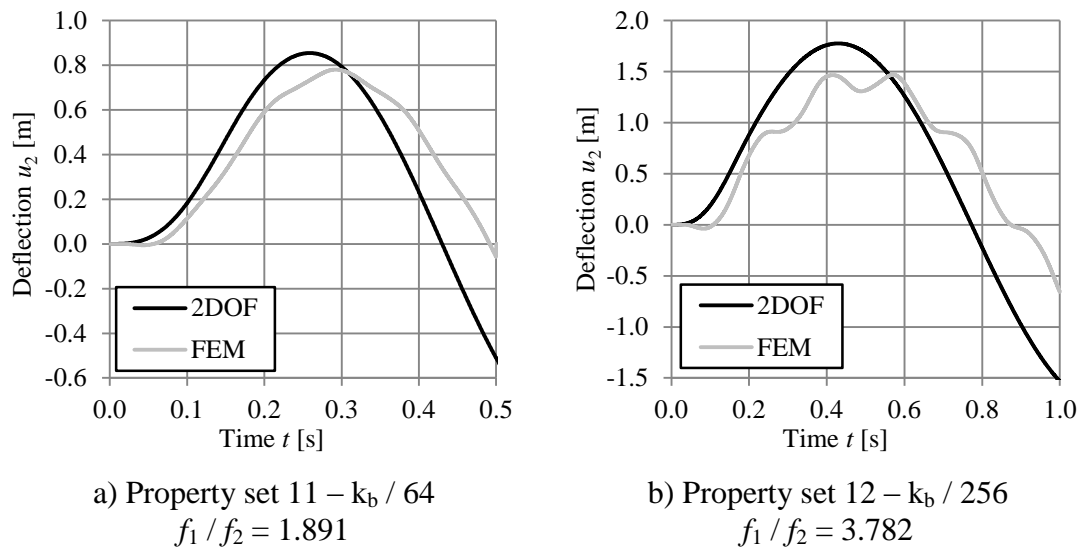
Figure 5.35   Comparison of how the deflection at midspan u_{mid} changes over time for $\alpha = 0.1$ for property sets 11 and 12.

5.3.7 Comparison of response assuming characteristic impulse

For collisions with high frequency ratios, the beam is much softer than the colliding object. This implies that almost all deformation takes place in the beam and that the duration of the impact is short compared to the period T_b of the beam. With this in mind, it is assumed that the impulse in such cases can be seen as a characteristic impulse, with an infinitely short duration. In Figure 5.36 it can be seen how the duration of the impulse decrease when the frequency ratio increases. This is made by changing the stiffness of the colliding object rather than stiffness of the beam, to make the difference easy to compare. The three highest frequency ratios appear to have an impulse that is short enough to be seen as characteristic, see also Figure 5.37. The same reasoning will be valid when changing the stiffness of the beam instead, but in this case the duration of the impact will remain almost constant while the period of the beam T_b increases. This concludes that the governing factor, for when it is reasonable to assume a characteristic impulse, will be the relationship between the duration of impact and the period of the beam.
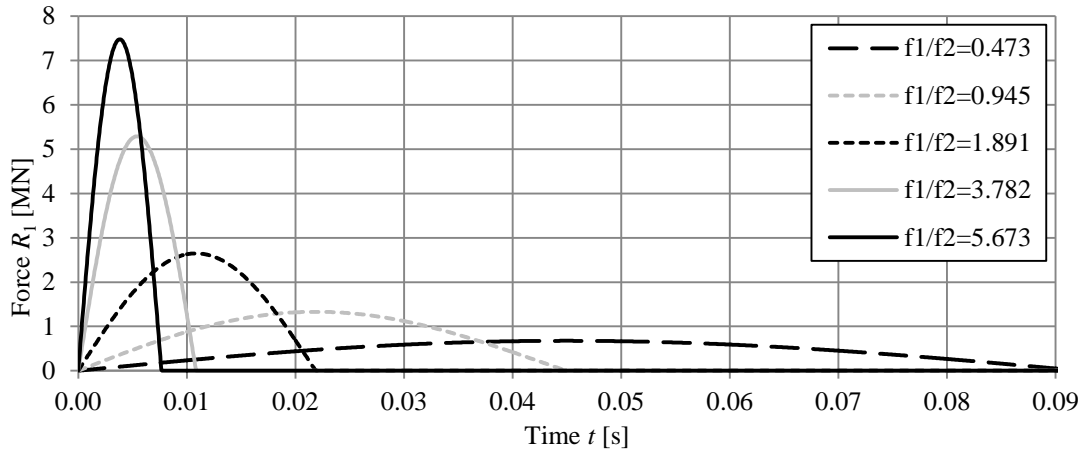
Figure 5.36   Illustration of the shape of the impulse for five different frequency ratios.

Whether this is true or not is investigated in this section by studying the reaction force from a characteristic impulse.

First, the deflection of the beam subjected to a characteristic impulse is written, according to section 2.3.2.2, as

$$u_{2,el} = \frac{I_c}{m_2 \cdot \omega_2} = \frac{I_c}{\sqrt{m_2 \cdot k_b}} \qquad (5.12)$$

where the characteristic impulse is defined as

$$I_c = 2 \cdot m_1 \cdot v_0 \qquad (5.13)$$

when the response is elastic. The reaction force can, by utilizing equation (3.2) and (5.7) together with (5.12), be written as

$$R_{A,char} = k_b \cdot u_{2,el} \cdot \beta \qquad (5.14)$$

This reaction force is now calculated for the property sets with highest frequency ratios, and the result is plotted together with the 2DOF and Biggs results in Figure 5.37. It can be seen that the characteristic impulse gives values that lies somewhere in between the 2DOF and Biggs response when the frequency ratio f_1 / f_2 is above 1.0. This is quite good results if you consider the simple formula for obtaining them, where only the masses, beam stiffness and initial velocity needs to be known. This formula can be used for rough estimates where the reaction force or displacement needs to be estimated with a simple method.
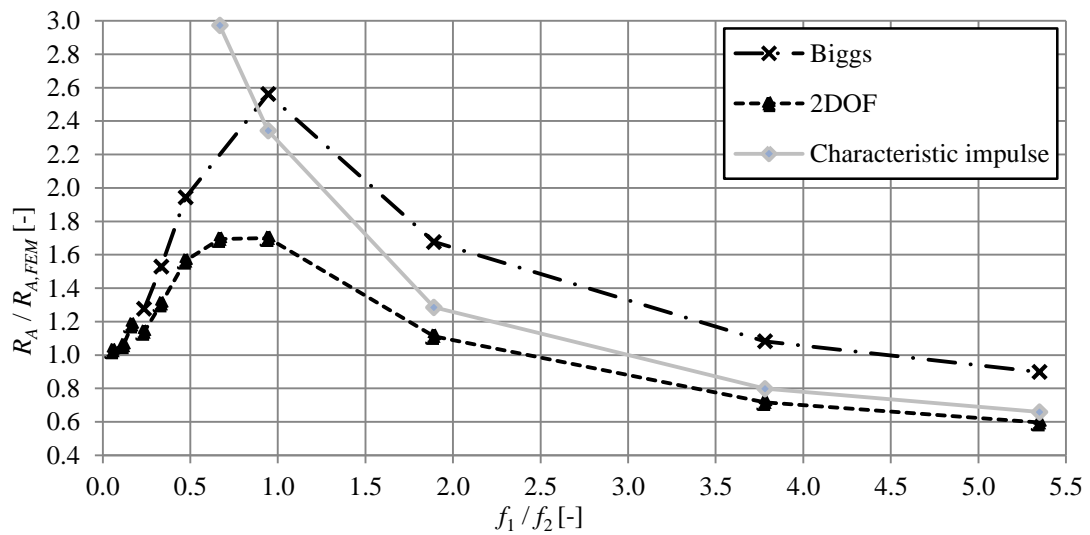
Figure 5.37   Illustration of how the ratio of the support reaction force $R_A / R_{A,FEM}$ when assuming a characteristic impulse varies with the frequency ratio, in comparison to the 2DOF and Biggs responses. Loading at α = 0.1.

5.4 Design example with a bilinear stiffness relationship

5.4.1 Orientation

In this section an example of an analysis is carried out and the aim is to come as close to a real life design problem as possible. The problem consists of analysing a column which is subjected to a collision impact from a moving vehicle, see Figure 5.38. The column is represented by the same elastic beam as was used in previous sections, for a detailed description see section 4.1.2. In order to better capture the real behaviour of a vehicle impact, as described in section 4.1.1, a bilinear load-displacement relationship for the spring representing the vehicle is utilized and the material response is fully plastic, meaning that the displacement remains constant at unloading. A fully plastic vehicle response is also what is assumed in Eurocode, with which a comparison will be conducted. Only the 2DOF model is used for analysis in this section because in ADINA it is not possible to use a plastic response for spring elements.

The analysis is carried out with, in addition to the one described above, five more load-displacement relationships for the vehicle in order to study the difference in response and determine if a simplified relationship can produce acceptable results, see Figure 5.38. The second relationship exhibits an elastic behaviour instead of plastic, the third and fifth relationship exhibits a linear plastic curve and the fourth and sixth a linear elastic curve.
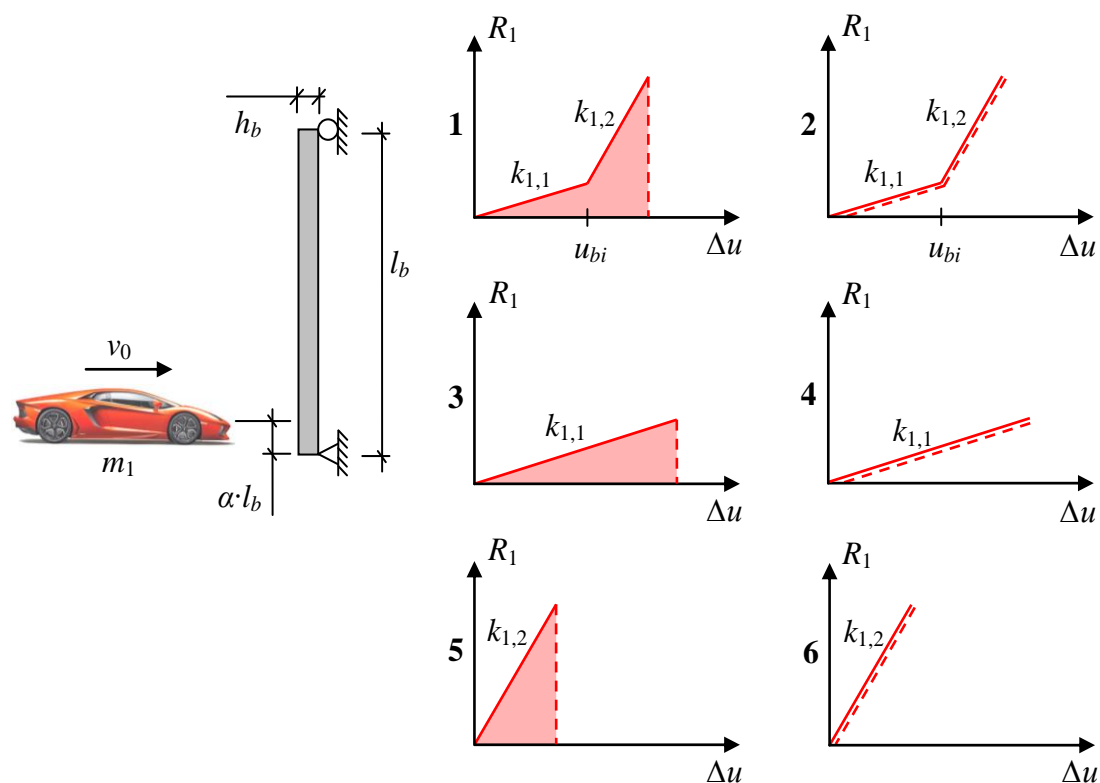
Figure 5.38   Illustration of the vehicle colliding with a beam representing a column and the six different load-displacement relationships for the vehicle studied in this example. The dashed line represents the unloading path.

The properties of both the beam and the vehicle are presented in Table 5.8. The stiffness $k_{1,1}$ is set to 300 kN/m in accordance with Eurocode, $k_{1,2}$ is four times greater, 1 200 kN/m and the change in stiffness is assumed to happen when the deformation of $k_{1,1}$ has reached 0.5 m, which is a reasonable assumption according to Figure 4.10.

The loading position is chosen to be at $\alpha = 0.1$, also in accordance with Eurocode. The stiffness of the beam k_b and the transformation factor $\kappa_{m,el}$ is calculated according to the method presented in section 0 where the transformation to a 2DOF system is described. The mass m_1 is specified as 1 500 kg for cars in Eurocode, and the velocity v_0 is stated as 25 m/s for motorways, so these values are chosen for the study. According to Eurocode the force should be applied as a distributed load with a height of 0.25 m. This small distribution, $\gamma = 0.05$, can according to section 0 be regarded as a point load.

Due to the relatively low frequency ratio in this example the 2DOF system will, according to Figure 5.27, produce a result that is a good estimate of the FE response. Therefore the 2DOF system can, in this case, be seen as a good reference and representation of reality.

Table 5.8   *Properties of the beam and the vehicle for use in the 2DOF model, see section 5.1 for explanation of variables.*

Beam	l_b	5 m
	m_b	3 600 kg
	$EI_b = E_c{\cdot}I_{II}$	18.302 MNm^2
	α	0.1
	k_b	54.23 MN/m
	$\kappa_{m,el}$	2.803
	m_2	10 092 kg
	f_b	11.67 Hz
Vehicle	m_1	1 500 kg
	v_0	25 m/s
	$k_{1,1}$	300 kN/m
	$k_{1,2}$	1 200 kN/m
	u_{bi}	0.5 m
	$f_{1,1}$	2.251 Hz
	$f_{1,2}$	4.502 Hz
Ratios	$f_{1,1} / f_b$	0.193
	$f_{1,2} / f_b$	0.386
	m_1 / m_2	0.149

5.4.2 Results using the 2DOF system

The results from the 2DOF system using the different load–displacement relationships are presented and compared with each other in the following sections. Only the forces are shown since it is the most important parameter and the displacement u_2 follows the same response as the force R_2.

5.4.2.1 Bilinear plastic behaviour – Material response 1

a)   b)
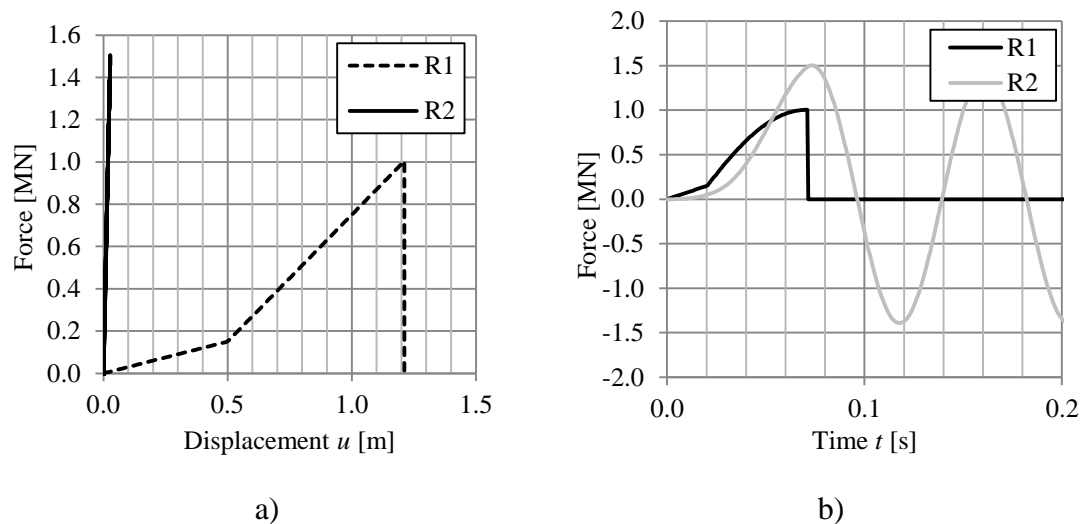
Figure 5.39   Force – Displacement curve and Force – Time curve using material response 1.

In Figure 5.39a the force R_1 is plotted against the deformation Δu and R_2 is plotted against u_2. It can clearly be seen by the shape of R_1 that the vehicle has a plastic material response with a bilinear stiffness. The beam is fully elastic and much stiffer than the vehicle which is confirmed by the shape of R_2. In Figure 5.39b it can be seen that the impulse from R_1 is cut off after reaching the maximum force value and this is when the impact is over. The velocity is at that time zero and the vehicle will change direction. This behaviour is typical for plastic material responses. The maximum force in the beam, seen in both Figure 5.39a and Figure 5.39b, is $R_2 = 1\ 504$ kN.

5.4.2.2 Bilinear elastic behaviour – Material response 2
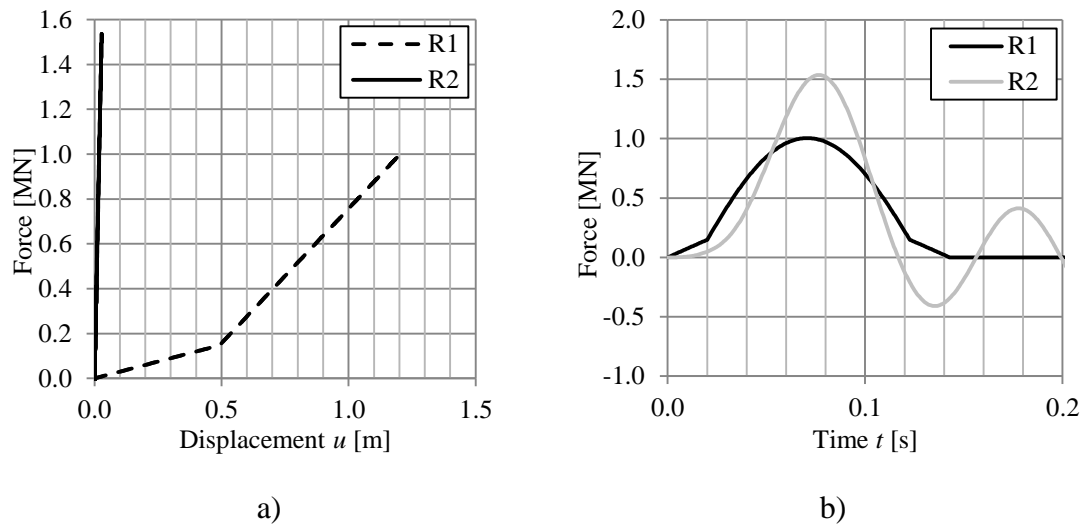
Figure 5.40   Force – Displacement curve and Force – Time curve using material response 2.

The material response of the vehicle is now fully elastic, which is seen in Figure 5.40a. The load R_1 now follows the same path both at loading and unloading, in the same way as the load in the beam R_2. Because of this the impulse is twice as large compared to Figure 5.39b, the maximum force in the second body is on the other hand not much larger than before, reaching a value of $R_2 = 1\ 536$ kN.

5.4.2.3 Linear plastic behaviour – Material response 3 and 5
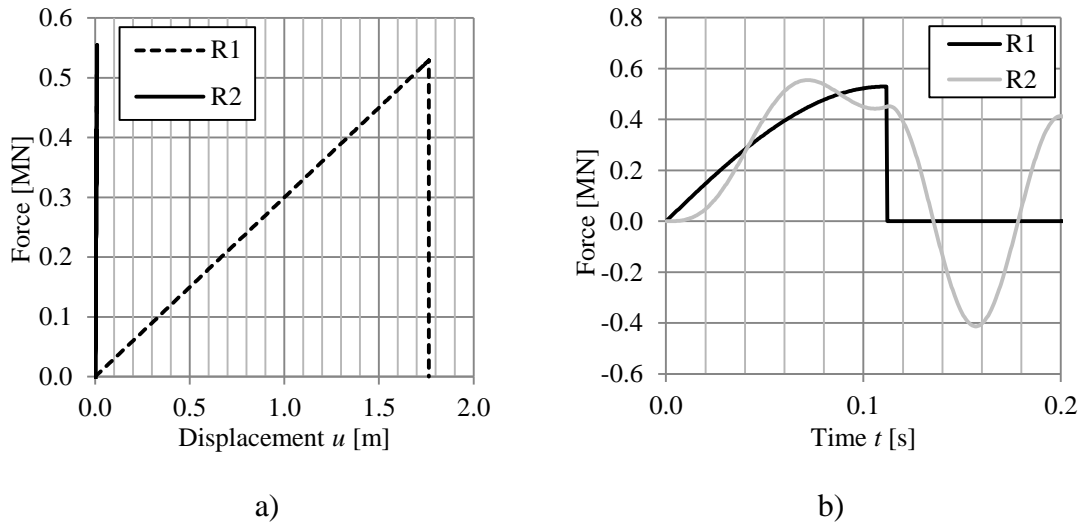
Figure 5.41 Force – Displacement curve and Force – Time curve using material response 3, stiffness $k_{1,1} = 300$ kN/m.

The material response of the vehicle is now linearly plastic using the lower stiffness $k_{1,1}$. Compared to the bilinear case the deformation Δu is much larger and the forces are lower, see Figure 5.41. However the work done by the vehicle, equal to the area under R_1, is about the same as before. The maximum force in the second body now reaches a value of $R_2 = 554.5$ kN.
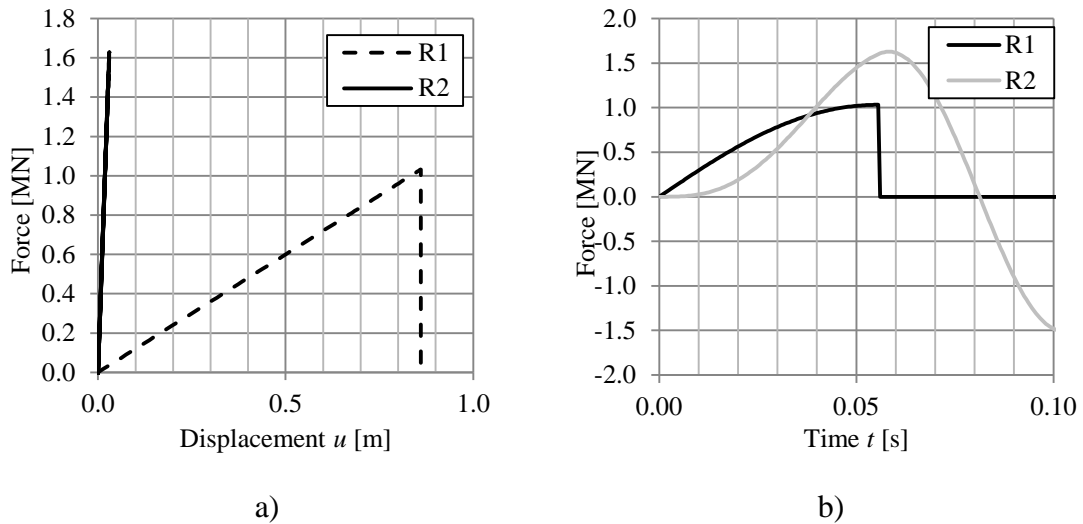
Figure 5.42 Force – Displacement curve and Force – Time curve using material response 5, stiffness $k_{1,2} = 1\ 200$ kN/m.

The material response of the vehicle is again linearly plastic but using the higher stiffness $k_{1,2}$. Compared to the bilinear case the deformation Δu is now smaller but the forces are a little bit larger, see Figure 5.42. The maximum force in the second body now reaches a value of $R_2 = 1\ 629$ kN, which is a good approximation of the response in the bilinear case.

5.4.2.4 **Linear elastic behaviour – Material response 4 and 6**
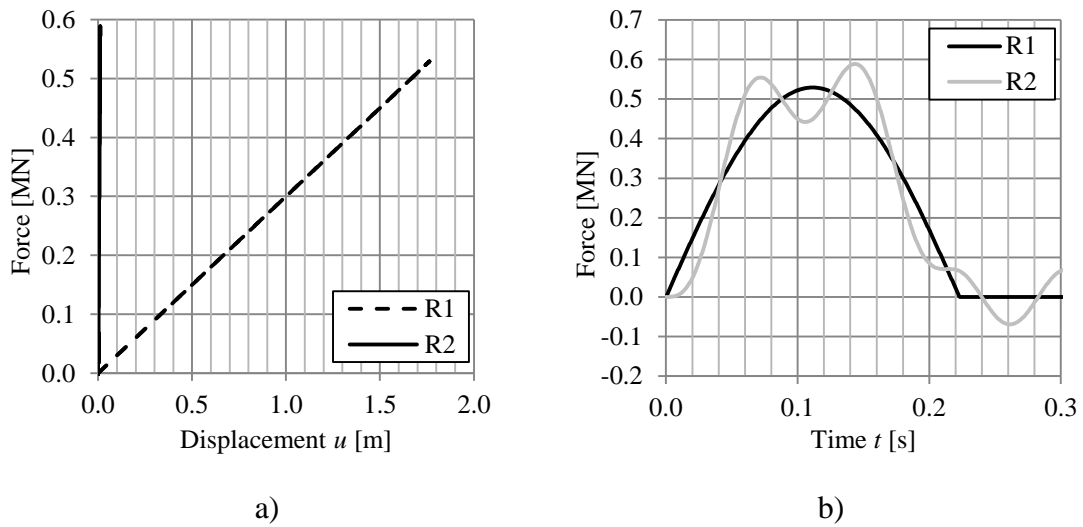
Figure 5.43   Force – Displacement curve and Force – Time curve using material response 4, stiffness $k_{1,1} = 300 \ kN/m$.
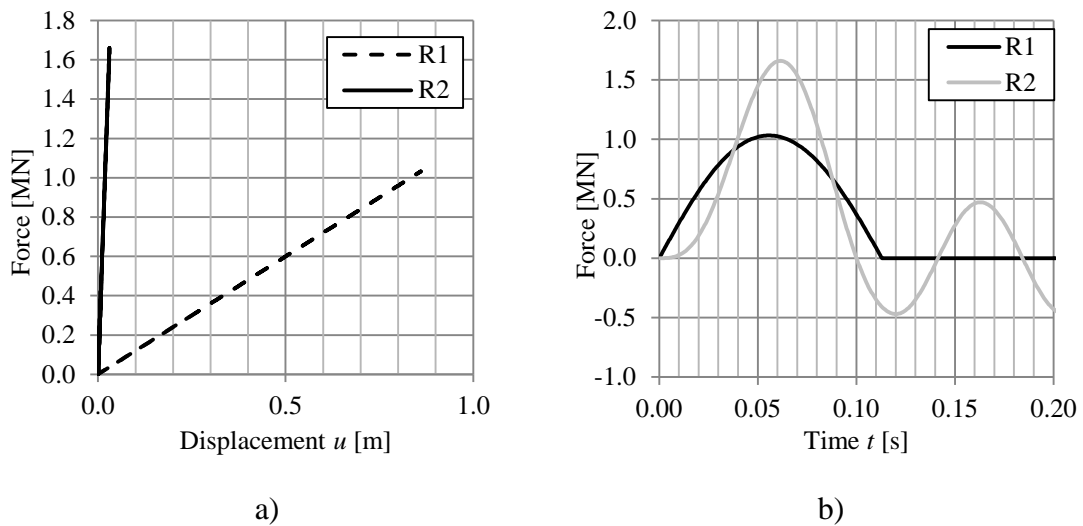
Figure 5.44   Force – Displacement curve and Force – Time curve using material response 6, stiffness $k_{1,2} = 1 \ 200 \ kN/m$.

The material response is now linearly elastic. The results for both forces are almost the same compared to the plastic case, with slightly higher values due to the larger impulse. The maximum force in the second body is for the lower stiffness $R_2 = 588.7$ kN and for the higher stiffness $R_2 = 1 \ 661$ kN.

5.4.2.5 Comparison between material responses

In Figure 5.45 the force in the beam R_2 is compared for the bilinear and linear material responses for both the elastic and plastic cases. The case with linear response and lower stiffness is omitted because of the lower force level.
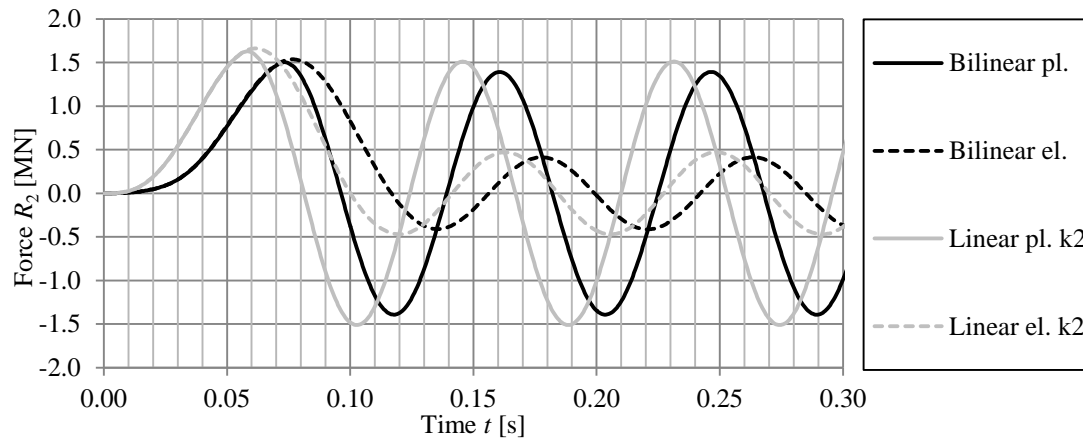
Figure 5.45   Force – Time curve for comparison between the different material responses.

For the elastic responses the maximum force R_2 is slightly larger, due to the double size of the impulse. However, for the plastic cases it can be seen that the amplitude of R_2 is larger after the initial impact compared to the elastic cases, i.e. at $t > 0.1$ seconds. This is due to that for the elastic case the force on the beam R_1 is still acting when the beam is moving in the negative direction, while for the plastic case the force on the beam R_1 stops acting when the vehicle changes direction. The difference in force between the different plastic and elastic material responses are presented in Table 5.9.

Table 5.9   Comparison between the different load – displacement relationships.

Material response	Plastic unloading		Elastic unloading		$\dfrac{R_{2,el}}{R_{2,pl}}$
	$R_{2,\mathrm{pl}}$ [kN]	$\dfrac{R_{2,pl}}{R_{2,pl,1}}$	$R_{2,\mathrm{el}}$ [kN]	$\dfrac{R_{2,el}}{R_{2,pl,1}}$	
Bilinear loading, response 1 and 2	1 504	1.000	1 536	1.021	1.021
Linear loading $k_{1,1}$, response 3 and 4	554.5	0.369	588.7	0.391	1.062
Linear loading $k_{1,2}$, response 5 and 6	1 629	1.083	1 661	1.104	1.020

As seen in Table 5.9 the ratio between elastic and plastic unloading is close to one, 1.021 when using the bilinear loading curve and 1.062 and 1.020 for the linear loading curves. It is also seen that the resulting load when using the bilinear curve is almost three times as large compared to when the linear curve with the lower stiffness $k_{1,1}$ is used. If instead the higher stiffness $k_{1,2}$ is used the resulting load in the beam is slightly overestimated compared to the bilinear curve, with about 8 percent for the plastic case and 10 percent for the elastic case.

This implies that, for the parameters used in this example, the linear response with high stiffness can be used for the vehicle to estimate the real behaviour of the collision impact. This is also on the safe side for both elastic and plastic material response.

5.4.3 Eurocode

The resulting force on the structure is calculated according to Eurocode 1-7, as described in section 4.3. Specifically it is in annex C, "Dynamic design for impact", that the design process is described.

The impact position for cars is given as 0.5 m above the ground in Eurocode, which is the same value as $\alpha \cdot l_b$ used for the 2DOF analysis. All other input values used are as given in Table 5.8.

The theory of hard impact given in Eurocode is used in this study because it states that the vehicle deforms more than the barrier. More precise it assumes a rigid barrier and a vehicle that deforms linearly, hence Eurocode neglects any bilinearity in the vehicle response. The code then states an expression for the maximum resulting dynamic interaction force F, which is given in equation (5.15)

$$F = v_r \cdot \sqrt{k_1 \cdot m_1} \tag{5.15}$$

where v_r is the object velocity at impact. This is the same expression as the dynamic load for a hard impact, derived in section 3.2.1.

If now the current values are inserted into equation (5.15), the response becomes

$$F = 25 \cdot \sqrt{300 \cdot 10^3 \cdot 1500} = 530.33 \, \text{kN} \tag{5.16}$$

This is the maximum dynamic force value that is acting on the outer surface of the structure, corresponding to R_1 in the 2DOF system. Eurocode then states that this value needs to be multiplied with an amplification factor φ_{dyn} to account for dynamic effects inside the structure, thus giving a force corresponding to R_2. It is not explicitly explained how the amplification factor should be calculated, only that a direct dynamic analysis is recommended to use. In fact the amplification factor corresponds well to the load factor β_{el} described in section 3.2.1, even though it is derived for elastic response instead of plastic. Using this load factor would increase the maximum force with about 10 percent in this case, see Figure 3.12. The force in the beam R_2 then becomes

$$R_2 = \beta_{el} \cdot F = 1.1 \cdot 530.33 = 583.36 \, \text{kN} \tag{5.17}$$

which is a good approximation of the linear plastic response obtained in section 5.4.2.3. Because of the great importance of the secondary stiffness $k_{1,2}$, seen in the previous section, it is now natural to instead use that stiffness in equation (5.15) to find a better correlation with the bilinear 2DOF model. By doing so and also multiplying with the corresponding load factor the force in the structure will get a better value

$$R_2 = 1.57 \cdot 25 \cdot \sqrt{1200 \cdot 10^3 \cdot 1500} = 1665.3 \, \text{kN} \tag{5.18}$$

The force is now a lot bigger compared to when using recommended values and it is even on the safe side of the bilinear 2DOF response. It can also be noted that the force is now really close to the 2DOF system when linear response with high stiffness is used, see Table 5.9.

5.4.4 Observations

The different material behaviours of the vehicle proved to give quite big differences in response with the stiffer part of the load-displacement curve to be governing. This is really interesting since, as mentioned before, Eurocode only assumes a linear material relationship with a relatively low stiffness. This leads to that the maximum force R_2 obtained according to Eurocode is only about 40 percent of the maximum force obtained from the 2DOF model using a bilinear material response. This proves that it sometimes can be dangerous to trust the values and formulas in Eurocode without having the proper background knowledge. It should also be mentioned that the stiffness values used for the bilinear material response in this example is much lower, about one third, compared to what was discovered in section 4.1.1, see Figure 4.10.

One would think that a better result would be obtained by using the higher secondary stiffness in the formula from Eurocode. Of course, this is also the case and the response, after multiplying with the load factor, becomes slightly higher compared to the bilinear plastic 2DOF system, meaning it is on the safe side.

Another conclusion from this example is how important the second stiffness is, especially when the velocity of the vehicle is high. On the other hand, for low velocities resulting in deformations below or close to the point of stiffness change, the first stiffness will be dominant.

It should also be pointed out that although the effect of plastic material response proved to be small in this example, the effect is believed to become much larger for collision impacts with a high frequency ratio. For these cases the response of the second body will be much slower than the response of the first. Thereby the entire impulse will be transferred before the second body reaches its maximum deflection, thus will the difference in size of impulse between elastic and plastic response make more difference.

5.4.5 Comparison

It can be interesting to investigate the correlation between Eurocode and the 2DOF model for different velocities when using the higher secondary stiffness value $k_{1,2}$. The load factor β_{el} used in the Eurocode calculation is again obtained from the diagram in Figure 3.12, and the values are presented in Table 5.10. Figure 5.46 shows a magnified version of the graph from Figure 3.12 with the coordinates marked by a cross. Eurocode also provides structural parameters for heavy vehicles and they are therefore included in this comparison. The same stiffness values should be used for all types of vehicles according to Eurocode, therefore the stiffness $k_{1,2}$ is used for both types of vehicle.

Table 5.10   Properties used for obtaining the load factor β_{el} in the example.

Vehicle	m_1 [kg]	$k_{1,2}$ [kN/m]	$f_{1,2}$ [Hz]	$\dfrac{m_1}{m_2}$	$\dfrac{f_{1,2}}{f_b}$	β_{el} [-]
Car	1 500	1 200	4.502	0.149	0.386	1.57
Heavy vehicle	30 000	1 200	1.007	2.973	0.086	1.08
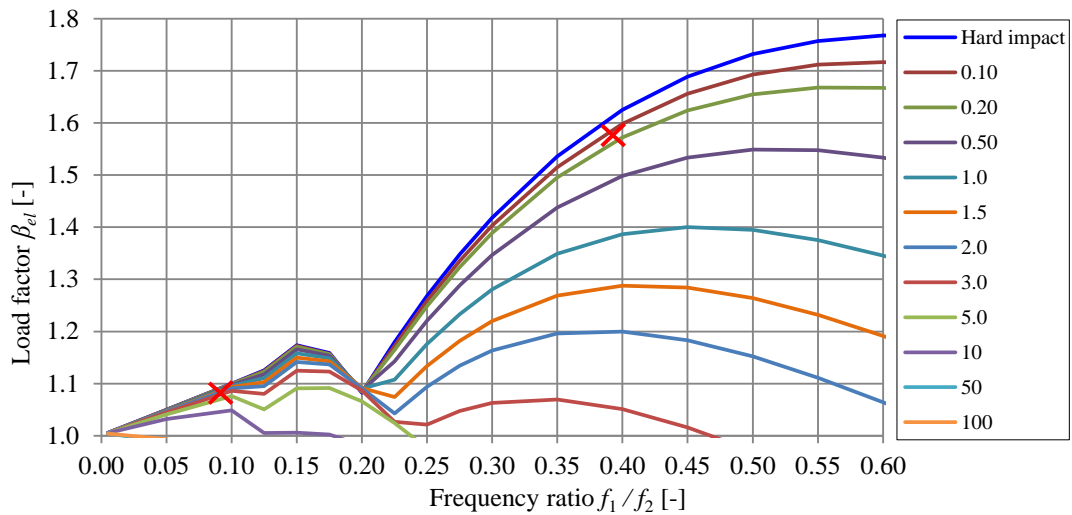
Figure 5.46   Load factor diagram with coordinates used in the example.

The comparison for different velocities can be seen in Figure 5.47 for the two types of vehicle. The correlation between Eurocode and the 2DOF model is acceptable for the case with the car, as long as the initial velocity is not too low. This is due to that the bilinear material response is used in the 2DOF system and the secondary stiffness $k_{1,2}$ will not influence the response at initial velocities under about 8 m/s, see Figure 5.47. At such low initial velocities Eurocode will overestimate the response with up to 170 percent. In these cases it would be wiser to use the lower stiffness $k_{1,1}$ in the Eurocode calculation. When the heavy vehicle is studied the correlation is very good. The bilinear response is still used for the vehicle but since the mass is very large the secondary stiffness is reached at a much lower velocity, about 1.6 m/s. This velocity can be obtained by using equation (5.19)

$$v_0 = u_{bi}\sqrt{\frac{k_{1,1}}{m_1}} \tag{5.19}$$

It should be noted that the stiffness still changes at the same force level and deformation as before, see Figure 5.39a.

a) Car

b) Heavy vehicle
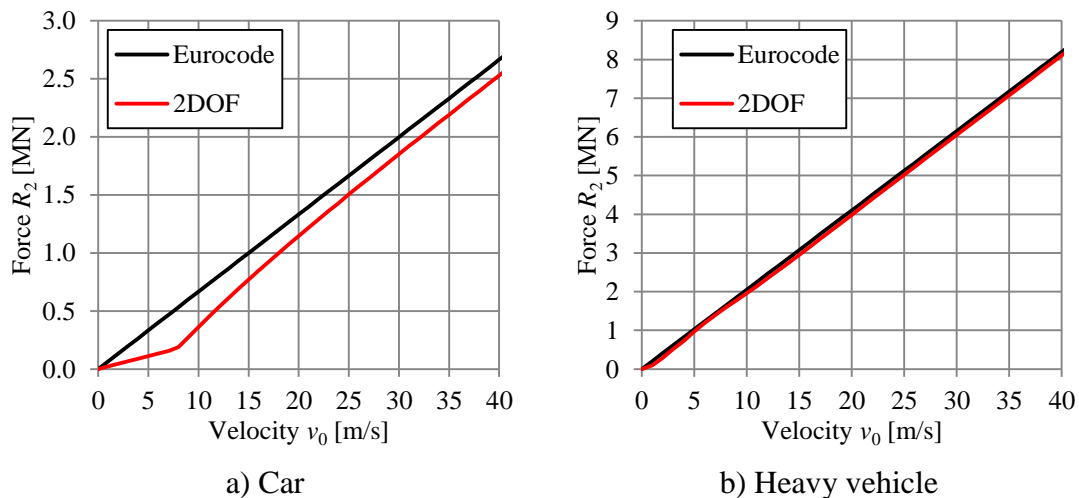
Figure 5.47   Comparison of resulting force in the beam between Eurocode and bilinear 2DOF for different initial velocities.

From this example it can be concluded that the method provided in Eurocode can be a good estimation in a design process, as long as the correct value of the vehicle stiffness and load factor is used. The method seems to always be on the safe side because it assumes a hard impact. It should though be noted that the results may not really be accurate for the highest velocities presented, due to the unknown response of the vehicles at such large corresponding deformations. This is especially important for the heavy vehicle where the deformation will be larger at the same velocity.

A suggestion for Eurocode would be to use a stiffness which depends on the initial velocity and mass of the colliding vehicle. This would give a response that was closer to the bilinear 2DOF response at different initial velocities. This would not be too complicated to introduce if only the properties of the bilinear material response is fully known. More detailed studies of the load-displacement relationship in vehicles during collision impact needs to be conducted. This needs to be made also for different initial velocities to determine if the bilinear material response is dependent on the velocity as well.

6 Final Remarks

The objective of this Master's thesis has been to investigate a collision impact and the resulting responses using both simplified and more advanced design approaches. The different methods, including a two degree of freedom (2DOF) system and a finite element (FE) model, have also been compared. This is made in order to see how well the simplified methods are able to describe the behaviour of a collision impact against a simply supported beam with elastic response.

6.1 Conclusions

The overall behaviour of an impact is not dependent on the individual properties of the involved objects but rather on the relationship between the properties. Therefore, a convenient parameter to use as a base in linear elastic analyses is the ratio of the eigenfrequencies of the two objects, which depends on the mass and stiffness of both objects.

For a 2DOF system the load factor β_{el} is a very convenient tool for obtaining the resisting force in the second body from the dynamic load of an hard impact. A good way of presenting the load factor is to plot it as a function of the frequency ratio and for different values of the mass ratio.

The response in a beam during a collision can be very different from when a static load is applied at the same position. This is more pronounced for collisions with high frequency ratios where, for example, the maximum moment might occur at a different section than at the point of impact.

For a collision on a simply supported beam, the correlation between the shear force from the 2DOF system and FE analysis greatly depends on the frequency ratio. The correlation is also different depending on the impact position. It is best when the frequency ratio is close to zero and around two. Between these values the 2DOF response is on the safe side for impacts close to the support, but the maximum shear force might be greatly overestimated. For frequency ratios above 2.5 the 2DOF system produces results that are on the unsafe side compared to the FE analysis. When using the conventional model, also referred to as Biggs model, to calculate the maximum shear force the results are larger compared to the 2DOF system for all frequency ratios. This implies that the Biggs response produces better results for high frequency ratios, although it will be unsafe as well if the ratio is high enough.

In opposite to the shear force, the maximum deflection of a beam obtained from the 2DOF model always has a good correlation with the FE analysis. It is also on the safe side for all frequency ratios treated in this thesis. This suggests that using the equivalent static load for obtaining the sectional forces may not be valid for high frequency ratios.

The load-displacement relationship for cars during a collision seems to have a bilinear response with a considerable stiffness increase after a certain deformation. Even though the overall behaviour obtained from crash tests are similar, it should be noted that there are some variation in the results depending on the model of the car and test method used. The material response of the colliding vehicle was successfully implemented in the 2DOF system and produced reasonable results. However, these were for some cases significantly different to what was found when using the linear

stiffness proposed by Eurocode. Furthermore, it was found that the 2DOF response can easily be estimated by utilizing the theory of hard impact and using an appropriate vehicle stiffness. This stiffness depends on the velocity at impact and should be higher for high velocities and lower for low velocities. Which stiffness to use is also highly dependent on the mass of the vehicle.

The theory of hard impact is also utilized in Eurocode but here the same stiffness is used for all types of vehicles and for all impact velocities, i.e. a linear response is assumed. This stiffness is also very low compared to what was found from the studied crash tests, indicating that the obtained response might be too low. A proposed revision for Eurocode is to use different vehicle stiffnesses for different type of roads and vehicles.

6.2 Recommendations of approach for analysis

The following recommendations are valid for analyses of collisions against simply supported beams.

- To estimate the shear force the 2DOF system should be used for frequency ratios below 2.5 and Biggs for frequency ratios between 2.5 and 4.5. For higher frequency ratios both the 2DOF system and Biggs will be on the unsafe side and an FE analysis may be necessary.
- For frequency ratios above 1.5 it is possible to make a rough estimation of the beam response using the deflection from the characteristic impulse. For the shear force this response will always lie between the 2DOF and Biggs responses.
- For vehicle impact against a rigid barrier, such as a heavy concrete structure, the response can be estimated by utilizing the theory of hard impact and using an appropriate vehicle stiffness. This will always give results on the safe side.

6.3 Further studies

In this thesis only elastic material response of the beam has been studied. To make the analysis more refined a plastic material behaviour should be implemented in the models in order to study what effect this might have on the beam response. Nonlinear response of the incoming object should also be investigated further.

To confirm that vehicles have a bilinear load-deflection curve more studies of crash tests need to be conducted. It is also of interest to study if this behaviour differs for different impact velocities and different types of vehicles, for example heavy trucks. Furthermore, it is important to determine what stiffnesses to use since these, from what is found in this thesis, seem to be much larger compared to what is given in Eurocode.

The correlation in shear force between the 2DOF system and FE analysis is, in this thesis, studied up to a frequency ratio of about five. But at this frequency ratio the tendency is that the correlation between the models will converge as the frequency ratio becomes even higher, with the 2DOF model producing results on the unsafe side. It also appears like the difference between the impact positions will disappear for high frequency ratios. These phenomena need to be investigated further to confirm that this really is the case.

A similar diagram as the one describing the load factor β_{el} as a function of the frequency ratio could be created, but this time for the FE responses, both shear force and moment, rather than the 2DOF response. This should be made for both an elastic and plastic material response for both objects. The diagram should include high frequency ratios to also make it valid for a so called soft impact.

In this thesis only collision against a simply supported beam is studied, but it could also be interesting to study a beam with other support conditions. Furthermore, it would be of interest to analyse a collision against a plate with different boundary conditions. It then needs to be investigated how the sectional forces should be calculated and how the response and crack pattern differs from static loading. In the same way as for the beam it should be determined how well a 2DOF system is able to describe the response of a plate.

The bending stiffness EI_b used in the FE analysis is modified by changing the value of the Young's modulus E, rather than changing the moment of inertia I. This means that also the wave speed in the material is changed and could be a reason why the response is so different for very soft beams. This potential problem should be investigated further by changing the beam stiffness by modifying the moment of inertia directly.

An intense impact on a concrete structure could cause spalling at the back of the structure. A study of this phenomenon should be carried out in order to be able to describe it in detail. It would also be useful to determine what simplified models to use in order to predict the size and velocity of the spalled concrete.

A modal analysis of the beam deflection shape could be made, by using Fourier transformations, in order to better understand the importance of each of the different eigenmodes for different impact positions.

7 References

ADINA R & D, Inc., 2014. *ADINA System 9.0 Release Notes,* Watertown: s.n.

Al-Thairy, H. & Wang, Y., 2013. An assesment of the current Eurocode 1 design methods for building structure steel columns under vehicle impact. *Journal of Constructional Steel Research,* Issue 88, pp. 164-171.

Biggs, J. M., 1964. *Introduction to Structural Dynamics.* Boston: McGraw-Hill Inc..

Cederwall, K., Lorentsen, M. & Östlund, L., 1990. *Betonghandboken - Konstruktion.* 2nd ed. Stockholm: Svensk byggtjänst.

CEN, 2004. *Eurocode 2: Design of concrete structures Part 1-1,* Stockholm: SIS Förlag AB.

CEN, 2010. *Eurocode 1 - Actions on structures - Part 1-7: General actions - Accidental actions,* Stockholm: SIS Förlag AB.

Craig Jr., R. R. & Kurdila, A. J., 2006. *Fundamentals of Structural Dynamics.* 2nd ed. Hoboken, New Jersey: John Wiley & Sons, Inc.

Dynamore GmbH, 2014. *Frontal Barrier Models.* [Online]
Available at: http://www.dynamore.de/en/products/models/front-barrier
[Accessed February 2014].

EURO NCAP, 2007. *Media player Fiat 500 pictures.* [Online]
Available at: http://www.euroncap.com/Player.aspx?nk=1bc0cec3-7e65-4838-b48c-313eef8a5361&t=2&sel=402bb7a8-480f-48cb-b92a-50792cfaf662
[Accessed February 2014].

EURO NCAP, 2014. *The tests explained - Frontal impact.* [Online]
Available at: http://www.euroncap.com/tests/frontimpact.aspx
[Accessed 21 February 2014].

Fortifikationsförvaltningen, 1973. *Provisoriska anvisningar för dimensionering av armerade betongkonstruktioner som skydd mot verkan av konventionella vapen inom närmissområde.* Bk 25:2 ed. Stockholm: Fortifikationsförvaltningen - Befästningsavdelningen.

Huibers, J. & de Beer, E., 2001. *Current front stiffness of European vehicles with regard to compatability,* The Netherlands: TNO Automotive Crash Safety Centre.

Johansson, M., 2014a. *Beräkningsmetodik Stötlast,* Gothenburg: Reinertsen Sverige AB.

Johansson, M., 2014b. *Personal communication and working notes* [Interview] (March 2014b).

Johansson, M. & Laine, L., 2012. *Bebyggelsens motståndsförmåga mot extrem dynamisk belastning, Del 3: Kapacitet hos byggnader,* s.l.: MSB.

Lundh, H., 2000. *Grundläggande Hållfasthetslära.* Stockholm: s.n.

Struble, D. E., 2014. *Automotive Accident Reconstruction: Practices and Principles.* Boca Raton: Taylor & Francis Group.

Takizawa, S., Higuchi, E. & Iwabe, T., 2005. *Study of load cell MDB crash tests for evaluation of frontal impact compatibility,* s.l.: Honda R&D Co. Ltd. , PSG Co. Ltd..

Tolman, S. S., 2008. *Analysis of Load Cell Barrier Data for Accident Reconstruction Applications,* Salt Lake City: Department of Mechanical Engineering, The Univeristy of Utah.

Volvo Cars, 2013. *The all-new Volvo V40 makes it Malaysian debut at Mid Valley.* [Online]
Available at:
http://www.volvocars.com/my/PublishingImages/news_events/2013/20130820_innovation3.jpg
[Accessed February 2014].

Wikipedia, 2014. *Crumple zone.* [Online]
Available at: http://en.wikipedia.org/wiki/Crumple_zone
[Accessed 19 February 2014].

Appendix A   Central difference method

The central difference method is summarized as a step by step algorithm in this appendix, see Table A.1, based on Craig Jr. and Kurdila (2006).

Table A.1   Algorithm for the central difference method, a tool for solving the equation of motion.

Step 0	(0.1) Input the mass, damping and stiffness matrices **M**, **C**, **K**
	(0.2) Calculate the LU factorization of **M**
	(0.3) Input the initial conditions u_0 and v_0
	(0.4) Set the simulation parameters including the time-step Δt
	(0.5) Calculate the initial acceleration from the equations of motion $$\ddot{u}_0 = \mathbf{M}^{-1}\big(F(0) - \mathbf{C} \cdot v_0 - \mathbf{K} \cdot u_0\big)$$
	(0.6) Calculate the LU-factorization of ' $$\frac{\mathbf{M}}{\Delta t^2} + \frac{\mathbf{C}}{2 \cdot \Delta t}$$
	(0.7) Calculate the starting displacement value from the equation $$u_{-\Delta t} = u_0 - \Delta t \cdot \dot{u}_0 + \frac{\Delta t^2}{2} \cdot \ddot{u}_0$$
Step 1	Loop for each time-step Δt
Step 2	Solve the displacements for the next time-step $$\mathbf{u}_{t+\Delta t} = \big(\Delta t^2 \mathbf{M}^{-1} + 2 \cdot \Delta t \mathbf{C}^{-1}\big)\left(\mathbf{F}(t) - \left(\mathbf{K} - \frac{2 \cdot \mathbf{M}}{\Delta t^2}\right)\mathbf{u}_t - \left(\frac{\mathbf{M}}{\Delta t^2} + \frac{\mathbf{C}}{2 \cdot \Delta t}\right)\mathbf{u}_{t-\Delta t}\right)$$
Step 3	Evaluate the set of velocities and accelerations as needed $$\dot{u}_t = \frac{u_{t+\Delta t} - u_{t-\Delta t}}{2 \cdot \Delta t}$$ $$\ddot{u}_t = \frac{u_{t+\Delta t} - 2 \cdot u_t + u_{t-\Delta t}}{\Delta t^2}$$
Step 4	set $t = t + \Delta t$ and continue to the next time-step

Appendix B Results 2DOF system without barrier

B.1 Elastic response

In this section results for Collision 1, Collision 2 and Collision 3 are presented, according to the analysis discussed in section 3.1.1.

Table B.1 Input parameters for the elastic classic collision analyses.

Case	m_1 [kg]	m_2 [kg]	k_1 [kN/m]	v_0 [m/s]
Collision 1	1 000	10 000	100	20
Collision 2	100 000	10 000	100	20
Collision 3	100 000	10 000	1 000	20

a)

b)

c)

d)
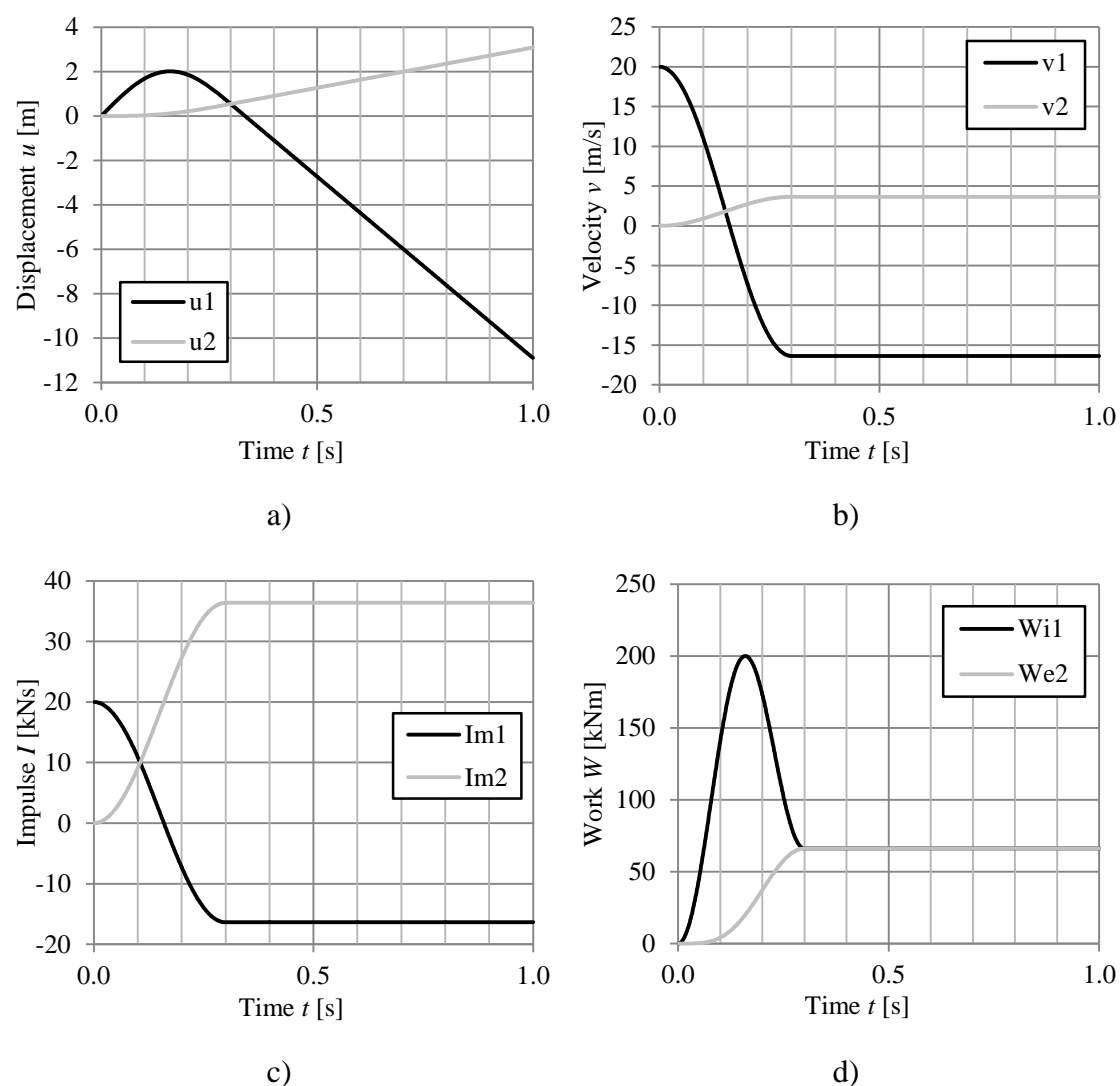
Figure B.1 Results from an elastic classic collision, Collision 1, where $m_1 = 1\ 000$ kg, $m_2 = 10\ 000$ kg, $k_1 = 100$ kN/m and $v_0 = 20$ m/s.
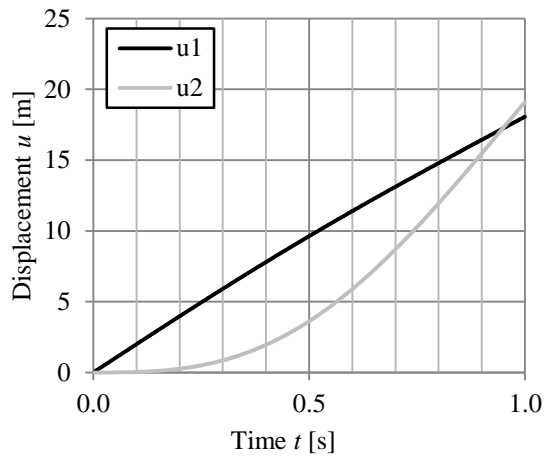
a)
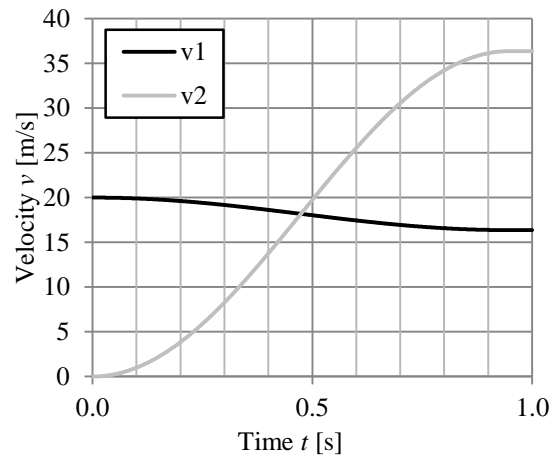
b)
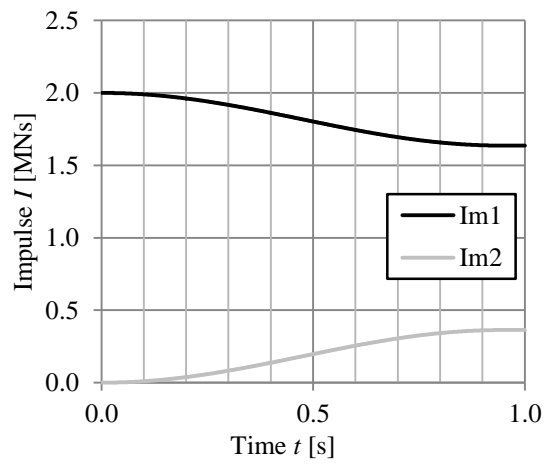
c)
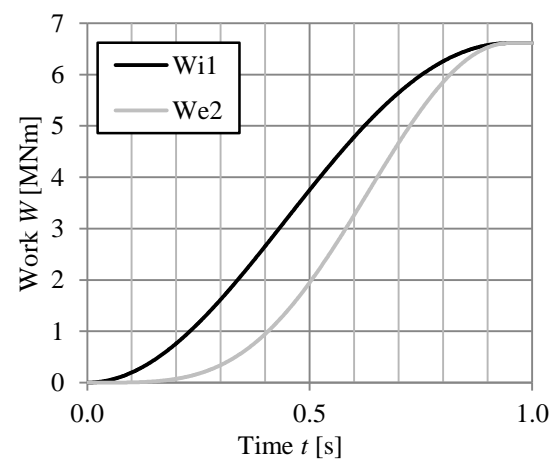
d)

Figure B.2   *Results from an elastic classic collision, Collision 2, where* $m_1 = 100\ 000$ kg, $m_2 = 10\ 000$ kg, $k_1 = 100$ kN/m *and* $v_0 = 20$ m/s.

a)

b)

c)

d)
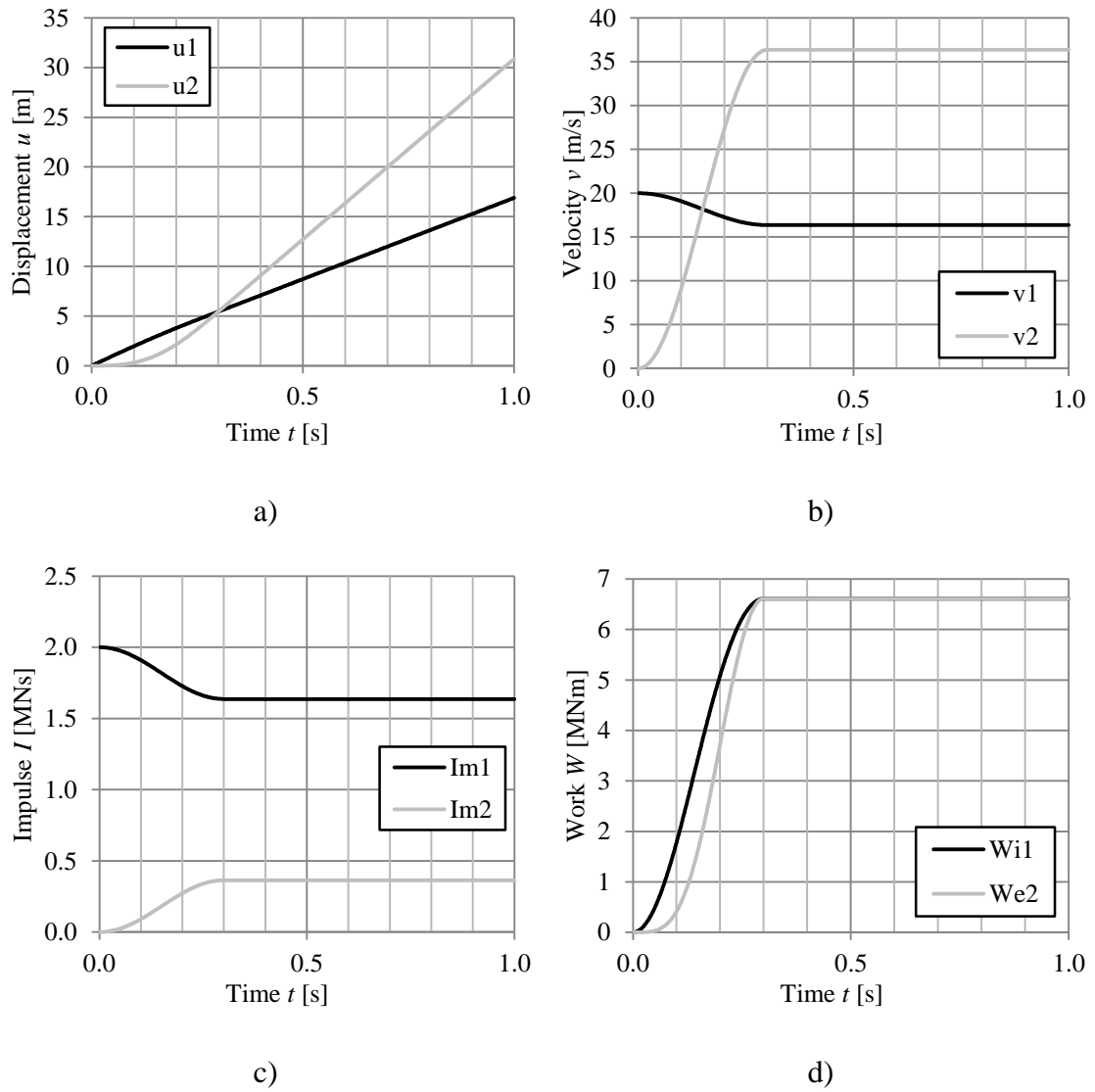
Figure B.3   Results from an elastic classic collision, Collision 3, where $m_1 = 100\ 000$ kg, $m_2 = 10\ 000$ kg, $k_1 = 1\ 000$ kN/m and $v_0 = 20$ m/s.

B.2 Plastic response

In this section results for Collision 4, Collision 5 and Collision 6 are presented, according to the analysis discussed in section 3.1.2.

Table B.2   Input parameters for the plastic classic collision analyses.

Case	m_1 [kg]	m_2 [kg]	k_1 [MN/m]	R_1 [kN]	v_0 [m/s]	e
Collision 4	1 000	10 000	100	200	20	0.033
Collision 5	100 000	10 000	100	200	20	0.011
Collision 6	100 000	10 000	100	400	20	0.021

a)

b)

c)

d)
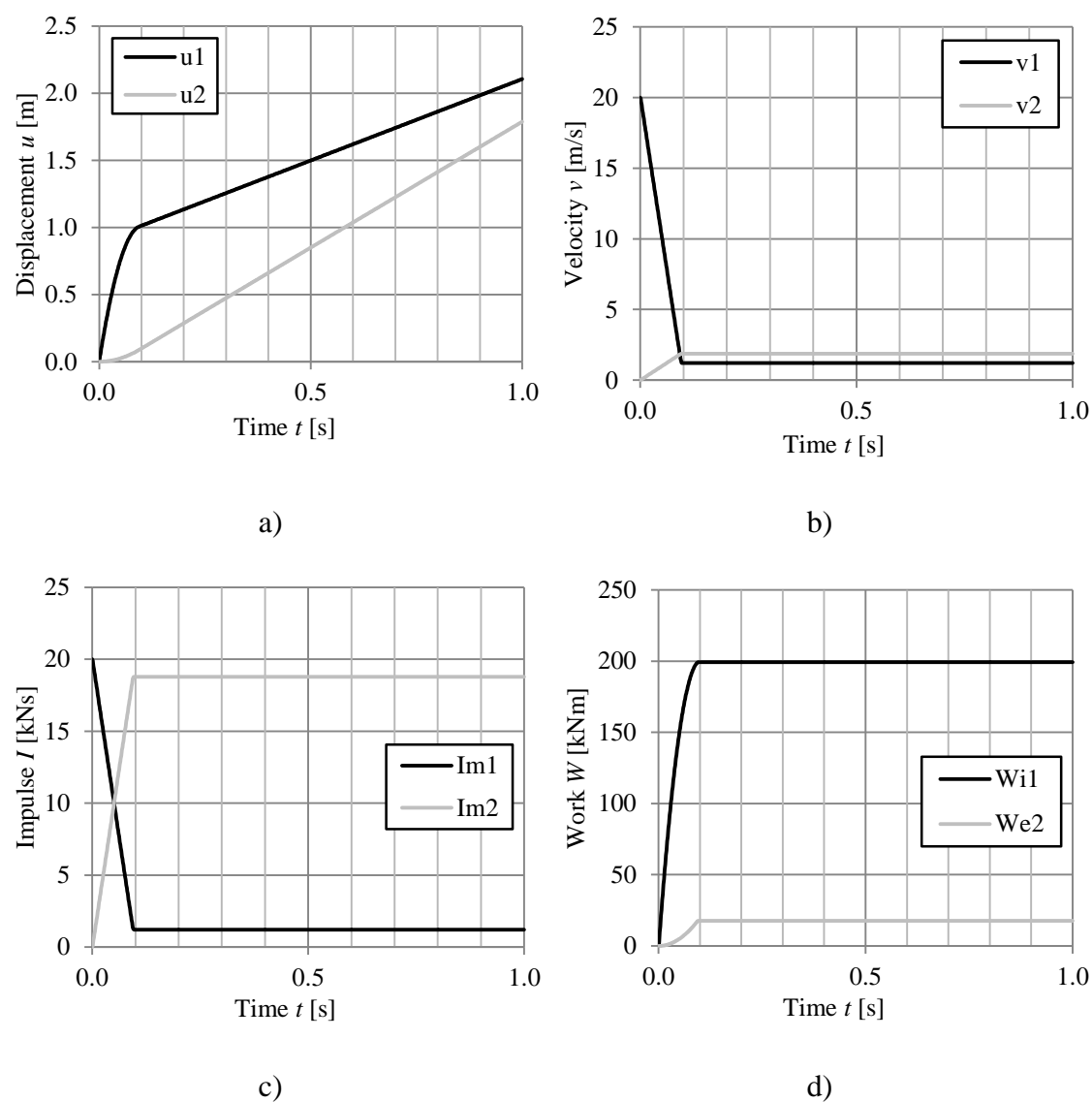
Figure B.4   Results from a plastic classic collision, Collision 4, where m_1 = 1 000 kg, m_2 = 10 000 kg, k_1 = 100 MN/m, R_1 = 200 kN and v_0 = 20 m/s.
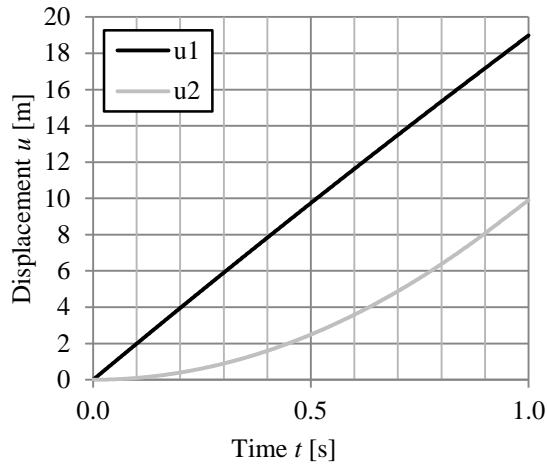
a)
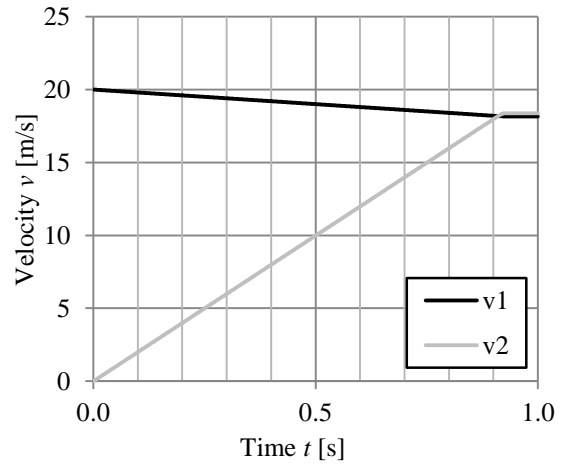
b)
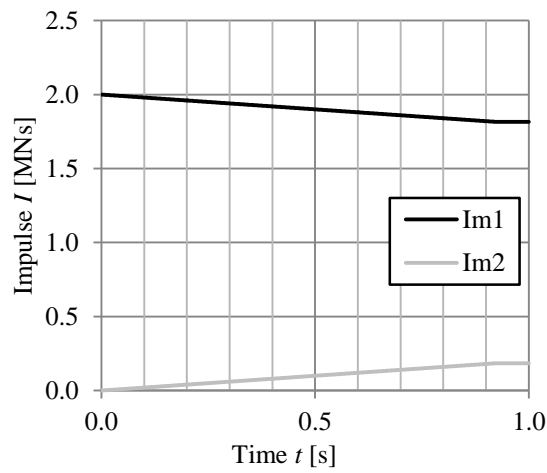
c)
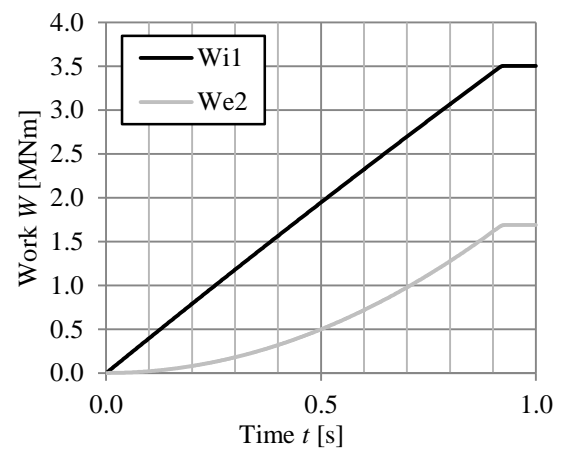
d)

Figure B.5   *Results from a plastic classic collision, Collision 5, where* $m_1 = 100\,000$ kg, $m_2 = 10\,000$ kg, $k_1 = 100$ MN/m, $R_1 = 200$ kN *and* $v_0 = 20$ m/s.

a)

b)

c)

d)
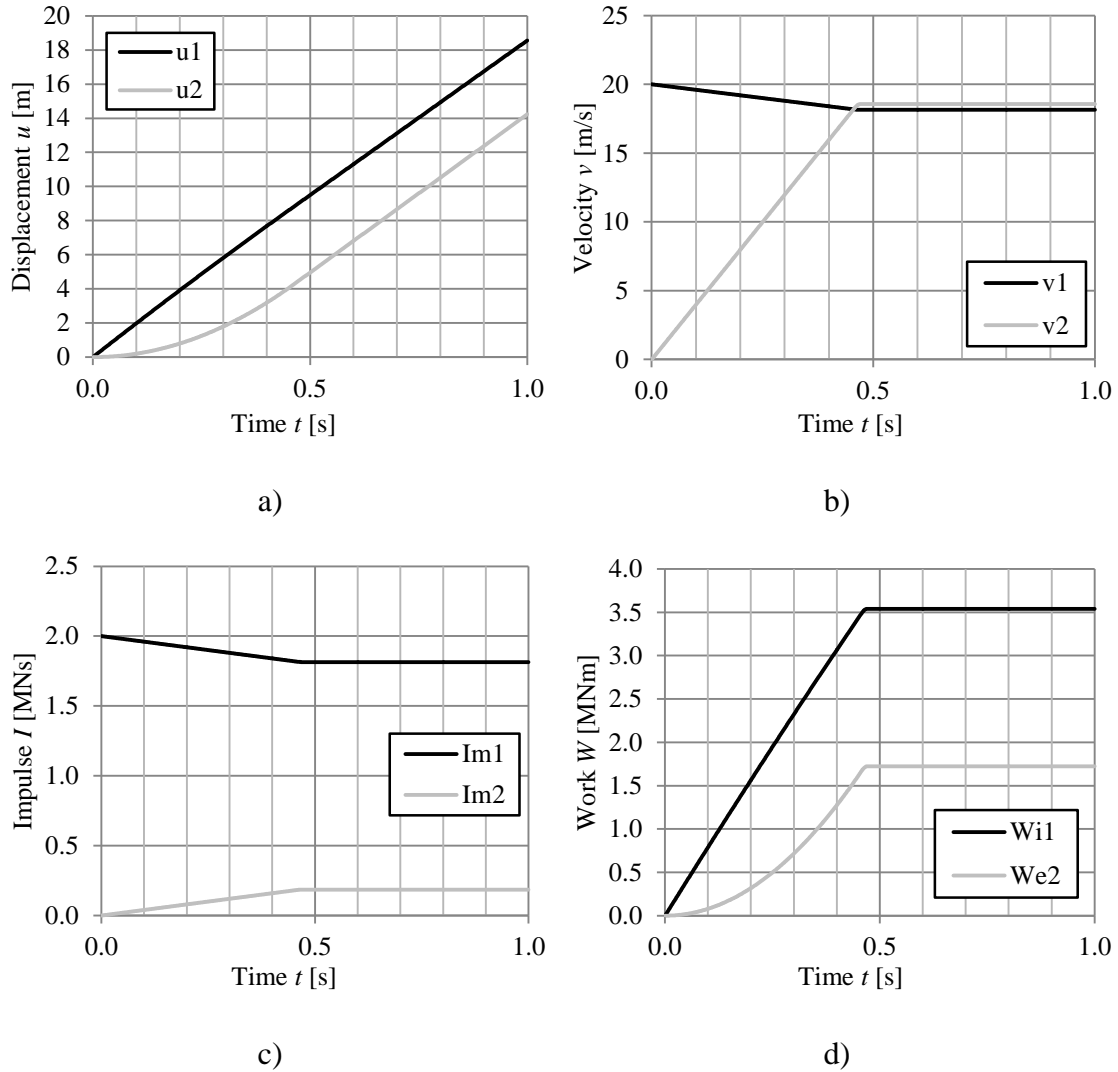
Figure B.6   *Results from a plastic classic collision, Collision 6, where* $m_1 = 100\ 000$ kg, $m_2 = 10\ 000$ kg, $k_1 = 100$ MN/m, $R_1 = 400$ kN   *and* $v_0 = 20$ m/s.

Appendix C   Results 2DOF system with barrier

C.1   Load factor β_{el}

In Johansson (2014a) a table and diagram showing the relation between the load factor β_{el} and the frequency ratio f_1 / f_2 is presented for different values of the mass ratio m_1 / m_2, this is shown in Tables C.1 and C.2 and Figure C.1.

Table C.1   Values for load factor β_{el}

f_1/f_2 [-]	Hard impact	$\beta_{el} = R_2 / F_{2,el}$ [-]										
		m_1 / m_2 [-]										
		0.10	0.20	0.50	1.0	1.5	2.0	3.0	5.0	10	50	100
0.000	1.000	1.000	1.000	1.000	1.000	1.000	1.000	1.000	1.000	1.000	1.000	1.000
0.005	1.006	1.005	1.005	1.005	1.005	1.005	1.005	1.005	1.005	1.005	1.004	1.004
0.050	1.050	1.050	1.049	1.049	1.048	1.047	1.046	1.044	1.041	1.032	0.986	0.993
0.100	1.100	1.099	1.099	1.098	1.095	1.093	1.091	1.086	1.076	1.048	0.874	0.925
0.125	1.125	1.124	1.122	1.118	1.110	1.103	1.095	1.080	1.050	1.005	0.802	0.651
0.150	1.174	1.172	1.171	1.166	1.158	1.150	1.141	1.125	1.091	1.006	0.874	0.578
0.175	1.158	1.157	1.156	1.153	1.148	1.143	1.137	1.123	1.092	1.002	0.672	0.517
0.200	1.083	1.084	1.085	1.087	1.090	1.091	1.091	1.086	1.066	0.981	0.615	0.461
0.225	1.180	1.172	1.165	1.143	1.108	1.074	1.042	1.027	1.024	0.949	0.563	0.420
0.250	1.268	1.258	1.249	1.221	1.176	1.134	1.094	1.021	0.976	0.915	0.515	0.382
0.275	1.348	1.335	1.323	1.288	1.233	1.182	1.134	1.047	0.927	0.879	0.479	0.352
0.300	1.418	1.403	1.389	1.347	1.281	1.220	1.164	1.063	0.899	0.843	0.447	0.324
0.350	1.536	1.515	1.495	1.437	1.349	1.269	1.196	1.069	0.873	0.776	0.389	0.281
0.400	1.625	1.598	1.572	1.498	1.387	1.288	1.200	1.051	0.830	0.713	0.347	0.248
0.450	1.689	1.656	1.624	1.534	1.400	1.284	1.183	1.016	0.777	0.655	0.310	0.221
0.500	1.732	1.693	1.655	1.549	1.395	1.264	1.152	0.971	0.722	0.602	0.281	0.200
0.550	1.757	1.712	1.668	1.548	1.375	1.232	1.111	0.920	0.667	0.552	0.256	0.182
0.600	1.768	1.717	1.668	1.534	1.345	1.192	1.064	0.867	0.627	0.506	0.235	0.167
0.650	1.766	1.710	1.656	1.510	1.308	1.146	1.014	0.814	0.605	0.465	0.217	0.154
0.700	1.755	1.693	1.635	1.478	1.266	1.098	0.964	0.763	0.583	0.429	0.202	0.143
0.750	1.736	1.670	1.608	1.442	1.220	1.049	0.913	0.714	0.560	0.405	0.188	0.133
0.800	1.710	1.640	1.575	1.402	1.173	0.999	0.863	0.667	0.537	0.386	0.177	0.125
0.850	1.680	1.607	1.538	1.359	1.126	0.951	0.816	0.624	0.513	0.367	0.166	0.118
0.900	1.646	1.570	1.499	1.315	1.078	0.903	0.770	0.583	0.489	0.349	0.157	0.111
0.950	1.609	1.531	1.458	1.270	1.032	0.858	0.727	0.548	0.466	0.332	0.149	0.105
1.000	1.571	1.490	1.416	1.225	0.986	0.815	0.687	0.518	0.445	0.316	0.141	0.100
1.125	1.471	1.387	1.310	1.117	0.883	0.721	0.606	0.456	0.397	0.281	0.126	0.089
1.250	1.373	1.288	1.211	1.020	0.797	0.648	0.543	0.408	0.358	0.253	0.113	0.080
1.375	1.283	1.198	1.122	0.936	0.725	0.588	0.492	0.377	0.325	0.230	0.103	0.073
1.500	1.200	1.116	1.042	0.864	0.666	0.538	0.450	0.350	0.298	0.210	0.094	0.067

Table C.2   Values for load factor β_{el} for hard impact.

f_1/f_2 [-]	β_{el} [-]	f_1/f_2 [-]	β_{el} [-]	f_1/f_2 [-]	β_{el} [-]
1.625	1.125	4.5	0.439	13	0.154
1.75	1.058	4.75	0.417	14	0.143
1.875	0.997	5	0.396	15	0.133
2	0.943	5.5	0.361	16	0.125
2.125	0.893	6	0.331	17	0.118
2.25	0.849	6.5	0.306	18	0.111
2.375	0.808	7	0.284	19	0.105
2.5	0.770	7.5	0.266	20	0.100
2.75	0.705	8	0.249	21	0.095
3	0.650	8.5	0.235	22	0.091
3.25	0.602	9	0.222	23	0.087
3.5	0.560	9.5	0.210	24	0.083
3.75	0.520	10	0.200	25	0.080
4	0.493	11	0.181		
4.25	0.465	12	0.166		
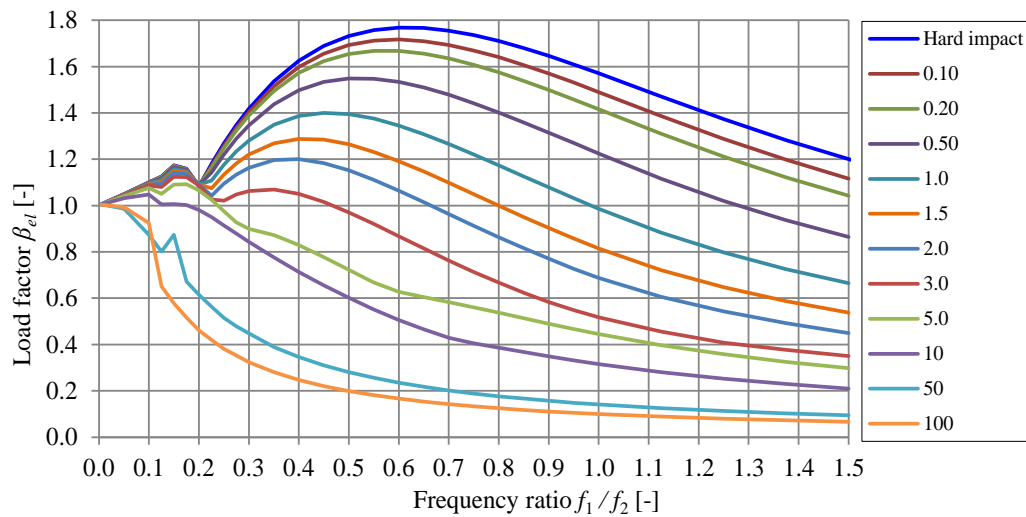
Figure C.1   Relationship between load factor β_{el} and frequency ratio f_1/f_2 for different relations of the mass ratio m_1/m_2.

C.2 Elastic response

The load factor diagram together with the coordinates for the different impact tests are presented in Figure C.2.
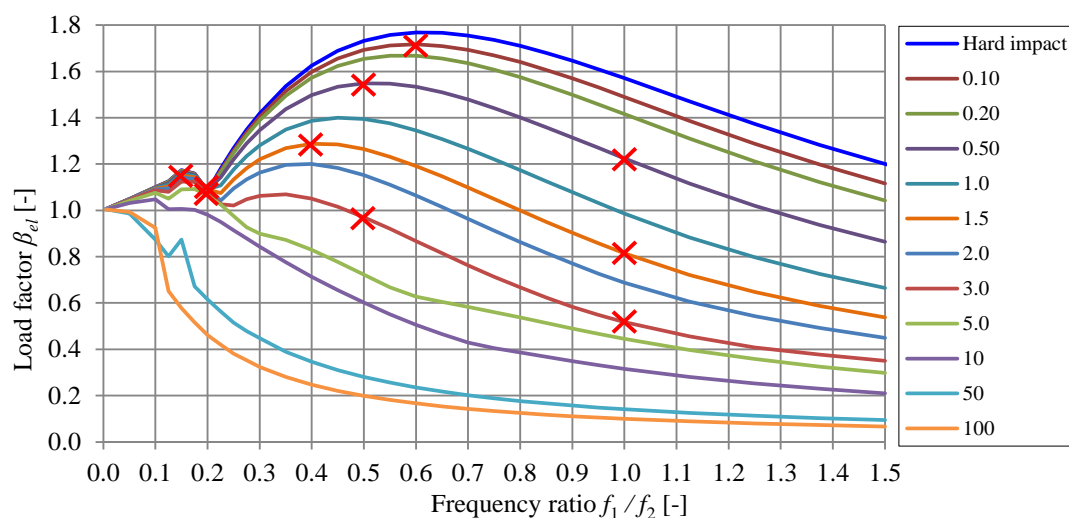
Figure C.2   Relationship between load factor β_{el} and frequency ratio f_1/f_2 for different relations of the mass ratio m_1/m_2.

All results from the analysis discussed in section 3.2.1 are presented in this section.

Table C.3   Table showing the coordinates in Figure C.1 of tested impacts

Impact test number	Mass ratio	Frequency ratio	Load factor β_{el}
1	0.1	0.6	1.72
2	0.5	0.5	1.55
3	1.5	0.4	1.29
4	0.2	0.2	1.08
5	2	0.2	1.09
6	0.2	0.15	1.17
7	2	0.5	0.97
8	3	1	0.52
9	1.5	1	0.81
10	0.5	1	1.22
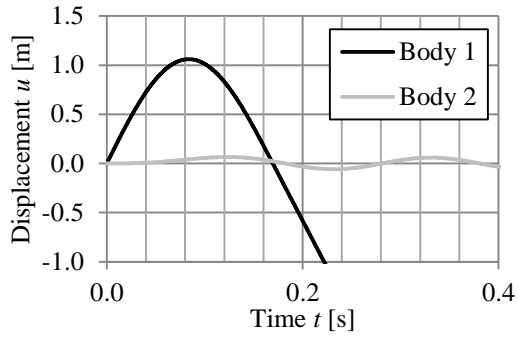
a) Displacement
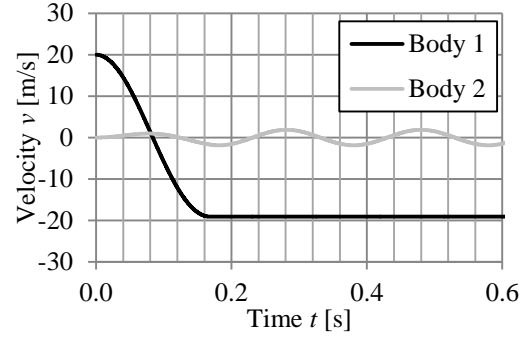
b) Velocity
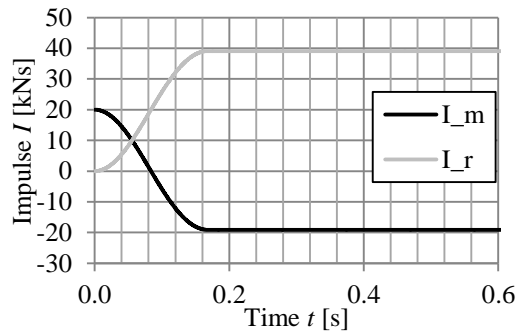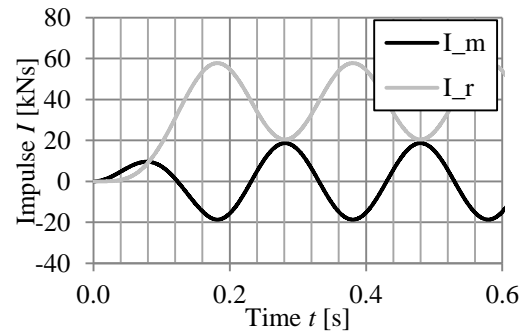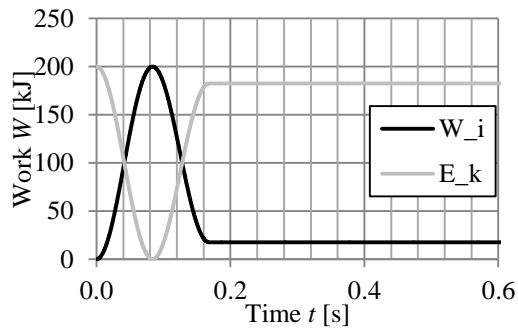
c) Impulse Body 1

d) Impulse Body 2

e) Kinetic energy - internal work body 1
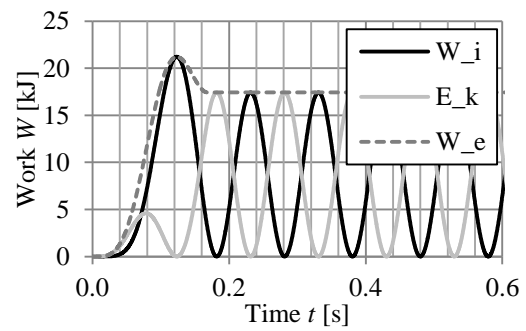
f) Kinetic energy - work body 2
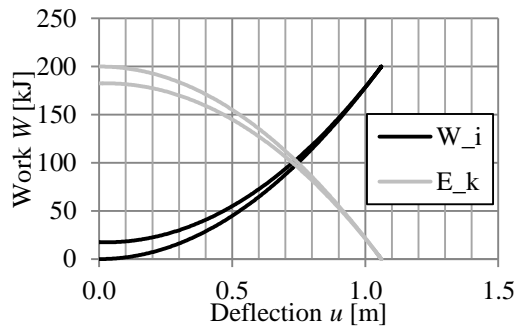
g) Kinetic energy - internal work body 1
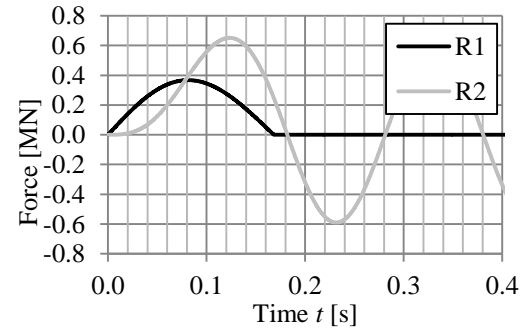
h) Load pulse

Figure C.3   Impact test number 1.
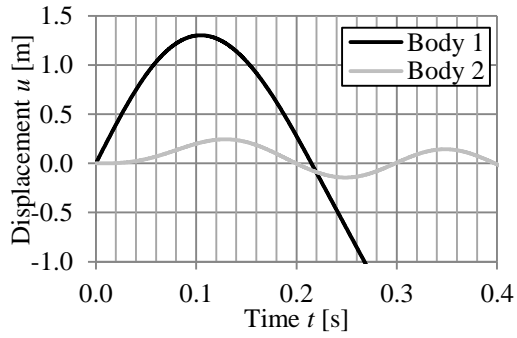
a) Displacement
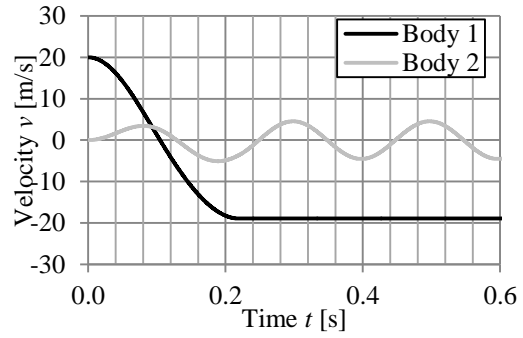
b) Velocity
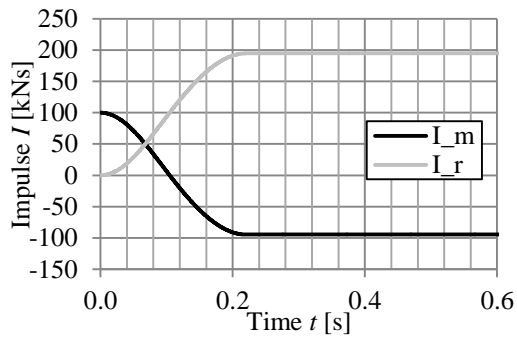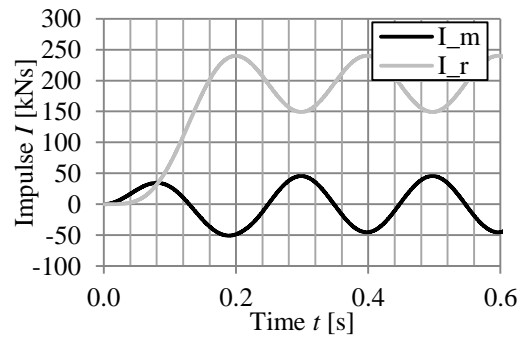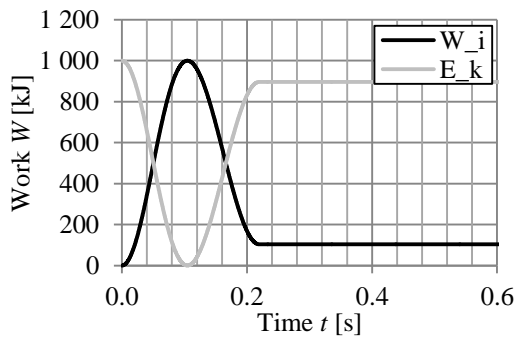
c) Impulse Body 1

d) Impulse Body 2

e) Kinetic energy - internal work body 1
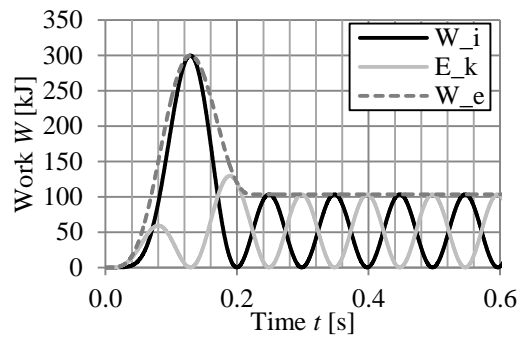
f) Kinetic energy - work body 2
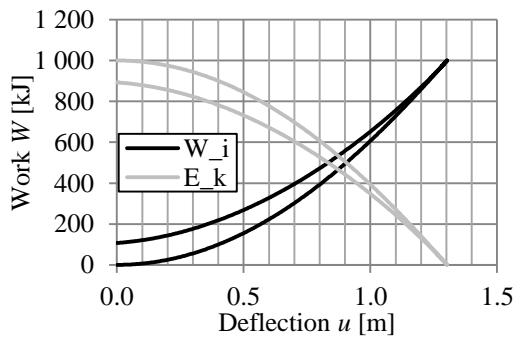
g) Kinetic energy - internal work body 1
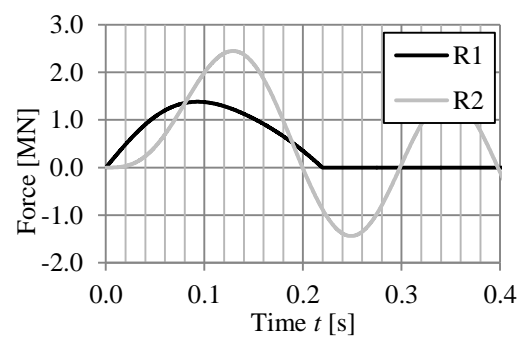
h) Load pulse

Figure C.4   Impact test number 2.
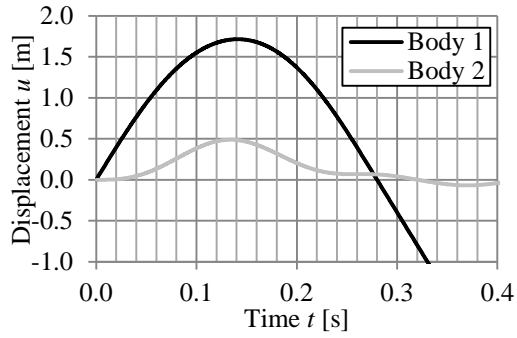
a) Displacement
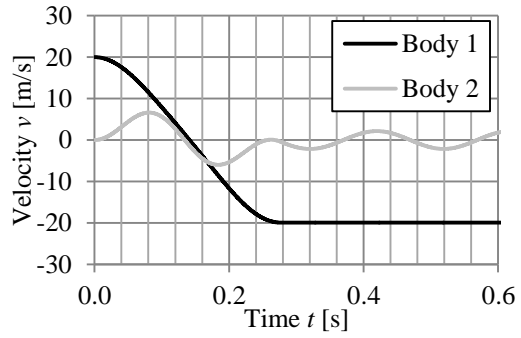
b) Velocity
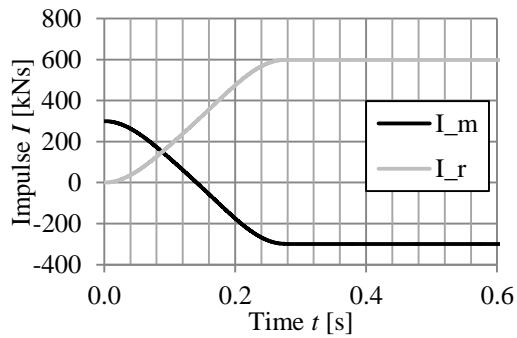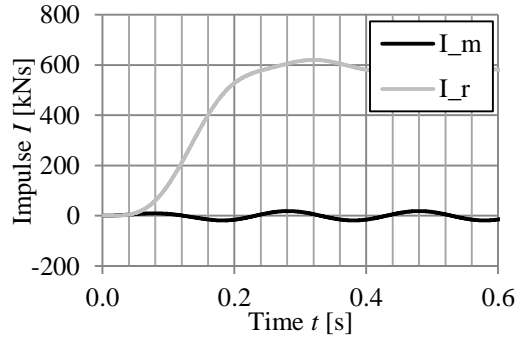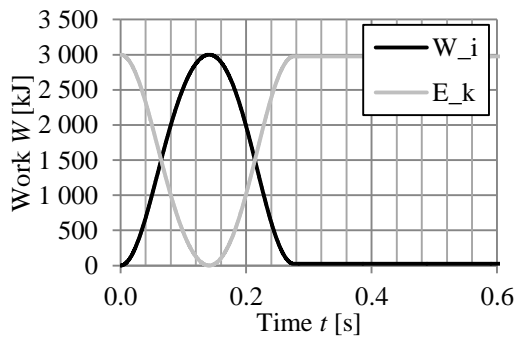
c) Impulse Body 1

d) Impulse Body 2

e) Kinetic energy - internal work body 1
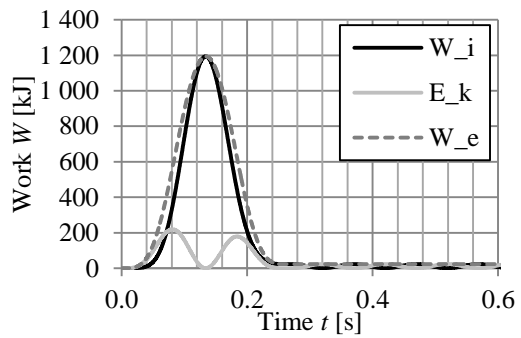
f) Kinetic energy - work body 2
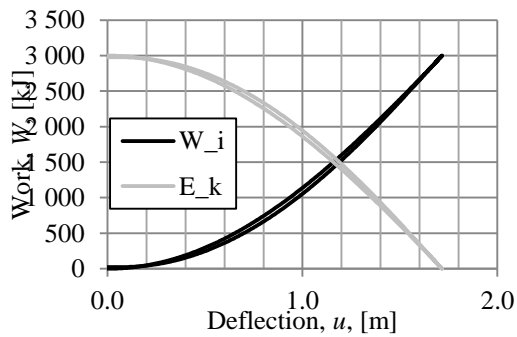
g) Kinetic energy - internal work body 1
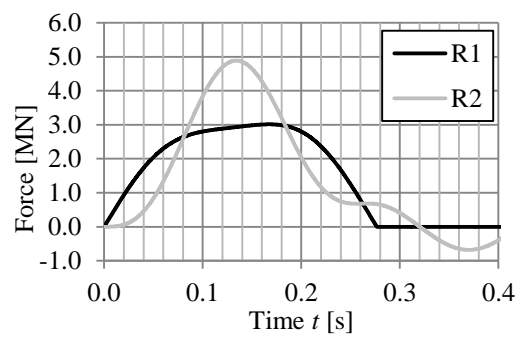
h) Load pulse

Figure C.5   Impact test number 3.
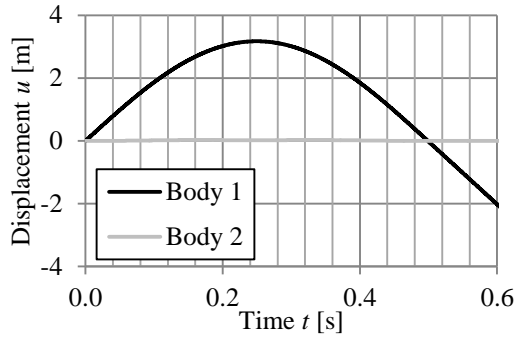
a) Displacement
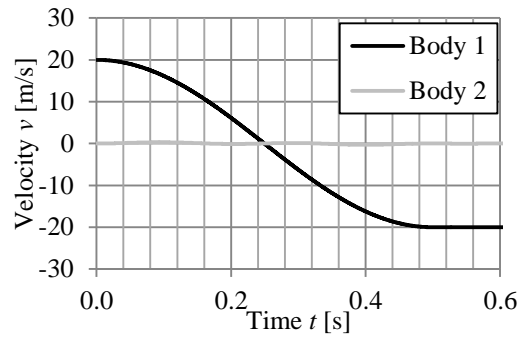
b) Velocity
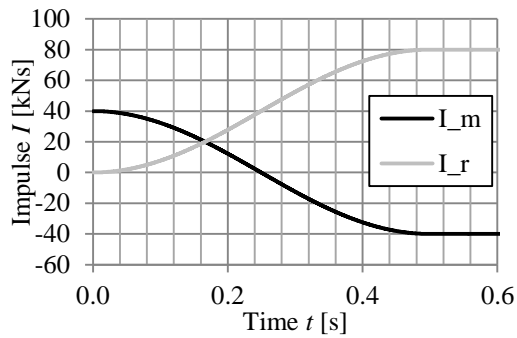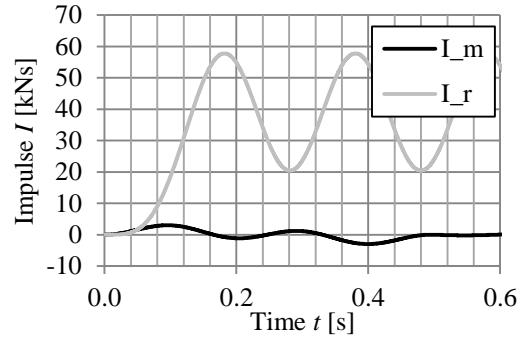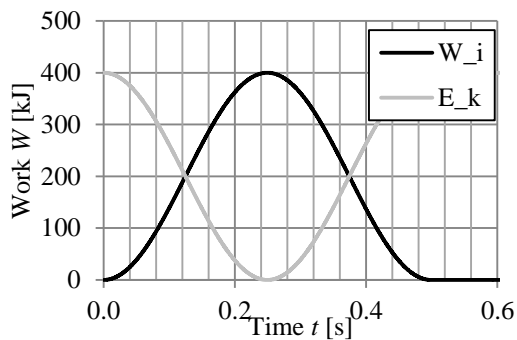
c) Impulse Body 1

d) Impulse Body 2

e) Kinetic energy - internal work body 1
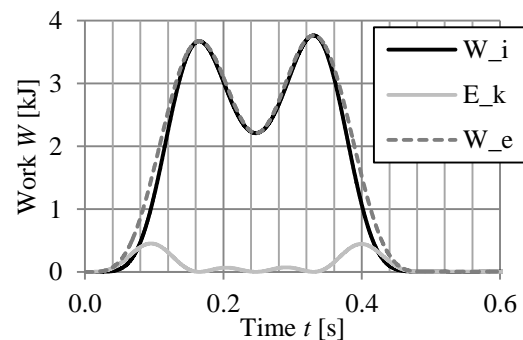
f) Kinetic energy - work body 2
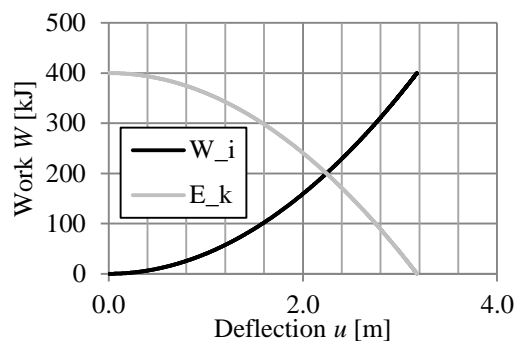
g) Kinetic energy - internal work body 1
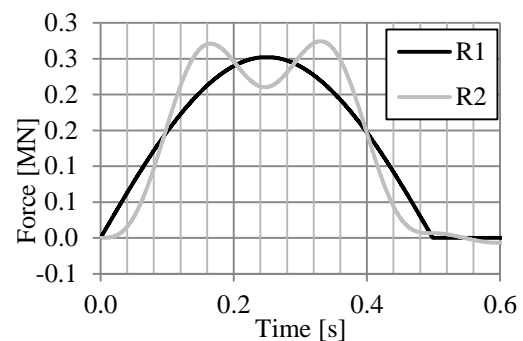
h) Load pulse

Figure C.6   Impact test number 4.
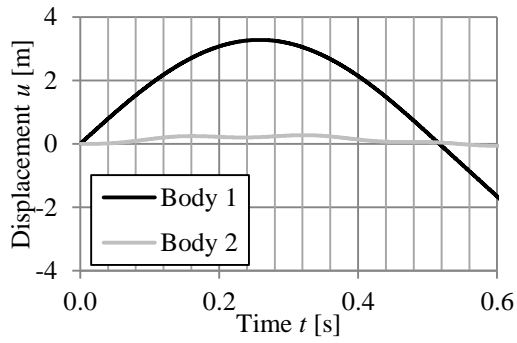
a) Displacement
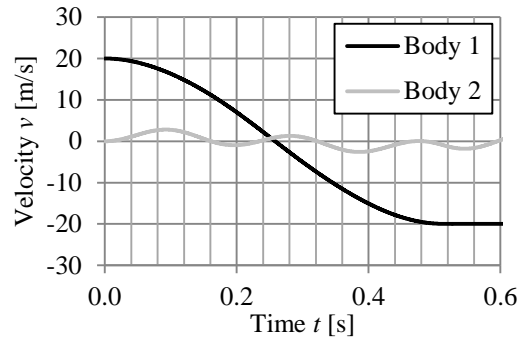
b) Velocity
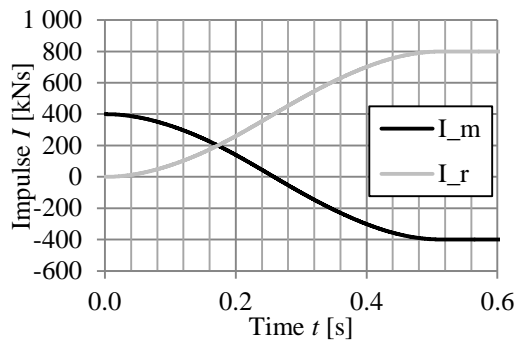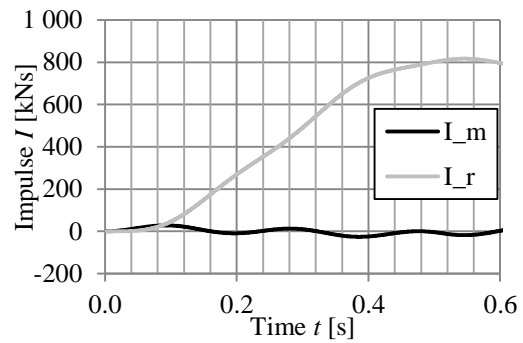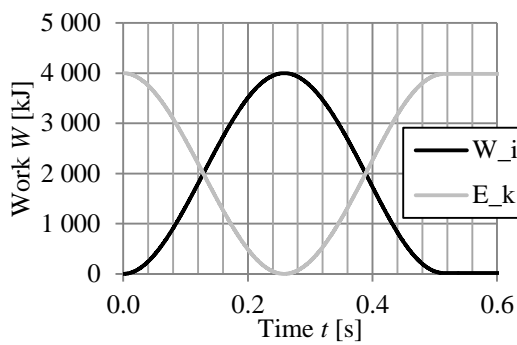
c) Impulse Body 1

d) Impulse Body 2

e) Kinetic energy - internal work body 1
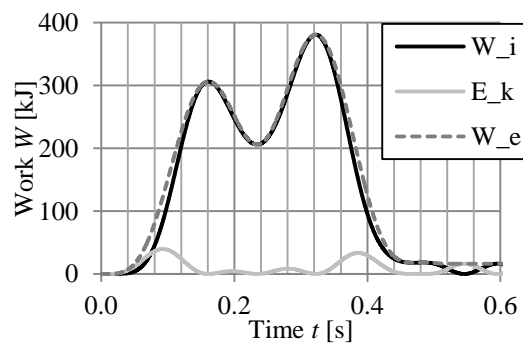
f) Kinetic energy - work body 2
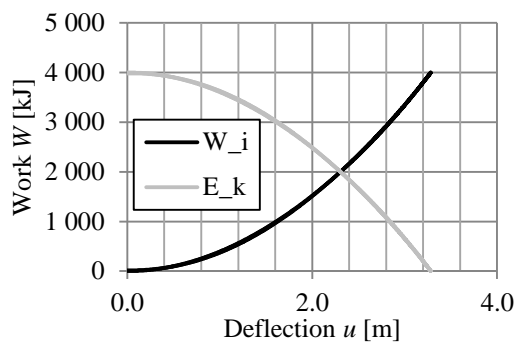
g) Kinetic energy - internal work body 1
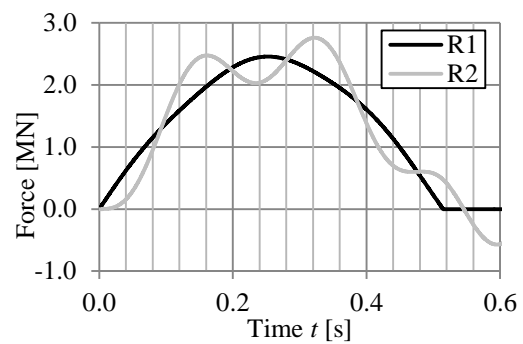
h) Load pulse

Figure C.7   Impact test number 5.
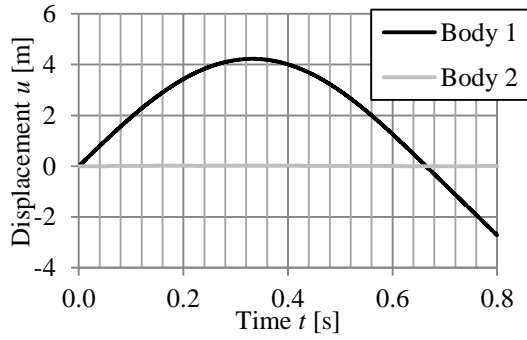
a) Displacement
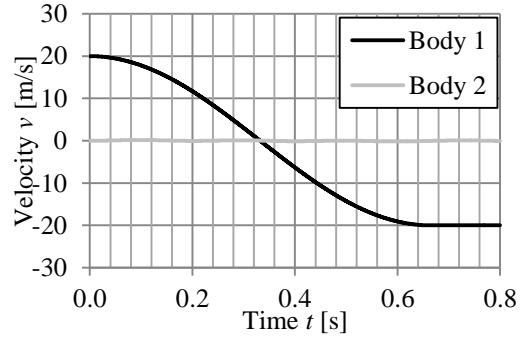
b) Velocity
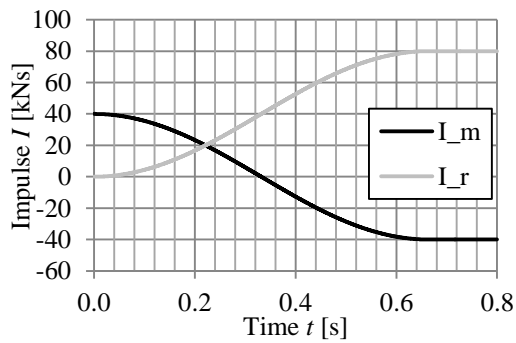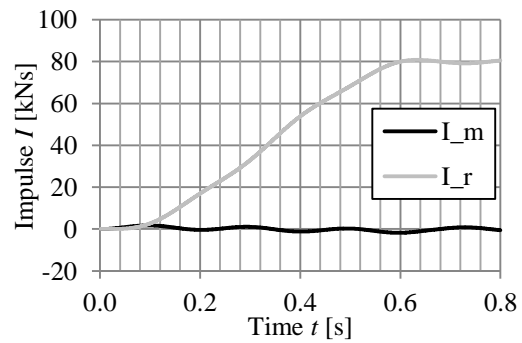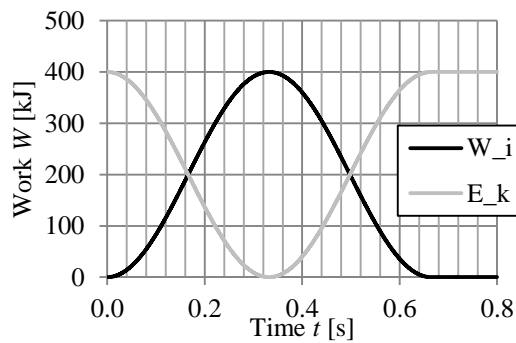
c) Impulse Body 1

d) Impulse Body 2

e) Kinetic energy - internal work body 1
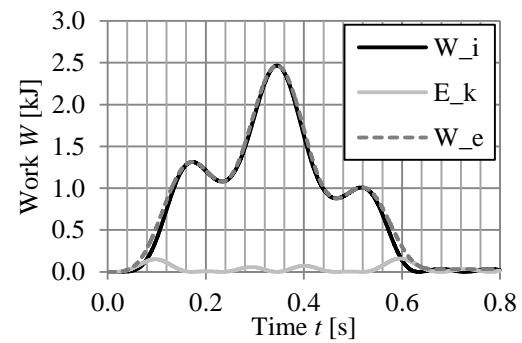
f) Kinetic energy - work body 2
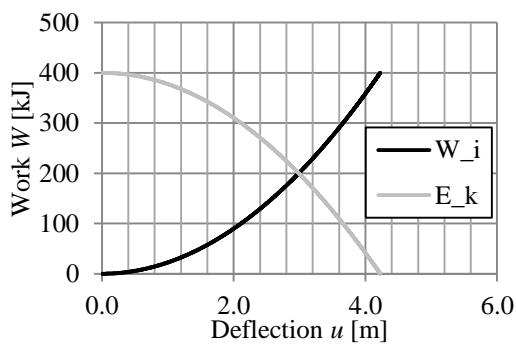
g) Kinetic energy - internal work body 1
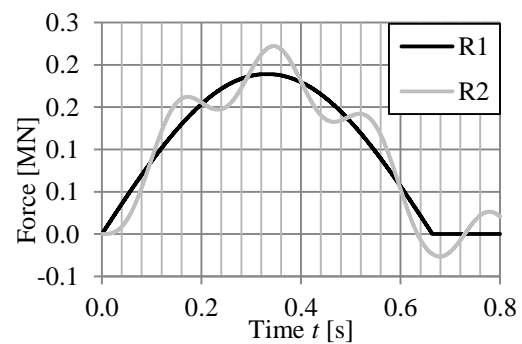
h) Load pulse

Figure C.8   Impact test number 6.
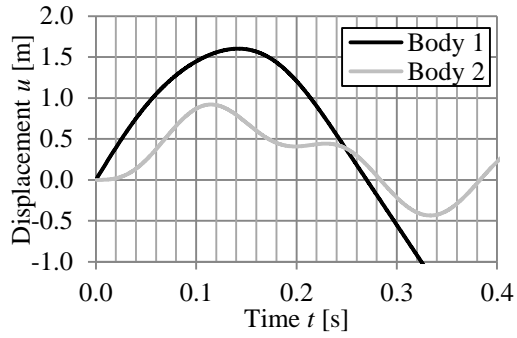
a) Displacement
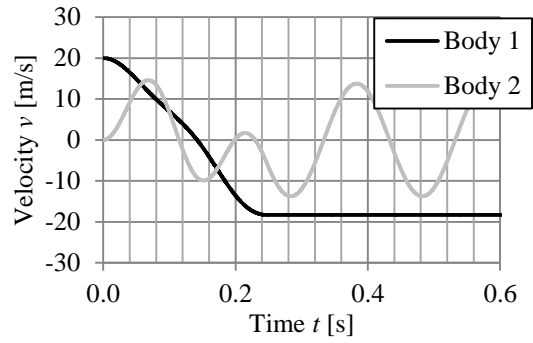
b) Velocity
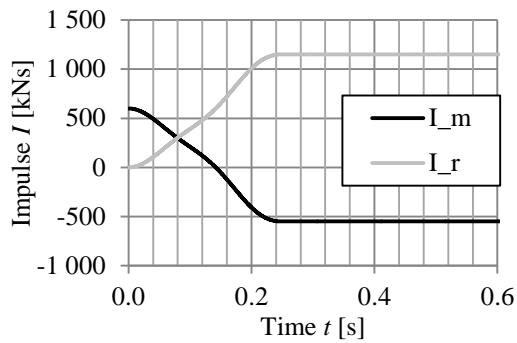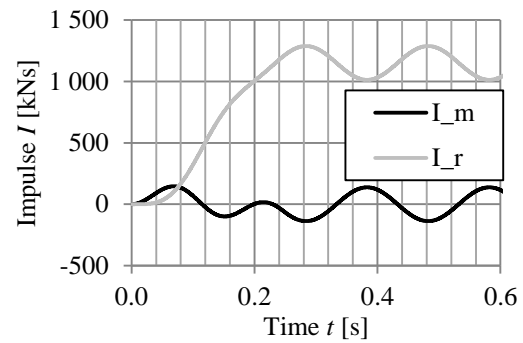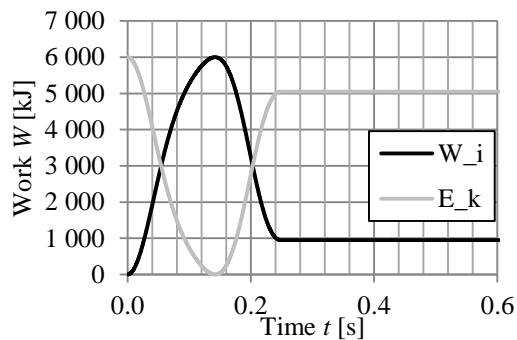
c) Impulse Body 1

d) Impulse Body 2

e) Kinetic energy - internal work body 1
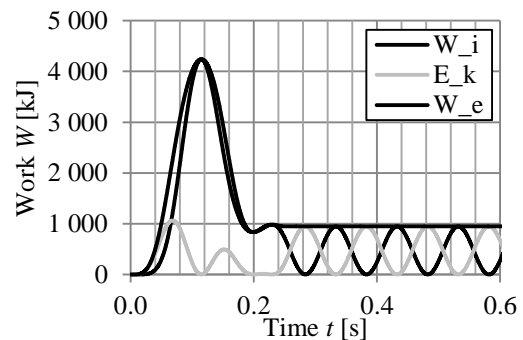
f) Kinetic energy - work body 2
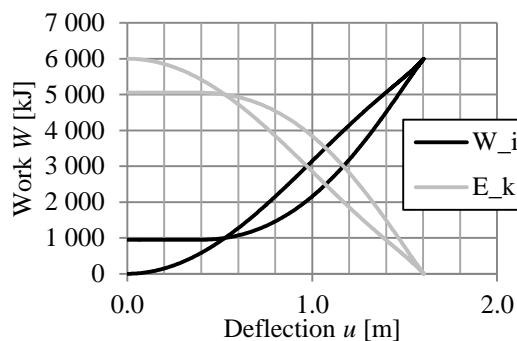
g) Kinetic energy - internal work body 1
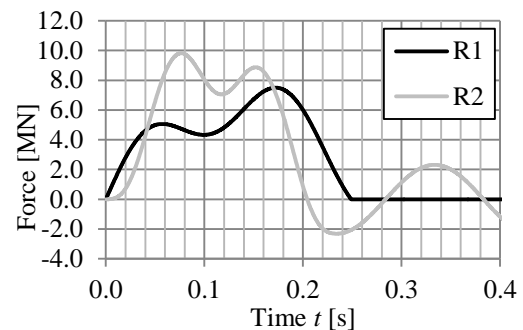
h) Load pulse

Figure C.9   Impact test number 7.
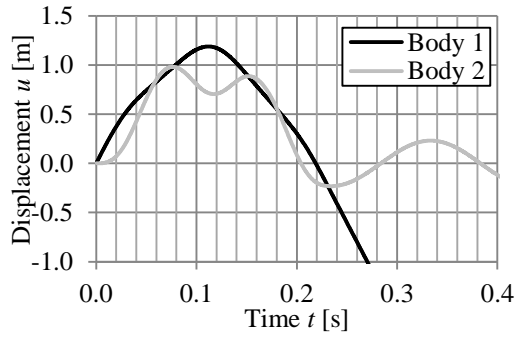
a) Displacement
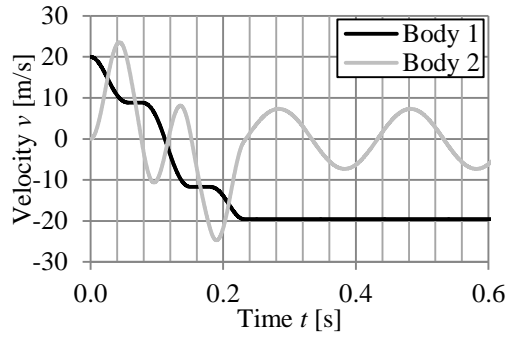
b) Velocity
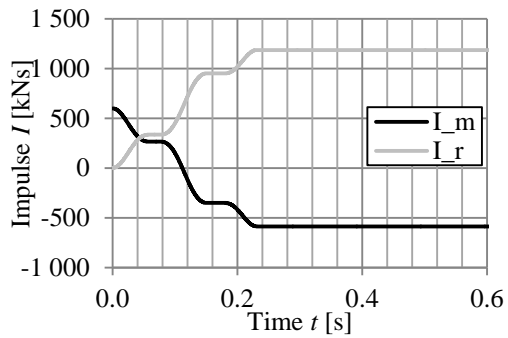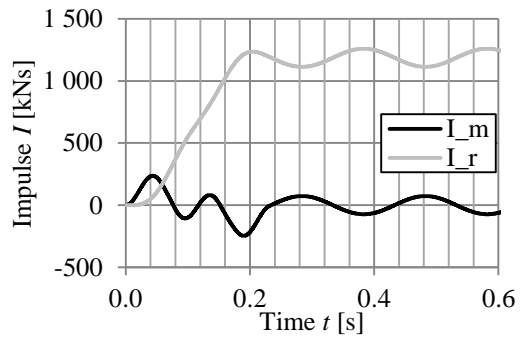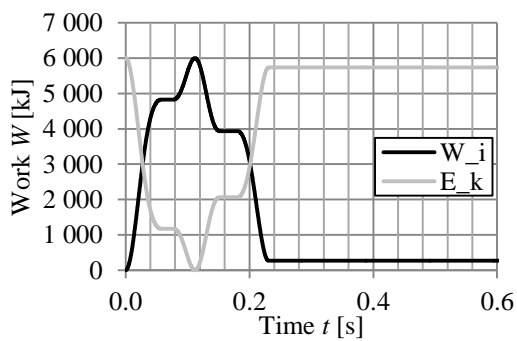
c) Impulse Body 1

d) Impulse Body 2

e) Kinetic energy - internal work body 1
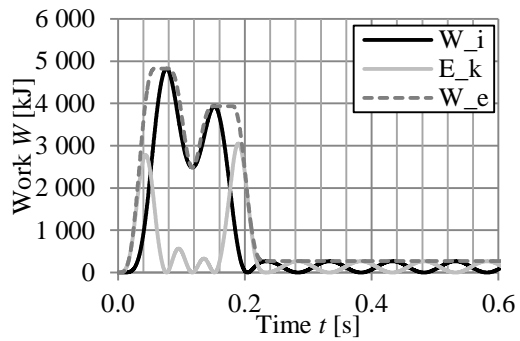
f) Kinetic energy - work body 2
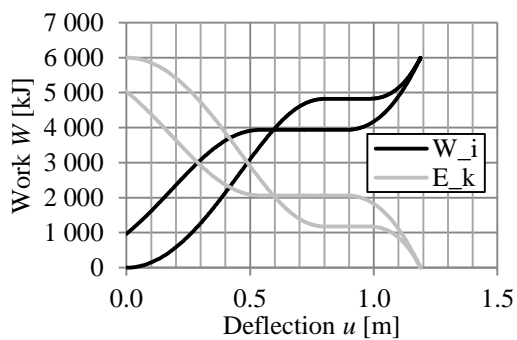
g) Kinetic energy - internal work body 1
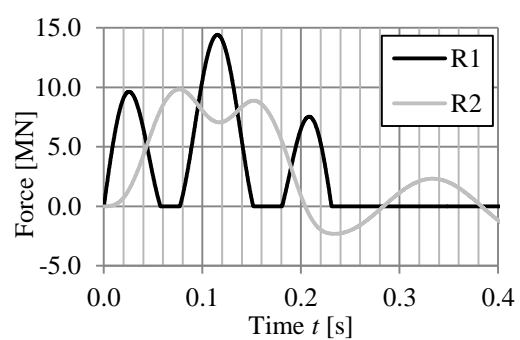
h) Load pulse

Figure C.10   Impact test number 8.
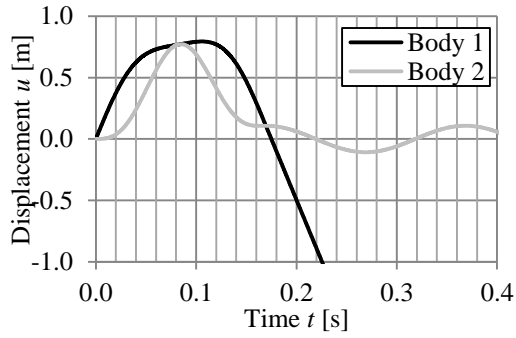
a) Displacement
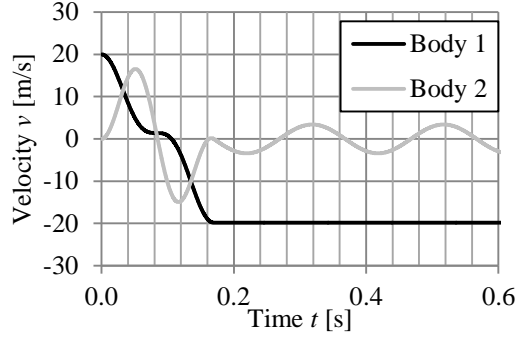
b) Velocity
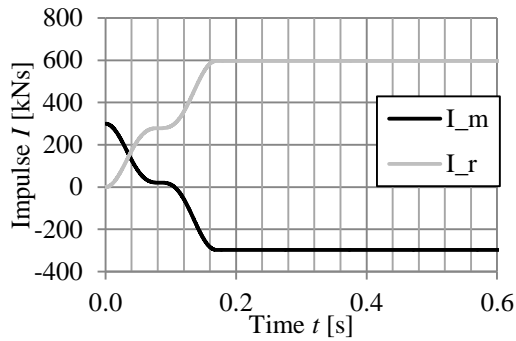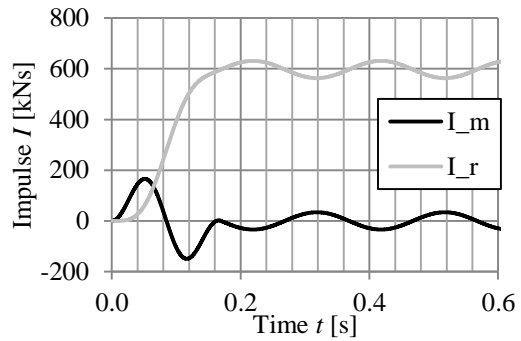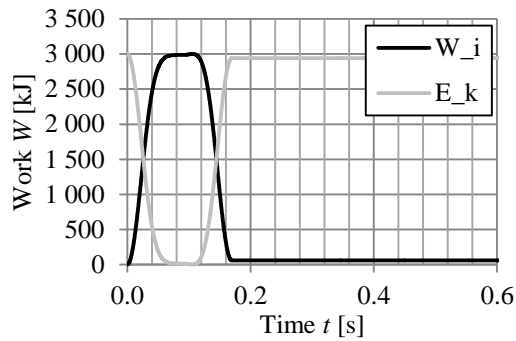
c) Impulse Body 1

d) Impulse Body 2

e) Kinetic energy - internal work body 1
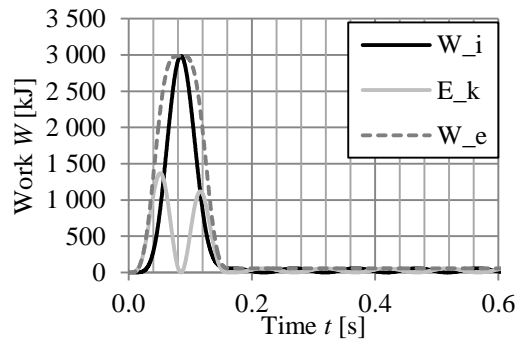
f) Kinetic energy - work body 2
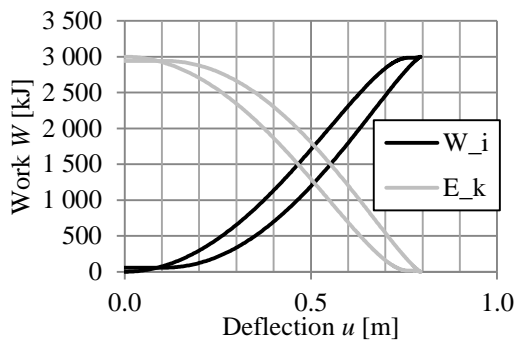
g) Kinetic energy - internal work body 1
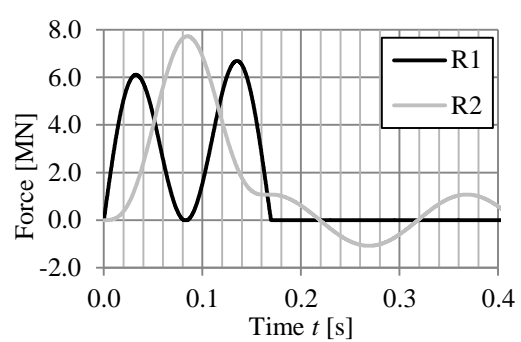
h) Load pulse

Figure C.11   Impact test number 9.
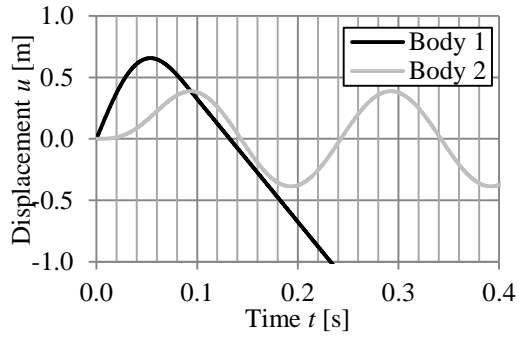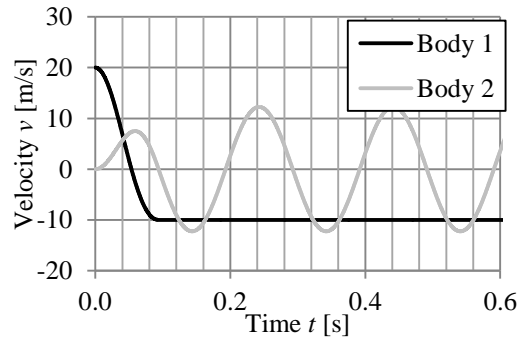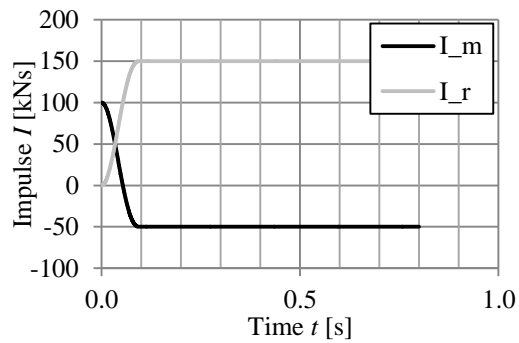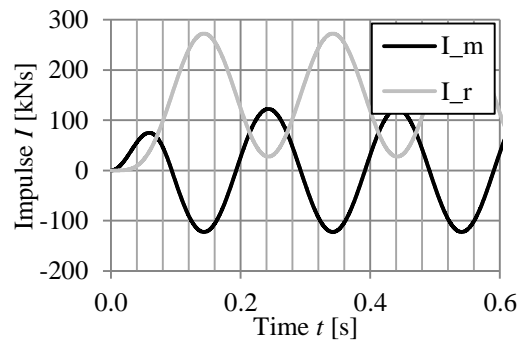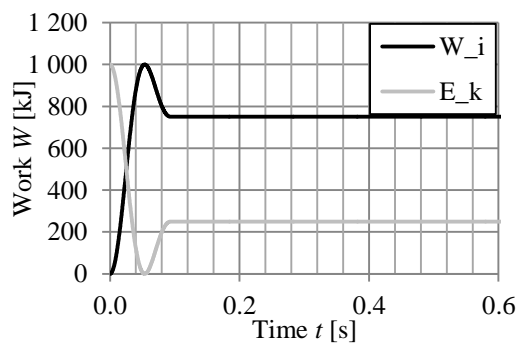
CHALMERS, *Civil and Environmental Engineering*, Master's Thesis 2014:80

a) Displacement

b) Velocity

c) Impulse Body 1

d) Impulse Body 2

e) Kinetic energy - internal work body 1
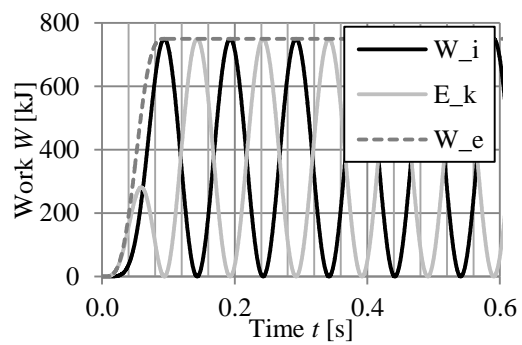
f) Kinetic energy - work body 2
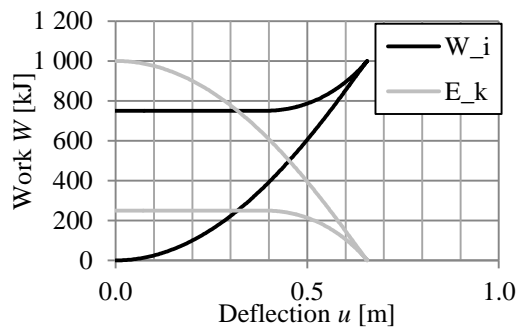
g) Kinetic energy - internal work body 1
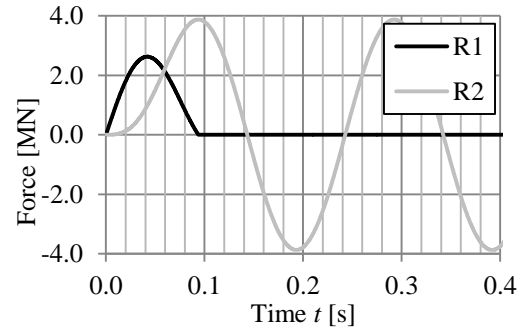
h) Load pulse

Figure C.12   *Impact test number 10.*

C.3 Elasto-plastic response

The elasto-plastic test uses the indata from Table C.4 as a base, then changes are made to one parameter at a time in order to find the impact of each parameter.

These results are not discussed in the main report but are included here since it might be interesting to see how a elasto-plastic system behaves.

Table C.4   Base parameters for the analysis in this section.

m_1	2 000	[kg]
m_2	10 000	[kg]
v_0	20	[m/s]
k_1	1	[MN/m]
k_2	100	[MN/m]
R_1	400	[N]
R_2	200	[N]
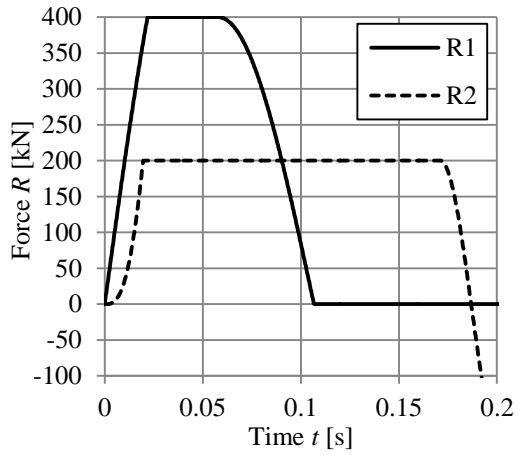
a) $m_1 = 1\,000$ kg
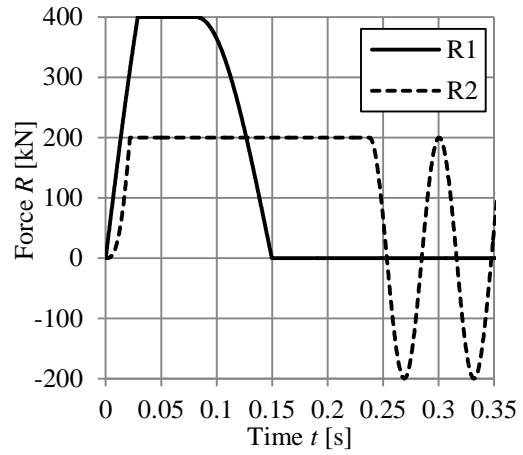
d) $v_0 = 15$ m/s
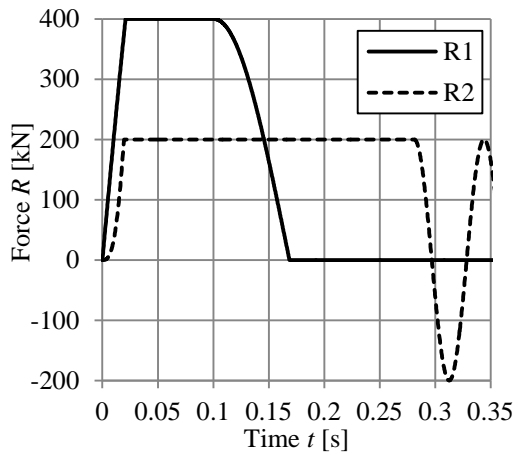
b) $m_1 = 2\,000$ kg
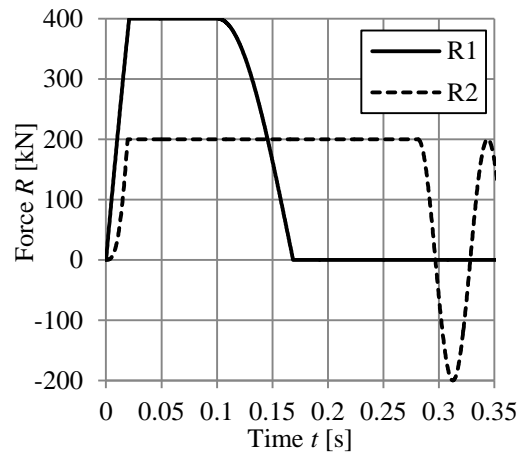
e) $v_0 = 20$ m/s
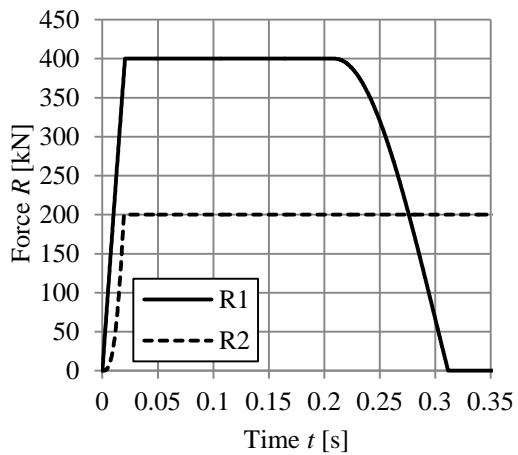
c) $m_1 = 5\,000$ kg
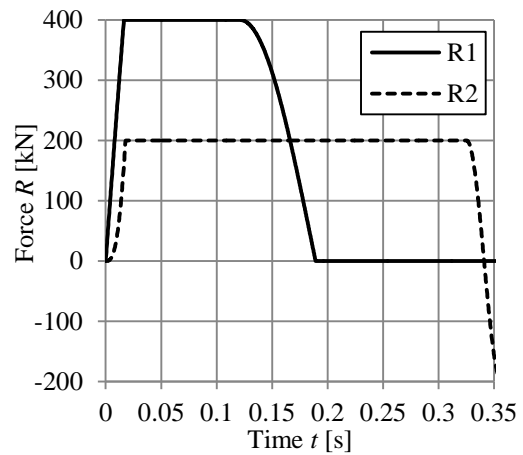
f) $v_0 = 25$ m/s

Figure C.13   a, b and c shows the load pulses for different mass of the impacting object, d, e and f shows the load pulses for different initial velocities.
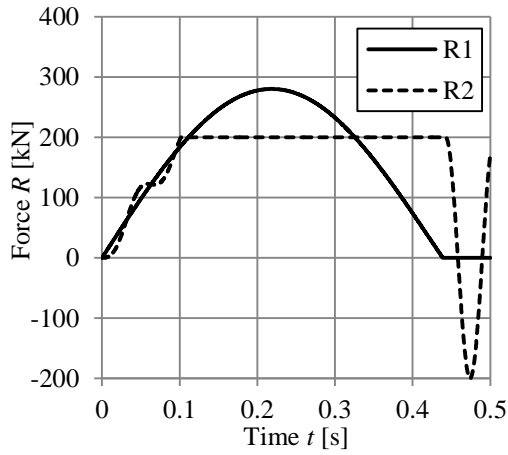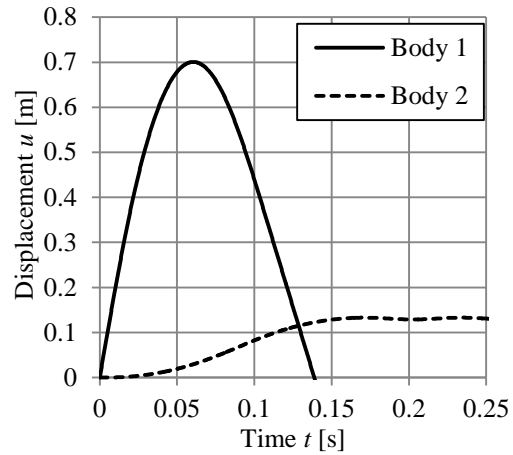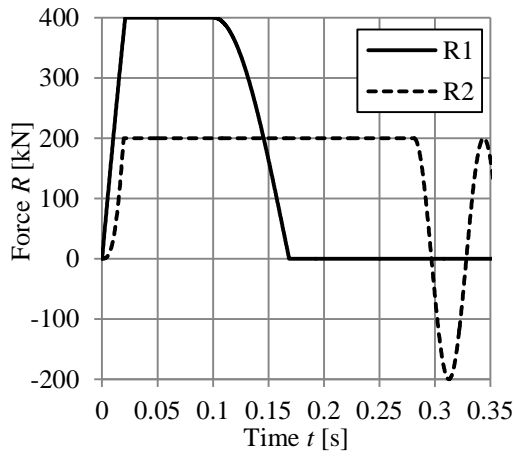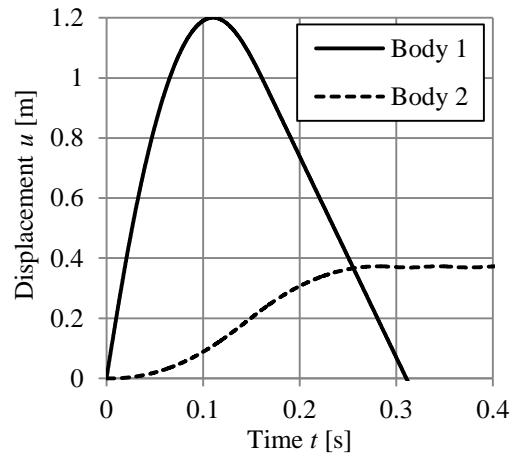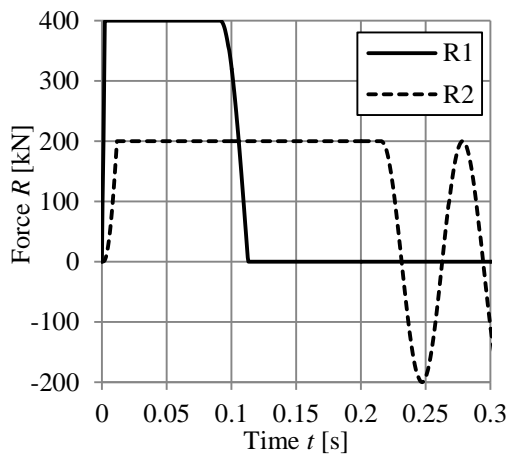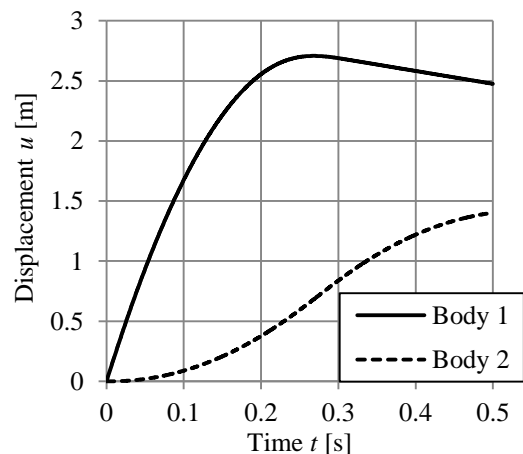
Figure C.14   a, b and c shows how the load pulses changes for different stiffness of the impacting object, d, e, and f shows the displacement for different values to mass 1.

CHALMERS, *Civil and Environmental Engineering*, Master's Thesis 2014:80
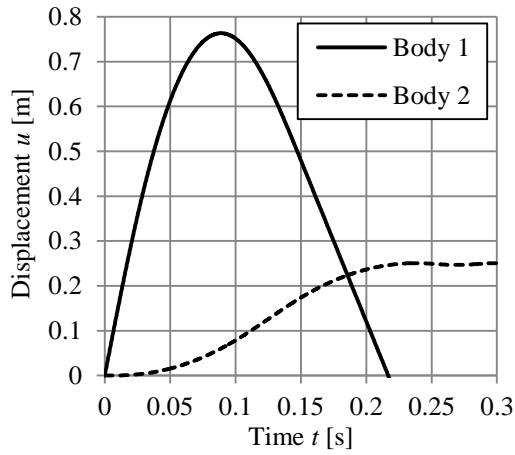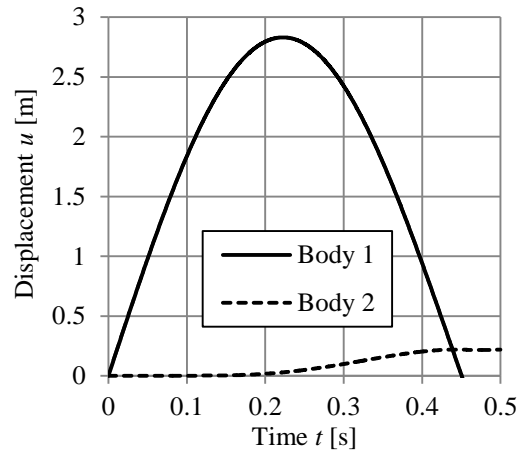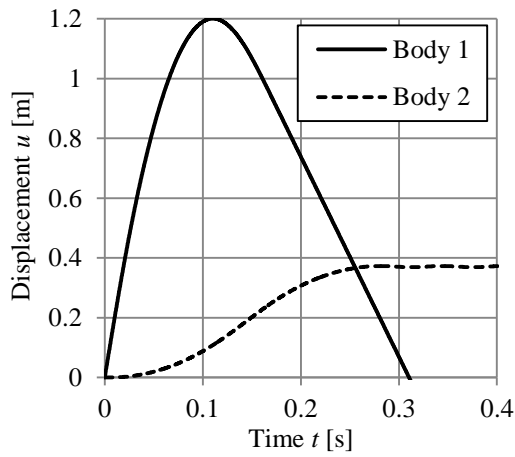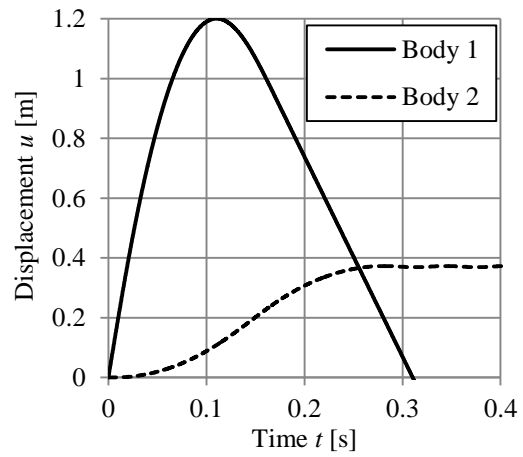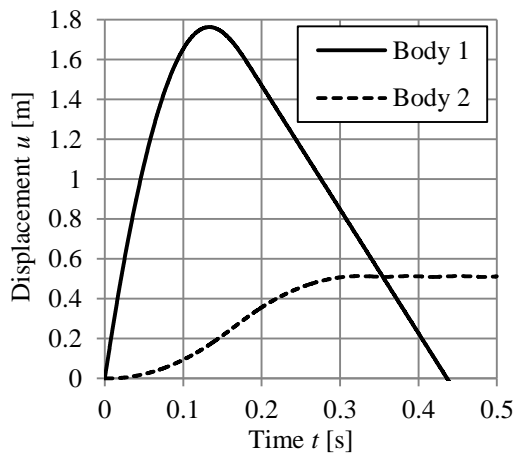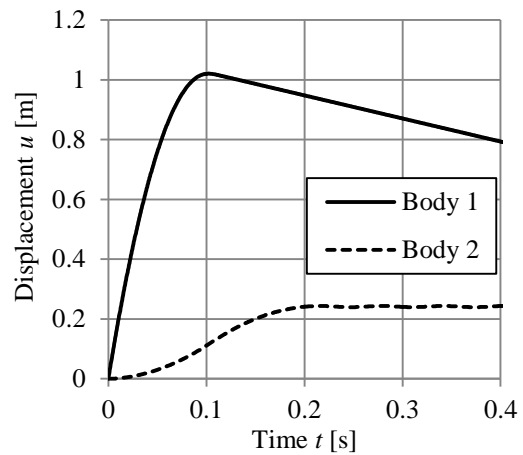
Figure C.15   a, b and c shows the displacement for different initial velocities of body 1, d, e and f shows the displacement for different values of the stiffness k_1.
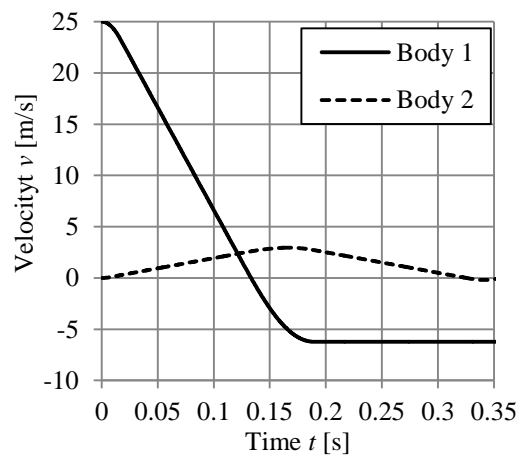
Figure C.16 a, b and c shows how the velocity changes for different values of mass 1, d, e and f show how the velocity changes for different values of the velocity v_0.

CHALMERS, *Civil and Environmental Engineering*, Master's Thesis 2014:80

Appendix D   2DOF Effect of impact position on a beam

In this appendix all the results from the analysis discussed in section 5.1 are presented.

D.1   Original beam
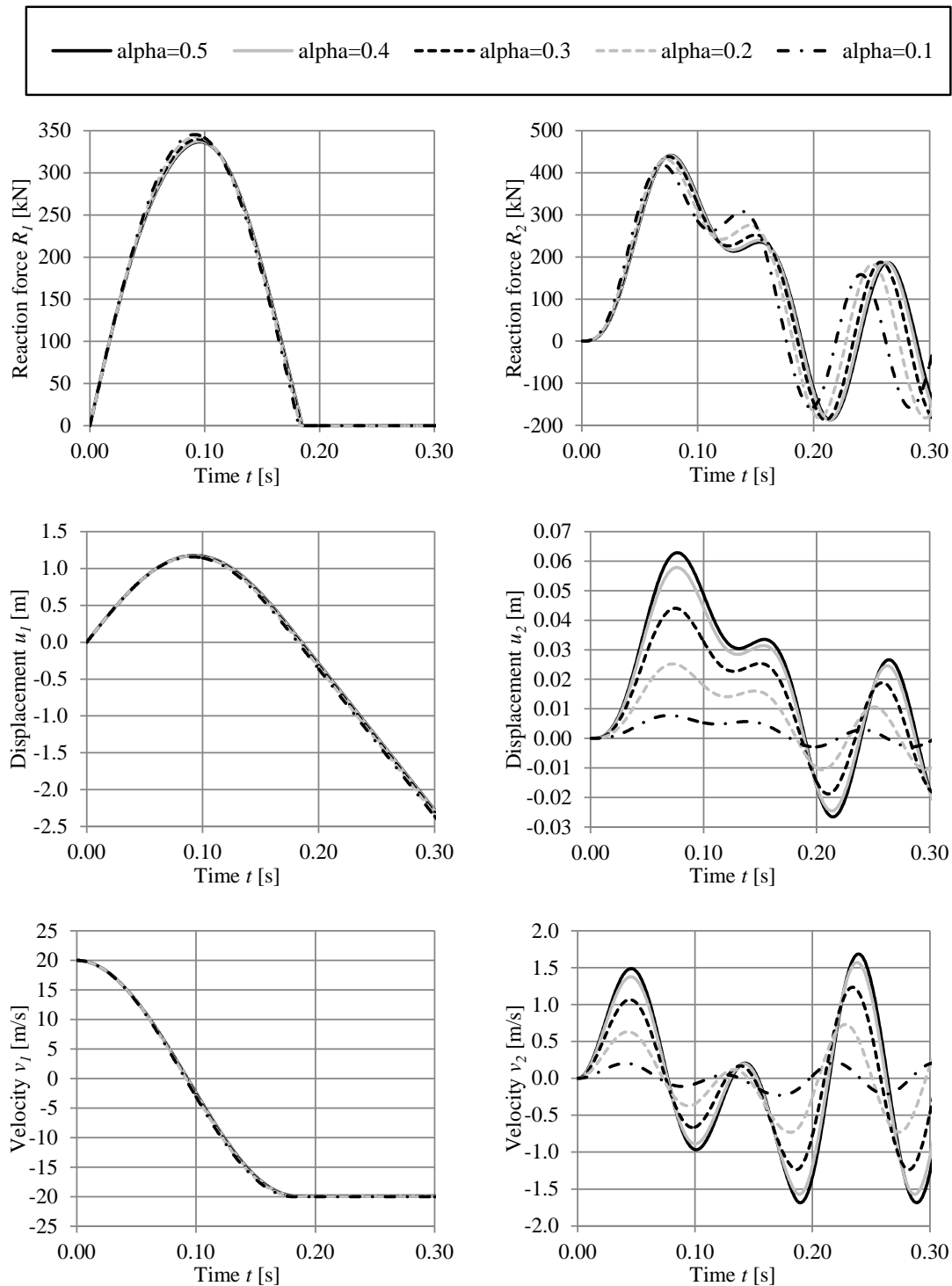
Figure D.1   Results from the simulated collision, describing the differences in position of impact for both the incoming object and the beam.

D.2 Stiffer beam
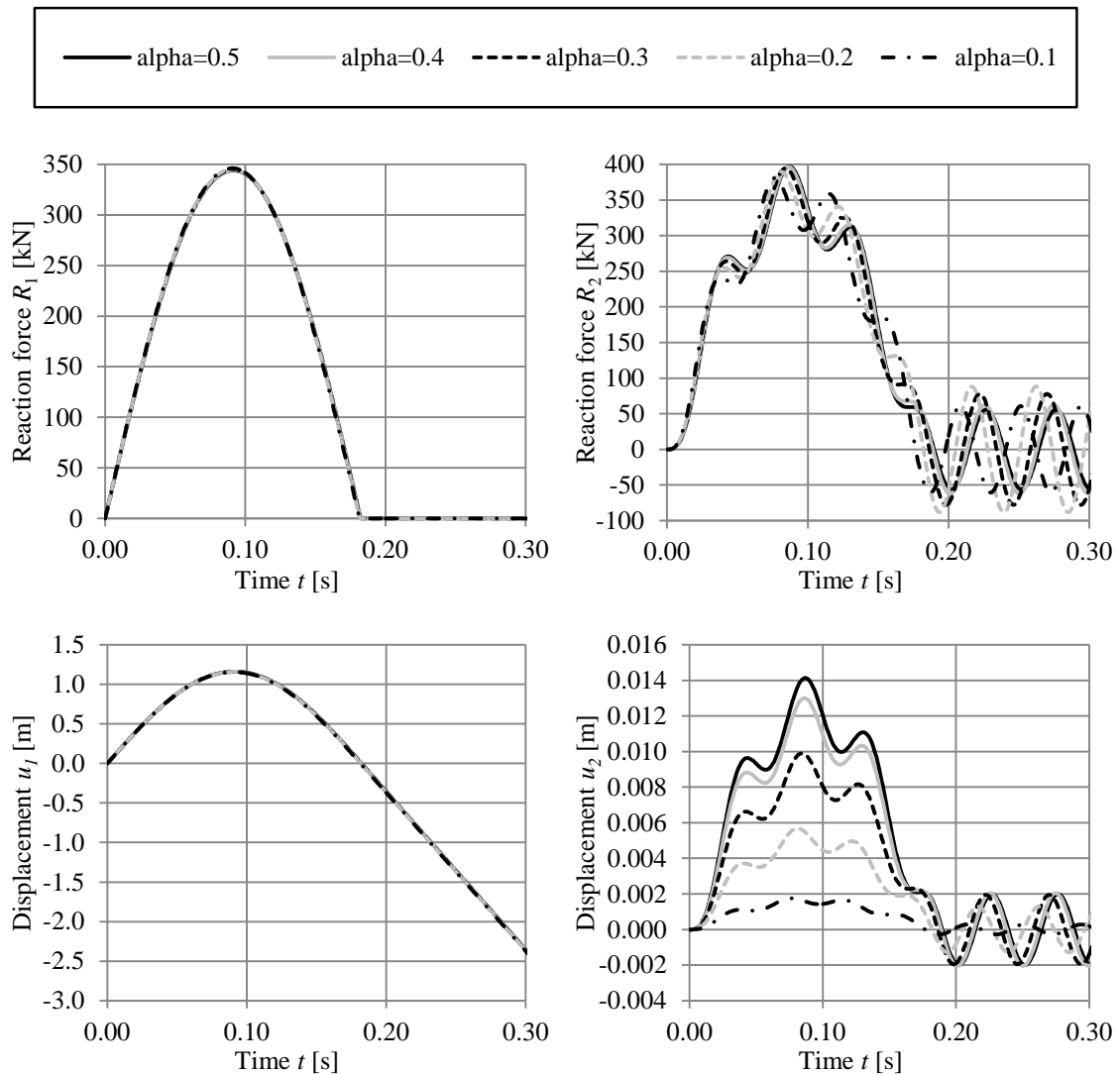
Figure D.2 *Results from the simulated collision with a stiffer beam, describing the differences in position of impact for both the incoming object and the beam.*

D.3   Softer beam
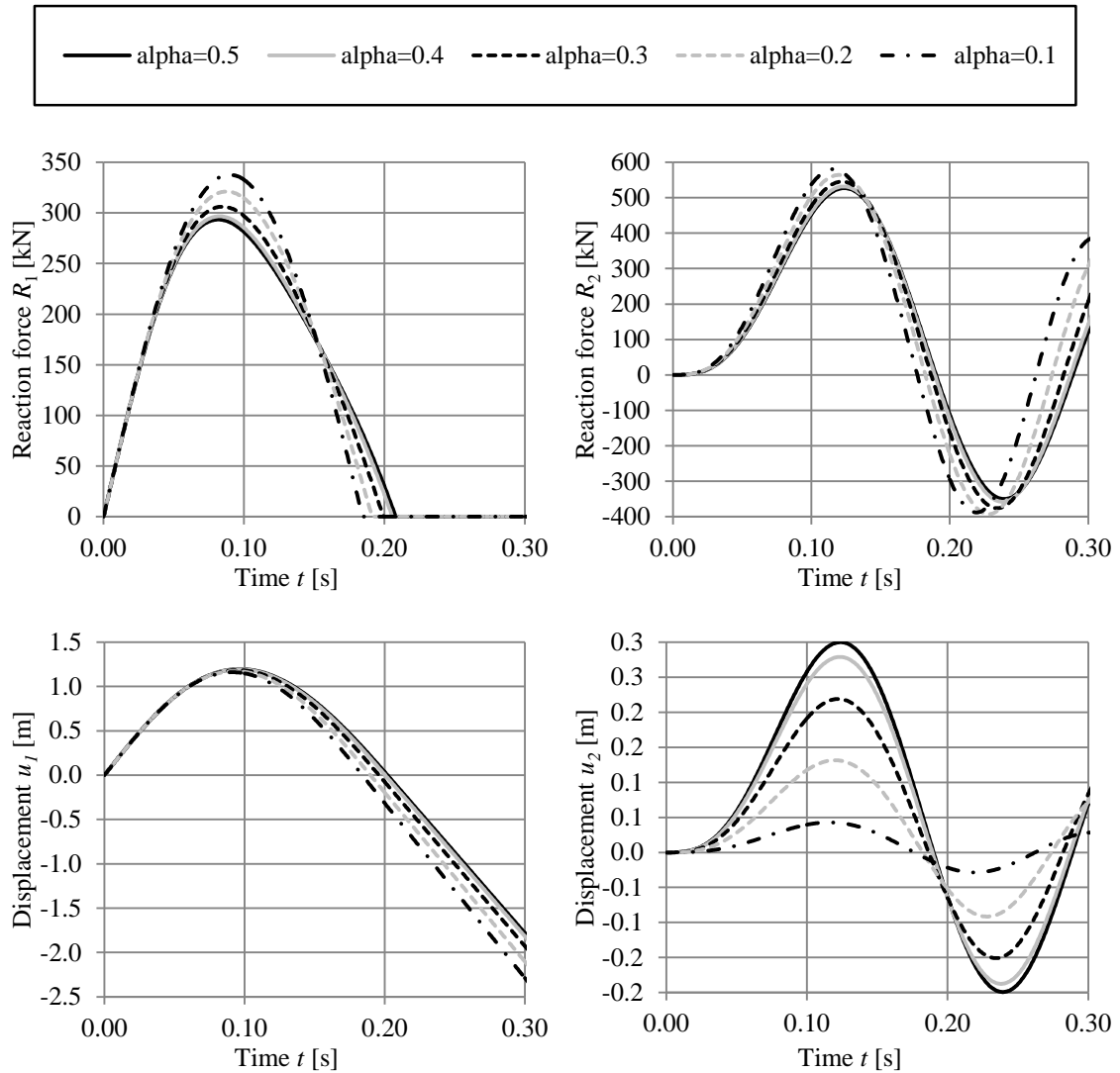
Figure D.3   *Results from the simulated collision with a softer beam, describing the differences in position of impact for both the incoming object and the beam.*

D.4 Stiffer colliding object
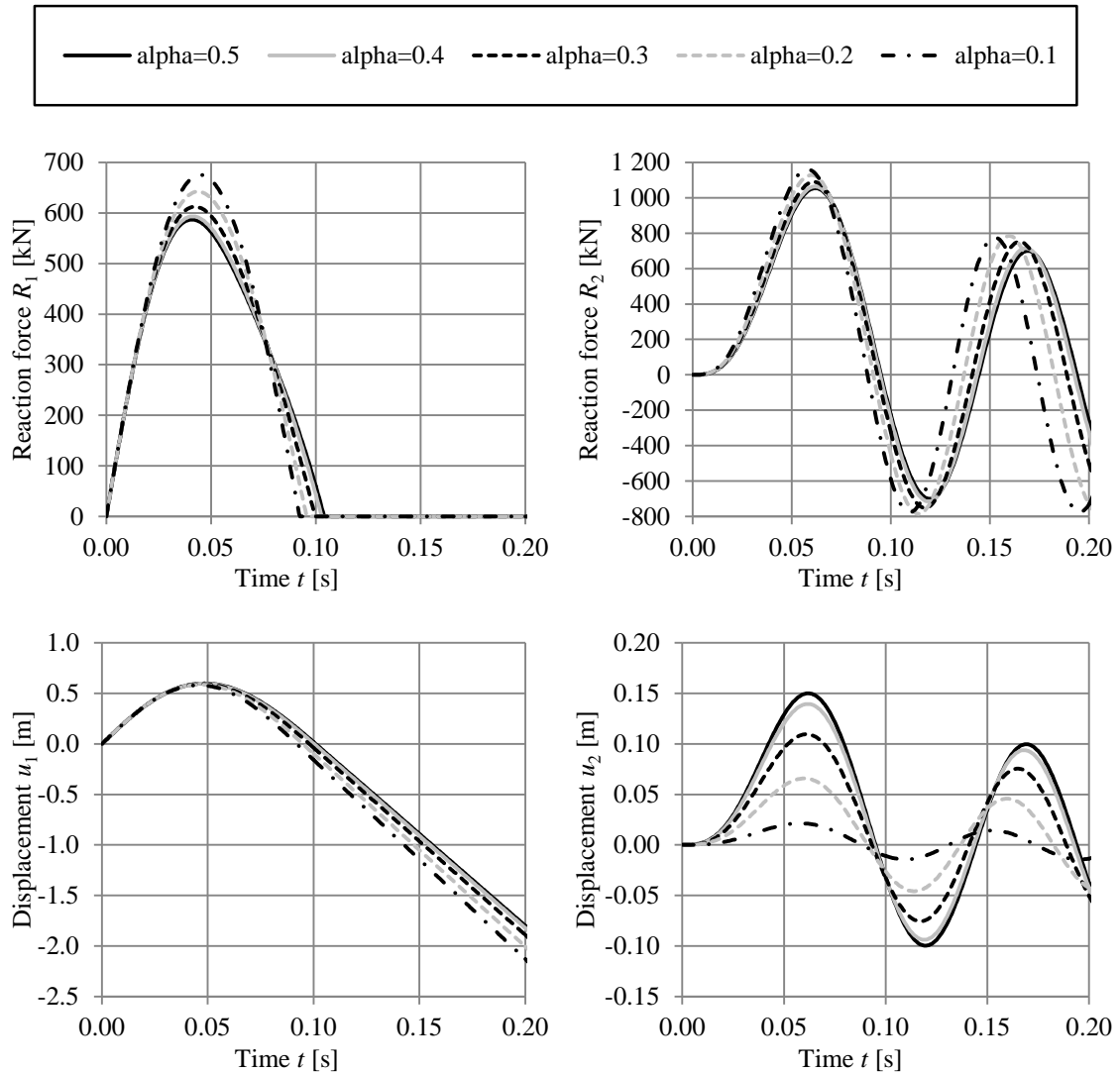
Figure D.4   Results from the simulated collision with a stiffer object, describing the differences in position of impact for both the incoming object and the beam.

D.5 Softer colliding object
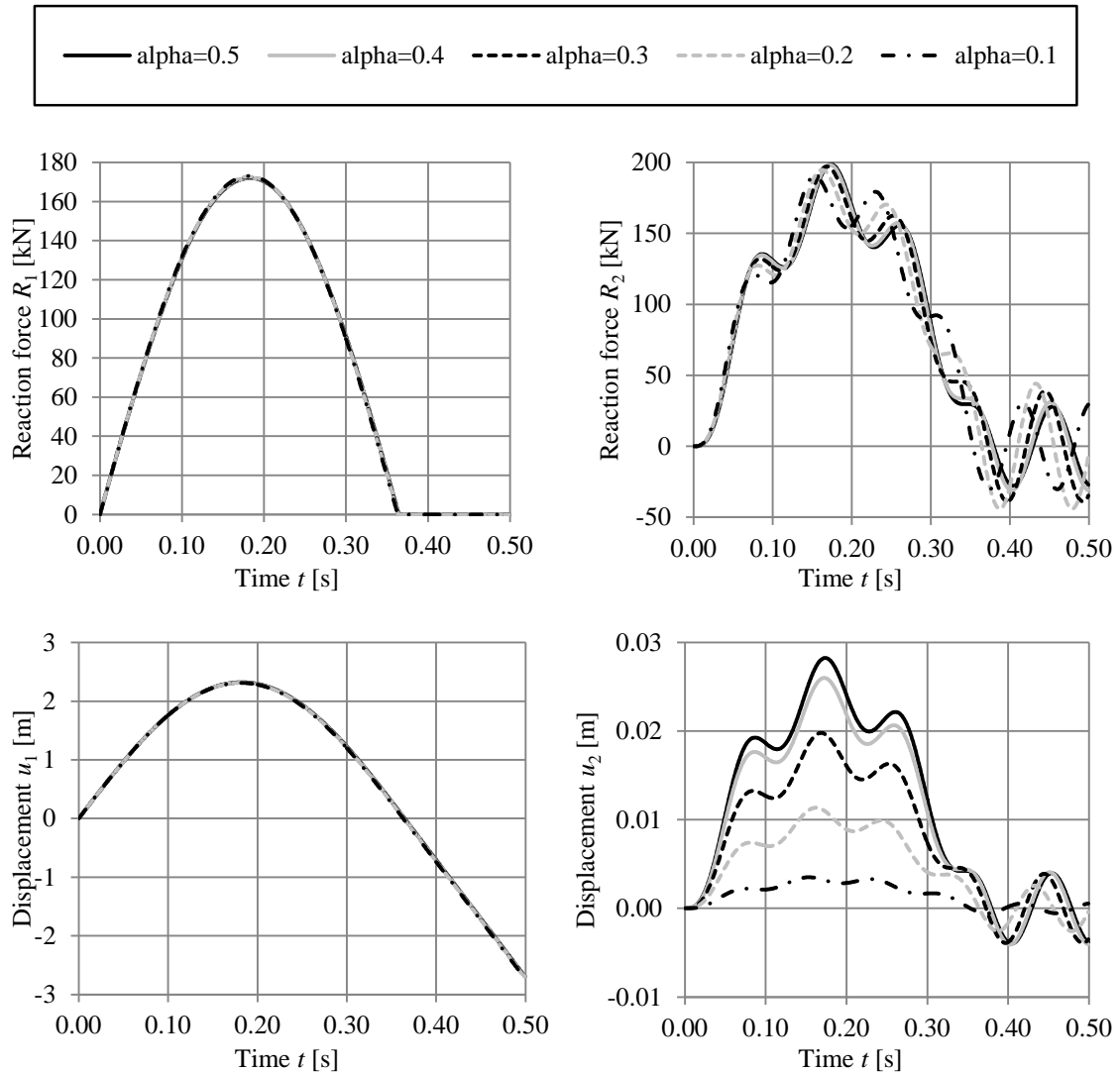
Figure D.5   Results from the simulated collision with a softer object, describing the differences in position of impact for both the incoming object and the beam.

Appendix E   Results from finite element analysis

In this appendix all the results from the analysis discussed in section 5.2 are presented. In Table E.1 the properties used in the different analyses can be seen.

Table E.1   The different set of properties used in each analysis.

Property set number	Spring stiffness k_1 [kN/m]	Equivalent Young's modulus E_{II} [GPa]
1	300	8.134
2	75	8.134
3	1 200	8.134
4	300	2.034
5	300	32.537

E.1   Original beam – Property set 1
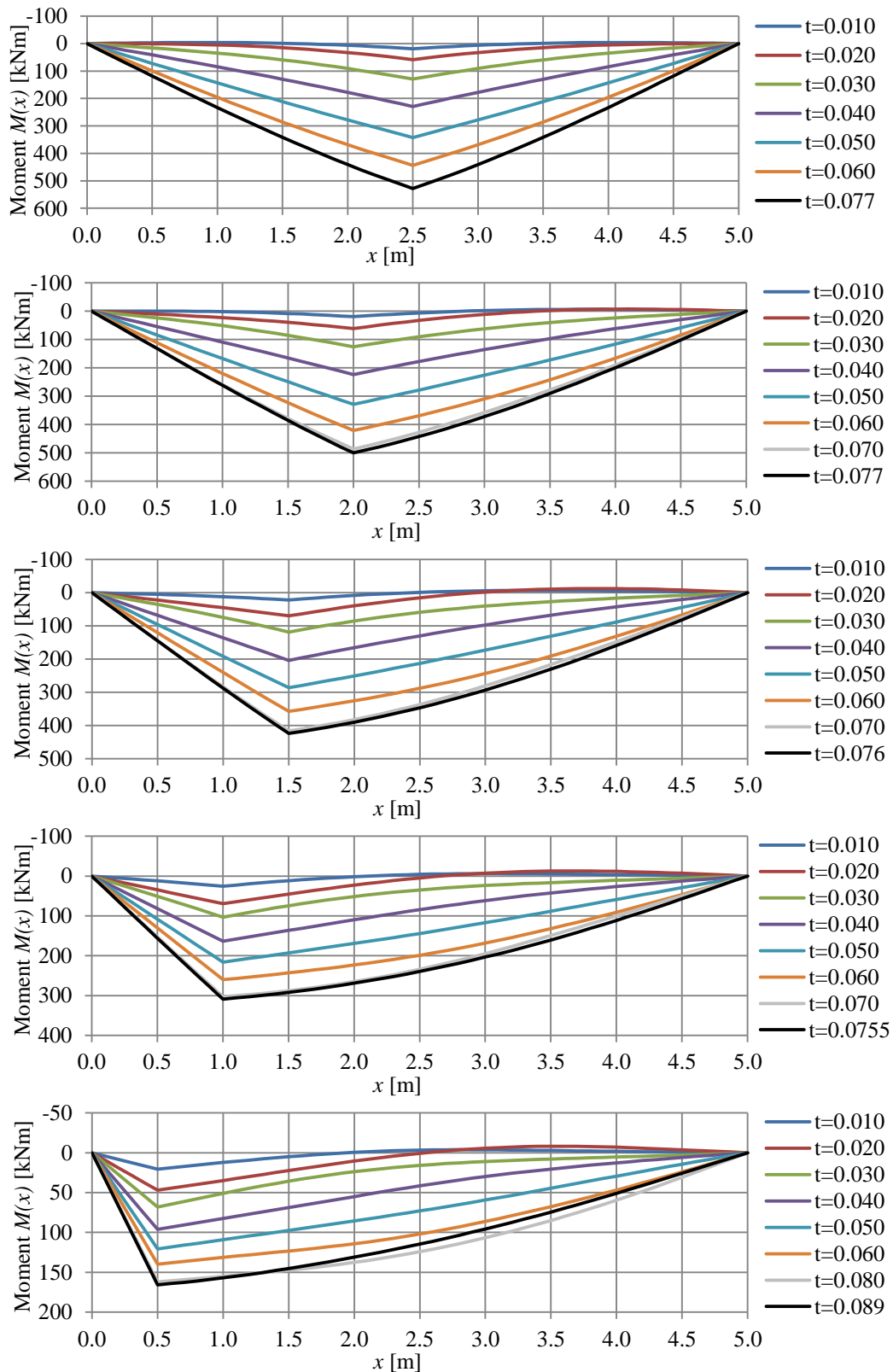
Figure E.1   Development of moment up to maximum moment over time for five different impact positions.
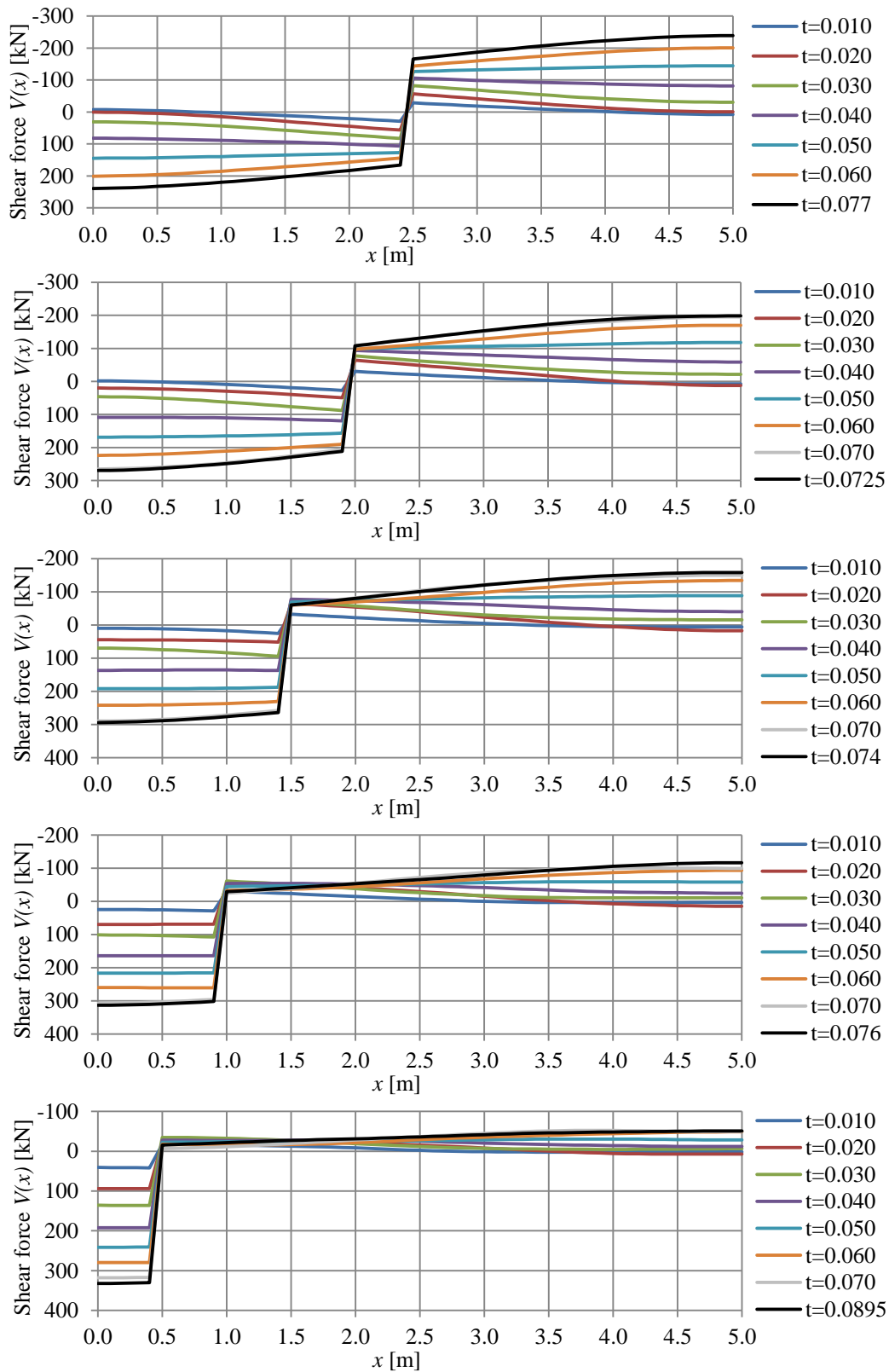
Figure E.2   Development up to maximum shear force over time for five different impact positions.
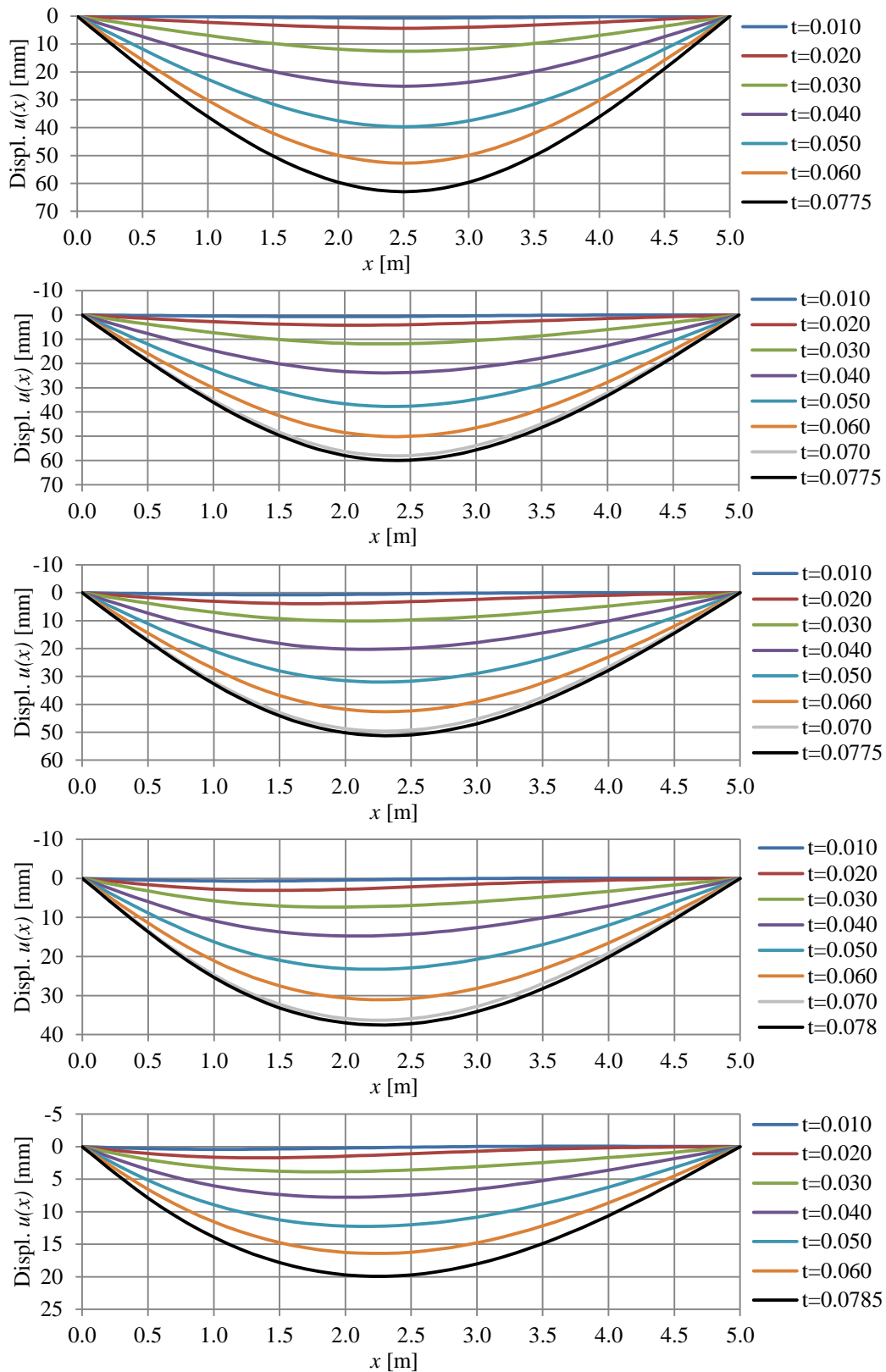
Figure E.3   Development up to maximum deflection over time for five different impact positions.

CHALMERS, *Civil and Environmental Engineering*, Master's Thesis 2014:80
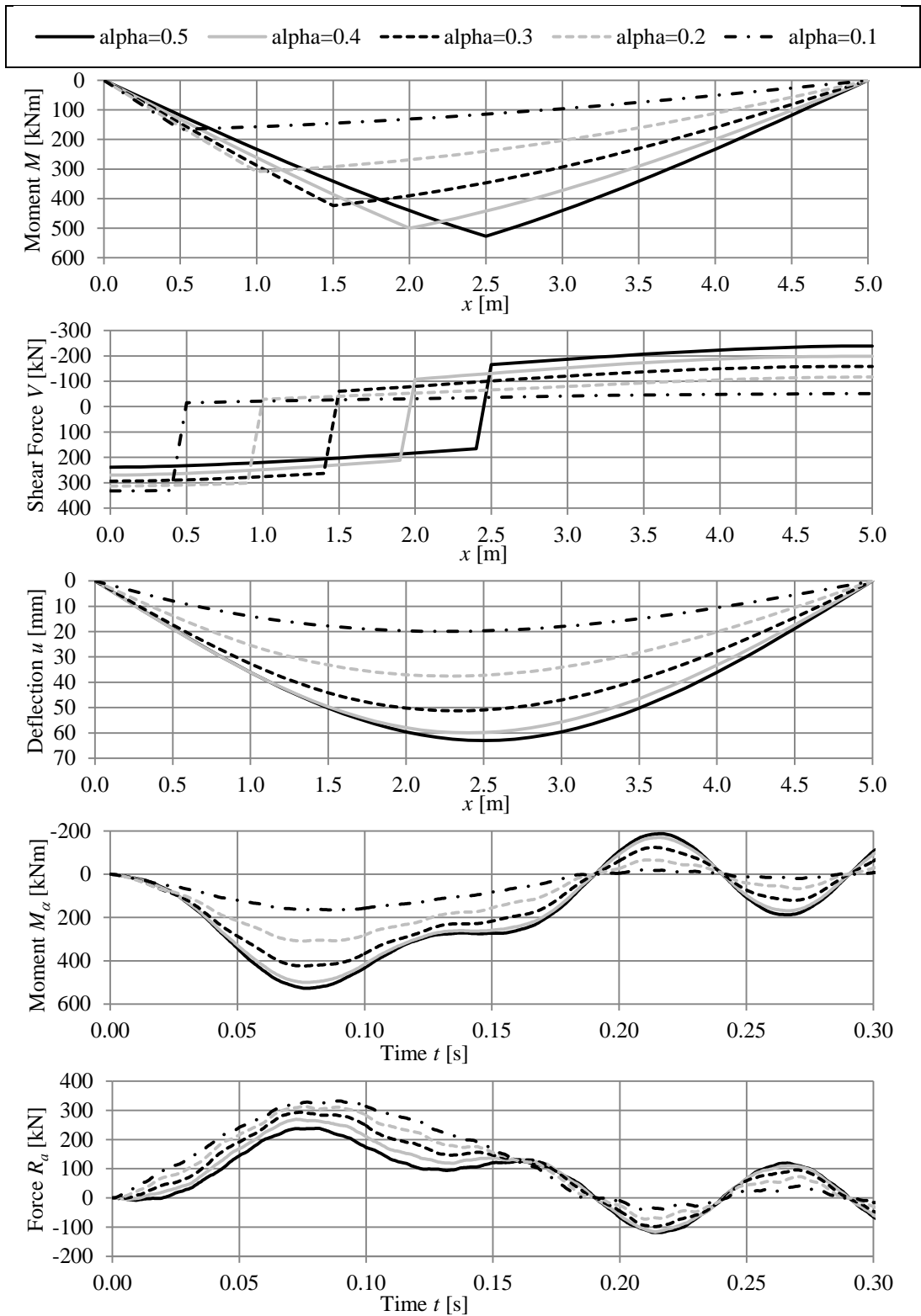
Figure E.4   Comparison of maximum responses for five different impact positions.

E.2   Stiffer beam – Property set 5
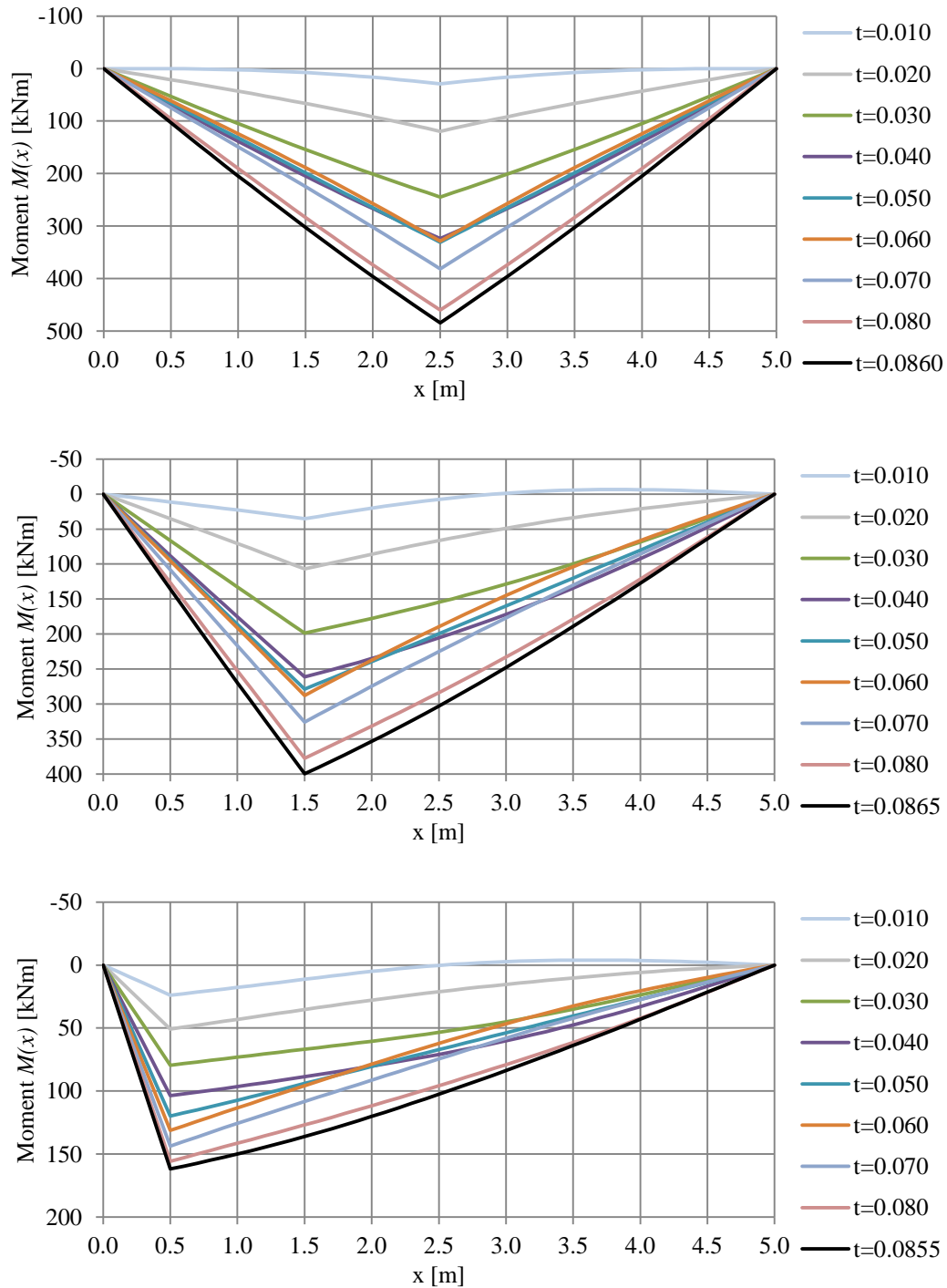
Figure E.5   Development of moment up to maximum moment over time for three different impact positions.

CHALMERS, *Civil and Environmental Engineering*, Master's Thesis 2014:80
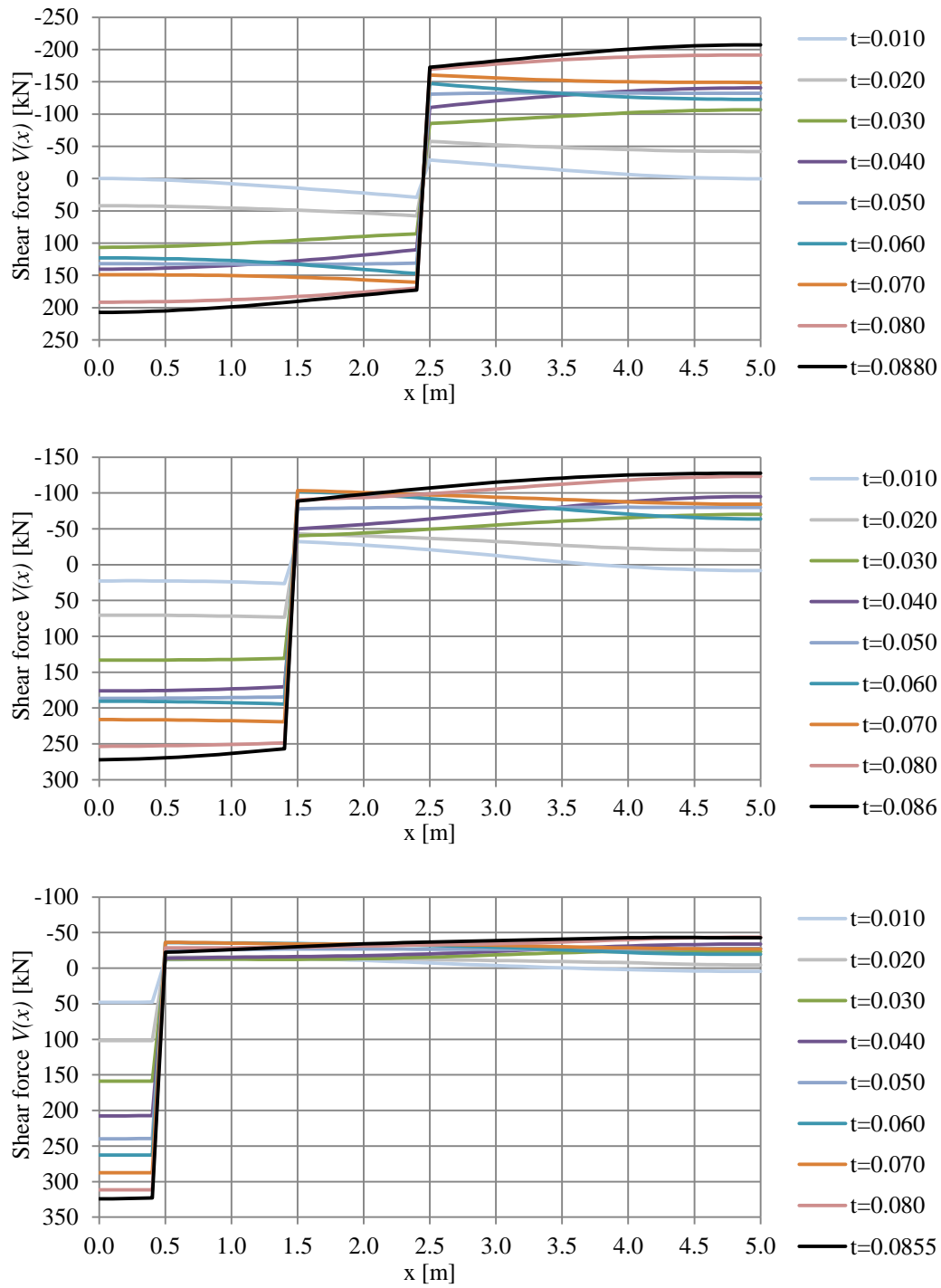
Figure E.6   Development up to maximum shear force over time for three different impact positions.
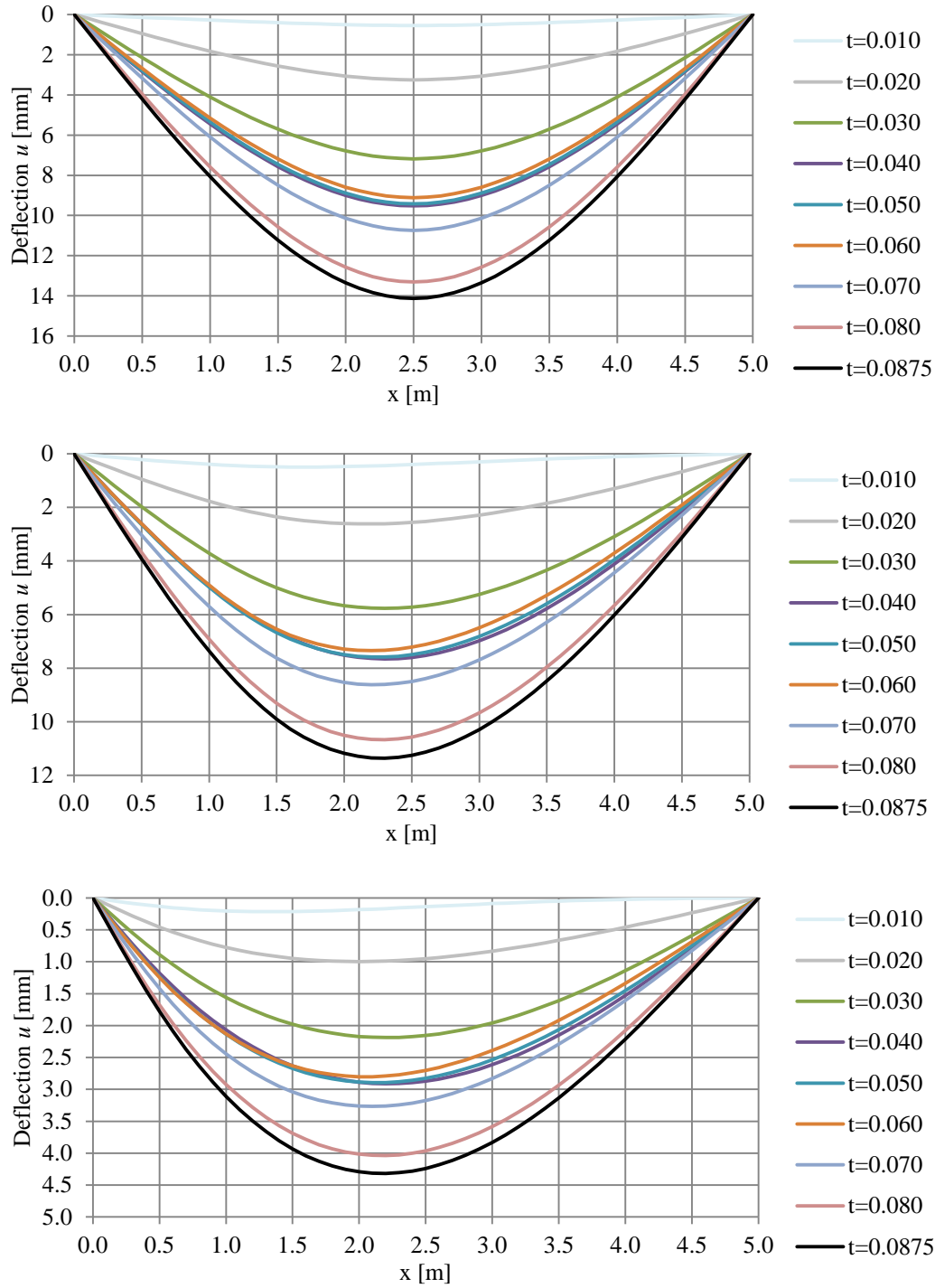
Figure E.7   Development up to maximum deflection over time for three different impact positions.
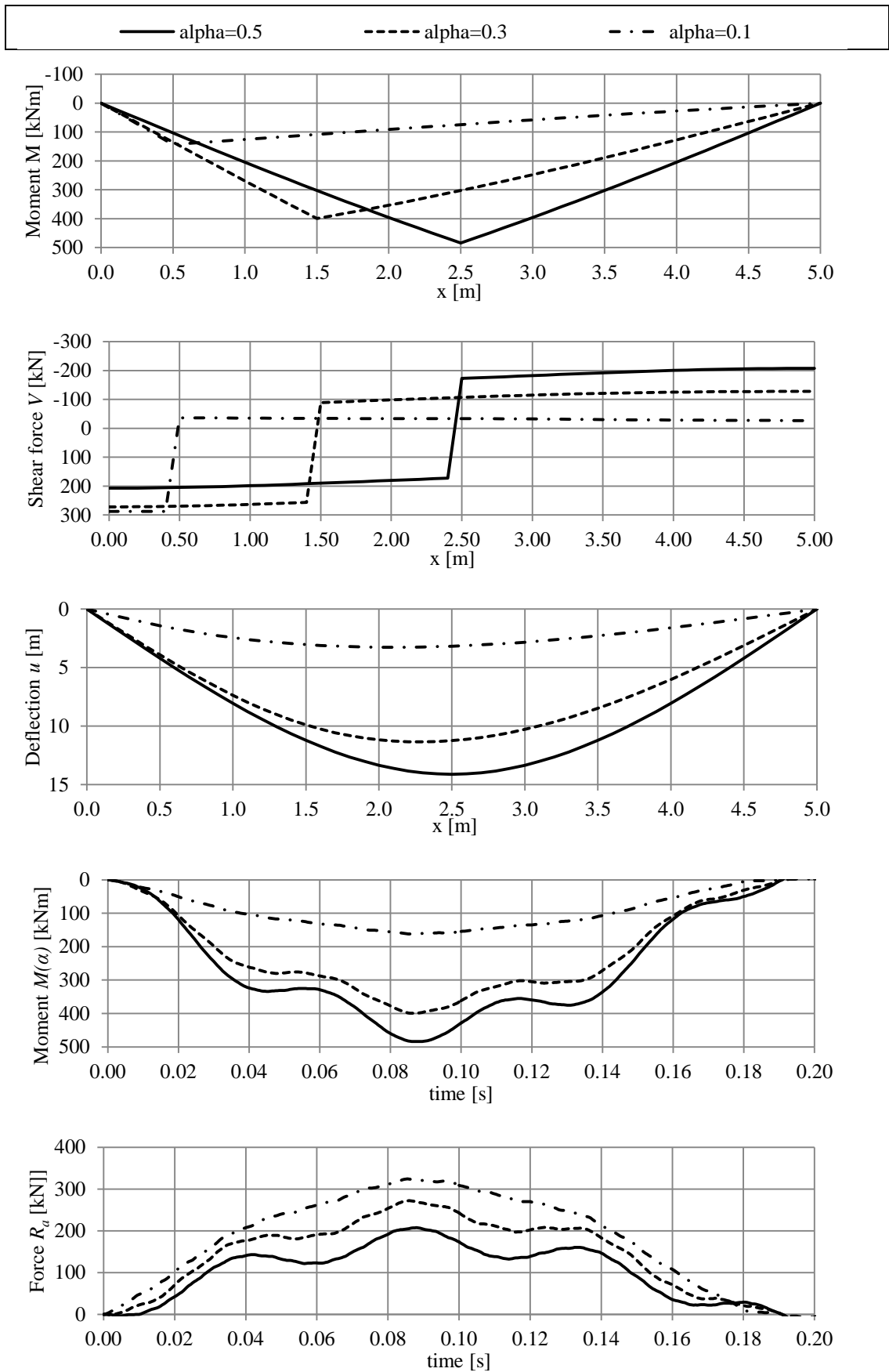
Figure E.8   Comparison of maximum responses for three different impact positions.

E.3   Softer beam – Property set 4
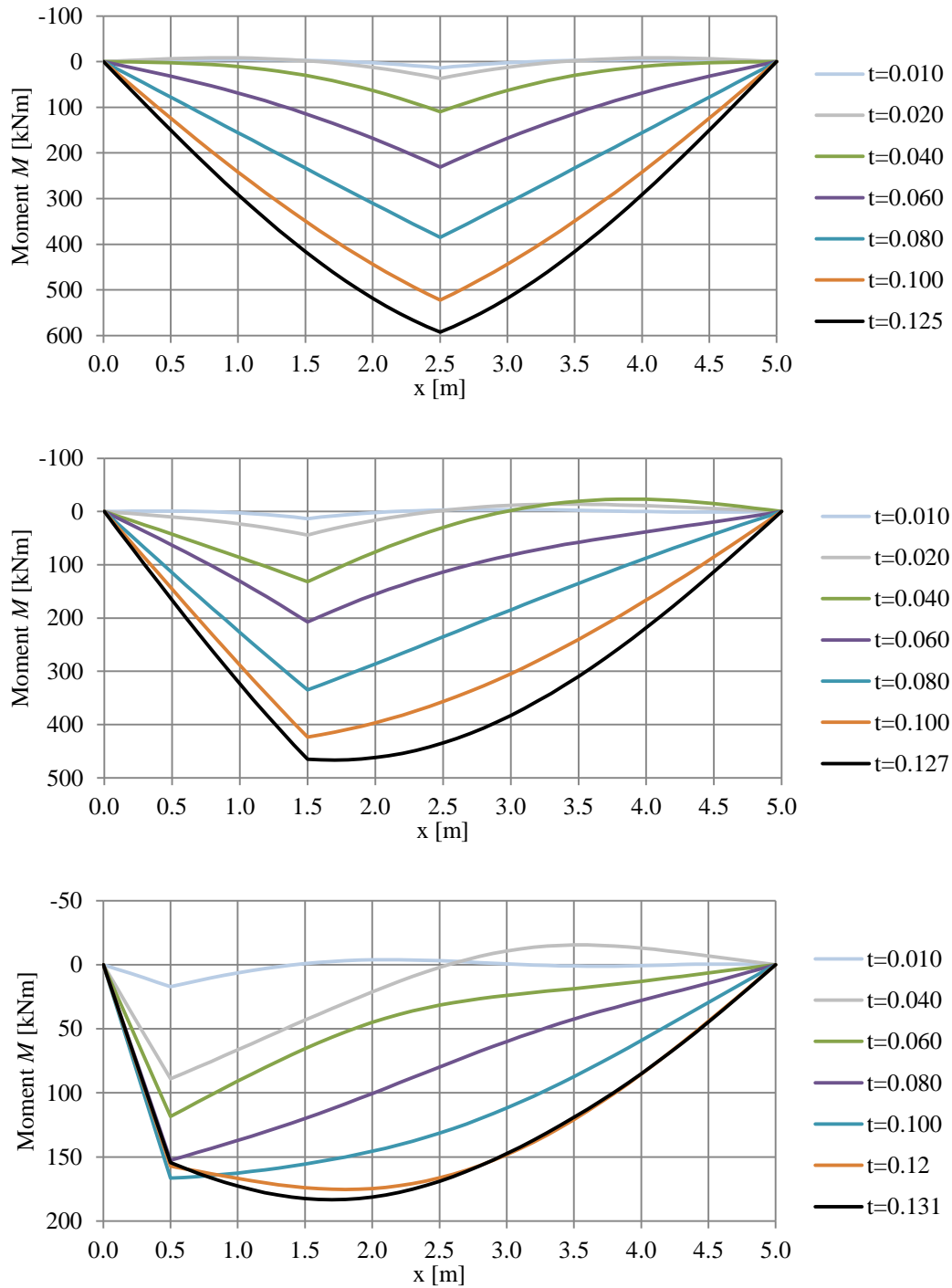
Figure E.9   Development of moment up to maximum moment over time for three different impact positions.

CHALMERS, *Civil and Environmental Engineering*, Master's Thesis 2014:80
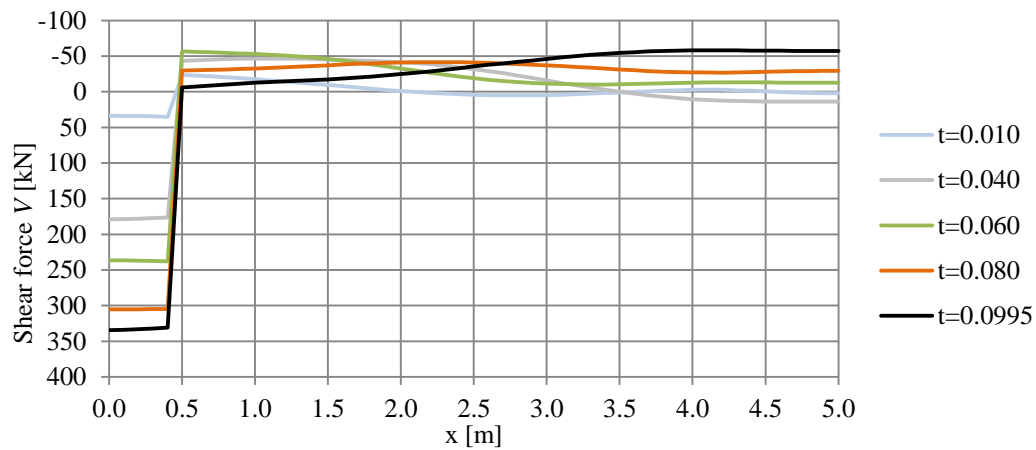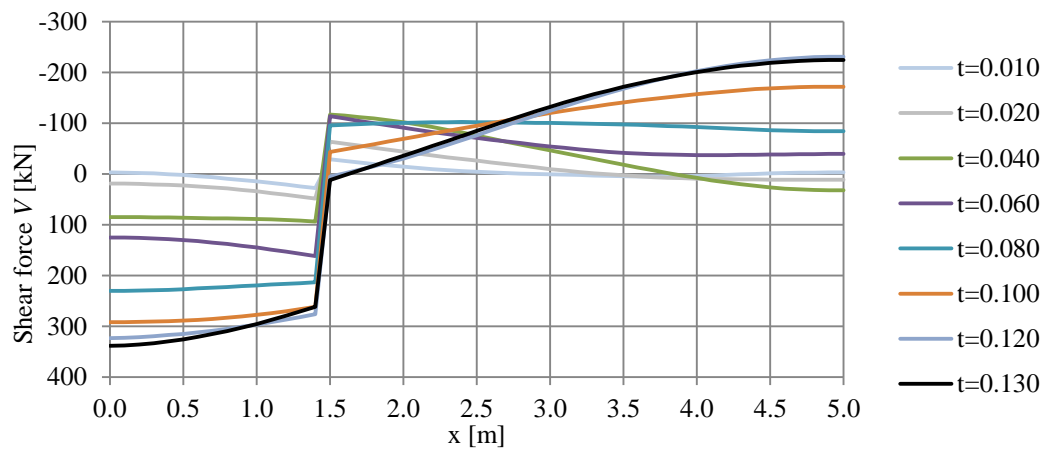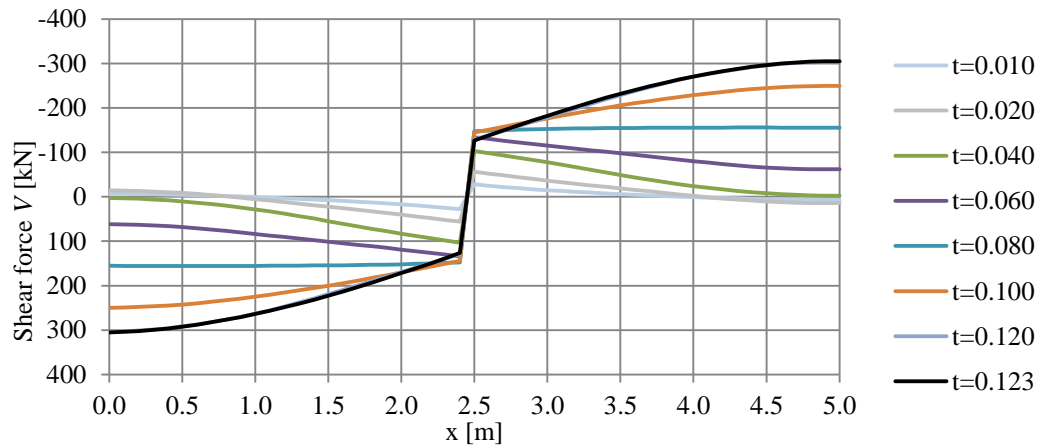
Figure E.10   Development up to maximum shear force over time for three different impact positions.
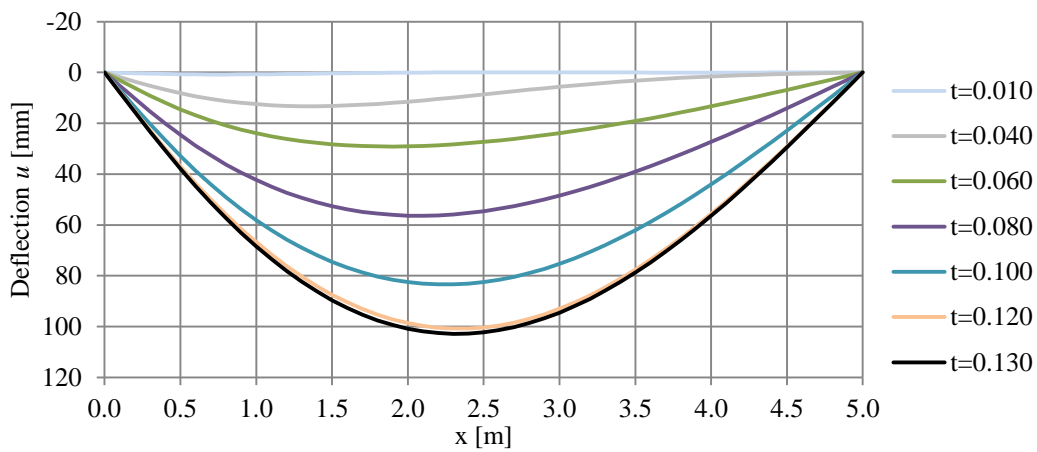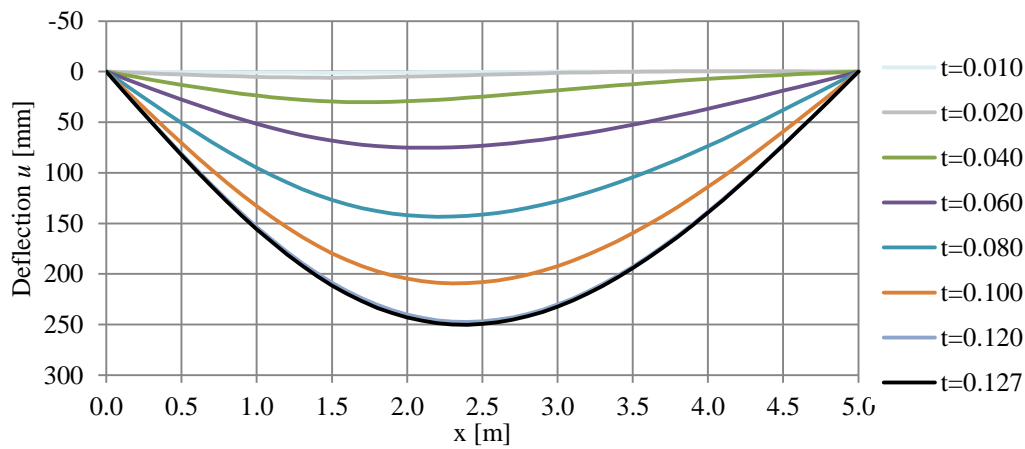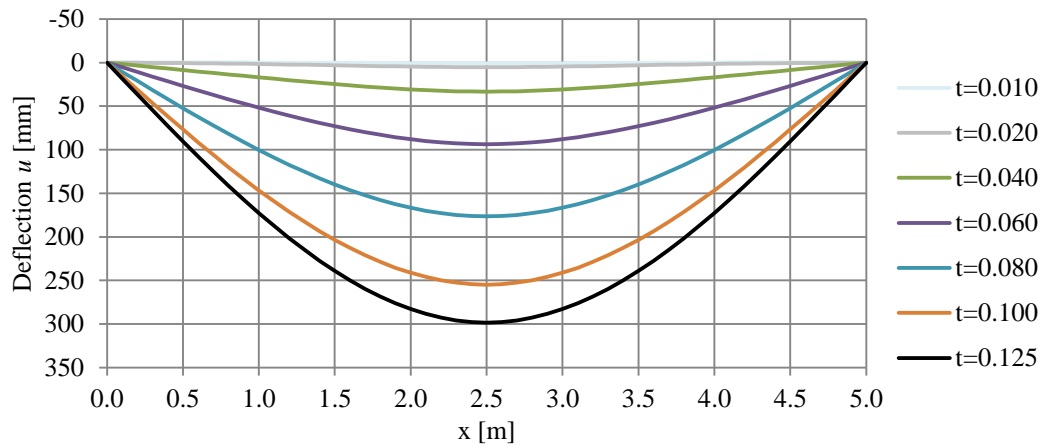
Figure E.11   Development up to maximum deflection over time for three different impact positions.
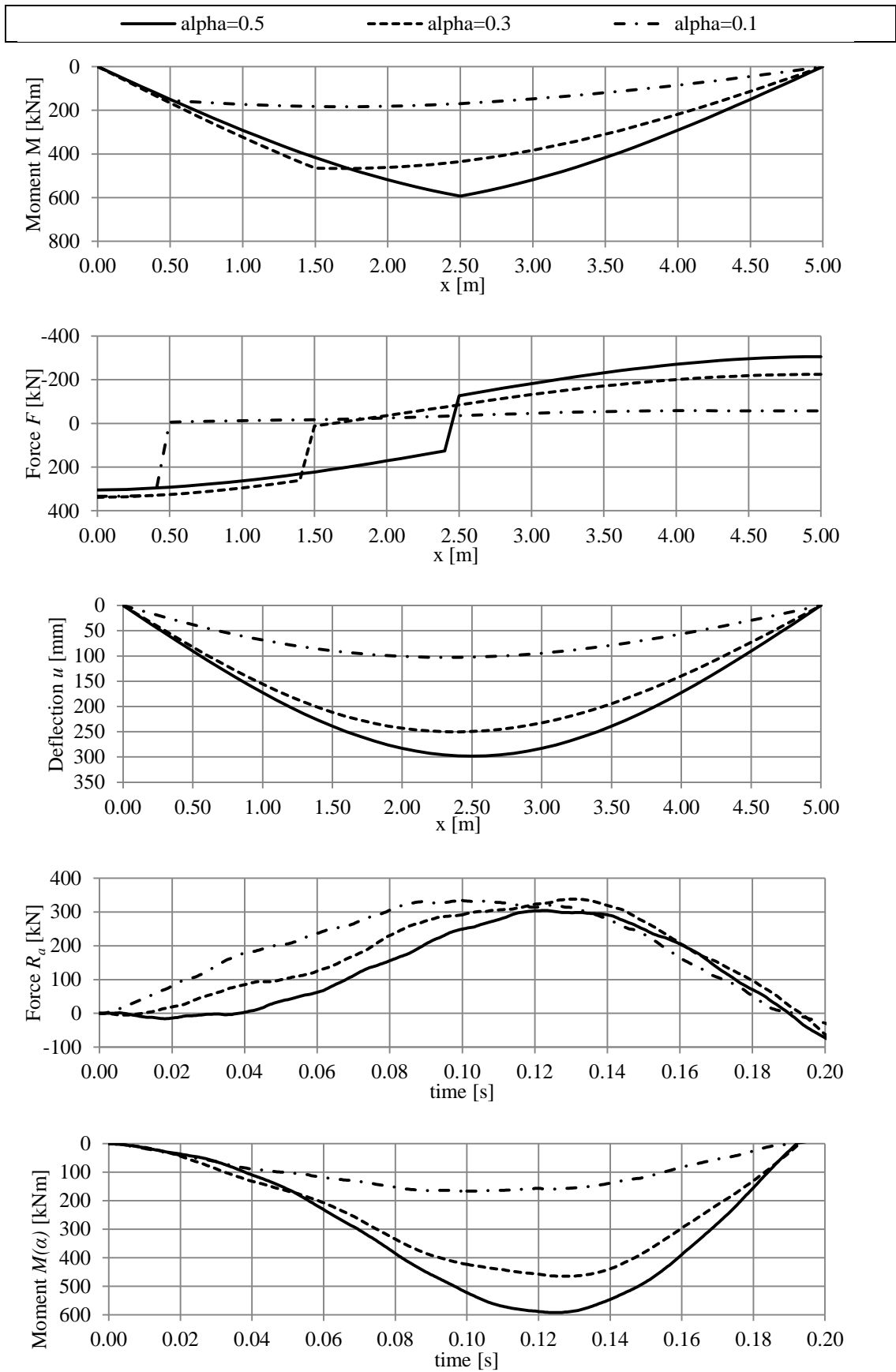
Figure E.12   Comparison of maximum responses for three different impact positions.

E.4 Stiffer colliding object – Property set 3
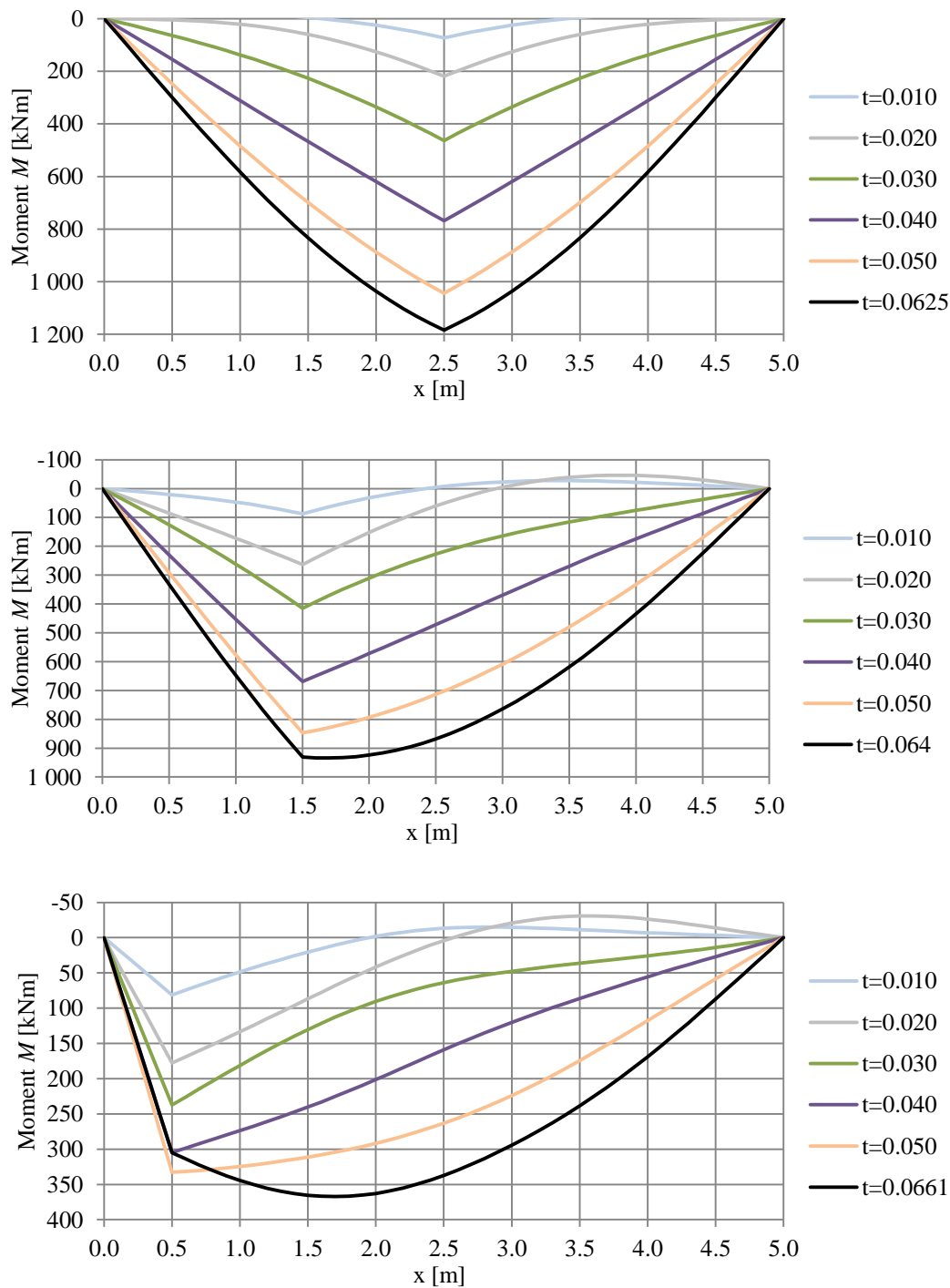
Figure E.13 Development of moment up to maximum moment over time for three different impact positions.
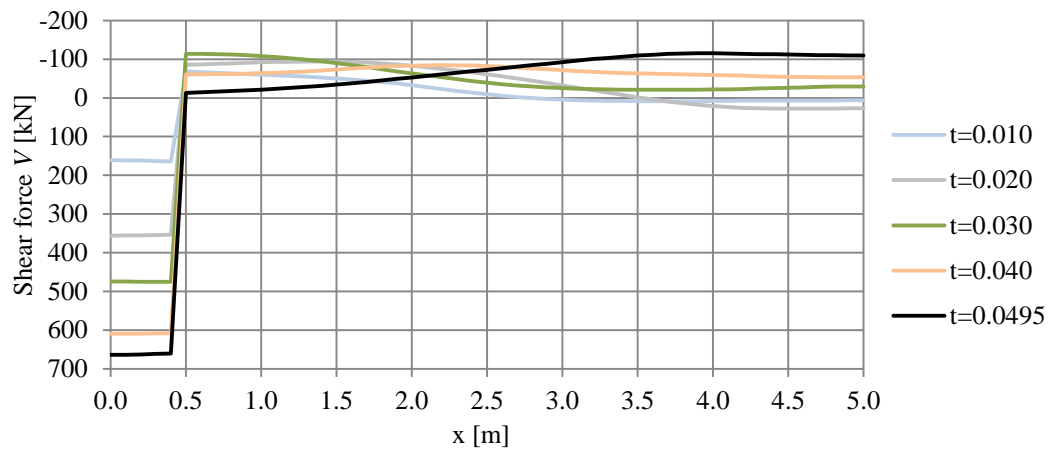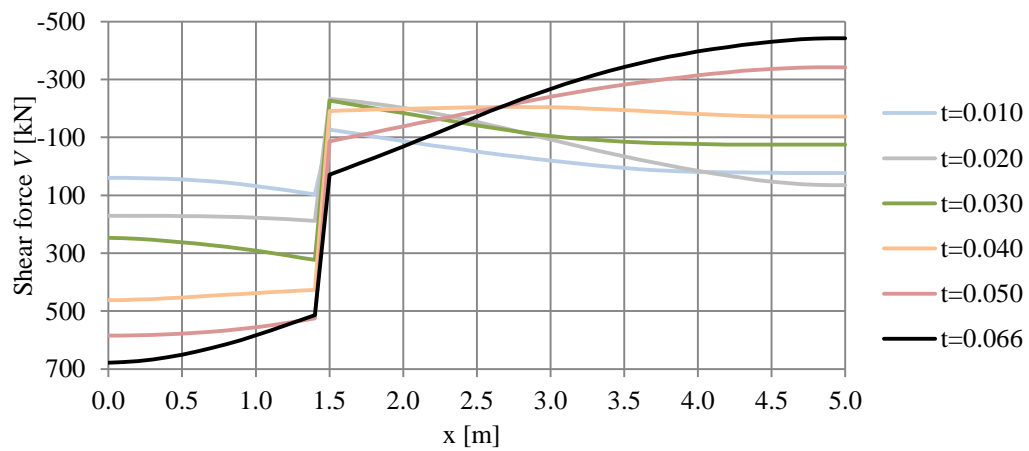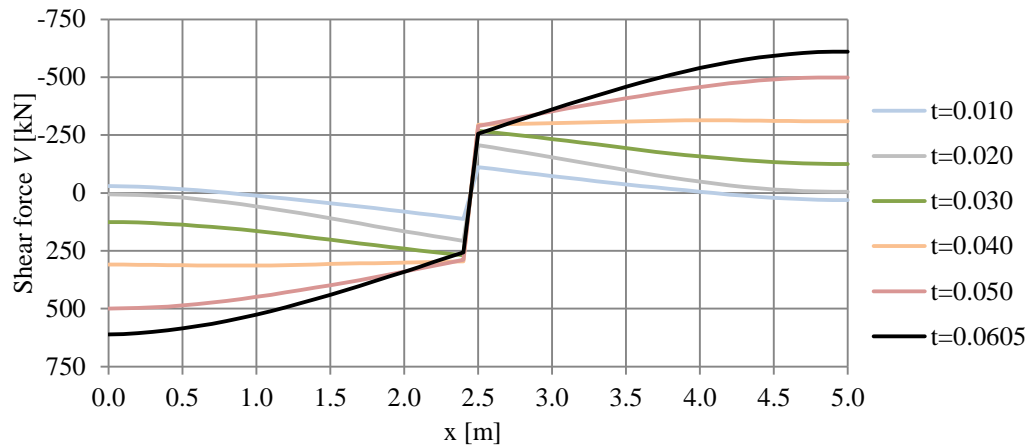
Figure E.14   Development up to maximum shear force over time for three different impact positions.
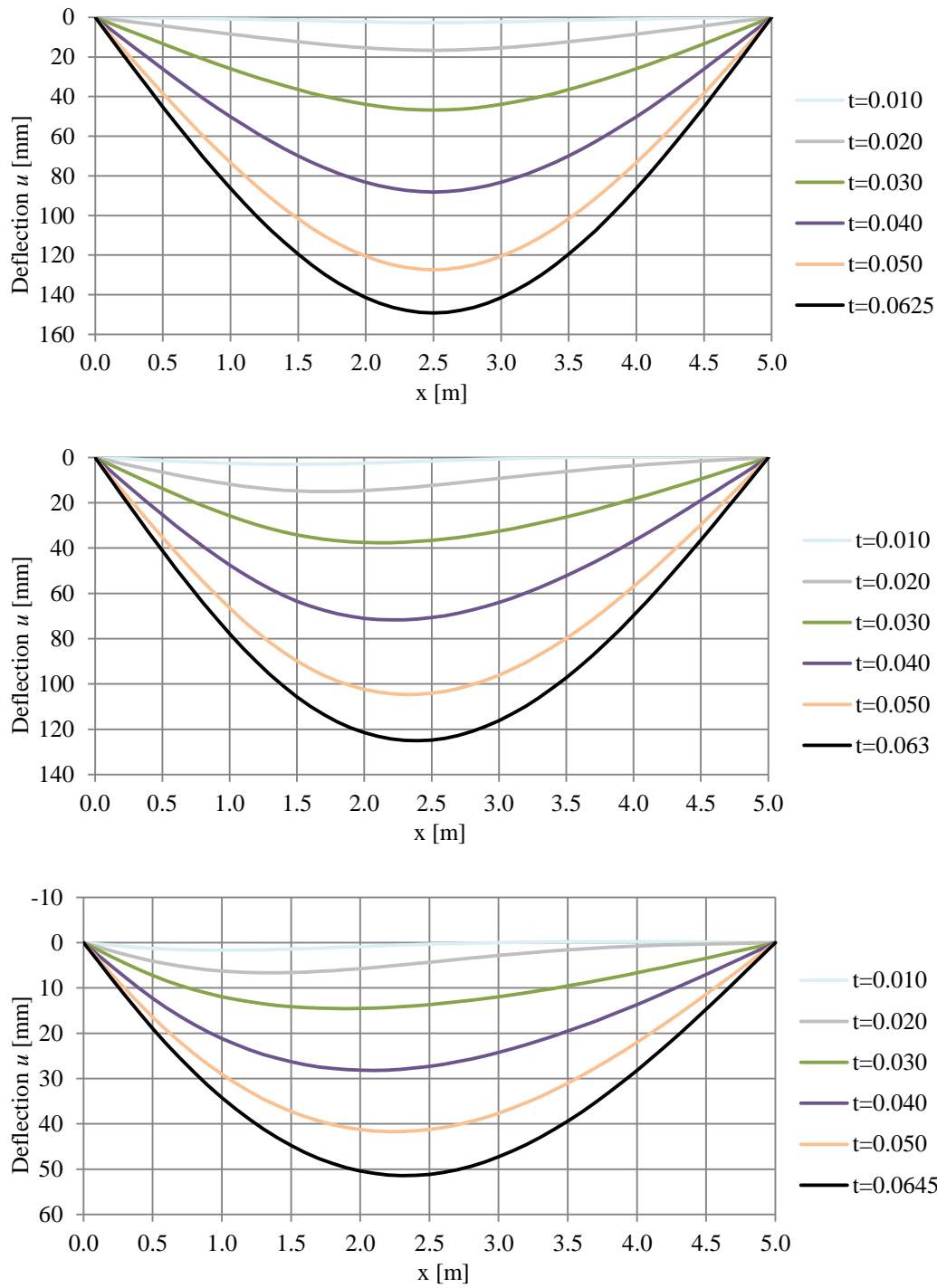
Figure E.15   Development up to maximum deflection over time for three different impact positions.

CHALMERS, *Civil and Environmental Engineering*, Master's Thesis 2014:80
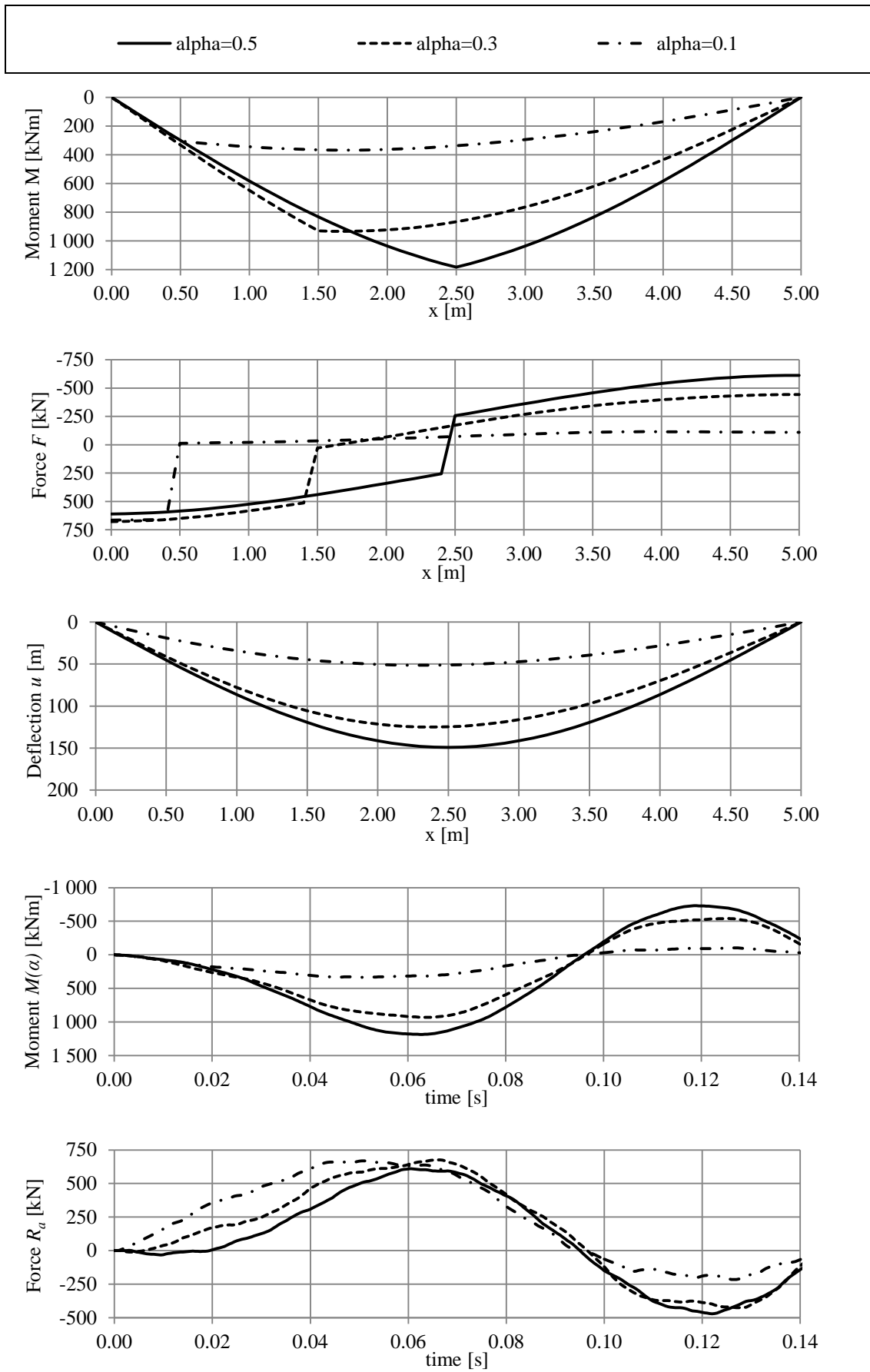
Figure E.16   Comparison of maximum responses for three different impact positions.

E.5   Softer colliding object – Property set 2
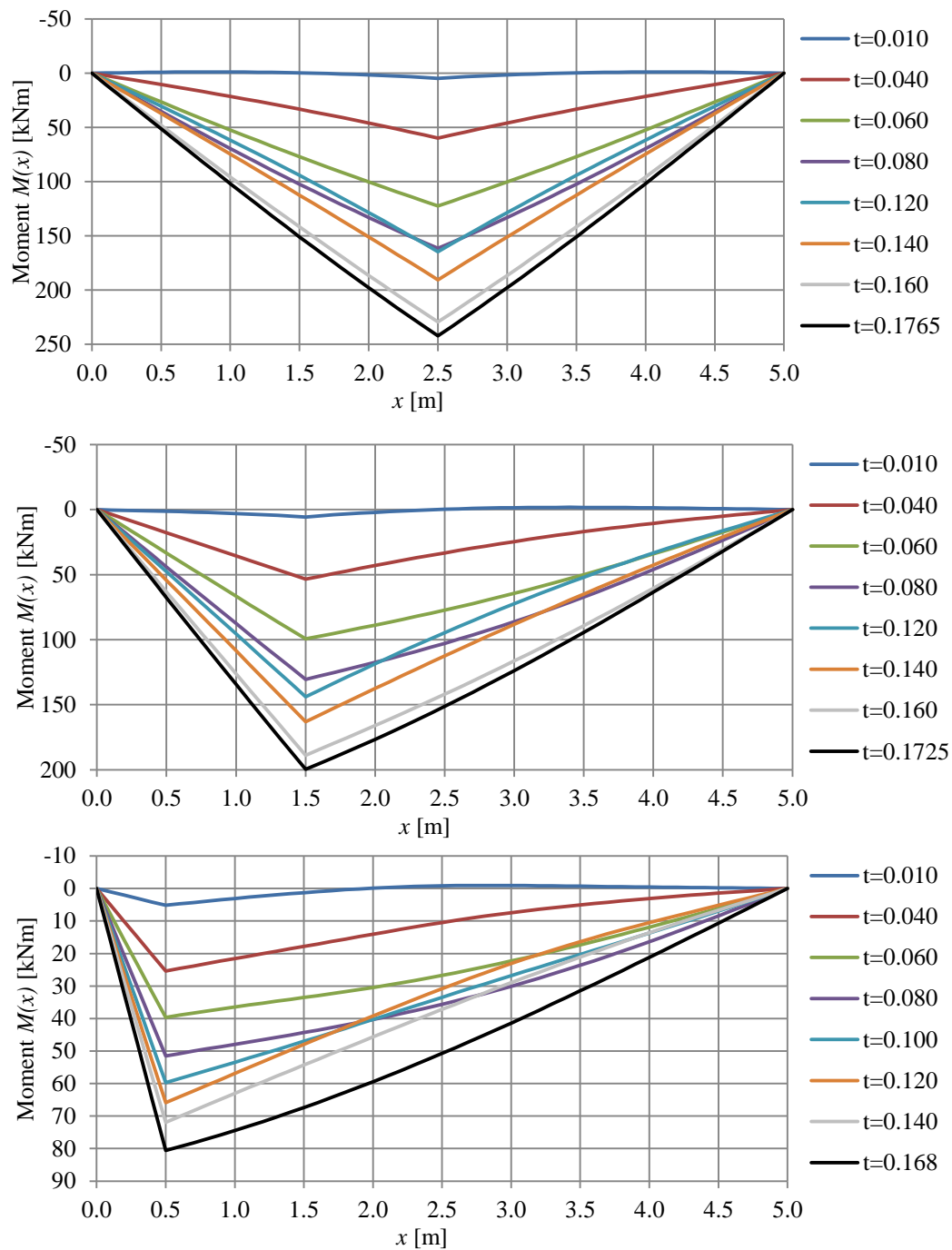
Figure E.17   Development of moment up to maximum moment over time for three different impact positions.
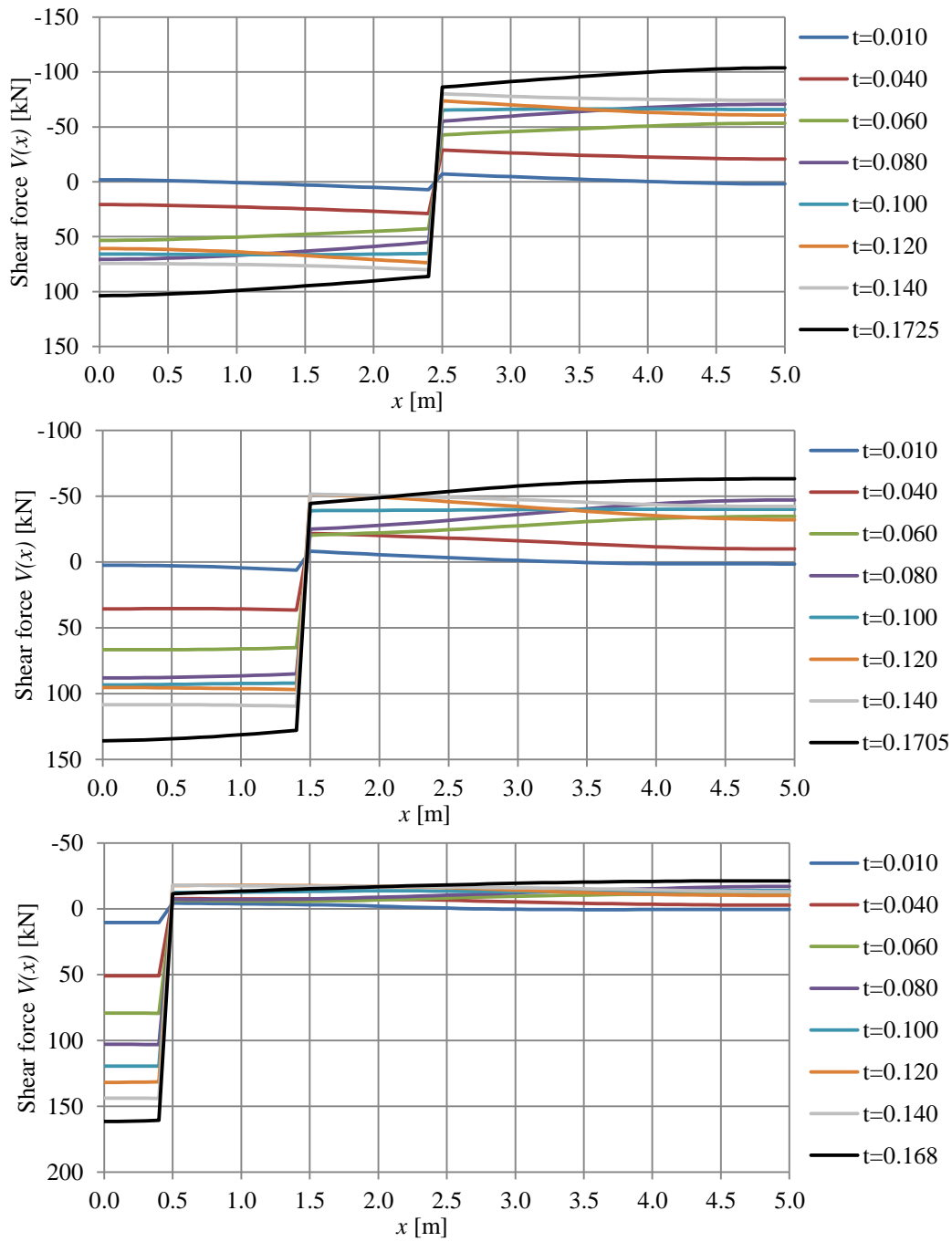
Figure E.18   Development up to maximum shear force over time for three different impact positions.
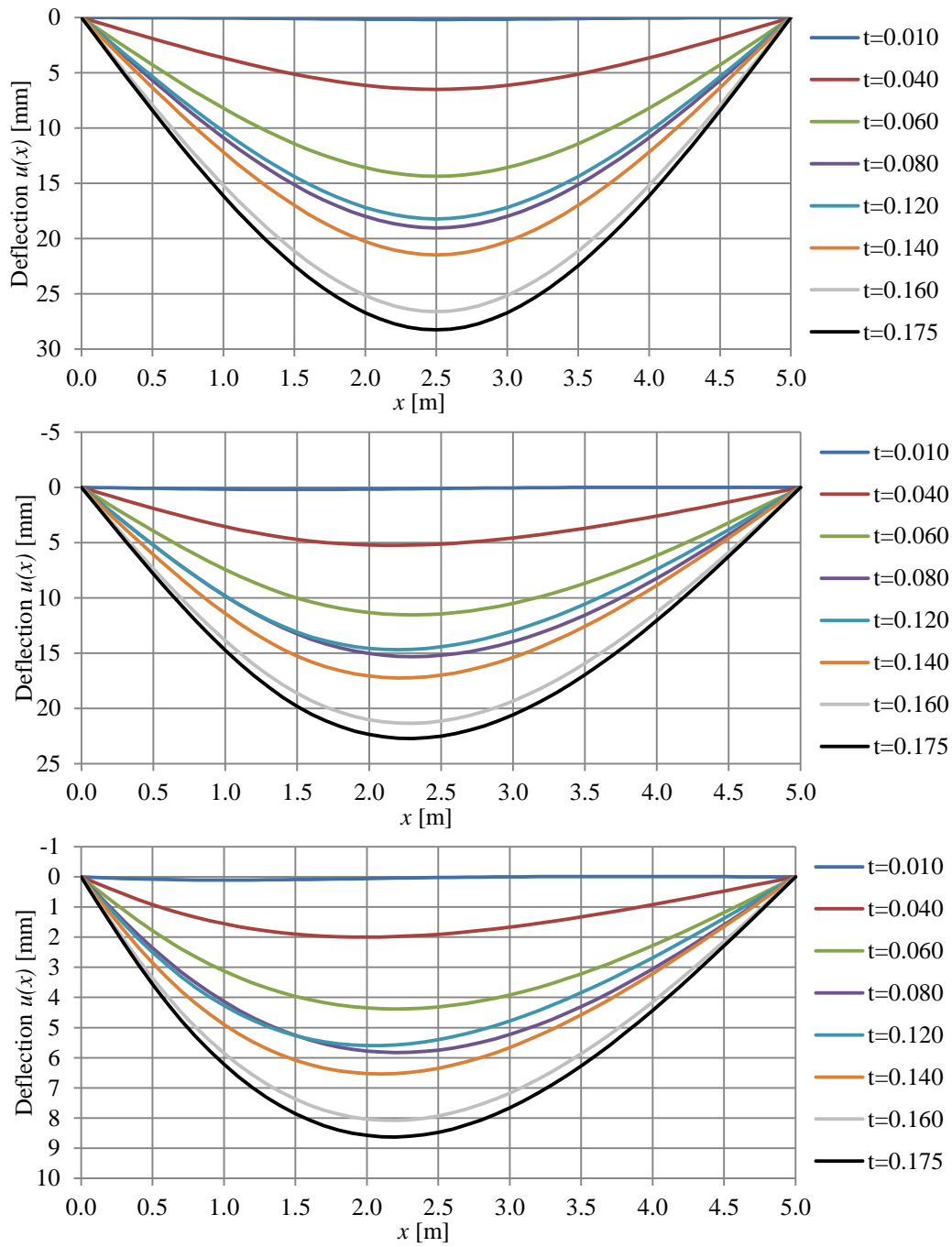
Figure E.19 *Development up to maximum deflection over time for three different impact positions.*
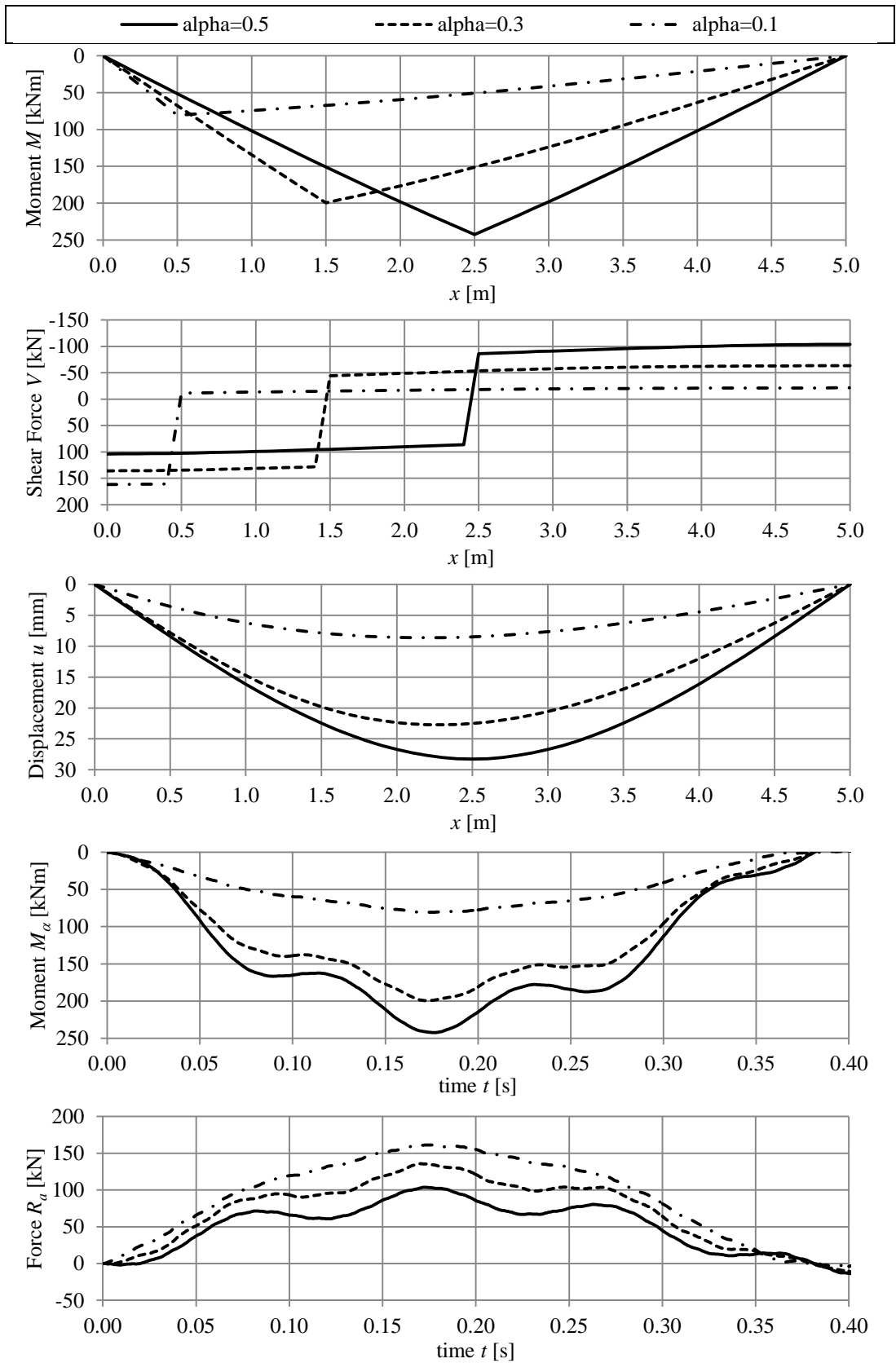
Figure E.20   Comparison of maximum responses for three different impact positions.

Appendix F Comparison of model responses

The comparison of responses from a collision modelled with the 2DOF system in MATLAB and with FEM software ADINA are presented in this appendix. The study in this section is based on the concrete beam described in section 4.1.2. The velocity v_0 of the incoming object is set to 20 m/s and the stiffness k_1 is set to 300 kN/m. These stiffnesses corresponds to property set 1, and the stiffnesses are then varied to create the other property sets, see Table F.1.

Table F.1   Input parameters for the different collision analyses.

α	Property set	k_1 [kN/m]	EI_b [MNm^2]	k_b [MN/m]	m_1 [kg]	m_2 [kg]	$\dfrac{m_1}{m_2}$	f_1 [Hz]	f_2 [Hz]	$\dfrac{f_1}{f_2}$
0.5	1	300	18.302	7.028	1 000	1 748.6	0.572	2.757	10.09	0.273
	2	75	18.302	7.028	1 000	1 748.6	0.572	1.378	10.09	0.137
	3	1 200	18.302	7.028	1 000	1 748.6	0.572	5.513	10.09	0.546
	4	300	4.576	1.757	1 000	1 748.6	0.572	2.757	5.045	0.546
	5	300	73.208	28.112	1 000	1 748.6	0.572	2.757	20.18	0.137
0.3	1	300	18.302	9.960	1 000	2 310.8	0.433	2.757	10.45	0.264
	2	75	18.302	9.960	1 000	2 310.8	0.433	1.378	10.45	0.132
	3	1 200	18.302	9.960	1 000	2 310.8	0.433	5.513	10.45	0.528
	4	300	4.576	2.490	1 000	2 310.8	0.433	2.757	5.225	0.528
	5	300	73.208	39.842	1 000	2 310.8	0.433	2.757	20.90	0.132
0.1	1	300	18.302	54.229	1 000	10 092	0.099	2.757	11.67	0.236
	2	75	18.302	54.229	1 000	10 092	0.099	1.378	11.67	0.118
	3	1 200	18.302	54.229	1 000	10 092	0.099	5.513	11.67	0.473
	4	300	4.576	13.557	1 000	10 092	0.099	2.757	5.833	0.473
	5	300	73.208	216.92	1 000	10 092	0.099	2.757	23.33	0.118

F.1   Original beam – Property set 1
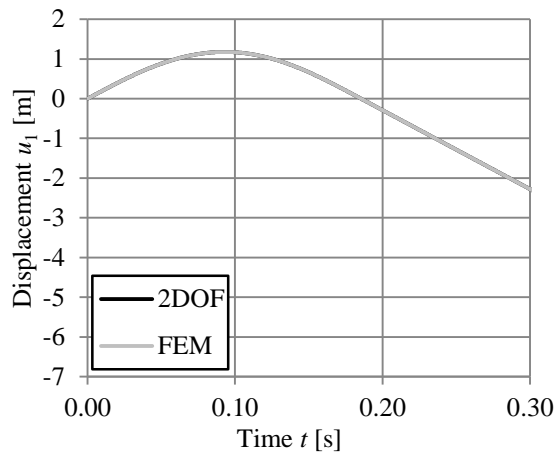
a) u_1, $\alpha = 0.5$
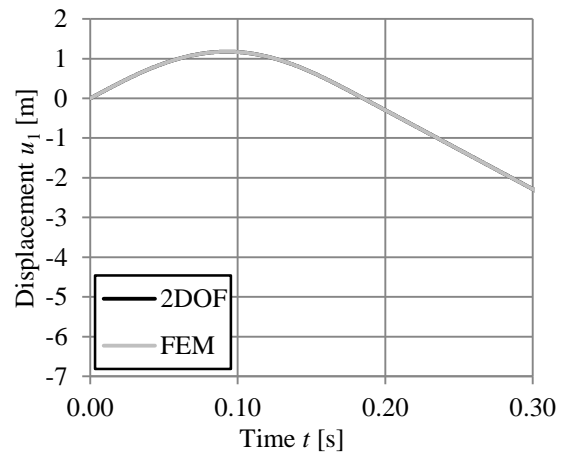
b) u_1, $\alpha = 0.4$
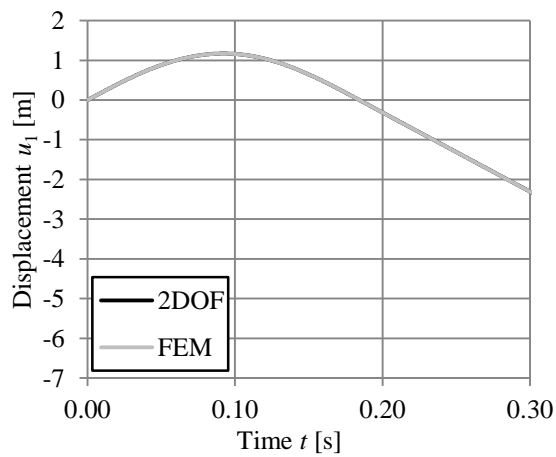
c) u_1, $\alpha = 0.3$
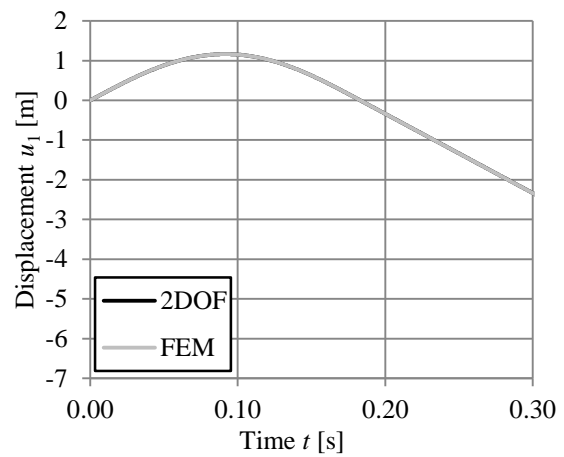
d) u_1, $\alpha = 0.2$
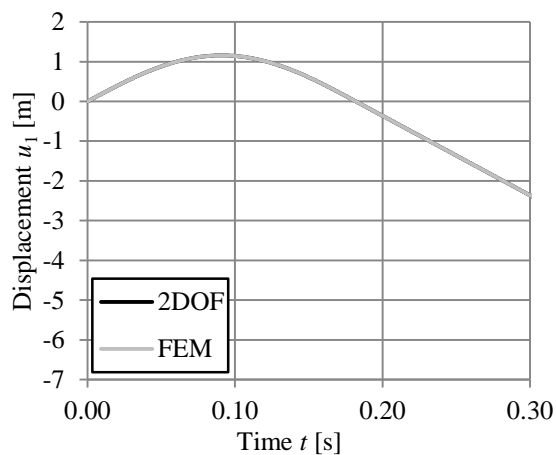
e) u_1, $\alpha = 0.1$

Figure F.1   Comparison of response in displacement u_1 over time between 2DOF and FEM, for five different positions of loading and with property set 1.
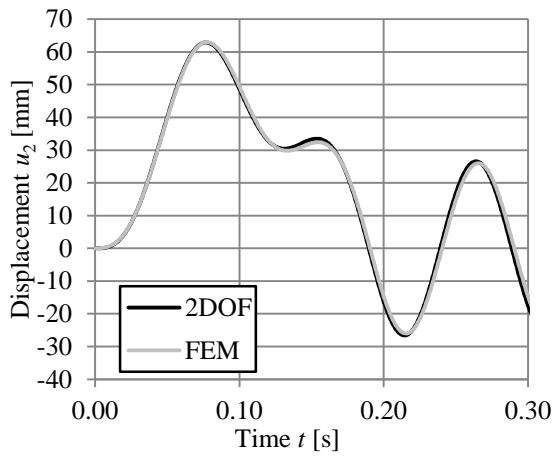
a) u_2, $\alpha = 0.5$
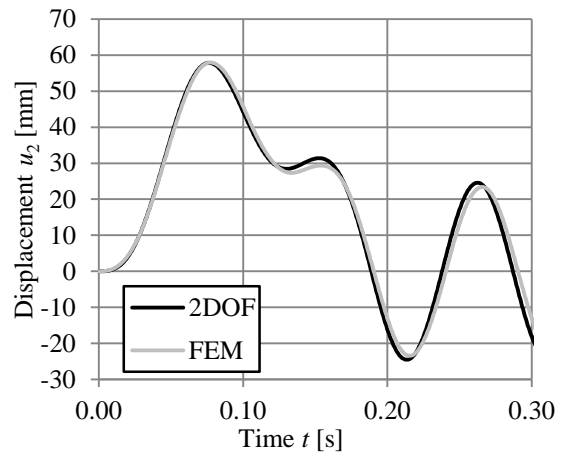
b) u_2, $\alpha = 0.4$
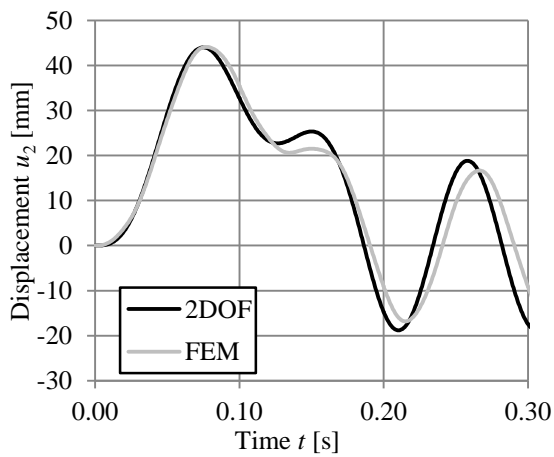
c) u_2, $\alpha = 0.3$
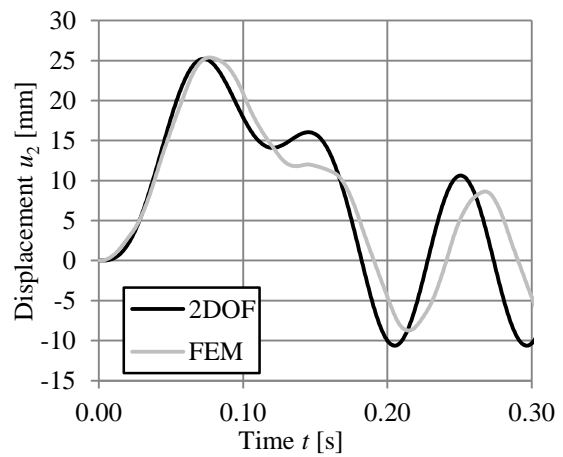
d) u_2, $\alpha = 0.2$
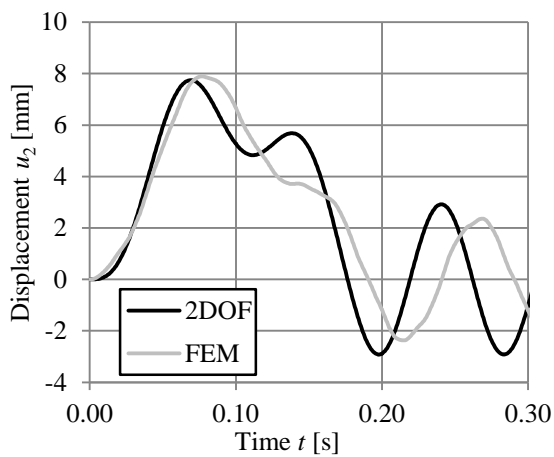
e) u_2, $\alpha = 0.1$

Figure F.2   Comparison of response in displacement u_2 over time between 2DOF and FEM, for five different positions of loading and with property set 1.
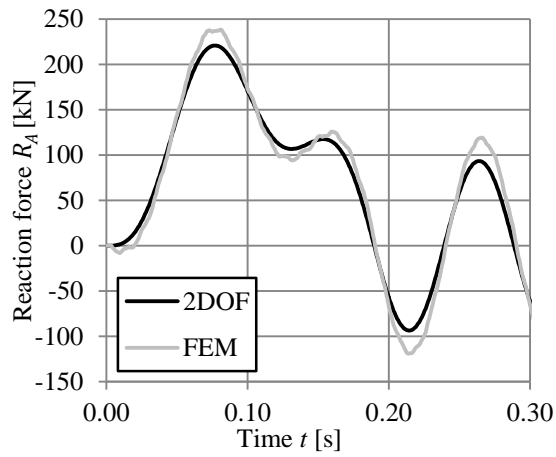
a) R_A, $\alpha = 0.5$
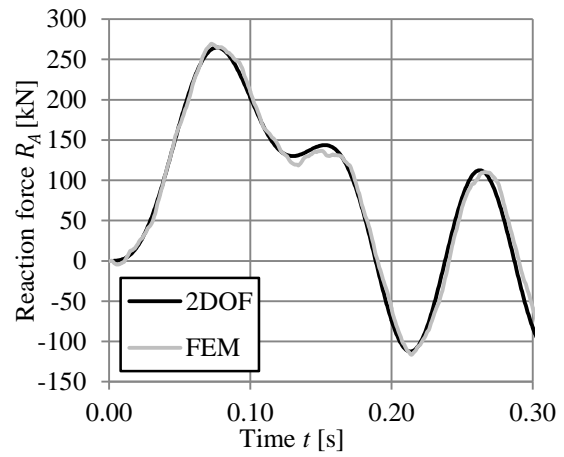
b) R_A, $\alpha = 0.4$
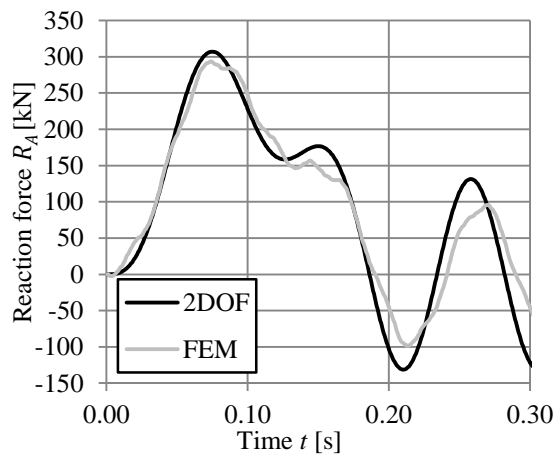
c) R_A, $\alpha = 0.3$
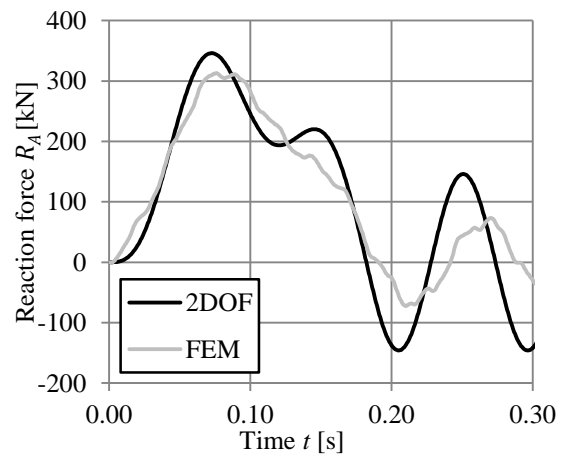
d) R_A, $\alpha = 0.2$
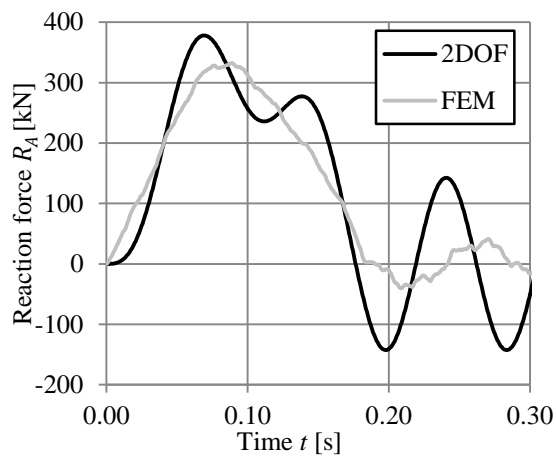
e) R_A, $\alpha = 0.1$

Figure F.3   Comparison of response in support reaction force R_A over time between 2DOF and FEM, for five different positions of loading and with property set 1.

a) M_α, $\alpha = 0.5$

b) M_α, $\alpha = 0.4$

c) M_α, $\alpha = 0.3$

d) M_α, $\alpha = 0.2$
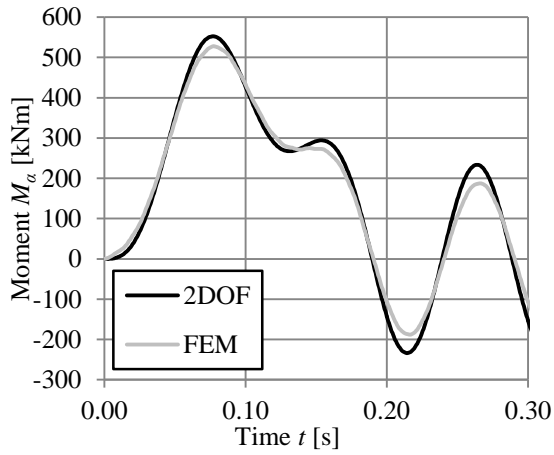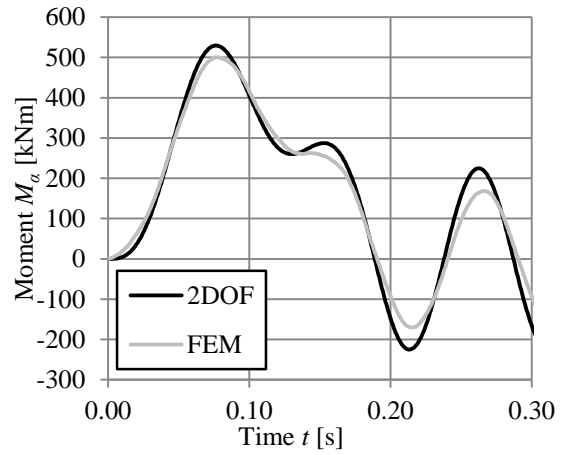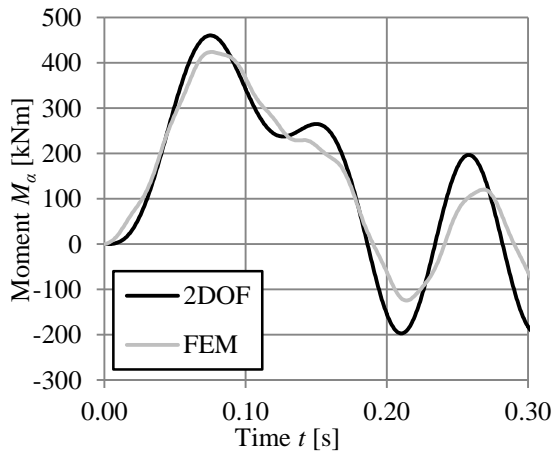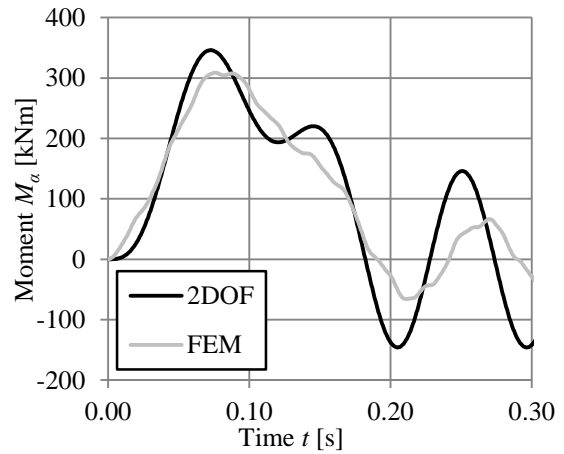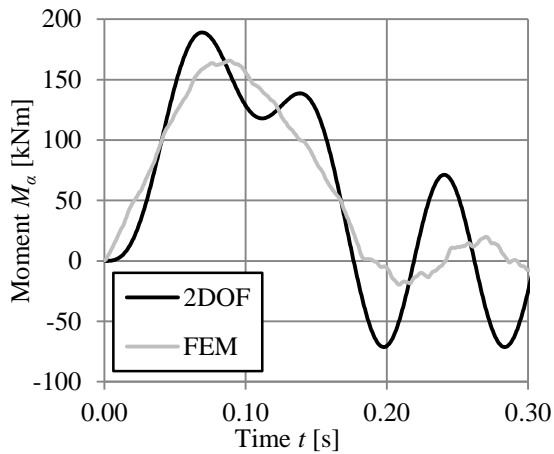
e) M_α, $\alpha = 0.1$

Figure F.4   *Comparison of response in moment M_α over time between 2DOF and FEM, for five different positions of loading and with property set 1.*
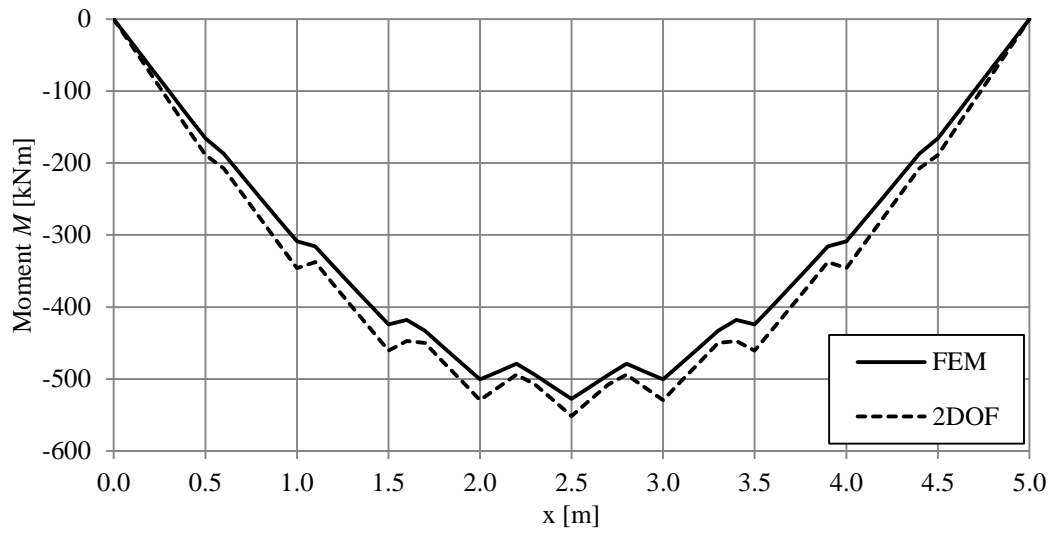
a) Moment Envelope
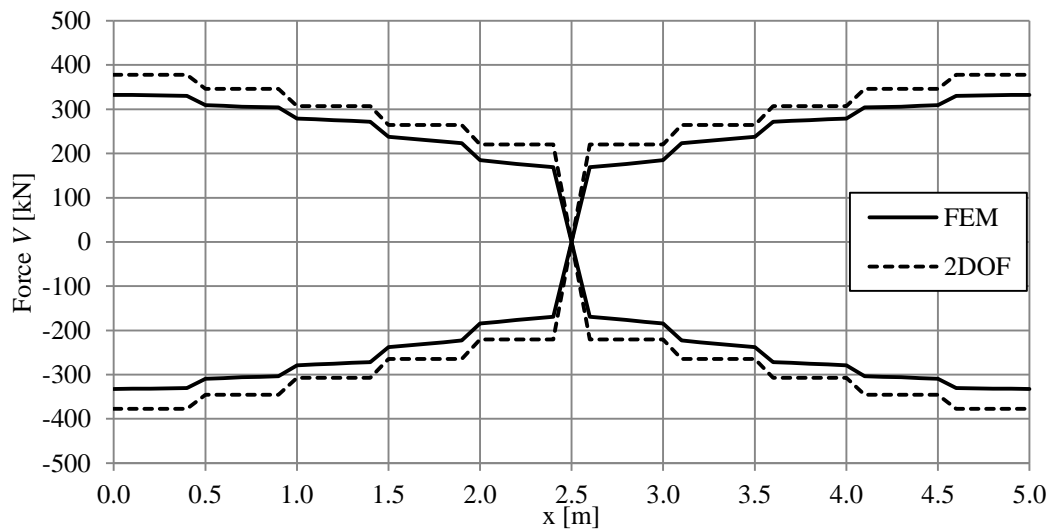
b) Shear Envelope

Figure F.5   Moment and shear envelope for property set 1

CHALMERS, *Civil and Environmental Engineering*, Master's Thesis 2014:80

F.2 Softer beam – Property set 4
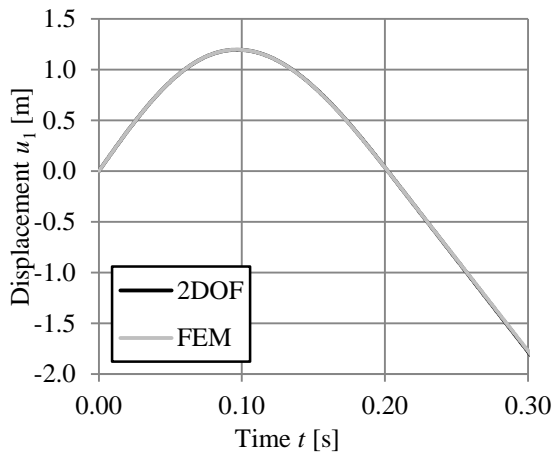
a) u_1, $\alpha = 0.5$
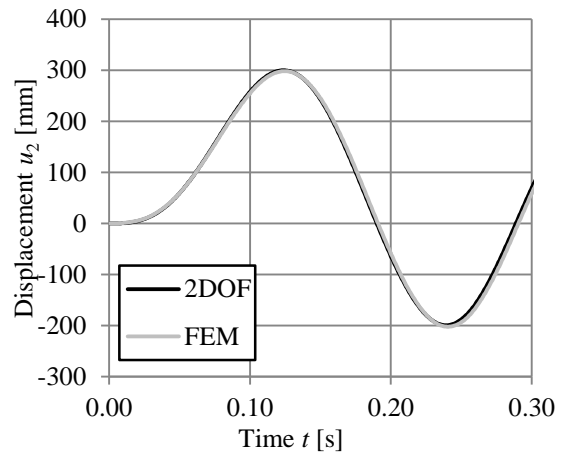
b) u_2, $\alpha = 0.5$
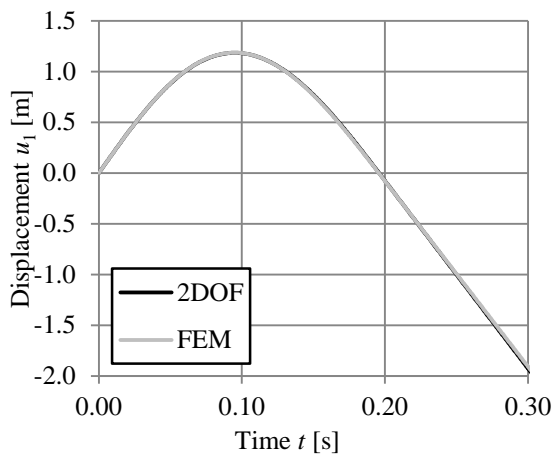
c) u_1, $\alpha = 0.3$
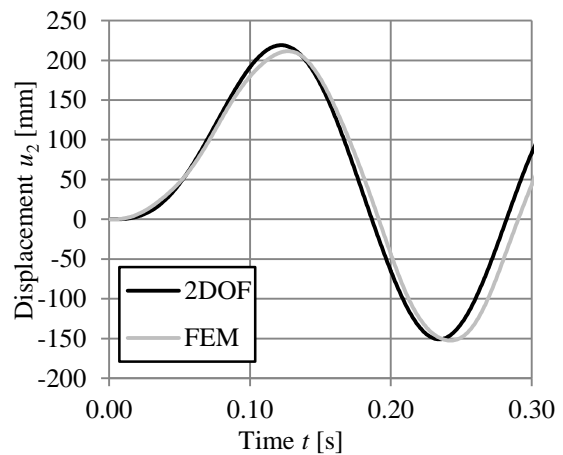
d) u_2, $\alpha = 0.3$
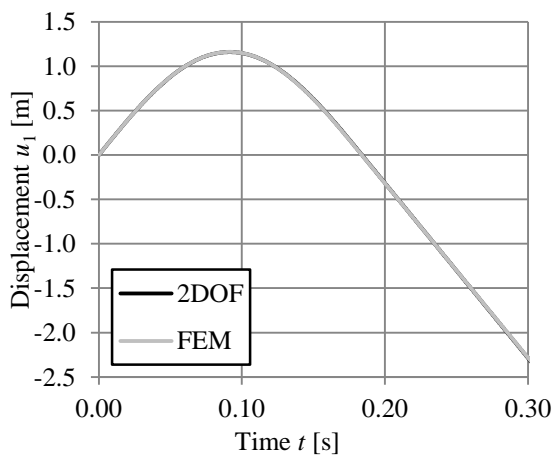
e) u_1, $\alpha = 0.1$
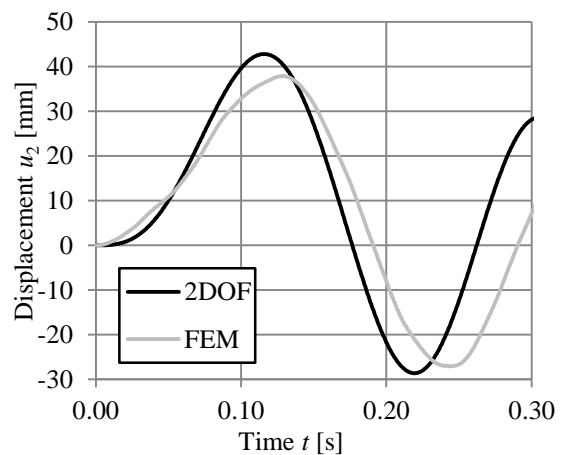
f) u_2, $\alpha = 0.1$

Figure F.6 Comparison of response in displacement u_1 and u_2 over time between 2DOF and FEM, for three different positions of loading and with property set 4.

a) R_A, $\alpha = 0.5$

b) M_α, $\alpha = 0.5$

c) R_A, $\alpha = 0.3$

d) M_α, $\alpha = 0.3$
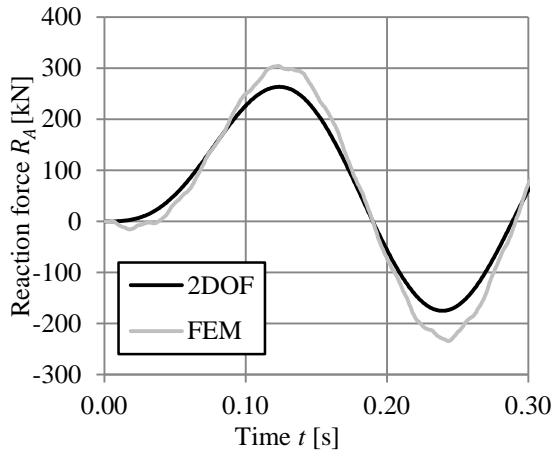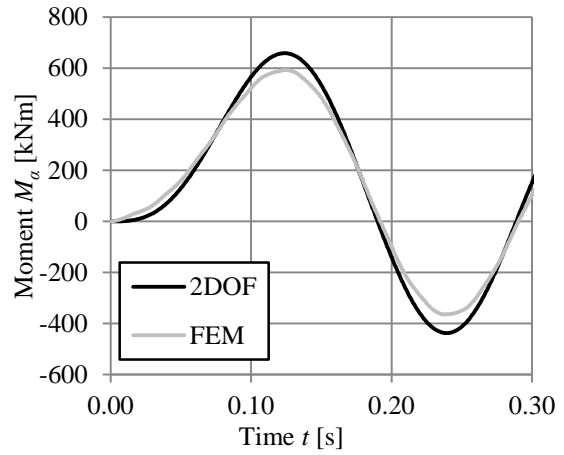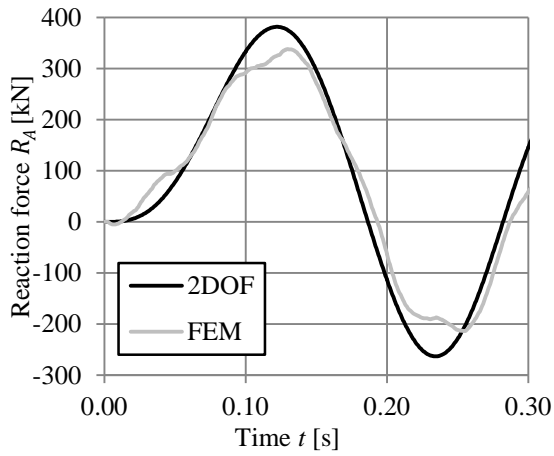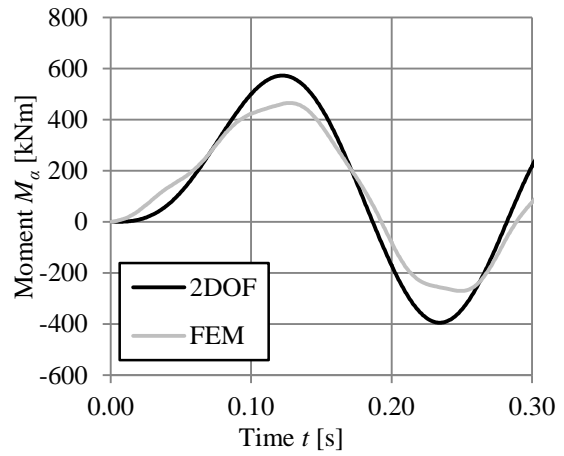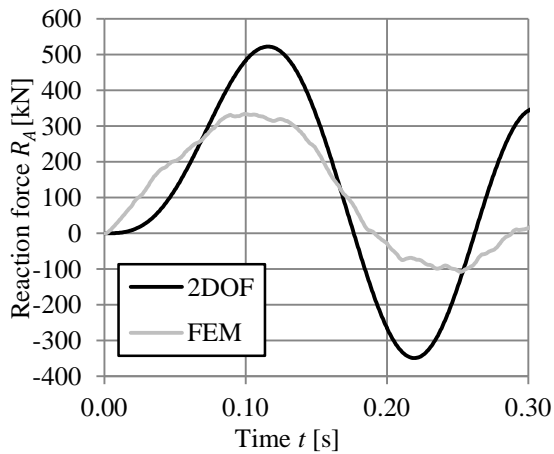
e) R_A, $\alpha = 0.1$
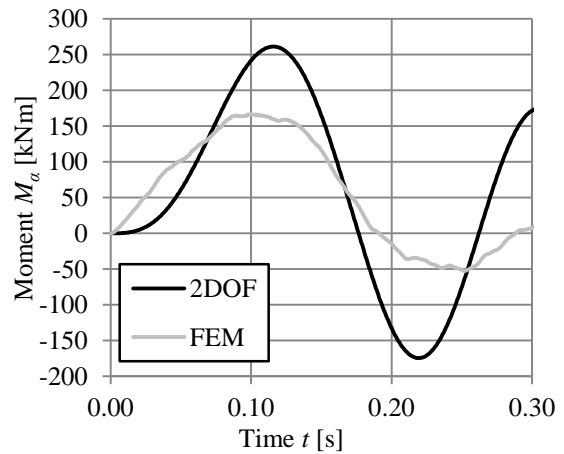
f) M_α, $\alpha = 0.1$

Figure F.7   *Comparison of response in support reaction force R_A and moment M_α over time between 2DOF and FEM, for three different positions of loading and with property set 4.*
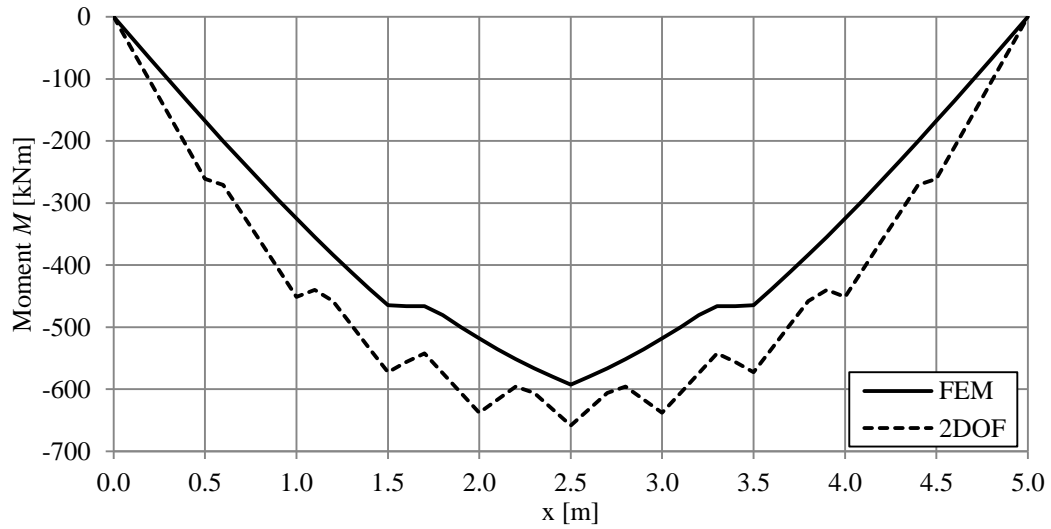
a) Moment Envelope
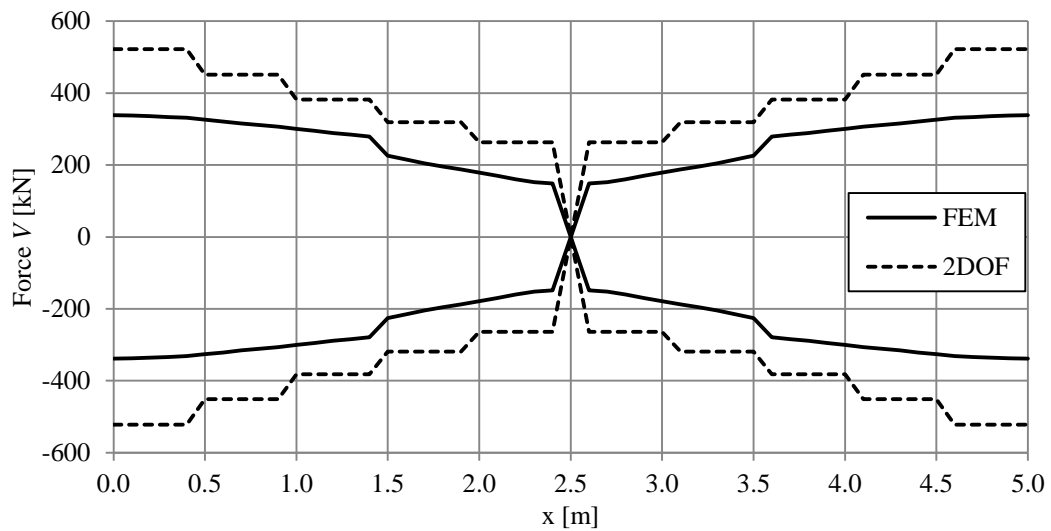
b) Shear Envelope

Figure F.8   Moment and shear envelope for property set 4.

F.3 Stiffer beam – Property set 5

a) u_1, $\alpha = 0.5$

b) u_2, $\alpha = 0.5$

c) u_1, $\alpha = 0.3$

d) u_2, $\alpha = 0.3$

e) u_1, $\alpha = 0.1$

f) u_2, $\alpha = 0.1$
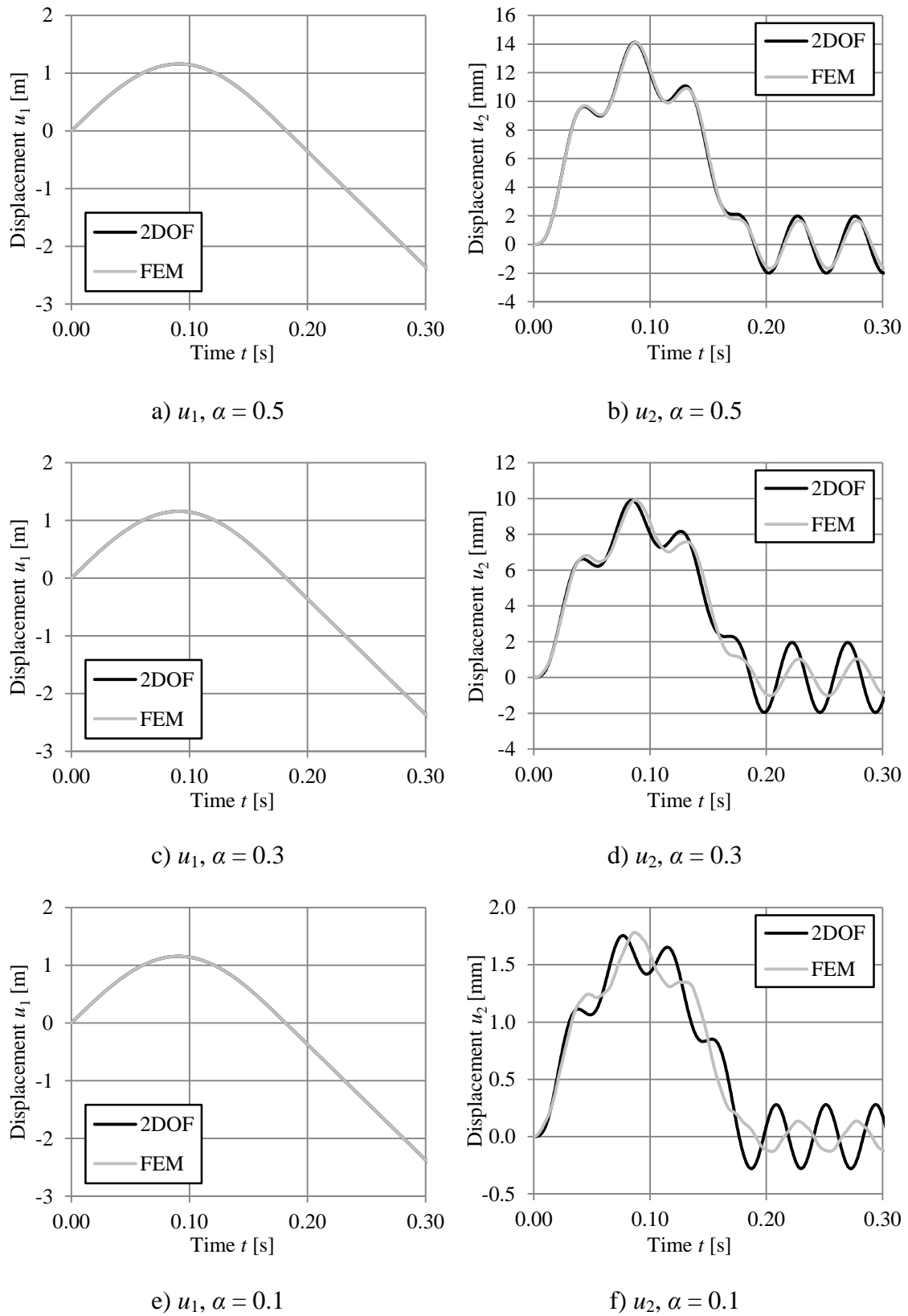
Figure F.9   Comparison of response in displacement u_1 and u_2 over time between 2DOF and FEM, for three different positions of loading and with property set 5.

CHALMERS, *Civil and Environmental Engineering*, Master's Thesis 2014:80

a) R_A, $\alpha = 0.5$

b) M_α, $\alpha = 0.5$

c) R_A, $\alpha = 0.3$

d) M_α, $\alpha = 0.3$
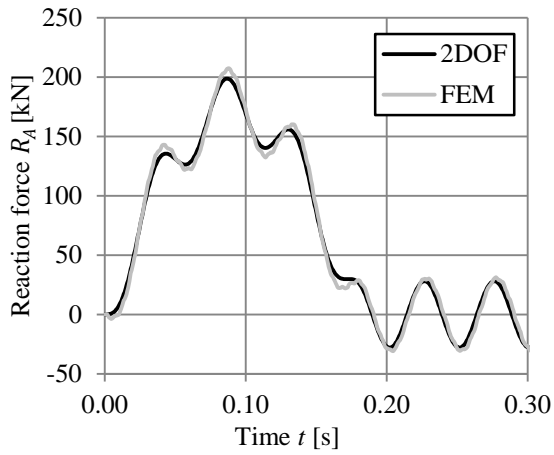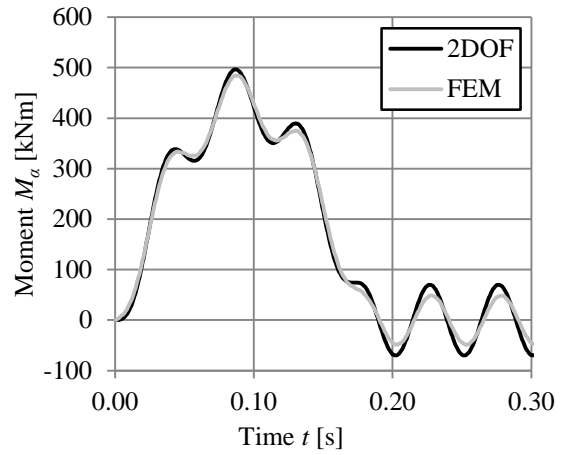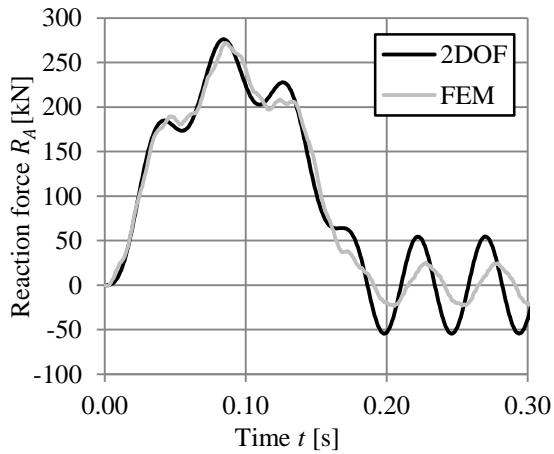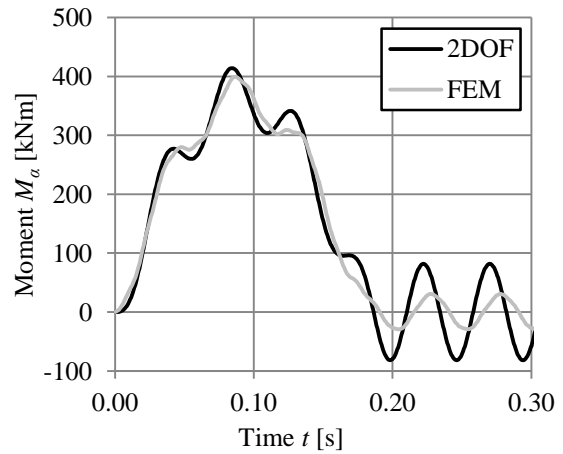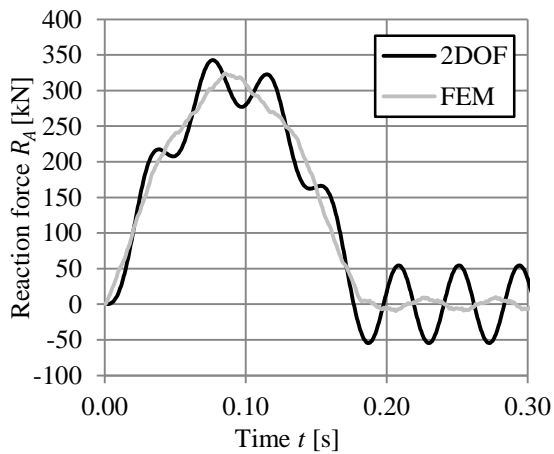
e) R_A, $\alpha = 0.1$
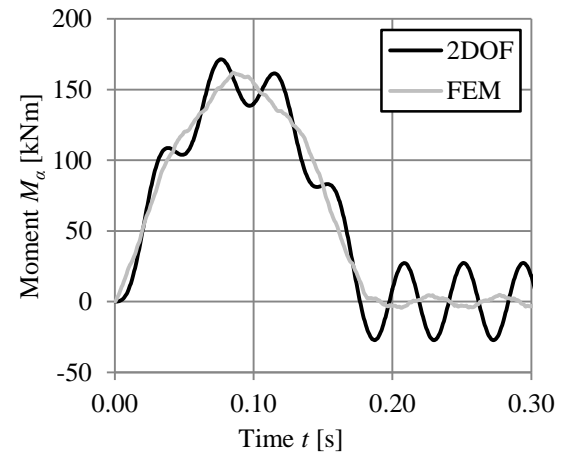
f) M_α, $\alpha = 0.1$

Figure F.10   Comparison of response in support reaction force R_A and moment M_α over time between 2DOF and FEM, for three different positions of loading and with property set 5.
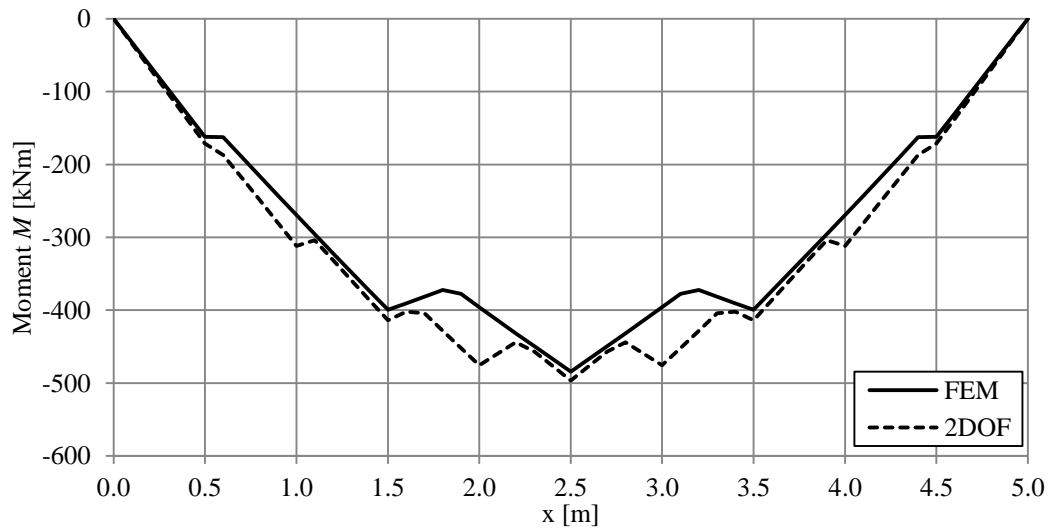
a) Moment Envelope
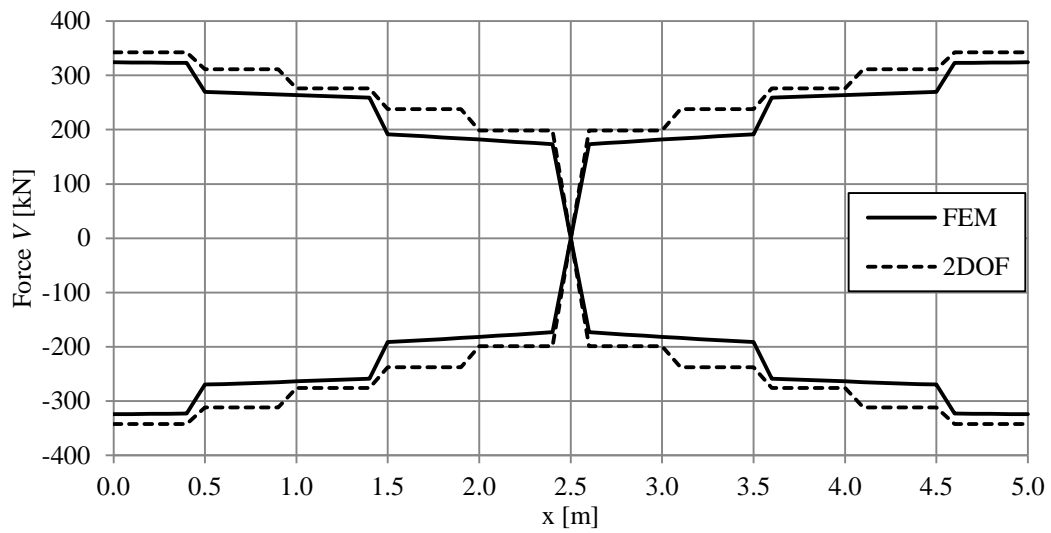
b) Shear Envelope

Figure F.11   Moment and shear envelope for property set 5.

CHALMERS, *Civil and Environmental Engineering*, Master's Thesis 2014:80

F.4 Softer colliding object – Property set 2

a) u_1, $\alpha = 0.5$

b) u_2, $\alpha = 0.5$

c) u_1, $\alpha = 0.3$

d) u_2, $\alpha = 0.3$

e) u_1, $\alpha = 0.1$

f) u_2, $\alpha = 0.1$
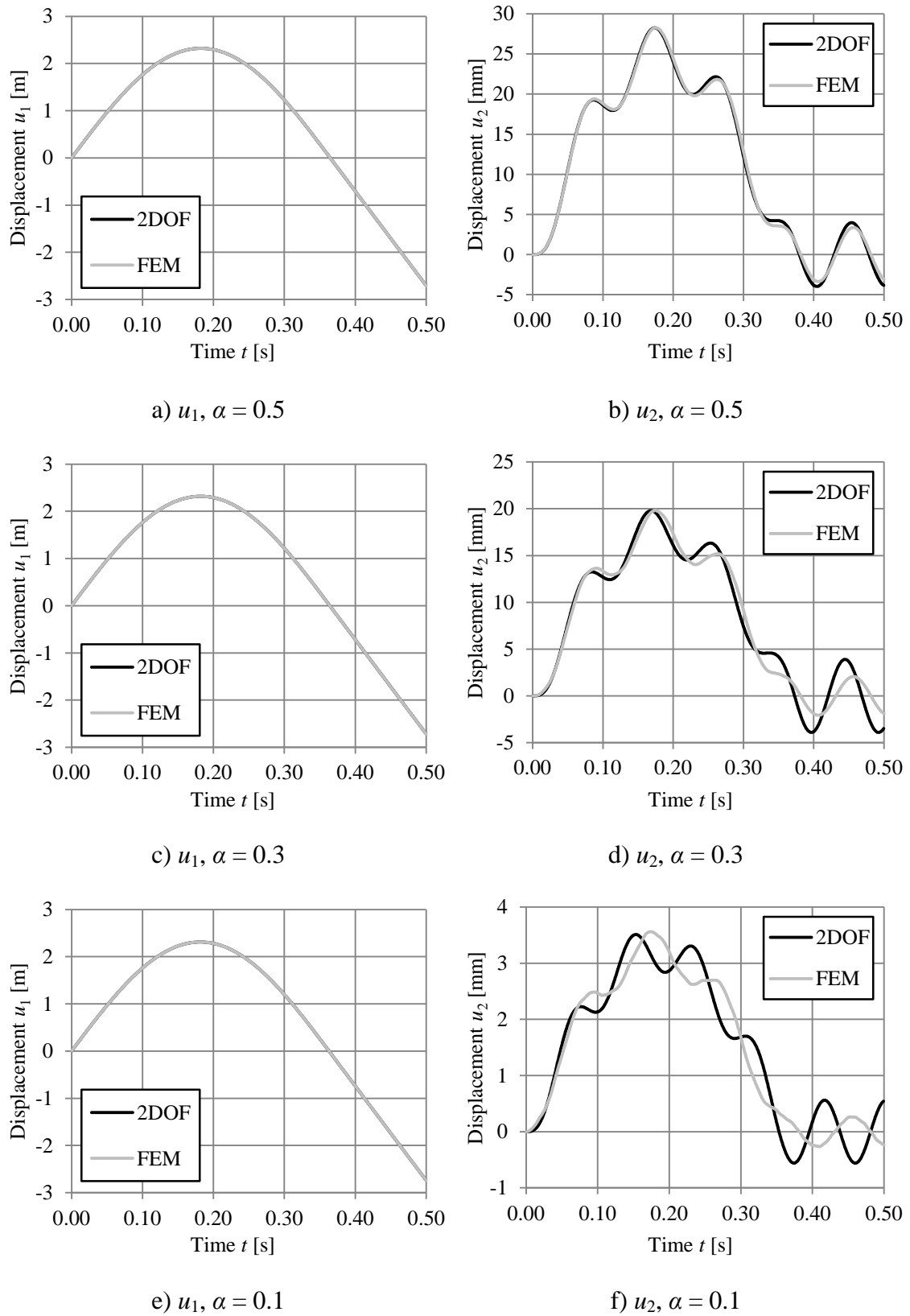
Figure F.12   Comparison of response in displacement u_1 and u_2 over time between 2DOF and FEM, for three different positions of loading and with property set 2.

a) R_A, $\alpha = 0.5$

b) M_α, $\alpha = 0.5$

c) R_A, $\alpha = 0.3$

d) M_α, $\alpha = 0.3$
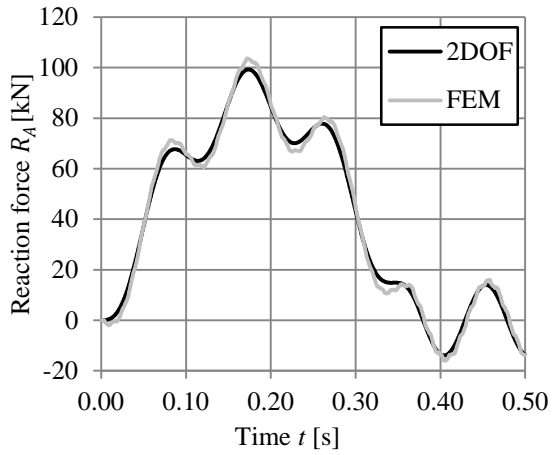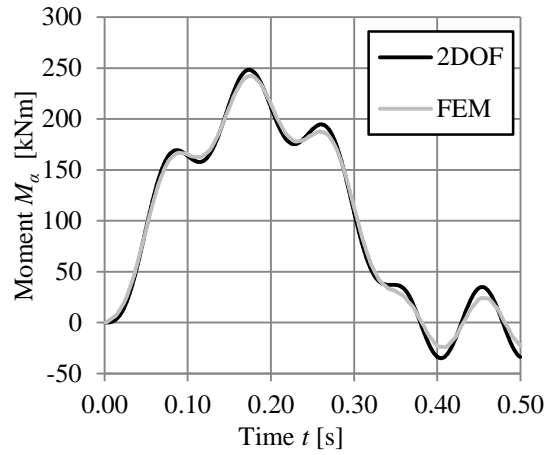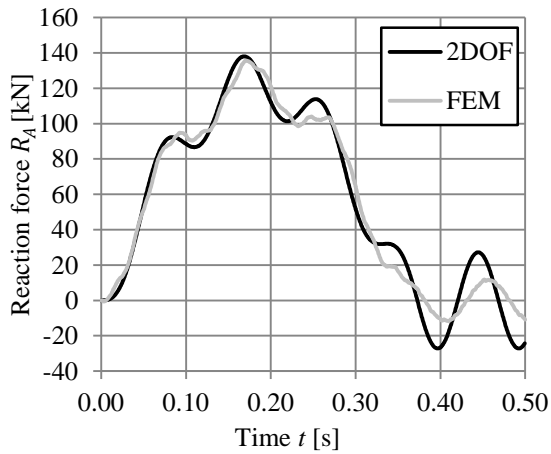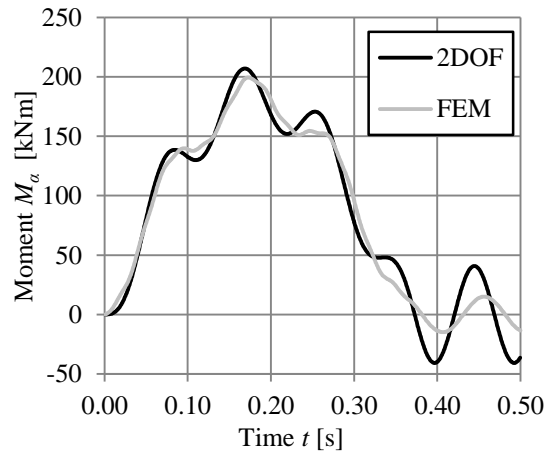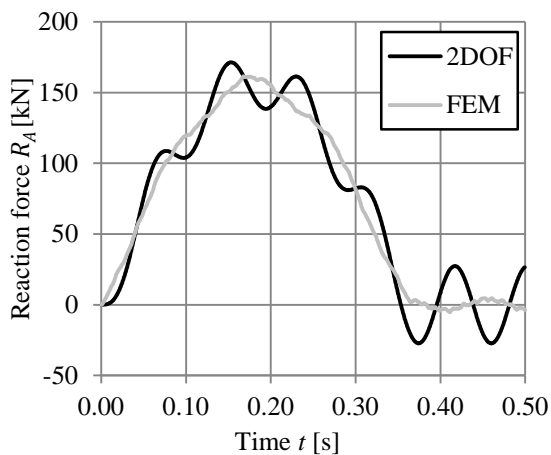
e) R_A, $\alpha = 0.1$
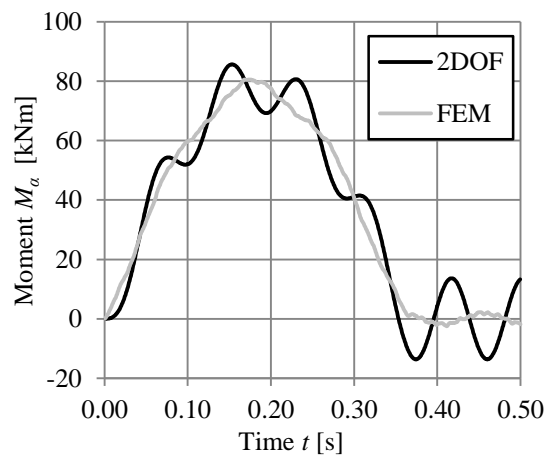
f) M_α, $\alpha = 0.1$

Figure F.13   Comparison of response in support reaction force R_A and moment M_α over time between 2DOF and FEM, for three different positions of loading and with property set 2.
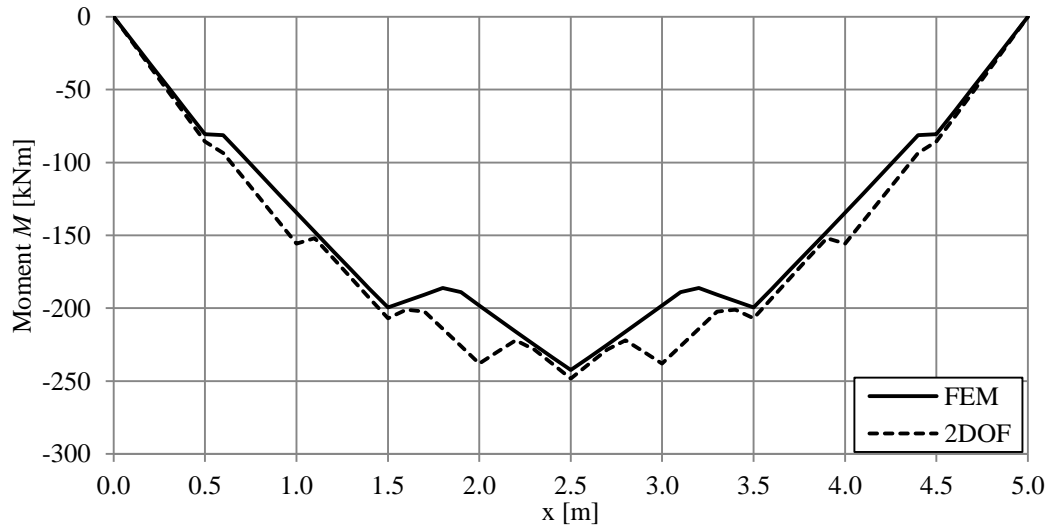
a) Moment Envelope
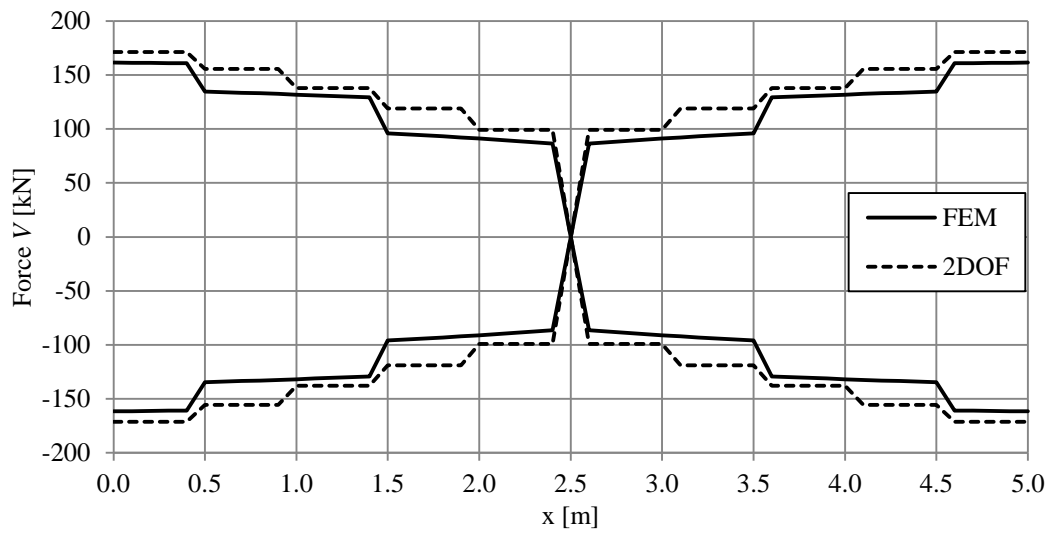
b) Shear Envelope

Figure F.14   Moment and shear envelope for property set 2.

F.5 Stiffer colliding object – Property set 3
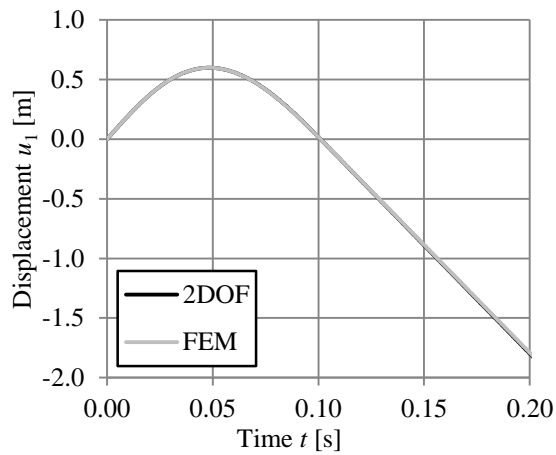
a) u_1, $\alpha = 0.5$
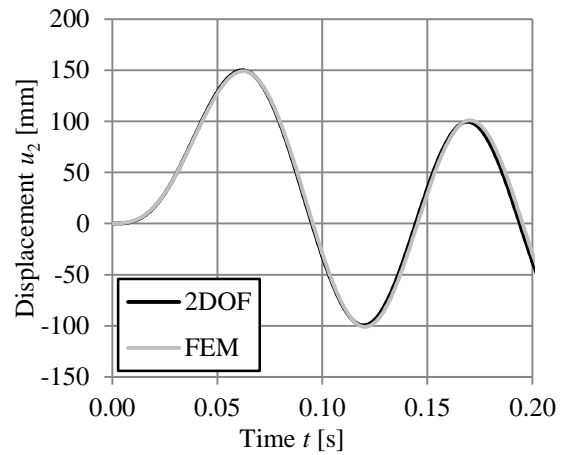
b) u_2, $\alpha = 0.5$
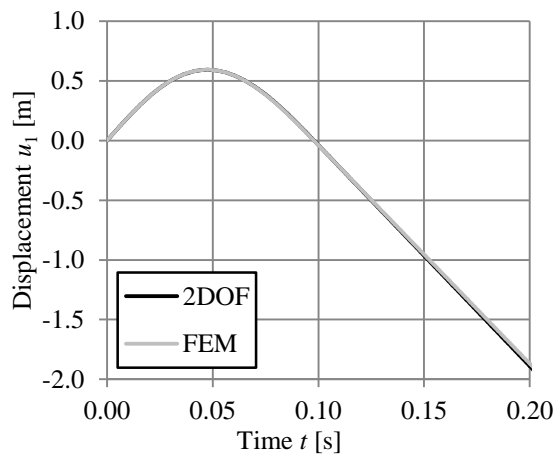
c) u_1, $\alpha = 0.3$
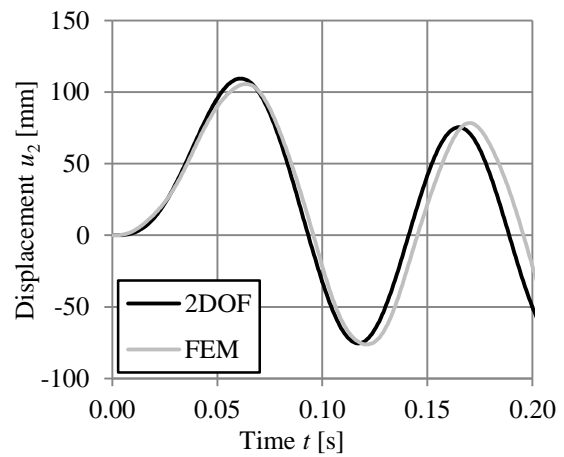
d) u_2, $\alpha = 0.3$
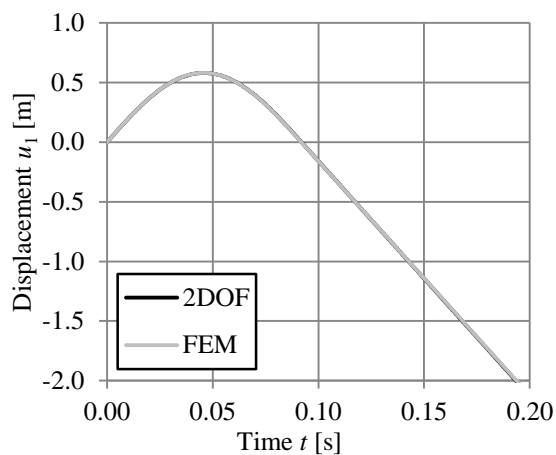
e) u_1, $\alpha = 0.1$
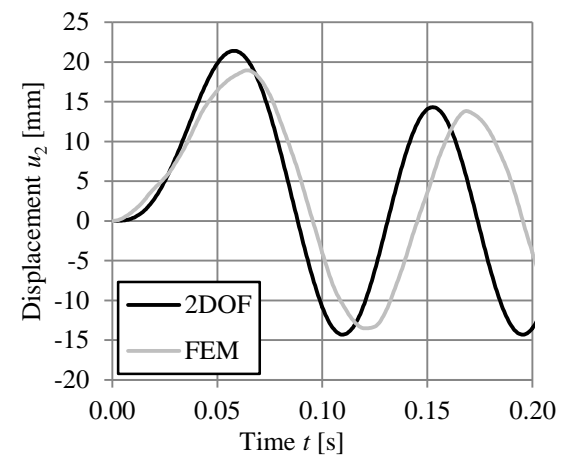
f) u_2, $\alpha = 0.1$

Figure F.15   *Comparison of response in displacement u_1 and u_2 over time between 2DOF and FEM, for three different positions of loading and with property set 3.*

a) R_A, $\alpha = 0.5$

b) M_α, $\alpha = 0.5$

c) R_A, $\alpha = 0.3$

d) M_α, $\alpha = 0.3$
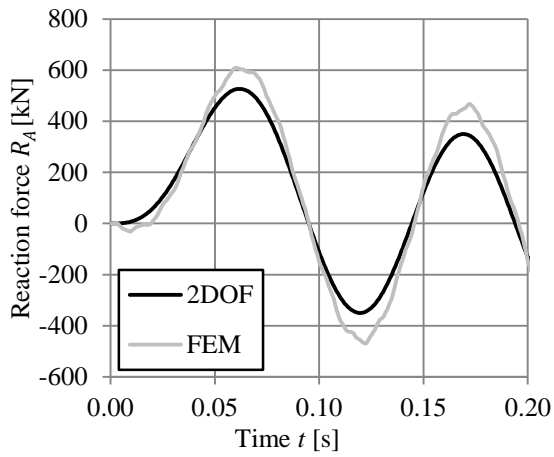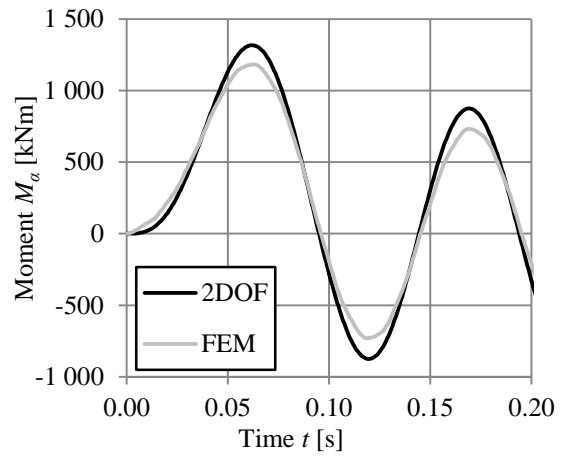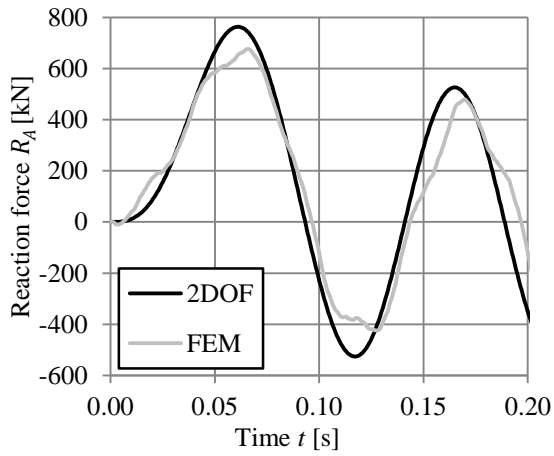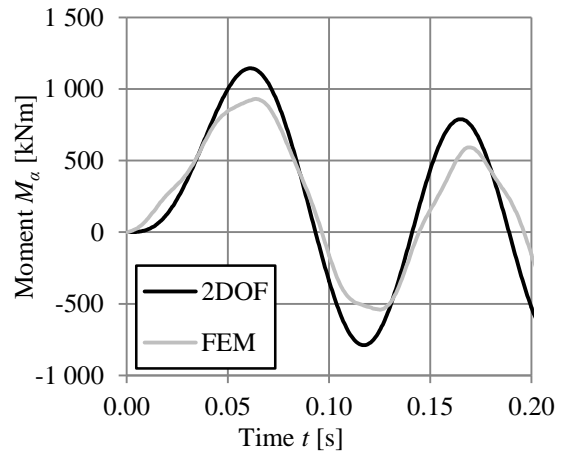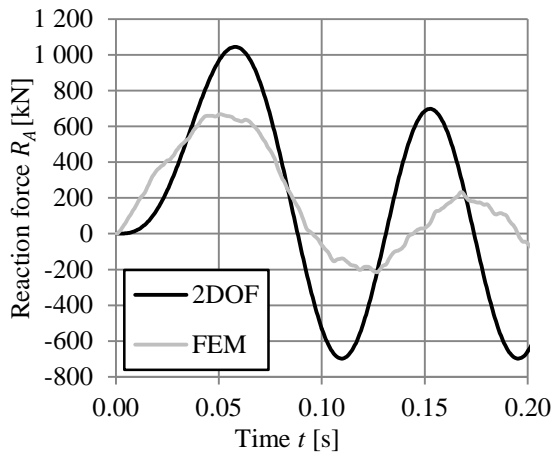
e) R_A, $\alpha = 0.1$
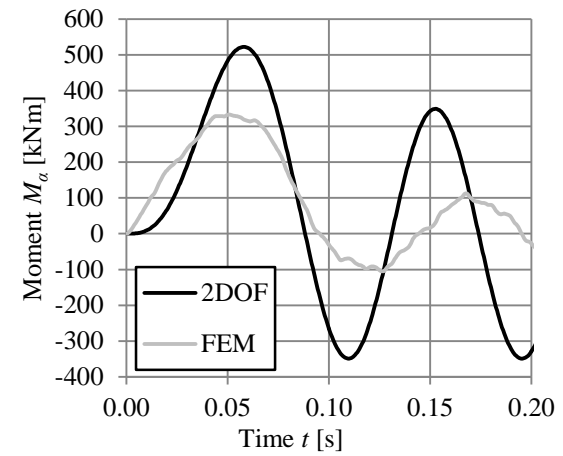
f) M_α, $\alpha = 0.1$

Figure F.16 *Comparison of response in support reaction force R_A and moment M_α over time between 2DOF and FEM, for three different positions of loading and with property set 3.*
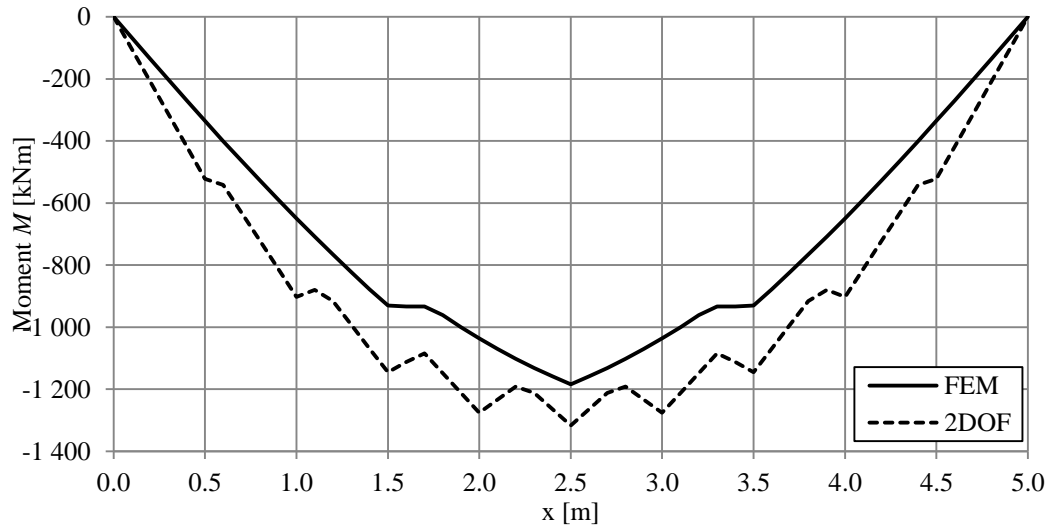
a) Moment Envelope
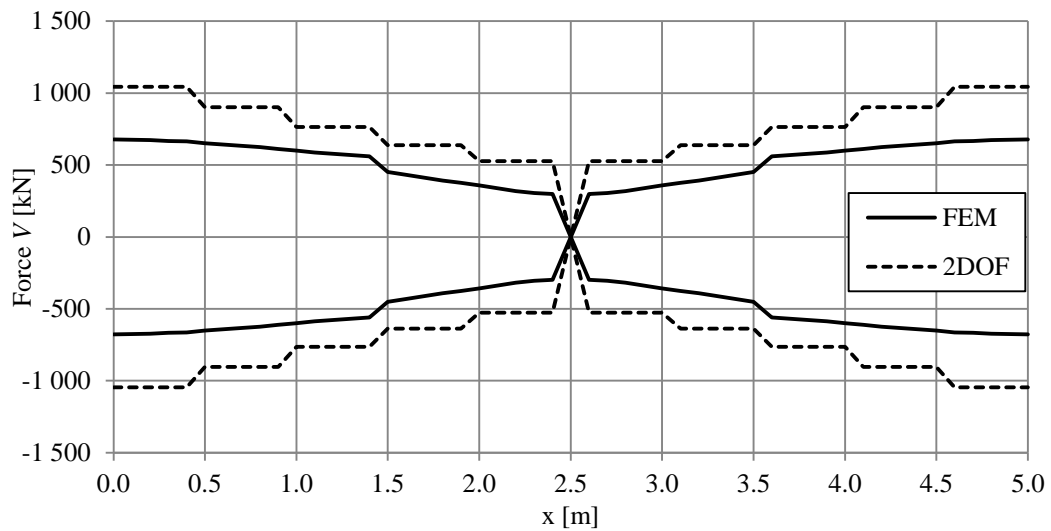
b) Shear Envelope

Figure F.17   Moment and shear envelope for property set 3.

CHALMERS, *Civil and Environmental Engineering*, Master's Thesis 2014:80

Appendix G   MathCad calculations

G.1   Beam transformation factors and stiffness

Transformation factors:

$\alpha := 0.5 \qquad \beta := 1 - \alpha = 0.5 \qquad\qquad \dfrac{3}{\alpha^2 \cdot \beta^2} = 48$

Point load:

$$\kappa_{m.pl} := \frac{1}{3} \cdot \alpha + \frac{1}{(\beta)^2} \cdot \left(\frac{1}{3} - \alpha + \alpha^2 - \frac{\alpha^3}{3} \right) = 0.333333$$

$$\kappa_{m.el} := \frac{\alpha^3}{28 \cdot \beta^2} + \frac{\left(23 \cdot \alpha^2 + 10 \cdot \alpha + 2\right) \cdot \beta}{105 \cdot \alpha^2} + \frac{\beta^2 - 2}{12 \cdot \alpha} - \frac{\alpha}{10 \cdot \beta^2} + \frac{1}{12 \cdot \alpha \cdot \beta^2} + \frac{\alpha}{10} = 0.485714$$

Stiffness of a beam:

$E_c := 30 GPa \qquad E_s := 200 GPa \qquad w_b := 1m \qquad h_b := 0.3m \qquad \alpha_s := \dfrac{E_s}{E_c} = 6.666667$

$s_{rebars} := 0.10m \qquad\qquad \phi := 16mm \qquad A_\phi := \dfrac{\pi \cdot \phi^2}{4} \qquad A_s := \dfrac{A_\phi}{s_{rebars}} \cdot w_b$

$c := 40mm \qquad d := h_b - c - \dfrac{\phi}{2} = 0.252m \qquad d' := h_b - d = 0.048m$

$x := 60.35mm \quad$ (guess) $\qquad x_{cc} := \dfrac{x}{3} = 0.020117m$

$A_{cc} := w_b \cdot x$

$A_{II} := A_{cc} + \left(\alpha_s - 1\right) \cdot A_s + \alpha_s \cdot A_s$

$$x_{II} := \frac{A_{cc} \cdot x_{cc} + \left(\alpha_s - 1\right) \cdot A_s \cdot d' + \alpha_s \cdot A_s \cdot d}{A_{II}} = 60.351289mm$$

$$I_{II} := \frac{w_b \cdot x^3}{12} + A_{cc} \cdot \left(x - x_{cc}\right)^2 + \left(\alpha_s - 1\right) \cdot A_s \cdot (x - d')^2 + \alpha_s \cdot A_s \cdot (d - x)^2 = 6.100744 \times 10^8 \cdot mm^4$$

$$I_I := \frac{w_b \cdot h_b^3}{12} = 2.25 \times 10^9 \cdot mm^4$$

$EI_b := E_c \cdot I_{II} = 1.830223 \times 10^7 \cdot N \cdot m^2 \qquad\qquad l := 5m$

$$k_b := \frac{3 \cdot EI_b}{l^3 \cdot \alpha^2 \cdot \beta^2} = 7.028057 \times 10^3 \cdot \frac{kN}{m}$$

ADINA indata:

Equivalent Youngs modulus:

$$E_{II} := \frac{I_{II}}{I_I} \cdot E_c = 8.134325 \, GPa$$

stiffer with a factor 4:

$$E_{4x} := E_{II} \cdot 4 = 32.537299 \, GPa$$

$$k_{b.4x} := \frac{3 \cdot E_{4x} \cdot I_I}{l^3 \cdot \alpha^2 \cdot \beta^2} = 2.811223 \times 10^4 \cdot \frac{kN}{m}$$

$$E_{4x} \cdot I_I = 7.320892 \times 10^7 \cdot N \cdot m^2$$

weaker with a factor 4:

$$E_{0.25x} := \frac{E_{II}}{4} = 2.033581 \, GPa$$

$$k_{b.0.25x} := \frac{3 \cdot E_{0.25x} \cdot I_I}{l^3 \cdot \alpha^2 \cdot \beta^2} = 1.757014 \times 10^3 \cdot \frac{kN}{m}$$

$$E_{0.25x} \cdot I_I = 4.575558 \times 10^6 \cdot N \cdot m^2$$

2DOF vs FEM comparison:

$$k_1 := 1 \cdot 300 \frac{kN}{m}$$

$$k_b = 7.028057 \times 10^3 \cdot \frac{kN}{m}$$

$$k_{use} := k_b \cdot \frac{1}{1} = 7.028057 \frac{MN}{m}$$

$$m_1 := 1000 \, kg$$

$$m_b := 3600 \, kg \qquad m_2 := \kappa_{m.el} m_b = 1.748571 \times 10^3 \, kg$$

$$f_1 := \frac{1}{2\pi} \sqrt{\frac{k_1}{m_1}} = 2.756644 \frac{1}{s} \qquad f_2 := \frac{1}{2 \cdot \pi} \sqrt{\frac{k_{use}}{m_2}} = 10.090114 \frac{1}{s}$$

$$\frac{f_1}{f_2} = 0.273203$$

Comparison of deflection with characteristic impulse and elastic respons

$$v_0 := 20 \frac{m}{s} \qquad I_k := 2m_1 \cdot v_0 = 40 \cdot kN \cdot s$$

$$u_2 := \frac{I_k}{\sqrt{m_2 \cdot k_{use}}} = 360.828372 \, mm$$

theoretical value of the beam deflection

$$F_{sta} := k_{use} \cdot u_2 = 2.535922 \times 10^3 \cdot kN$$

$$R_A := F_{sta} \cdot \beta = 1.267961 \times 10^3 \cdot kN$$

Appendix H   MATLAB algorithms

H.1   2DOF system - main algorithm

```
%---------------------- 2-DOF SYSTEM --------------------------

% A program that calculates the response of a 2-DOF system
containing

% 2 masses and 2 springs connected to a fixed support. This
system

% represents a collision between two bodies and works for both
plastic

% and elastic response plus a bilinear material relationship with
linear

% plastic behaviour.

%

% Developed for the Master's Thesis "Design with regard to
collision impact"

% by Erik Asplund and Daniel Steckmest

%

% Last modified: 2014-05-26

%--------------------------------------------------------------

%--------------------------------------------------------------

clear all

close all

clc

%%-------------------------------------------------------------

%--------------INDATA------------------------------------------

m1=1500;       %Mass of body 1 [kg]

m2=10092;      %Mass of body 2 [kg]


k1=300e3;      %Stiffness of spring 1 [N/m]

k1_2=4*k1;        %Stiffness of second stiffer part of spring 1
response

k2=10e6;       %Stiffness of spring 2 [N/m]


R1=400e100;    %Load capacity of body 1 [N]

R2=400e100;    %Load capacity of body 2 [N]


v0=[25;0];         %Initial velocity of body 1 and 2 [m/s]

U_Rd=[1e100 1e100]; %Ultimate plastic deformation [m]

u_stiffness=0.5;      %After what displ. the change in stiffness
occurs [m]

%-------------Beam Parameters----------------------------------

%position of impact load

alpha=0.5;

beta=1-alpha;


%mass

h=0.3;          %Height of beam [m]

w=1;            %Width of beam  [m]

l=5;            %Lenght of beam [m]

rho=2400;       %Density of beam [kg/m^3]

m_beam=h*w*l*rho;   %Mass of beam [kg]


%beam stiffness

EI_b=1.830223e7;    %bending stiffness of beam

EI_b=(1/64)*EI_b;
```

```
k2=3*EI_b/(l^3*alpha^2*beta^2);  %Beam stiffness used in 2DOF


%transformation factor from beam to 2DOF

kappa_m_el=alpha^3/(28*beta^2)+(23*alpha^2+10*alpha+2)*beta/(105*
alpha^2)...

    +(beta^2-2)/(12*alpha)-
alpha/(10*beta^2)+1/(12*alpha*beta^2)+alpha/10;


%transformed mass used in 2DOF

m2=kappa_m_el*m_beam;

%--------------------------------------------------------------


% Mass matrix

M=[m1 0;

    0 m2];


% Stiffness matrix

K=[k1 -k1;

   -k1  k1+k2];


K_el=[k1 k2 k1_2];             %elastic stiffnesses

U_el=[R1/k1 R2/k2 u_stiffness]; %maximum elastic displacement


%Calculating the eigenvalues and eigenvectors using a direct

%eigenvalue solver

[Lambda, Egv]=eigen(K,M);


%--- Central difference method --------------------------

%Following the algorithm presented in Craig Jr, Kurdila (2006)


%Initial conditions

u0=zeros(length(K),1);  %Displacement

a0=zeros(length(K),1);  %Acceleration

p0=zeros(length(K),1);  %External force


%Calculating the time step

%h_crit=2/max(sqrt(Lambda));     %critical time step

% h=0.01*h_crit;                  %decreased time step, increased
precision

% t_analysis=0.6;               %time period for analysis [s]

% n=ceil(t_analysis/h);         %number of iterations

n=1000;    %using a predefined number of steps

h=0.0005;   %using a predefined time step


%Starting values

u_n_minus1=u0-h*v0+(h^2/2)*a0;

p_n=p0;


%Predefining

u=zeros(length(K),n);        %Displacement

v=zeros(length(K),n);        %Velocity

a=zeros(length(K),n);        %Acceleration
```

```
U_pl=zeros(length(K),n);    %Plastic deformation

R=zeros(length(K),n);       %Reaction forces

du=zeros(1,n);              %Deformation of spring 1

k=zeros(2,n);              %stiffness vector

Wi=zeros(length(K),n);      %Internal work

We=zeros(length(K),n);      %External work

Ek=zeros(length(K),n);      %Kinetic energy

Im=zeros(length(K),n);      %Impulse of mass

I_R=zeros(length(K),n);     %Impulse of reaction force

R_biggs=zeros(n,1);

kkk=zeros(1,n);



for i=1:n

    %Since an elasto-plastic material model is used the stiffness
matrix,

    %K, is updated in each iteration. Also the reaction forces
are

    %calculated.

    [U_pl,        R,        du,        K,        k1,
k2,kkk]=Rforce(u,du,i,U_el,U_pl,U_Rd,K_el,R,kkk);


    k(:,i)=[k1;k2]; %stiffness vector


    %Right hand side terms of the iteration in central difference
method

    RHSn=p_n-(K-(2/(h^2))*M)*u(:,i)-((1/h^2)*M)*u_n_minus1;


    %Solves the displacement for the next timestep

    u(:,i+1)=((1/h^2)*M)\RHSn;


    %Calculating velocity and acceleration for each timestep

    if i==1

        v(:,i)=v0;

        a(:,i)=a0;

    else

        v(:,i)=(u(:,i+1)-u(:,i-1))/(2*h);

        a(:,i)=(u(:,i+1)-2*u(:,i)+u(:,i-1))/h^2;

    end


    %Calculating internal and external work, kinetic energies and
impulse

    if i==1 %Skips the first step

    else

    dWi(1)=(R(1,i)+R(1,i-1))/2*(u(1,i)-u(1,i-1));

    Wi(1,i)=Wi(1,i-1)+dWi(1);


    dWi(2)=(R(2,i)+R(2,i-1))/2*(u(2,i)-u(2,i-1));

    Wi(2,i)=Wi(2,i-1)+dWi(2);


    dWe(2)=(R(1,i)+R(1,i-1))/2*(u(2,i)-u(2,i-1));

    We(2,i)=We(2,i-1)+dWe(2);


    dI_R(1)=(R(1,i)+R(1,i-1))/2*h;

    I_R(1,i)=I_R(1,i-1)+dI_R(1);
```

```
    dI_R(2)=(R(2,i)+R(2,i-1))/2*h;

    I_R(2,i)=I_R(2,i-1)+dI_R(2);

    end


    Ek(:,i)=(M*v(:,i).^2)/2;

    Im(:,i)=M*v(:,i);


    %Reactionforce according to Biggs

    a_1=1.357;

    a_2=-0.457;

    R_biggs(i)=a_1*R(2,i)+a_2*R(1,i);


    %Updating the values

    u_n_minus1=u(:,i);

end


%---values for comparison with classic theory---

if v(1,n)>0

    Ek3=Ek(1,n)+Ek(2,n);

else

    Ek3=Ek(2,n);

end


E_k_ratio(1)=Ek3/Ek(1,1);

e=(v(2,n)-v(1,n))/v0(1);

------------------------------------------------


%Remove the last values in the displacement vector since not
needed

u(:,n+1)=[];

%%


%-------------------------------------------------------------
%Plotting the graphs
%-------------------------------------------------------------
t=linspace(0,h*n,n);  %Creates a time vector to be able to plot


figure(1)

plot(t,u(1,:),'m');

hold on

plot(t,u(2,:),'r--')

%plot(t,du)

title('Displacement for mass 1 and 2 ')

legend('Displacement    mass    1    ',    'Displacement    mass    2',
'Location','SouthWest')

xlabel('Time [s]')

ylabel('Displacement [m]')


figure(2)

plot(t,v(1,:),'m');

hold on

plot(t,v(2,:),'r--')

title('Velocity for mass 1 and 2 ')

legend('Velocity mass 1 ','Velocity mass 2')

xlabel('Time [s]')
```

```
ylabel('Velocity [m/s]')


figure(3)

plot(t,a(1,:),'m');

hold on

plot(t,a(2,:),'r--')

title('Acceleration for mass 1 and 2 ')

legend('Acceleration    mass    1    ','Acceleration    mass
2','Location','SouthEast')

xlabel('Time [s]')

ylabel('Acceleration [m/s^2]')


figure(4)

plot(t,k)

title('Change in stiffness ')

legend('k1 ','k2')

xlabel('Time [s]')

ylabel('Stiffness [N/m]')


figure(5)

plot(t,Wi(1,:),'m');

hold on

plot(t,We(1,:),'r')

plot(t,Ek(1,:),'b')

title('Work and kinetic energy mass 1 ')

legend('Internal work mass 1 ','External work mass 1'...

        ,'Kinetic energy mass 1','Location','NorthEast')

xlabel('Time [s]')

ylabel('Work, W [J]')


figure(6)

plot(t,Wi(2,:),'m');

hold on

plot(t,We(2,:),'r')

plot(t,Ek(2,:),'b')

title('Work and kinetic energy mass 2 ')

legend('Internal work mass 2 ','External work mass 2'...

      ,'Kinetic energy mass 2','Location','NorthEast')

xlabel('Time [s]')

ylabel('Work, W [J]')


figure(7)

plot(t,Im(1,:),'m');

hold on

plot(t,I_R(1,:),'r')

title('Impulse mass 1')

legend('Impulse of mass','Impulse of reaction force'...

      ,'Location','NorthEast')

xlabel('Time [s]')

ylabel('Work, W [J]')


figure(8)

plot(t,Im(2,:),'m');

hold on

plot(t,I_R(2,:),'r')
```

```
title('Impulse mass 2 ')

legend('Impulse of mass','Impulse of reaction force'...

      ,'Location','NorthEast')

xlabel('Time [s]')

ylabel('Work, W [J]')


figure(9)

plot(t,R(1,:),'m');

hold on

plot(t,R(2,:),'r')

plot(t,R_biggs,'b')

title('Load - Deformation curve ')

legend('R1','R2'...

      ,'Location','NorthEast')

xlabel('Time [s]')

ylabel('Load, [N]')


figure(10)

plot(du,R(1,:),'m');

hold on

plot(u(2,:),R(2,:),'r')

xlim([0 max(max(u))])

title('Load - Deformation curve ')

legend('R1','R2'...

      ,'Location','NorthEast')

xlabel('Deformation [m]')

ylabel('Load, [N]')

max(u(2,:))
```

H.2   2DOF system - function file

```
function[U_pl,R,du,K,k1,k2,kkk]=Rforce(u,du,i,U_el,U_pl,U_
Rd,K_el,R,kkk)

%--------------------------------------------------------
---------

% Function file that updates the stiffness matrix and the
reaction forces

% when using the central difference method to solve a 2-
DOF system using a

% elastic, plastic or elasto-plastic linear/bilinear
material model.

%

% Developed for the Master's Thesis "Design with regard to
collision impact"

% by Erik Asplund and Daniel Steckmest

%

% Last modified: 2014-05-26

%--------------------------------------------------------

%--------------------------------------------------------


du(i)=u(1,i)-u(2,i);


%------ONLY USE FOR LINEAR PLASTIC BEHAVIOUR-----

Q=0;

if i==1

elseif du(i)<max(du)

    du(i)=max(du);   %make sure the deformation stays at
the max value

    Q=1;

end

-----------------------------------------------


%calculate the additional plastic deformation

U_max=[max(du(1:i-1)) max(u(2,1:i-1))];

%for body 1

if du(i)>U_el(1) && du(i)>U_max(1)

    dU_pl(1)=du(i)-max(U_max(1),U_el(1));

else

    dU_pl(1)=0;

end

%for body 2

if u(2,i)>U_el(2) && u(2,i)>U_max(2)

    dU_pl(2)=u(2,i)-max(U_max(2),U_el(2));

else

    dU_pl(2)=0;

end


%calculation of plastic deformation

if i==1

else

    U_pl(:,i)=dU_pl'+U_pl(:,i-1);

end


%Calculation of reaction forces

%for body 1

if du(i)<0 || U_pl(1,i)>U_Rd(1) || Q==1

    R(1,i)=0;
```

```
elseif du(i)>U_el(3)

    %R(1,i)=max(0,K_el(3)*(du(i)-U_pl(1,i)));

    %R(1,i)=max(0,R(1,i-1)+K_el(3)*(du(i)-du(i-1)-
U_pl(1,i)));

    R(1,i)=max(0,U_el(3)*K_el(1)+K_el(3)*(du(i)-U_el(3)-
U_pl(1,i)));

    kkk(i)=1;

else

    R(1,i)=max(0,K_el(1)*(du(i)-U_pl(1,i)));

    kkk(i)=0.5;

end

%for body 2

if U_pl(2,i)>U_Rd(2)

    R(2,i)=0;

else

    R(2,i)=K_el(2)*(u(2,i)-U_pl(2,i));

end


%update the values for the stiffnesses

%for body 1

if du(i)==0

    k1=K_el(1);

elseif U_pl(1)>U_Rd(1)

    k1=0;

else

    k1=R(1,i)/du(i);

end


%for body 2

if u(2,i)==0

    k2=K_el(2);

elseif U_pl(2)>U_Rd(2)

    k2=0;

else

    k2=R(2,i)/u(2,i);

 end

 %assembly of stiffness matrix

K=[k1 -k1;

    -k1  k1+k2];
```

H.3   Classic theory

```
%---------------------------------------------------------------
% Collision impact according to classical theory
%---------------------------------------------------------------
clc

clear all

close all


%Indata
m1=1000;

m2=10000;

v0=20;

M=[m1 m2];


%Coefficient of restitution
e=0;      % 1 = elstic impact     0 = plastic impact


%Kinetic energy before impact
E_k0=m1*v0(1).^2/2


%Momentum before impact
p_0=m1*v0(1)



%Velocity after impact
v_cl(:,1)=v0(1)*(m1-(e*m2))/(m1+m2);

v_cl(:,2)=v0(1)*((1+e)*m1)/(m1+m2);


%Kinetic energy after impact
E_k=M.*v_cl.^2/2;


%Kinetic energy actiong in the same direction as mass 2, exterior work on
%second body


if v_cl(1)>0

    E_k(3)=E_k(1)+E_k(2);
else

    E_k(3)=E_k(2);
end


%Energy quota, shows how much of the initial kinetic energy that is
%continuing in the direction of body 2
v_cl

E_k

E_k_q=E_k(3)/E_k0
```

Appendix I ADINA command files

I.1 ADINA-IN command file for setting up the model

```
* Command file created from session file information stored
within AUI database

*--- Database created 28 March 2014, 00:00:00 ---*

*--- by ADINA: AUI version 9.0.1 ---*

*

DATABASE NEW SAVE=NO PROMPT=NO

FEPROGRAM ADINA

CONTROL FILEVERSION=V90

*

FEPROGRAM PROGRAM=ADINA

*

CONTROL  PLOTUNIT=PERCENT  VERBOSE=YES  ERRORLIM=0  LOGLIMIT=0
UNDO=5,

     PROMPTDE=UNKNOWN AUTOREPA=YES DRAWMATT=YES DRAWTEXT=EXACT,

     DRAWLINE=EXACT DRAWFILL=EXACT AUTOMREB=YES ZONECOPY=NO,

     SWEEPCOI=YES   SESSIONS=YES   DYNAMICT=YES   UPDATETH=YES
AUTOREGE=NO,

     ERRORACT=CONTINUE FILEVERS=V90 INITFCHE=NO SIGDIGIT=6,

     AUTOZONE=YES PSFILEVE=V0 ELEMENT-=REPEAT

*

FEPROGRAM PROGRAM=ADINA

*

MASTER ANALYSIS=DYNAMIC-DIRECT-INTEGRATION MODEX=EXECUTE,

     TSTART=0.00000000000000         IDOF=0         OVALIZAT=NONE
FLUIDPOT=AUTOMATIC,

     CYCLICPA=1 IPOSIT=STOP REACTION=YES INITIALS=NO FSINTERA=NO,

     IRINT=DEFAULT CMASS=NO SHELLNDO=AUTOMATIC AUTOMATI=OFF,

     SOLVER=SPARSE CONTACT-=CONSTRAINT-FUNCTION,

     TRELEASE=0.00000000000000   RESTART-=NO   FRACTURE=NO   LOAD-
CAS=NO,

     LOAD-PEN=NO SINGULAR=YES STIFFNES=0.000100000000000000,

     MAP-OUTP=NONE    MAP-FORM=NO    NODAL-DE=''    POROUS-C=NO
ADAPTIVE=0,

     ZOOM-LAB=1  AXIS-CYC=0  PERIODIC=NO  VECTOR-S=GEOMETRY EPSI-
FIR=NO,

     STABILIZ=NO STABFACT=1.00000000000000E-10 RESULTS=PORTHOLE,

     FEFCORR=NO BOLTSTEP=1 EXTEND-S=YES CONVERT-=NO DEGEN=YES,

     TMC-MODE=NO ENSIGHT-=NO IRSTEPS=1 INITIALT=NO TEMP-INT=NO,

     ESINTERA=NO  OP2GEOM=NO  INSITU-D=NO  OP2ERCS=ELEMENT  2DPL-
AX=YZ-Z

*

ANALYSIS DYNAMIC-DIRECT-INTEGRATION METHOD=NEWMARK,

     DELTA=0.500000000000000 ALPHA=0.250000000000000,

     THETA=1.40000000000000 TIMESTEP=TOTALTIME NCRSTEP=1,

     CRSTEP=0.00000000000000 MASS-SCA=1.00000000000000,

     DTMIN1=0.00000000000000 DTMIN2=0.00000000000000,

     GAMMA=0.500000000000000 MIDLOAD=TIMEFUNCTION,

     GAMAP=0.540000000000000

*

COORDINATES POINT SYSTEM=0

@CLEAR

1 0.00000000000000 0.00000000000000 0.00000000000000 0

2 2.50000000000000 0.00000000000000 0.00000000000000 0

3 5.00000000000000 0.00000000000000 0.00000000000000 0
```

```
4 2.50000000000000 2.50000000000000 0.00000000000000 0

@

*

LINE STRAIGHT NAME=1 P1=1 P2=2

*

LINE STRAIGHT NAME=2 P1=2 P2=3

*

MATERIAL      ELASTIC       NAME=1      E=8.13400000000000E+09
NU=0.200000000000000,

     DENSITY=2400.00000000000 ALPHA=0.00000000000000 MDESCRIP=,

'Concrete'

*

CROSS-SECTIO RECTANGULAR NAME=1 WIDTH=1.00000000000000,

     HEIGHT=0.300000000000000              SC=0.00000000000000
TC=0.00000000000000,

     TORFAC=1.00000000000000 SSHEARF=0.00000000000000,

     TSHEARF=0.00000000000000 ISHEAR=NO SQUARE=NO

*

LINE-ELEMDAT BEAM

@CLEAR

1 1 1 0  'DEFAULT'  'DEFAULT' 0.00000000000000 0.00000000000000
'NO',

     0.00000000000000 0.00000000000000 0.00000000000000

2 1 1 0  'DEFAULT'  'DEFAULT' 0.00000000000000 0.00000000000000
'NO',

     0.00000000000000 0.00000000000000 0.00000000000000

@

*

FIXITY NAME=SIMPLY_SUPPORTED

@CLEAR

 'X-TRANSLATION'

 'Y-TRANSLATION'

 'Z-TRANSLATION'

 'X-ROTATION'

 'Y-ROTATION'

 'OVALIZATION'

 'FLUID-POTENTIAL'

 'PORE-FLUID-PRESSURE'

 'TEMPERATURE'

 'BEAM-WARP'

@

*

FIXITY NAME=SIMPLY_SUPPORTED_ROLLER

@CLEAR

 'Y-TRANSLATION'

 'Z-TRANSLATION'

 'X-ROTATION'

 'Y-ROTATION'

 'OVALIZATION'

 'FLUID-POTENTIAL'

 'PORE-FLUID-PRESSURE'

 'TEMPERATURE'

 'BEAM-WARP'
```

```
@

*

FIXITY NAME=SPRING_TOP

@CLEAR

 'X-TRANSLATION'

 'Z-TRANSLATION'

 'X-ROTATION'

 'Y-ROTATION'

 'Z-ROTATION'

 'OVALIZATION'

 'FLUID-POTENTIAL'

 'PORE-FLUID-PRESSURE'

 'TEMPERATURE'

 'BEAM-WARP'

@

*

FIXBOUNDARY POINTS FIXITY=ALL

@CLEAR

1 'SIMPLY_SUPPORTED'

3 'SIMPLY_SUPPORTED_ROLLER'

4 'SPRING_TOP'

@

PROPERTY NONLINEAR-K NAME=1 RUPTURE=NO

@CLEAR

-1.00000000000000 -300000.000000000

0.00000000000000 0.00000000000000

1.00000000000000 0.00000000000000

@

*

PROPERTYSET NAME=1 K=0.00000000000000 M=0.00000000000000,

     C=0.00000000000000 NONLINEA=YES NK=1 NM=0 NC=0

*

MASSES POINTS

@CLEAR

4     0.00000000000000     1000.00000000000     0.00000000000000
0.00000000000000,

     0.00000000000000 0.00000000000000

@

*

EGROUP BEAM NAME=1 SUBTYPE=THREE-D DISPLACE=DEFAULT MATERIAL=1
RINT=5,

     SINT=DEFAULT TINT=DEFAULT RESULTS=FORCES INITIALS=NONE,

     CMASS=DEFAULT RIGIDEND=NONE MOMENT-C=NO RIGIDITY=1,

     MULTIPLY=1000000.00000000 RUPTURE=ADINA OPTION=NONE,

     BOLT-TOL=0.00000000000000 DESCRIPT='Beam' SECTION=1,

     PRINT=DEFAULT SAVE=DEFAULT TBIRTH=0.00000000000000,

     TDEATH=0.00000000000000 SPOINT=2 BOLTFORC=0.00000000000000,

     BOLTNCUR=0 TMC-MATE=1 BOLT-NUM=0 BOLT-LOA=0.00000000000000,

     WARP=NO ENDRELEA=ACCURATE

*

EGROUP SPRING NAME=2 PROPERTY=1 RESULTS=FORCES NONLINEA=NO,

     SKEWSYST=NO OPTION=NONE DESCRIPT='spring' PRINT=DEFAULT,

     SAVE=DEFAULT                        TBIRTH=0.00000000000000
TDEATH=0.00000000000000,

     6DOF-SPR=NO

*


SPRING POINTS

@CLEAR

1  4  2  2  2  1    'DEFAULT'    'DEFAULT'  0.00000000000000
0.00000000000000

@

*

SUBDIVIDE LINE NAME=1 MODE=LENGTH SIZE=0.100000000000000

@CLEAR

2

@

*

GLINE NODES=2 AUXPOINT=0 NCOINCID=ENDS NCENDS=12,

     NCTOLERA=1.00000000000000E-05        SUBSTRUC=0        GROUP=1
MIDNODES=CURVED,

     XO=0.00000000000000 YO=0.00000000000000 ZO=1.00000000000000,

     XYZOSYST=SKEW

@CLEAR

1

2

@

*

TIMESTEP NAME=DEFAULT

@CLEAR

1000 0.000500000000000000

@

*

INITIAL VELOCITIES SUBSTRUC=0 REUSE=1

@CLEAR

1 0.00000000000000 -20.0000000000000 0.00000000000000,

     0.00000000000000 0.00000000000000 0.00000000000000,

     0.00000000000000

@

*

EGROUP BEAM NAME=1 SUBTYPE=THREE-D DISPLACE=DEFAULT MATERIAL=1
RINT=5,

     SINT=DEFAULT TINT=DEFAULT RESULTS=STRESSES INITIALS=NONE,

     CMASS=DEFAULT RIGIDEND=NONE MOMENT-C=NO RIGIDITY=1,

     MULTIPLY=1000000.00000000 RUPTURE=ADINA OPTION=NONE,

     BOLT-TOL=0.00000000000000 DESCRIPT='Beam' SECTION=1,

     PRINT=DEFAULT SAVE=DEFAULT TBIRTH=0.00000000000000,

     TDEATH=0.00000000000000 SPOINT=2 BOLTFORC=0.00000000000000,

     BOLTNCUR=0 TMC-MATE=1 BOLT-NUM=0 BOLT-LOA=0.00000000000000,

     WARP=NO ENDRELEA=ACCURATE

*

EGROUP SPRING NAME=2 PROPERTY=1 RESULTS=STRESSES NONLINEA=NO,

     SKEWSYST=NO OPTION=NONE DESCRIPT='spring' PRINT=DEFAULT,

     SAVE=DEFAULT                        TBIRTH=0.00000000000000
TDEATH=0.00000000000000,

     6DOF-SPR=NO

****

*** ADINA OPTIMIZE=SOLVER FILE=,

***        'Q:\1_Projekt\EXJOBB\Daniel_Erik_2014\ADINA\a=0,5\SS-
Beam_a=0,

*** 5.dat' FIXBOUND=YES OVERWRIT=YES
```

I.2   ADINA-PLOT command file for extracting the result

```
NODEPOINT NAME=U1 SUBSTRUC=0 REUSE=1 NODE=1

*

NODEPOINT NAME=U2 SUBSTRUC=0 REUSE=1 NODE=2

*

NODEPOINT NAME=RA SUBSTRUC=0 REUSE=1 NODE=3

*

NODEPOINT NAME=RB SUBSTRUC=0 REUSE=1 NODE=52

*

NODEPOINT NAME=Mid SUBSTRUC=0 REUSE=1 NODE=2

*

*********CHANGE     TO     CORRECT     COORDINATE     FOR     EACH
IMPACT*****************

*

ELPOINT  NAME=U2_element  SUBSTRUC=0  REUSE=1  GROUP=1  ELEMENT=26
LAYER=1,

     OPTION=LABEL LABEL=1

*

ELLINE NAME=BEAM_COMPLETE SUBSTRUC=0 REUSE=1 GROUP=1 ELEMENT=1,

     LAYER=1 OPTION=LABEL LABEL=1 FACTOR=1.00000000000000

@CLEAR

0 1 1 1 1  'LABEL' 0 1 1 0.00000000000000 0.00000000000000,

     0.00000000000000 1.00000000000000

0 1 1 2 1  'LABEL' 0 1 1 0.00000000000000 0.00000000000000,

     0.00000000000000 1.00000000000000

0 1 1 3 1  'LABEL' 0 1 1 0.00000000000000 0.00000000000000,

     0.00000000000000 1.00000000000000

0 1 1 4 1  'LABEL' 0 1 1 0.00000000000000 0.00000000000000,

     0.00000000000000 1.00000000000000

0 1 1 5 1  'LABEL' 0 1 1 0.00000000000000 0.00000000000000,

     0.00000000000000 1.00000000000000

0 1 1 6 1  'LABEL' 0 1 1 0.00000000000000 0.00000000000000,

     0.00000000000000 1.00000000000000

0 1 1 7 1  'LABEL' 0 1 1 0.00000000000000 0.00000000000000,

     0.00000000000000 1.00000000000000

0 1 1 8 1  'LABEL' 0 1 1 0.00000000000000 0.00000000000000,

     0.00000000000000 1.00000000000000

0 1 1 9 1  'LABEL' 0 1 1 0.00000000000000 0.00000000000000,

     0.00000000000000 1.00000000000000

0 1 1 10 1  'LABEL' 0 1 1 0.00000000000000 0.00000000000000,

     0.00000000000000 1.00000000000000

0 1 1 11 1  'LABEL' 0 1 1 0.00000000000000 0.00000000000000,

     0.00000000000000 1.00000000000000

0 1 1 12 1  'LABEL' 0 1 1 0.00000000000000 0.00000000000000,

     0.00000000000000 1.00000000000000

0 1 1 13 1  'LABEL' 0 1 1 0.00000000000000 0.00000000000000,

     0.00000000000000 1.00000000000000

0 1 1 14 1  'LABEL' 0 1 1 0.00000000000000 0.00000000000000,

     0.00000000000000 1.00000000000000

0 1 1 15 1  'LABEL' 0 1 1 0.00000000000000 0.00000000000000,

     0.00000000000000 1.00000000000000

0 1 1 16 1  'LABEL' 0 1 1 0.00000000000000 0.00000000000000,

     0.00000000000000 1.00000000000000

0 1 1 17 1  'LABEL' 0 1 1 0.00000000000000 0.00000000000000,

     0.00000000000000 1.00000000000000
```

```
0 1 1 18 1  'LABEL' 0 1 1 0.00000000000000 0.00000000000000,

     0.00000000000000 1.00000000000000

0 1 1 19 1  'LABEL' 0 1 1 0.00000000000000 0.00000000000000,

     0.00000000000000 1.00000000000000

0 1 1 20 1  'LABEL' 0 1 1 0.00000000000000 0.00000000000000,

     0.00000000000000 1.00000000000000

0 1 1 21 1  'LABEL' 0 1 1 0.00000000000000 0.00000000000000,

     0.00000000000000 1.00000000000000

0 1 1 22 1  'LABEL' 0 1 1 0.00000000000000 0.00000000000000,

     0.00000000000000 1.00000000000000

0 1 1 23 1  'LABEL' 0 1 1 0.00000000000000 0.00000000000000,

     0.00000000000000 1.00000000000000

0 1 1 24 1  'LABEL' 0 1 1 0.00000000000000 0.00000000000000,

     0.00000000000000 1.00000000000000

0 1 1 25 1  'LABEL' 0 1 1 0.00000000000000 0.00000000000000,

     0.00000000000000 1.00000000000000

0 1 1 26 1  'LABEL' 0 1 1 0.00000000000000 0.00000000000000,

     0.00000000000000 1.00000000000000

0 1 1 27 1  'LABEL' 0 1 1 0.00000000000000 0.00000000000000,

     0.00000000000000 1.00000000000000

0 1 1 28 1  'LABEL' 0 1 1 0.00000000000000 0.00000000000000,

     0.00000000000000 1.00000000000000

0 1 1 29 1  'LABEL' 0 1 1 0.00000000000000 0.00000000000000,

     0.00000000000000 1.00000000000000

0 1 1 30 1  'LABEL' 0 1 1 0.00000000000000 0.00000000000000,

     0.00000000000000 1.00000000000000

0 1 1 31 1  'LABEL' 0 1 1 0.00000000000000 0.00000000000000,

     0.00000000000000 1.00000000000000

0 1 1 32 1  'LABEL' 0 1 1 0.00000000000000 0.00000000000000,

     0.00000000000000 1.00000000000000

0 1 1 33 1  'LABEL' 0 1 1 0.00000000000000 0.00000000000000,

     0.00000000000000 1.00000000000000

0 1 1 34 1  'LABEL' 0 1 1 0.00000000000000 0.00000000000000,

     0.00000000000000 1.00000000000000

0 1 1 35 1  'LABEL' 0 1 1 0.00000000000000 0.00000000000000,

     0.00000000000000 1.00000000000000

0 1 1 36 1  'LABEL' 0 1 1 0.00000000000000 0.00000000000000,

     0.00000000000000 1.00000000000000

0 1 1 37 1  'LABEL' 0 1 1 0.00000000000000 0.00000000000000,

     0.00000000000000 1.00000000000000

0 1 1 38 1  'LABEL' 0 1 1 0.00000000000000 0.00000000000000,

     0.00000000000000 1.00000000000000

0 1 1 39 1  'LABEL' 0 1 1 0.00000000000000 0.00000000000000,

     0.00000000000000 1.00000000000000

0 1 1 40 1  'LABEL' 0 1 1 0.00000000000000 0.00000000000000,

     0.00000000000000 1.00000000000000

0 1 1 41 1  'LABEL' 0 1 1 0.00000000000000 0.00000000000000,

     0.00000000000000 1.00000000000000

0 1 1 42 1  'LABEL' 0 1 1 0.00000000000000 0.00000000000000,

     0.00000000000000 1.00000000000000

0 1 1 43 1  'LABEL' 0 1 1 0.00000000000000 0.00000000000000,

     0.00000000000000 1.00000000000000

0 1 1 44 1  'LABEL' 0 1 1 0.00000000000000 0.00000000000000,
```

```
    0.00000000000000 1.00000000000000                              0 1 35 1.00000000000000

0 1 1 45 1  'LABEL' 0 1 1 0.00000000000000 0.00000000000000,         0 1 36 1.00000000000000

    0.00000000000000 1.00000000000000                              0 1 37 1.00000000000000

0 1 1 46 1  'LABEL' 0 1 1 0.00000000000000 0.00000000000000,         0 1 38 1.00000000000000

    0.00000000000000 1.00000000000000                              0 1 39 1.00000000000000

0 1 1 47 1  'LABEL' 0 1 1 0.00000000000000 0.00000000000000,         0 1 40 1.00000000000000

    0.00000000000000 1.00000000000000                              0 1 41 1.00000000000000

0 1 1 48 1  'LABEL' 0 1 1 0.00000000000000 0.00000000000000,         0 1 42 1.00000000000000

    0.00000000000000 1.00000000000000                              0 1 43 1.00000000000000

0 1 1 49 1  'LABEL' 0 1 1 0.00000000000000 0.00000000000000,         0 1 44 1.00000000000000

    0.00000000000000 1.00000000000000                              0 1 45 1.00000000000000

0 1 1 50 1  'LABEL' 0 1 1 0.00000000000000 0.00000000000000,         0 1 46 1.00000000000000

    0.00000000000000 1.00000000000000                              0 1 47 1.00000000000000

0 1 1 50 1  'LABEL' 0 2 1 0.00000000000000 0.00000000000000,         0 1 48 1.00000000000000

    0.00000000000000 1.00000000000000                              0 1 49 1.00000000000000

@                                                                  0 1 50 1.00000000000000

********MOVE  NODE  2  TO  CORRECT  POSITION  FOR  EACH  LOAD       0 1 51 1.00000000000000
APPLICATION*********
                                                                   0 1 52 1.00000000000000
*
                                                                   @
NODELINE NAME=BEAM_NODE_LIST SUBSTRUC=0 REUSE=1 NODE=1,
                                                                   ****************************************************************
    FACTOR=1.00000000000000                                        *********

@CLEAR                                                             *

0 1 3 1.00000000000000                                             FRAME LOWER=0.00000000000000 UPPER=0.00000000000000 ROTATION=0,

0 1 4 1.00000000000000                                                  LINE=YES SIZE=SURFACE ISOSIZE=4.00000000000000,

0 1 5 1.00000000000000                                                  WIDTH=100.000000000000 HEIGHT=100.000000000000,

0 1 6 1.00000000000000                                                  XOFFSET=0.00000000000000 YOFFSET=0.00000000000000 INDEX=YES,

0 1 7 1.00000000000000                                                  CUTMARK=NO        WINDOW=PREVIOUS        UNITLOWE=PERCENT
                                                                   UNITUPPE=PERCENT,
0 1 8 1.00000000000000
                                                                       UNITWIDT=PERCENT UNITHEIG=PERCENT UNITXOFF=PERCENT,
0 1 9 1.00000000000000
                                                                       UNITYOFF=PERCENT UPDATE=NO ASPECT=1.33333337306976,
0 1 10 1.00000000000000
                                                                       CHARSIZE=0.250000000000000 UNITCHAR=CM HSTRING=' ',
0 1 11 1.00000000000000
                                                                       ADINATEX=VERTICAL
0 1 12 1.00000000000000
                                                                   *
0 1 13 1.00000000000000
                                                                   RESPONSESHOW        XVARIABL=TIME        XPOINT=U2_element
0 1 14 1.00000000000000                                            YVARIABL=NODAL_MOMENT-S,

0 1 15 1.00000000000000                                                 YPOINT=U2_element RESPRANG=DEFAULT XSMOOTHI=DEFAULT,

0 1 16 1.00000000000000                                                 YSMOOTHI=DEFAULT    XRESULTC=DEFAULT    YRESULTC=DEFAULT
                                                                   GRAPH=YES,
0 1 17 1.00000000000000
                                                                       CURVEDEP=DEFAULT XAXIS=DEFAULT_X YAXIS=DEFAULT_Y,
0 1 18 1.00000000000000
                                                                       GRAPHDEP=DEFAULT SUBFRAME=DEFAULT LIST=NO
0 1 19 1.00000000000000
                                                                   *
0 1 20 1.00000000000000
                                                                   SAVEBMP FILENAME='Results\Moment_u2.jpg',
0 1 21 1.00000000000000
                                                                       SIZE=FRAME SCALE=1.00000000000000 XSIZE=640 YSIZE=480
0 1 22 1.00000000000000
                                                                   *
0 1 23 1.00000000000000
                                                                   FRAME LOWER=0.00000000000000 UPPER=0.00000000000000 ROTATION=0,
0 1 24 1.00000000000000
                                                                       LINE=YES SIZE=SURFACE ISOSIZE=4.00000000000000,
0 1 25 1.00000000000000
                                                                       WIDTH=100.000000000000 HEIGHT=100.000000000000,
0 1 26 1.00000000000000
                                                                       XOFFSET=0.00000000000000 YOFFSET=0.00000000000000 INDEX=YES,
0 1 27 1.00000000000000
                                                                       CUTMARK=NO        WINDOW=PREVIOUS        UNITLOWE=PERCENT
0 1 2 1.00000000000000                                             UNITUPPE=PERCENT,

0 1 28 1.00000000000000                                                 UNITWIDT=PERCENT UNITHEIG=PERCENT UNITXOFF=PERCENT,

0 1 29 1.00000000000000                                                 UNITYOFF=PERCENT UPDATE=NO ASPECT=1.33333337306976,

0 1 30 1.00000000000000                                                 CHARSIZE=0.250000000000000 UNITCHAR=CM HSTRING=' ',

0 1 31 1.00000000000000                                                 ADINATEX=VERTICAL

0 1 32 1.00000000000000                                            *

0 1 33 1.00000000000000                                            RESPONSESHOW        XVARIABL=TIME        XPOINT=U2_element
                                                                   YVARIABL=NODAL_FORCE-T,
0 1 34 1.00000000000000
```

```
        YPOINT=U2_element RESPRANG=DEFAULT XSMOOTHI=DEFAULT,

        YSMOOTHI=DEFAULT      XRESULTC=DEFAULT      YRESULTC=DEFAULT
GRAPH=YES,

        CURVEDEP=DEFAULT XAXIS=DEFAULT_X YAXIS=DEFAULT_Y,

        GRAPHDEP=DEFAULT SUBFRAME=DEFAULT LIST=NO
*
SAVEBMP FILENAME='Results\Force_u2.jpg',

        SIZE=FRAME SCALE=1.00000000000000 XSIZE=640 YSIZE=480

*
FRAME LOWER=0.00000000000000 UPPER=0.00000000000000 ROTATION=0,

        LINE=YES SIZE=SURFACE ISOSIZE=4.00000000000000,

        WIDTH=100.000000000000 HEIGHT=100.000000000000,

        XOFFSET=0.00000000000000 YOFFSET=0.00000000000000 INDEX=YES,

        CUTMARK=NO         WINDOW=PREVIOUS         UNITLOWE=PERCENT
UNITUPPE=PERCENT,

        UNITWIDT=PERCENT UNITHEIG=PERCENT UNITXOFF=PERCENT,

        UNITYOFF=PERCENT UPDATE=NO ASPECT=1.33333337306976,

        CHARSIZE=0.250000000000000 UNITCHAR=CM HSTRING=' ',

        ADINATEX=VERTICAL
*
RESPONSESHOW   XVARIABL=TIME   XPOINT=U1   YVARIABL=Y-DISPLACEMENT
YPOINT=U1,

        RESPRANG=DEFAULT XSMOOTHI=DEFAULT YSMOOTHI=DEFAULT,

        XRESULTC=DEFAULT           YRESULTC=DEFAULT          GRAPH=YES
CURVEDEP=DEFAULT,

        XAXIS=DEFAULT_X YAXIS=DEFAULT_Y GRAPHDEP=DEFAULT,

        SUBFRAME=DEFAULT LIST=NO
*
SAVEBMP FILENAME='Results\u1_graph.jpg',

        SIZE=FRAME SCALE=1.00000000000000 XSIZE=640 YSIZE=480

*
FRAME LOWER=0.00000000000000 UPPER=0.00000000000000 ROTATION=0,

        LINE=YES SIZE=SURFACE ISOSIZE=4.00000000000000,

        WIDTH=100.000000000000 HEIGHT=100.000000000000,

        XOFFSET=0.00000000000000 YOFFSET=0.00000000000000 INDEX=YES,

        CUTMARK=NO         WINDOW=PREVIOUS         UNITLOWE=PERCENT
UNITUPPE=PERCENT,

        UNITWIDT=PERCENT UNITHEIG=PERCENT UNITXOFF=PERCENT,

        UNITYOFF=PERCENT UPDATE=NO ASPECT=1.33333337306976,

        CHARSIZE=0.250000000000000 UNITCHAR=CM HSTRING=' ',

        ADINATEX=VERTICAL
*
RESPONSESHOW   XVARIABL=TIME   XPOINT=U2   YVARIABL=Y-DISPLACEMENT
YPOINT=U2,

        RESPRANG=DEFAULT XSMOOTHI=DEFAULT YSMOOTHI=DEFAULT,

        XRESULTC=DEFAULT           YRESULTC=DEFAULT          GRAPH=YES
CURVEDEP=DEFAULT,

        XAXIS=DEFAULT_X YAXIS=DEFAULT_Y GRAPHDEP=DEFAULT,

        SUBFRAME=DEFAULT LIST=NO
*
SAVEBMP FILENAME='Results\u2_graph.jpg',

        SIZE=FRAME SCALE=1.00000000000000 XSIZE=640 YSIZE=480

*
FRAME LOWER=0.00000000000000 UPPER=0.00000000000000 ROTATION=0,

        LINE=YES SIZE=SURFACE ISOSIZE=4.00000000000000,

        WIDTH=100.000000000000 HEIGHT=100.000000000000,

        XOFFSET=0.00000000000000 YOFFSET=0.00000000000000 INDEX=YES,


        CUTMARK=NO         WINDOW=PREVIOUS         UNITLOWE=PERCENT
UNITUPPE=PERCENT,

        UNITWIDT=PERCENT UNITHEIG=PERCENT UNITXOFF=PERCENT,

        UNITYOFF=PERCENT UPDATE=NO ASPECT=1.33333337306976,

        CHARSIZE=0.250000000000000 UNITCHAR=CM HSTRING=' ',

        ADINATEX=VERTICAL

*
RESPONSESHOW  XVARIABL=TIME   XPOINT=RA   YVARIABL=Y-REACTION
YPOINT=RA,

        RESPRANG=DEFAULT XSMOOTHI=DEFAULT YSMOOTHI=DEFAULT,

        XRESULTC=DEFAULT           YRESULTC=DEFAULT          GRAPH=YES
CURVEDEP=DEFAULT,

        XAXIS=DEFAULT_X YAXIS=DEFAULT_Y GRAPHDEP=DEFAULT,

        SUBFRAME=DEFAULT LIST=NO
*
SAVEBMP FILENAME='Results\R_graph.jpg',

        SIZE=FRAME SCALE=1.00000000000000 XSIZE=640 YSIZE=480
*
FRAME LOWER=0.00000000000000 UPPER=0.00000000000000 ROTATION=0,

        LINE=YES SIZE=SURFACE ISOSIZE=4.00000000000000,

        WIDTH=100.000000000000 HEIGHT=100.000000000000,

        XOFFSET=0.00000000000000 YOFFSET=0.00000000000000 INDEX=YES,

        CUTMARK=NO         WINDOW=PREVIOUS         UNITLOWE=PERCENT
UNITUPPE=PERCENT,

        UNITWIDT=PERCENT UNITHEIG=PERCENT UNITXOFF=PERCENT,

        UNITYOFF=PERCENT UPDATE=NO ASPECT=1.33333337306976,

        CHARSIZE=0.250000000000000 UNITCHAR=CM HSTRING=' ',

        ADINATEX=VERTICAL

*
RESPONSESHOW   XVARIABL=TIME   XPOINT=mid   YVARIABL=Y-DISPLACEMENT
YPOINT=mid,

        RESPRANG=DEFAULT XSMOOTHI=DEFAULT YSMOOTHI=DEFAULT,

        XRESULTC=DEFAULT           YRESULTC=DEFAULT          GRAPH=YES
CURVEDEP=DEFAULT,

        XAXIS=DEFAULT_X YAXIS=DEFAULT_Y GRAPHDEP=DEFAULT,

        SUBFRAME=DEFAULT LIST=NO
*
SAVEBMP FILENAME='Results\u_midpoint_graph.jpg',

        SIZE=FRAME SCALE=1.00000000000000 XSIZE=640 YSIZE=480
*
FRAME LOWER=0.00000000000000 UPPER=0.00000000000000 ROTATION=0,

        LINE=YES SIZE=SURFACE ISOSIZE=4.00000000000000,

        WIDTH=100.000000000000 HEIGHT=100.000000000000,

        XOFFSET=0.00000000000000 YOFFSET=0.00000000000000 INDEX=YES,

        CUTMARK=NO         WINDOW=PREVIOUS         UNITLOWE=PERCENT
UNITUPPE=PERCENT,

        UNITWIDT=PERCENT UNITHEIG=PERCENT UNITXOFF=PERCENT,

        UNITYOFF=PERCENT UPDATE=NO ASPECT=1.33333337306976,

        CHARSIZE=0.250000000000000 UNITCHAR=CM HSTRING=' ',

        ADINATEX=VERTICAL

*
RESPONSESHOW   XVARIABL=TIME   XPOINT=RB   YVARIABL=Y-REACTION
YPOINT=RB,

        RESPRANG=DEFAULT XSMOOTHI=DEFAULT YSMOOTHI=DEFAULT,

        XRESULTC=DEFAULT           YRESULTC=DEFAULT          GRAPH=YES
CURVEDEP=DEFAULT,

        XAXIS=DEFAULT_X YAXIS=DEFAULT_Y GRAPHDEP=DEFAULT,

        SUBFRAME=DEFAULT LIST=NO

*
```

```
SAVEBMP FILENAME='Results\RB_graph.jpg',

    SIZE=FRAME SCALE=1.00000000000000 XSIZE=640 YSIZE=480

*

FRAME LOWER=0.00000000000000 UPPER=0.00000000000000 ROTATION=0,

    LINE=YES SIZE=SURFACE ISOSIZE=4.00000000000000,

    WIDTH=100.000000000000 HEIGHT=100.000000000000,

    XOFFSET=0.00000000000000 YOFFSET=0.00000000000000 INDEX=YES,

    CUTMARK=NO          WINDOW=PREVIOUS          UNITLOWE=PERCENT
UNITUPPE=PERCENT,

    UNITWIDT=PERCENT UNITHEIG=PERCENT UNITXOFF=PERCENT,

    UNITYOFF=PERCENT UPDATE=NO ASPECT=1.33333337306976,

    CHARSIZE=0.250000000000000 UNITCHAR=CM HSTRING=' ',

    ADINATEX=VERTICAL

*

MESHPLOT MESHSTYL=DEFAULT ZONENAME=WHOLE_MODEL RESPONSE=DEFAULT,

    MODELDEP=DEFAULT        VIEW=DEFAULT        MESHWIND=DEFAULT
PLOTAREA=DEFAULT,

    SUBFRAME=DEFAULT ELDEPICT=DEFAULT NODEDEPI=DEFAULT,

    BOUNDEPI=DEFAULT GPDEPICT=DEFAULT GLDEPICT=DEFAULT,

    GSDEPICT=DEFAULT GVDEPICT=DEFAULT MESHREND=DEFAULT,

    MESHANNO=DEFAULT FRONDEPI=DEFAULT CONDEPIC=DEFAULT,

    VSDEPICI=DEFAULT CRACKDEP=DEFAULT RESULTCO=DEFAULT,

    CUTSURFA=DEFAULT ELFACESE=0 ELEDGESE=0

*

MOVIESHOOT LOAD-STEP TSTART=EARLIEST  TEND=LATEST  FRAMES=100
MOVIENUM=1

*

SAVEAVI FILENAME='Results\vid.avi',

    SPEED=5 XSIZE=640 YSIZE=480 MOVIENUM=1 SIZE=FRAME,

    SCALE=1.00000000000000 COLORBIT=16

*

RESPRANGE      LOAD-STEP      NAME=LISTA      TSTART=EARLIEST
TEND=0.200000000000000,

    INCREMEN=TINCREMENT TINCREME=0.0100000000000000

*

Filelist o=File f='Results\Moment+shear.text'

LINELIST       LINENAME=BEAM_COMPLETE       SMOOTHIN=DEFAULT
RESULTCO=DEFAULT,

    RESPOPTI=RESPRANGE RESPONSE=DEFAULT RESPRANG=LISTA,

    VARIABLE=NODAL_MOMENT-S NODAL_FORCE-T

*

Filelist o=File f='Results\max_moment+shear_time.text'

LINEMAX     LINENAME=BEAM_COMPLETE     TYPE=ABSMAX     NUMBER=1
SMOOTHIN=DEFAULT,

    RESULTCO=DEFAULT RESPOPTI=RESPRANGE RESPONSE=DEFAULT,

    RESPRANG=DEFAULT VARIABLE=NODAL_MOMENT-S NODAL_FORCE-T

*

Filelist o=File f='Results\Deflection_time.text'

LINELIST       LINENAME=BEAM_NODE_LIST       SMOOTHIN=DEFAULT
RESULTCO=DEFAULT,

    RESPOPTI=RESPRANGE RESPONSE=DEFAULT RESPRANG=LISTA,

    VARIABLE=Y-DISPLACEMENT

*

Filelist o=File f='Results\max_deflection_time.text'

LINEMAX    LINENAME=BEAM_NODE_LIST     TYPE=ABSMAX     NUMBER=1
SMOOTHIN=DEFAULT,

    RESULTCO=DEFAULT RESPOPTI=RESPRANGE RESPONSE=DEFAULT,

    RESPRANG=DEFAULT VARIABLE=Y-DISPLACEMENT
```

```
*

Filelist o=File f='Results\Ra.text'

POINTLIST POINTNAM=RA SMOOTHIN=DEFAULT RESULTCO=DEFAULT,

    RESPOPTI=RESPRANGE RESPONSE=DEFAULT RESPRANG=DEFAULT,

    VARIABLE=Y-REACTION

*

Filelist o=File f='Results\Rb.text'

POINTLIST POINTNAM=RB SMOOTHIN=DEFAULT RESULTCO=DEFAULT,

    RESPOPTI=RESPRANGE RESPONSE=DEFAULT RESPRANG=DEFAULT,

    VARIABLE=Y-REACTION

*

Filelist o=File f='Results\u_topspring.text'

POINTLIST POINTNAM=U1 SMOOTHIN=DEFAULT RESULTCO=DEFAULT,

    RESPOPTI=RESPRANGE RESPONSE=DEFAULT RESPRANG=DEFAULT,

    VARIABLE=Y-DISPLACEMENT

*

Filelist o=File f='Results\u_bottomspring.text'

POINTLIST POINTNAM=U2 SMOOTHIN=DEFAULT RESULTCO=DEFAULT,

    RESPOPTI=RESPRANGE RESPONSE=DEFAULT RESPRANG=DEFAULT,

    VARIABLE=Y-DISPLACEMENT

*

Filelist o=File f='Results\u_midpoint.text'

POINTLIST POINTNAM=mid SMOOTHIN=DEFAULT RESULTCO=DEFAULT,

    RESPOPTI=RESPRANGE RESPONSE=DEFAULT RESPRANG=DEFAULT,

    VARIABLE=Y-DISPLACEMENT

*

Filelist o=File f='Results\Moment_impactnode_t.text'

POINTLIST POINTNAM=U2_element SMOOTHIN=DEFAULT RESULTCO=DEFAULT,

    RESPOPTI=RESPRANGE RESPONSE=DEFAULT RESPRANG=DEFAULT,

    VARIABLE=NODAL_MOMENT-S

*

Filelist o=File f='Results\Force_impactnode_t.text'

POINTLIST POINTNAM=U2_element SMOOTHIN=DEFAULT RESULTCO=DEFAULT,

    RESPOPTI=RESPRANGE RESPONSE=DEFAULT RESPRANG=DEFAULT,

    VARIABLE=NODAL_FORCE-T

*

********Moment
envelope**************************************************

*

RESPONSE ENVELOPE NAME=ENVELOPE_MIN TYPE=MINIMUM OPTION=RANGE,

    TSTART=EARLIEST TEND=LATEST INCREMEN=AVAILABLE,

    TINCREME=1.00000000000000 NSTEP=1 INTERPOL=NO NSKIP=0

*

Filelist o=File f='Results\Moment_env_min.text'

LINEEXCEED        LINENAME=BEAM_COMPLETE        TYPE=MINIMUM
VALUE=0.00000000000000,

    SMOOTHIN=DEFAULT RESULTCO=DEFAULT RESPOPTI=RESPONSE,

    RESPONSE=ENVELOPE_MIN                RESPRANG=DEFAULT
VARIABLE=NODAL_MOMENT-S

*

RESPONSE ENVELOPE NAME=ENVELOPE_ABSMAX TYPE=ABSMAX OPTION=RANGE,

    TSTART=EARLIEST TEND=LATEST INCREMEN=AVAILABLE,

    TINCREME=1.00000000000000 NSTEP=1 INTERPOL=NO NSKIP=0

*

Filelist o=File f='Results\Moment_env_absmax.text'

LINEEXCEED        LINENAME=BEAM_COMPLETE        TYPE=ABSMAX
VALUE=0.00000000000000,
```

```
     SMOOTHIN=DEFAULT RESULTCO=DEFAULT RESPOPTI=RESPONSE,

     RESPONSE=ENVELOPE_ABSMAX RESPRANG=DEFAULT,

     VARIABLE=NODAL_MOMENT-S
*

*****Shear                                                  force
envelope*************************************************

*

RESPONSE ENVELOPE NAME=ENVELOPE_MAX TYPE=MAXIMUM OPTION=RANGE,

     TSTART=EARLIEST TEND=LATEST INCREMEN=AVAILABLE,

     TINCREME=1.00000000000000 NSTEP=1 INTERPOL=NO NSKIP=0

*

Filelist o=File f='Results\Shear_env_min.text'

LINEEXCEED          LINENAME=BEAM_COMPLETE          TYPE=MINIMUM
VALUE=0.00000000000000,

     SMOOTHIN=DEFAULT RESULTCO=DEFAULT RESPOPTI=RESPONSE,

     RESPONSE=ENVELOPE_MIN RESPRANG=DEFAULT VARIABLE=NODAL_FORCE-
T

*

Filelist o=File f='Results\Shear_env_max.text'

LINEEXCEED          LINENAME=BEAM_COMPLETE          TYPE=MAXIMUM
VALUE=0.00000000000000,

     SMOOTHIN=DEFAULT RESULTCO=DEFAULT RESPOPTI=RESPONSE,

     RESPONSE=ENVELOPE_MAX RESPRANG=DEFAULT VARIABLE=NODAL_FORCE-
T

*

Filelist o=File f='Results\Shear_env_absmax.text'

LINEEXCEED          LINENAME=BEAM_COMPLETE          TYPE=ABSMAX
VALUE=0.00000000000000,

     SMOOTHIN=DEFAULT RESULTCO=DEFAULT RESPOPTI=RESPONSE,

     RESPONSE=ENVELOPE_ABSMAX                       RESPRANG=DEFAULT
VARIABLE=NODAL_FORCE-T

*******************************************************************
```